Topology optimisation by invariants of anisotropic lattice structures

Nassim Kesmia

Université Gustave Eiffel

PARIS EST SUP — ÉCOLE DOCTORALE Sciences, Ingénierie et Environnement

Université Gustave Eiffel

École doctorale Sciences, Ingénierie et Environnement

Thèse

Pour obtenir le grade de

DOCTEUR de l'Université Gustave Eiffel

Spécialité : Mécanique.

Présentée et soutenue par :

Nassim KESMIA

Optimisation topologique par invariants des structures Lattices anisotropes

---

Pour une soutenance le 29 septembre 2023 devant le jury composé de:

M. Aurélien Vattré	Ingénieur de recherche, DMAS - Office national d'études et de recherches aérospatiales (ONERA)	Rapporteur
M. Rafael Estevez	Professeur des universités, SIMaP - Université Grenoble Alpes	Rapporteur
M. Marc François	Professeur des universités, GeM - Nantes université	Examinateur
M. Djimedo Kondo	Professeur des universités, ∂'Alembert - Sorbonne université	Examinateur
M. Nicolas Auffray	Professeur des universités, ∂'Alembert - Sorbonne université	Directeur
M. Boris Desmorat	Maître de conférences, ∂'Alembert - Sorbonne université	Co-directeur
M. Giuseppe Rosi	Maître de conférences, MSME - Université Paris-Est Créteil	Encadrant

Résumé

Les matériaux architecturés sont des matériaux qui présentent une mésostructure entre leur macrostructure et leur microstructure. Ils sont connus pour avoir de nombreuses propriétés intéressantes telles qu'un bon rapport rigidité/poids, guidage d'ondes et absorption d'énergie. Il est important d'utiliser toutes ces propriétés de manière optimale, ce qui peut être fait à l'aide d'outils d'optimisation de la topologie. Assurer la tenue mécanique tout en ayant des propriétés optimales reste, jusqu'à présent, un problème. Les matériaux architecturés sont connus pour avoir un comportement mécanique particulier où l'on trouve deux modes de ruine : (1) la plasticité (ou rupture) en traction et (2) le flambage (ou plasticité) en compression. Ils sont donc fortement anisotropes et présentent des dissymétries (en traction et en compression). Il est nécessaire de définir un critère de tenue mécanique capable de décrire précisément ce comportement afin d'assurer la tenue mécanique de la structure optimisée. Dans la littérature, de multiples approches sont disponibles lorsqu'il s'agit de définir un critère prenant en compte l'anisotropie. Nous trouvons (i) la théorie de la représentation des groupes, (ii) les transformations linéaires et (iii) l'utilisation de polynômes de degré supérieur. Parmi toutes ces approches, nous nous intéressons au critère (iii). Les critères polynomiaux se sont révélés efficaces et précis dans la modélisation de l'anisotropie d'ordre élevé et dans la modélisation des dissymétries en traction/compression.

Avec le développement rapide des méthodes de fabrication additive, il est absolument nécessaire de garantir la résistance mécanique tout en ayant des propriétés optimales. Cela peut se faire en imposant un critère mécanique établi, généralement exprimé dans l'espace des contraintes (par exemple Von Mises), comme contrainte dans un problème d'optimisation de la topologie. Le problème qui en résulte est connu sous le nom de problème d'optimisation topologique sous contrainte. Ce type de problème présente de nombreuses difficultés numériques, et de nombreux auteurs l'étudient afin de le rendre plus pratique pour les applications industrielles.

Notre étude se limitera à la 2D pour un comportement élastique linéaire statique où le matériau considéré est un "Lattice 2D" triangulaire équilatéral. Pour ce matériau, un critère de seuil, qui permet de modéliser approximativement la dissymétrie traction/compression, a été établi. Le critère est ensuite considéré comme une contrainte dans un problème d'optimisation de la topologie, qui est résolu avec la méthode SIMP en utilisant l'algorithme de Lagrangien augmenté (une approche basée sur le gradient). Le matériau est considéré comme continu (par homogénéisation).

Abstract

Architectured materials are materials that present a mesostructure between their macrostructure and their microstructure. They are known to have many interesting properties such as a good stiffness/weight ratio, wave guide, energy absorption. It is important to use all these properties in an optimal way and this can be done with the help of topology optimisation tools. Ensuring mechanical strength while having optimal properties remains, until now, a problem. Architectured materials are known to have a particular mechanical behaviour where two modes of failure can be found: (1) plasticity (or brittleness) in tension and (2) buckling (or plasticity) in compression. They are therefore highly anisotropic and exhibit asymmetries (in tension and in compression). It is necessary to define a failure criterion capable of accurately describing this behaviour in order to ensure the mechanical strength of the optimised structure. In the literature, multiple approaches are available when it comes to to define a criterion that takes into account the anisotropy. We find (i) the group representation theory, (ii) linear transformations and (iii) the use of a higher degree polynomials . From all these approaches, we are interested on the (iii). Polynomial criteria have been shown to be efficient and accurate in modelling high-order anisotropy and in modelling dissymmetries in traction/compression.

With the fast development of additive manufacturing methods, ensuring the mechanical strength while having optimal properties is absolutely worth it. This can be done by imposing an established mechanical criterion, generally expressed in the stress space (e.g. Von Mises), as a constraint in a topology optimisation problem. The resulted problem is known as a stress constrained topology optimisation problem. This kind of problem exhibits lot of numerical issues, many authors are studying it in order to make it more convenient for industrial applications.

Our study will be limited to 2D for a static linear elastic behaviour where the considered material is an equilateral triangular honeycomb. For this material, a threshold criterion, that allows the tension/compressive strength dissymmetry to be modelled approximately, has been established. The criterion is then considered as a constraint in a topology optimisation problem, which is solved with SIMP method using the augmented Lagrangian algorithm (a gradient based approach). The material is considered continuous (through homogenisation).

Contents

List of Figures

Introduction: Optimal design of lattice structures

Contents

This thesis is a part of the *MOMAP* project (measurement and optimisation of architectured periodic materials). It is funded by the French National Research Agency (ANR). It is held on in the Multi-scale Modelling and Simulation Laboratory (MSME) at the Gustave Eiffel University. The subject of the thesis is "Topological optimisation of anisotropic lattice structures using invariants". It will be carried out in two phases. The first phase is theoretical and aims to propose an versatile analytical expression describing the mechanical strength limit of the architectured materials. The second phase is numerical and focuses on topological optimisation where, in the process, the proposed criterion will be implemented and considered as a constraint.

The current chapter, as an introduction, gives the context and the objective the thesis. The outline is as follows: The first section gives briefly the definition and the interests of using architectured material. The second speaks, in a very general manner, about topology optimisation and the purpose of apply it. The last section gives the context of this thesis by introducing the project MOMAP.

Architectured materials

The definition of architecture materials remains until now kind of ambiguous it covers a very large range of materials [72]. A lot of versions exist in literature [79, 142, 112]. They share some similarities as they also have some differences. Only thing they share is that all they have a micro structure from which we can identify the effective properties.

Kromm et al. [112] provided the following definition: "the architectured material refers to the notions of materials combination and structure, and as consequence, it focuses the attention on observation scale. An architectured material is defined by the association of several non-miscible materials disposed following predefined morphology such that a representative elementary volume has at least one dimension that is very small in comparison of the part in composes". This definition is accurate and introduce the notion of scale which is mainly used to distinguish architectured materials from bulk materials.

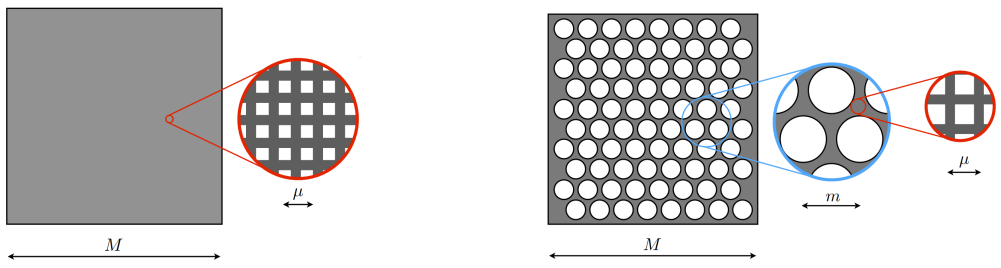

(a) A normal material with a macrostructure and a microstructure whose scales are well separated ($\mu << M$)

(b) An architectured material presenting 3 scales of structures

Figure 2: The difference between an architectured material and standard one

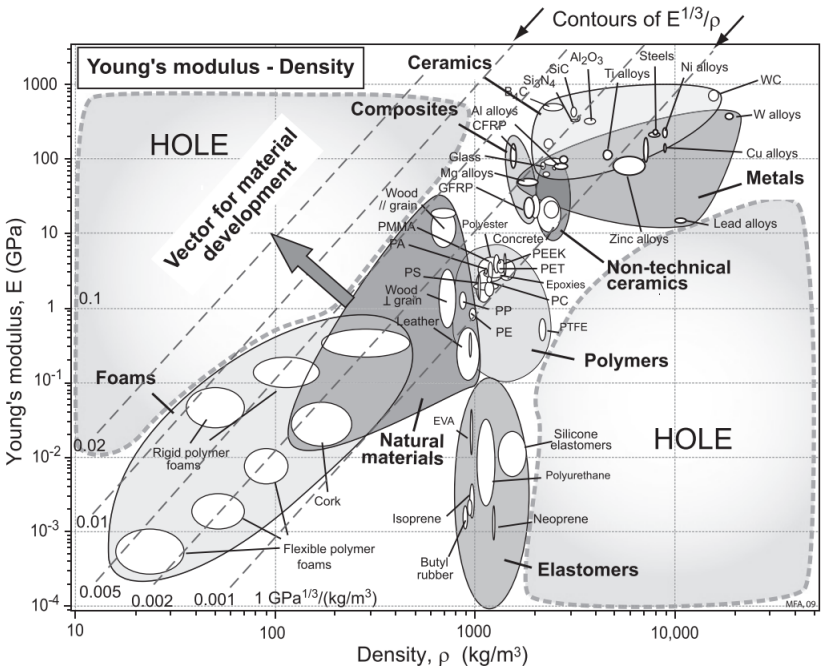

Figure 3: The modulus–density ratio space, Part of the space is occupied by the known materials, while part is empty (the "holes") [12].

A better resumed definition is proposed by Poncelet et al. [144], a material is said to be architectured (i) if it presents between its microstructure and its macrostrucutre one or more other scales of organisation of matter (called mesostructiure) and (ii) if the intermediate scales of organised are comparable with the those of the macrostructure, but separate with the one of microstructure (see figure 2).

As mentioned previously, architectured covers huge range of material and according to Ashby [12], it can give the possibility of covering the holes illustrated in his material diagram (see figure 3). Some examples of sub-classes of architectured materials are given below and illustrated in figure 4:

- Composites (solid, regular or random materials).
- Sandwich structures (solid, regular or random materials).
- Cellular materials (hollow, regular or random) [79].

Cellular materials are part of architectural materials consisting mainly of voids and walls surrounding. Because of their structure, cellular materials are very good candidates for filling the zones of interest in Ashby diagrams.

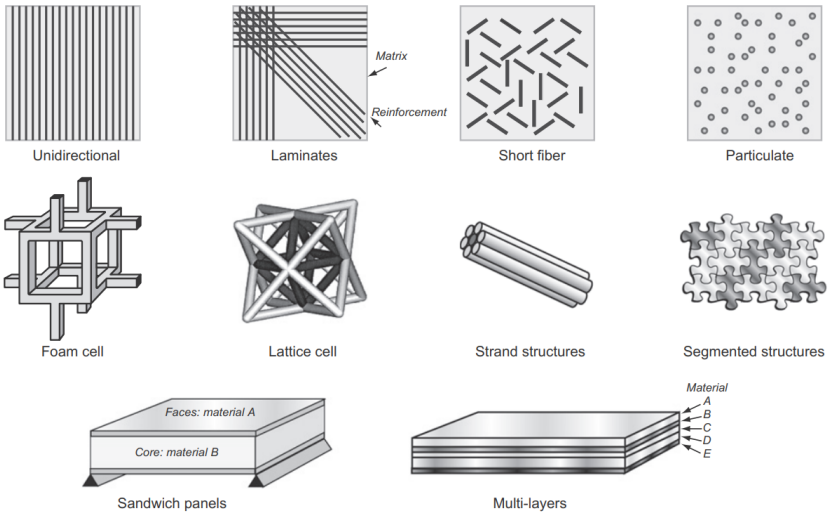

Figure 4: Examples of architectured materials with differing configurations [12].

Interests

Architectured materials are known for their interesting priorities in various industrial purposes such as good stiffness-weight ratio, acoustic, thermal conductivity and absorbing impacts energy, ... In general, the proprieties of architectured materials are resumed in the following points:

1. A good strong stiff/ weight ratio. Indeed, architectured materials can have a low percentage of matter which allows reaching a very low density and at the same time, they can have relatively a high Young's modulus. An example is given of of Cellulose foams [79] which have a density of $1.5mg/m^3$ and Young's modulus of $25GPa$. Its yield strength can reach $350MPa$.

2. Several acoustic proprieties are found. Architectured materials are known to have great damping effects on wave propagation depending on its morphology [124]. Controlling and guiding the wave propagation is possible. An example of cloaking effects is given by Chen et al. [49]. Another example is given by Giuseppe et al. [149] where they found out that it feasible to guide the wave in the hexagonal lattice structure considering Strain-Gradient elasticity continuum model and using available optimisation tools.

3. Some classes of architectured materials are known for low thermal expansion and high impacts energy absorption which required for aerospace industrial applications. Examples is provided by Craig et al. and Lehman et al. for thermal expansion in a bimaterial lattices [118, 174]. A theoretical example of resisting shock loading of honeycombs (2D Lattice) is provided by Hutchinson et al. [99].

4. With architectured materials, some unusual special characteristics can be found. For example a class called *auxetic materials*. They are known to have a negative Poisson's coefficient. They exist few in nature however, they can be artificially manufactured. The reader is invited to read the review carried out by Pasternak et al. [139] where examples of microstructures, that are able to generate auxetic effects, are available. Another example of materials called *double-negative metamaterials* [88] is provided. It is defined as a class of materials with effective properties of a negative Poisson's ratio and negative stiffness.

Lattice structures

In this thesis is focused on *Lattice materials*. It remains a subclass of architectured materials and it is considered as a part of cellular materials (examples in figure 5). A definition is provided by Phani et al. [142]. It is defined as a spatially periodic network of structural elements, such as rods, beams, plates, or shells. One of main characteristics is a spatially ordered pattern of unit cells in a periodic or semi-periodic manner. A unit cell is an interconnected network of structural elements. It is important to note that structural elements can be made of bulk materials or composites, which means that the multi-scale aspect can be present.

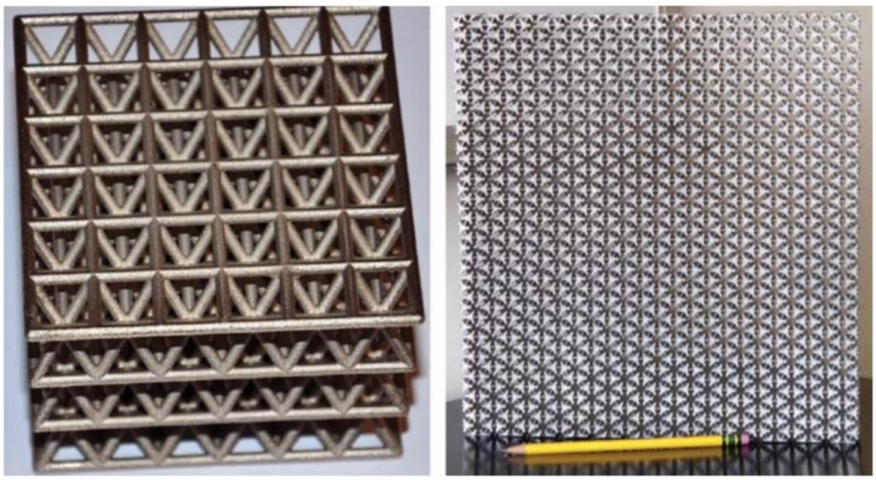

(a) **(b)**

Figure 5: Lattice materials formed from a periodic network of beams: (a) ultralight nanometal truss hybrid lattice; (b) pentamode lattice [142].

Phani et al. [142] pointed out on how to differentiate lattice materials from other materials and structures displayed in figure 6. Some of these are actually spatially ordered network of structural elements hence, the definition above gives us the impression that they are the same thing. Phani et al. stated that the spatial periodic network of beams is called *lattice material* if The deformation length scale is at length scale of the structural elements. In others words, a scale separation rule (e.g., between microstructure and macrostructure)

must be respected, the figure 6 shows how the scale separation scale is with comparison to a truss bridge structure.

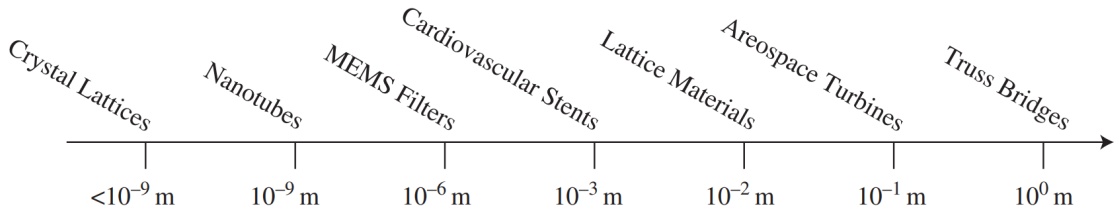

Figure 6: Periodic material and structures and their length scale (m=meter, MEMS = MicroElectroMechanical Systems) [142].

The following statements resume the reasons why the study is focused on lattice materials:

1. All the interests mentioned are present, making them very multifunctional. Since they are periodic (or semi periodic) and characterised by a unit cell, it is possible to control their properties by means of optimisation tools for the sake of better performance.
2. The high development of mathematical modelling tools for lattice material when it comes to their behaviour (static/dynamic). It is important to note that homogenisation approaches play an important role to characterise periodic lattice material and elaborate a continuum model [144, 173].
3. Lattice materials are now possible to make specially the fast development of additive manufacturing methods [183].

Optimisation

Lattice material are known to have a very interesting properties [142] which are possible to control. For a defined application, it is worth to get best desired performance and this is possible by the means of optimisation tools. Optimisation consists of mathematical approaches used to minimise (or maximise), with respect to defined variables, a cost function. The variable can be subject to constraints. It is applied in mechanical engineering where there are numerous applications for several purposes [31]. The reader is invited to read the section 4 for more details on how structural optimisation is preformed. A focus is put on topology optimisation which consist of founding optimal distribution of matter for defined problem.

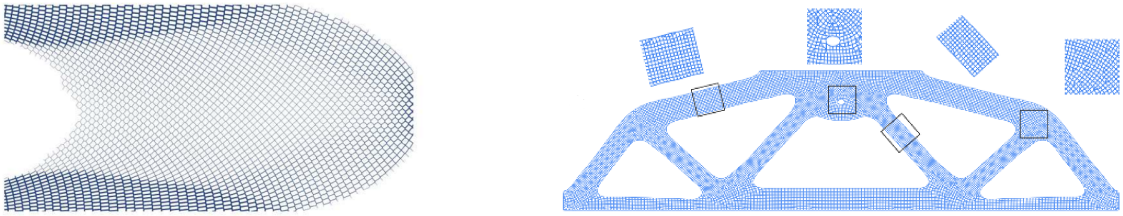

(a) (b)

Figure 7: Optimised Lattice structure designs ([104] for (a), [195] for (b)).

In this document, the conducted study will focus on using the topology optimisation of 2D lattice structures (structures made of lattice material). Many authors managed to do that [7, 104, 195, 42]. The optimal lattice designs, illustrated in figure 7, can be obtained using the so-called *homogenisation* or *SIMP* (Simple Isotropic Material Penalisation) method and, subsequently, by applying a *dishomogenisation* approach. Lattice material are known to have a particular mechanical behaviour where two modes of failure can be found: (1) plasticity (or brittleness) in traction and (2) buckling (or plasticity) in compression. Ensuring the mechanical strength while having optimal properties is absolutely worth it. This can be done by imposing an established mechanical criterion, generally expressed in the stress space (e.g. Von Mises), as a constraint in the topology optimisation problem. The resulted problem is known as a stress based topology optimisation problem. Moreover, lattice materials are often anisotropic therefore orientation (additional to the topology) can be considered as an additional variable in the optimisation problem. The study is divided into two main phases: (i) the establishment of a strength criterion, and (ii) its implementation in a topology optimisation problem.

Project MOMAP

The MOMAP project ("Modélisation et Optimisation des Milieux Architecturés Périodiques") is led by Marc François (professor at Nantes university) and funded by the ANR ("Agence Nationale de la Recherche"), bringing together several laboratories and organisms (see figure 8).

Figure 8: The laboratories and the organisms that are involved in project MOMAP.

The mechanical strength (tension/compression asymmetry) and the lack of control tools for lattice materials are obstacles to their development and more widespread industrial use. This project therefore aims to provide tools for developing the use of architectural materials in engineering to make them structural materials. As illustrated the project is focusing on 3 main following topic:

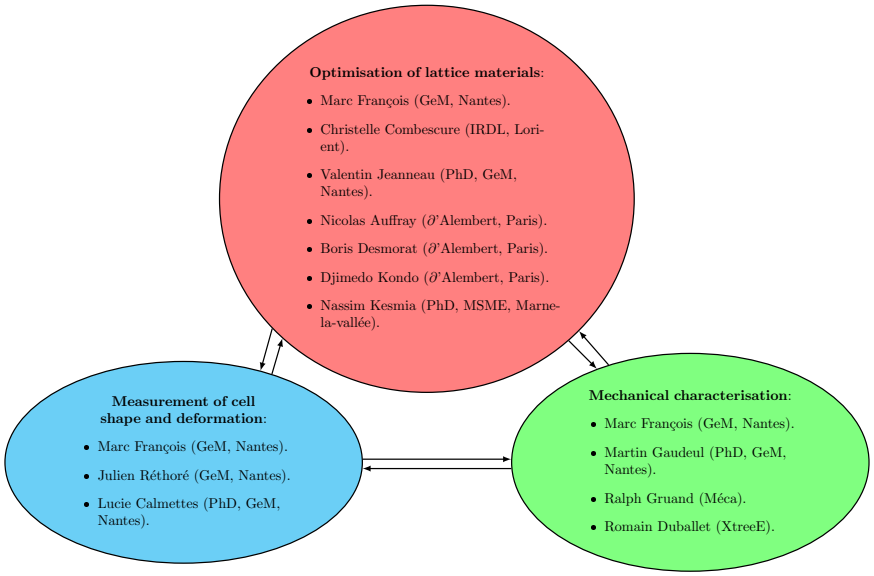

Figure 9: The three main topic of project MOMAP with the members involved.

1. *Optimisation of lattice materials:* The objective is to provide an optimisation algorithm for lattice structure taking into account the elasticity threshold. The study focus on studying the 2D triangular lattices. The aim is to provide optimal designs of lattice structures for experimental testing (for the two other axes). 2 thesis are present in this axis:

   (a) The first thesis has the objective to establish the relation between different geometric parameters of the unit cell and effective elasticity tensors [47]. Moreover, in the stress space, the discrete elasticity limit must established considering the plasticity and buckling instabilities. All this work (first step) is carried out by Jeanneau [102].

   (b) The second thesis aims to establish analytically a threshold criterion for the discrete elastic strength limit established by Jeanneau (for triangular lattices). This work is carried out in the first part of the document. Once done, the established threshold will implemented in a topology optimisation problem in the second part of the document.

2. *Mechanical characterisation:* The objective is to design and manufacture a specific mechanical test set-up for lattice materials that can be used to induce all possible deformation tensors while limiting edge effects and allowing the X-ray tomography this work was carried out by Gaudeul (in his internship).

3. *Measurement of cell shape and deformation:* The objective is to provide an algorithm based on virtual image correlation (VIC) to find the shape defects present in the architectural material after it has been manufactured and tested. The work is carried out by Calmettes in her thesis.

Part I

Towards a versatile threshold criterion

Chapter 1

Classical threshold criteria: a review

Contents

In solid mechanics, we define criterion as loading or a stress limit for which if it is reached, we will have a transition in the mechanical behaviour e.g. from elasticity to plasticity. It is important to have an idea of what the authors have done in order to theoretically establish a criterion that meets the requirements in terms of accuracy and fidelity with experimental tests. In this chapter, a review about some available criteria in the literature is presented. They are classified according to 2 main aspects: (i) The 1st one is material symmetry. A material can be isotropic, it means that their properties remain the same in all in direction with respect to a defined base reference. Meanwhile, an anisotropic material has properties that do not remain the same in all in directions[1]. (ii) The 2nd point is the loading symmetry. Some materials behave differently when they are subject to tension or to compression stresses. It is very common feature for architectured materials, we can give example of lattice structures where two modes of failure can be found, plasticity in traction and buckling in compression [79]. It is important to see how different authors managed to establish criteria for both isotropic and anisotropic materials with such a mechanical aspect. Mathematically, a criterion is usually represented by the following equation:

$$F(\underset{\sim}{\sigma}) = \sigma_{lim},$$

where the state variable $\underset{\sim}{\sigma}$ is the Cauchy stress tensor (in linear elasticity). $\sigma_{lim} \in \mathbb{R}_+^*$ is the threshold stress and F is called threshold function. We denote $\{\sigma_1, \sigma_2, \sigma_3\}$ as principal stresses of stress tensor (defined as its eigenvalues). The deviatoric part is denoted $\underset{\sim}{s}$ where $\{s_1, s_2, s_3\}$ are its principal stresses. This notation is adopted for this chapter.

The plan of this chapter is as follows: First section speaks about available isotropic criteria. The second section is for anisotropic criteria. In the third section, some established criteria for lattice materials will be discussed.

Remarks

1. Most of reviewed threshold criteria are coming from plasticity studies [19, 150, 126].
2. Some of threshold criteria here are introduced in 3D ($\mathbb{R}^3$). The proprieties of stress tensors are not the same as in 2D (as showed section 2.2). Nonetheless, all 3D threshold functions can be reduced to 2D (plane stress) with simple simplifications.

[1] In this case, we can particularly find subsets of anisotropic materials e.g. orthotropic materials.

1.1 Isotropic criteria

A criterion associated to an isotropic material is the one that is independent of its the orientation. Therefore, a criterion is said to be isotropic if and only if its threshold function F is completely invariant under any orthogonal transformation $\mathbf{g}$ of $\underset{\sim}{\sigma}$ (rotations, mirrors), we write:

$$F(\underset{\sim}{\mathbf{g}}^T \underset{\sim}{\sigma} \underset{\sim}{\mathbf{g}}) = F(\underset{\sim}{\sigma}) \qquad \forall \underset{\sim}{\mathbf{g}} \in \mathrm{O}(2), \tag{1.1}$$

where $\mathrm{O}(2)$ is the groups of orthogonal transformations and $(.^T)$ is the transpose. In this case F can be written as a function of the invariants of $\underset{\sim}{\sigma}$.

1.1.1 Symmetric criteria

A criterion is said to be symmetric only if [169]:

$$F(\underset{\sim}{\sigma}) = F(-\underset{\sim}{\sigma}),$$

geometrically, in the stress space $(\{\sigma_{11}, \sigma_{22}, \sigma_{12}\})$, it is interpreted as a surface having a central point symmetry with respect to the origin $\{0, 0, 0\}$.

Tresca 1864 (3D)

It is one of the oldest criterion [152]. It is based on the fact that the crystallographic max-dense planes gliding (i.e. plasticity) are caused by shear stress. So the yielding occurs when the maximum shear is reached. The criterion is written as follows:

$$\max\{|\sigma_1 - \sigma_2|, |\sigma_2 - \sigma_3|, |\sigma_3 - \sigma_1|\} = \sigma_{lim}, \tag{1.2}$$

where σ_1, σ_2 and σ_3 are principal stresses, σ_{lim} is the threshold stress (also called yield stress in plasticity).

This is a shear based criterion, it means that it is independent of the hydrostatic pressure. Hence, the red axis of the hexagonal prism (see figure 1.1) is the hydrostatic axis.

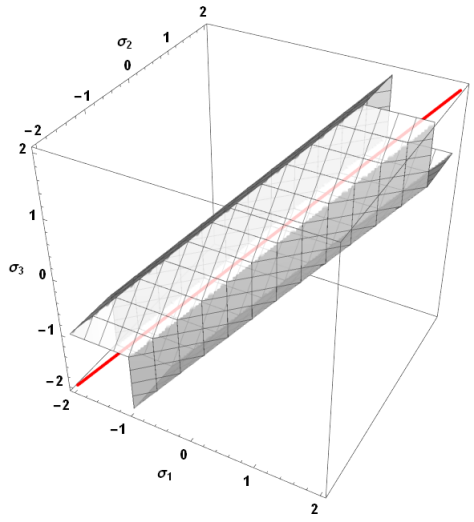

Figure 1.1: Threshold surface of Tresca criterion for $\sigma_{lim} = 1$.

Von-Mises 1913 (3D)

It is the most common criterion for isotropic pressure independent materials. It was introduced by Huber [98] and Von Mises [129]. The criterion is formulated based on the energy of distortion. When it reaches a threshold point, a transition from elasticity to plasticity occurs.

The energy of deformation W_f has two parts : volumetric energy W_s and the deviatoric (distortion) energy W_d meaning:

$$W_f = W_s + W_d, \tag{1.3}$$

and W_d is given by:

$$W_d = \frac{1+\nu}{6E}\left[(\sigma_1 - \sigma_2)^2 + (\sigma_2 - \sigma_3)^2 + (\sigma_3 - \sigma_1)^2\right], \tag{1.4}$$

where E is the Young's modulus and ν is the Poisson's coefficient. In an uniaxial loading ($\sigma_2 = 0$ and $\sigma_3 = 0$), The yielding (threshold stress is reached) occurs when $\sigma_1 = \sigma_{lim}$. In this case, the deviatoric energy is given by:

$$W_d = \frac{1+\nu}{6E} 2\sigma_{lim}^2. \tag{1.5}$$

Hence, the Von-Mises criterion is written as follows:

$$\frac{1+\nu}{6E} 2\sigma_{lim}^2 = \frac{1+\nu}{6E} \left[(\sigma_1 - \sigma_2)^2 + (\sigma_2 - \sigma_3)^2 + (\sigma_3 - \sigma_1)^2\right]. \tag{1.6}$$

At the end we have:

$$\frac{1}{2}\left[(\sigma_1 - \sigma_2)^2 + (\sigma_2 - \sigma_3)^2 + (\sigma_3 - \sigma_1)^2\right] = \frac{3}{2} \underset{\sim}{\mathrm{s}} : \underset{\sim}{\mathrm{s}} = \sigma_{lim}^2, \tag{1.7}$$

where,

$$\underset{\sim}{\mathrm{s}} = \underset{\sim}{\sigma} - \frac{1}{3}\mathrm{tr}(\underset{\sim}{\sigma})\underset{\sim}{\mathrm{I}}, \tag{1.8}$$

is the deviatoric part of the stress tensor $\underset{\sim}{\sigma}$. The obtained threshold function is a homogeneous polynomial of degree 2 in $\underset{\sim}{\mathrm{s}}$. It is independent of hydrostatic pressure (figure 1.2). It is important to notice in planar stress, (figure 1.3) the criterion is dependant on the 2D hydrostatic pressure.

Remark In 2D, the stress tensor is given by

$$[\underset{\sim}{\sigma}^{2D}] = \begin{bmatrix} \sigma_{11} & \sigma_{12} \\ \sigma_{12} & \sigma_{22} \end{bmatrix}. \tag{1.9}$$

In this case the deviatoric stress is given by:

$$\underset{\sim}{\mathrm{s}}^{2D} = \underset{\sim}{\sigma}^{2D} - \frac{1}{2}\mathrm{tr}(\underset{\sim}{\sigma}^{2D})\underset{\sim}{\mathrm{I}}^{2D}. \tag{1.10}$$

In this case W_d is given by:

$$W_d = \frac{1+\nu}{4E}(\sigma_1 - \sigma_2)^2, \tag{1.11}$$

which means that Von Mises criterion, is given by the following equation:

$$(\sigma_1 - \sigma_2)^2 = 2\underset{\sim}{\mathrm{s}}^{2D} : \underset{\sim}{\mathrm{s}}^{2D} = \sigma_{lim}^2. \tag{1.12}$$

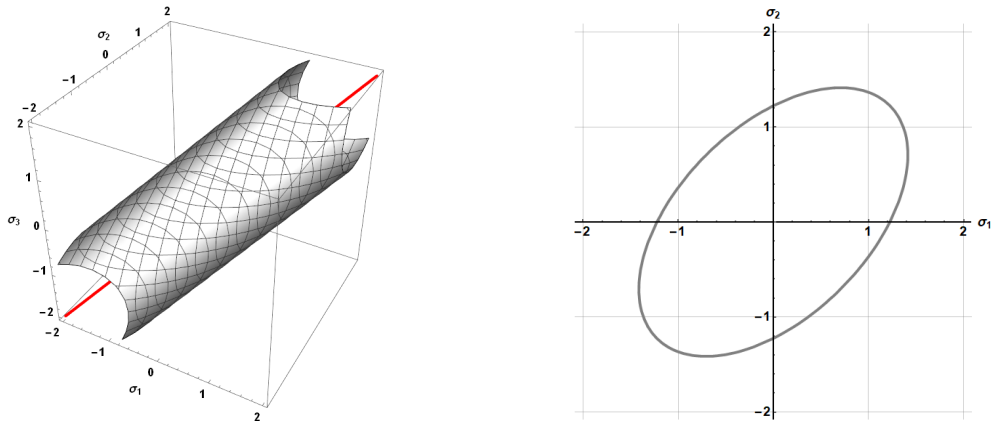

(a) 3d surface in the space $\{\sigma_1, \sigma_2, \sigma_3\}$ (b) Plane $\sigma_3 = 0$

Figure 1.2: Threshold surface of Von Mises criterion for $\sigma_{lim} = 1$ (principal stresses). The red line is hydrostatic axis.

The figure 1.2 represents the 3D Von Mises criterion surface in function of principal stresses ($\mathbb{R}^3$) and it has a cylinder shape. The red line is the axis of the cylinder and corresponds to the hydrostatic axis (of direction $\{1, 1, 1\}$). This form is due the fact that the criterion is independent from the hydrostatic pressure. The figures 1.3 and 1.4 represent the surface the Von Mises criterion in function of stress spatial components $\{\sigma_{11}, \sigma_{22}, \sqrt{2}\sigma_{12}\}$ hence, planar stress assumption is considered. The two represented surfaces are different, one is an ellipsoid and other is and cylinder of which the axis is 2D hydrostatic axis (red line). Mathematically, the difference between the two comes from the fact that the surface in figure 1.3 comes from 3D criterion by

simplifying $\sigma_3 = 0$ in equation (1.7). The other one, in figure 1.4, comes directly from equation (1.12). The difference is due to the deviatoric part of the stress tensor being defined from two different assumptions (look at equations (1.8) and (1.10)). The conclusion is that the 3D von Mises criterion is independent of 3D hydrostatic pressure but, it is dependant of 2D hydrostatic pressure. Meanwhile, the 2D Von Mises criterion is completely independent of 2D hydrostatic pressure which explains the cylindrical form in figures 1.4.

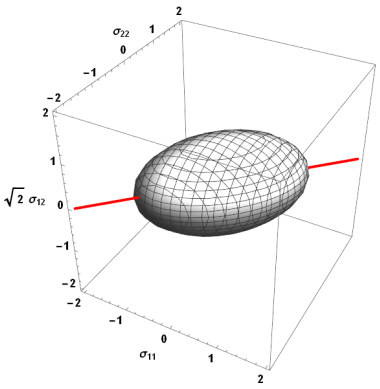

Figure 1.3: Tri-component representation of threshold surface of 3D Von Mises criterion under planar stress assumption for $\sigma_{lim} = 1$.

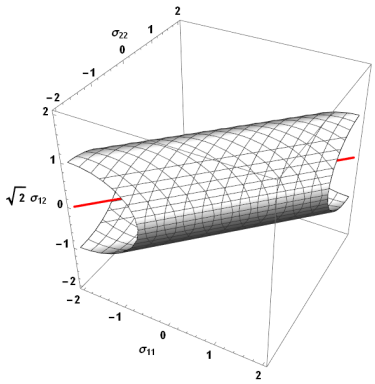

Figure 1.4: Tri-component representation of threshold surface of 2D Von Mises creterion for $\sigma_{lim} = 1$.

Hershey/Hosford 1972 (3D)

Hershey [87] and Hosford [94] proposed the following isotropic criterion for metallic materials:

$$(\sigma_1 - \sigma_2)^m + (\sigma_2 - \sigma_3)^m + (\sigma_3 - \sigma_1)^m = (2\sigma_{lim})^m, \tag{1.13}$$

in which m is a parameter that depends on the crystallographic structure of the metallic material. The criterion is a generalisation of Tresca and Von-Mises. While $m = 2$ the Von Mises criterion is retrieved, while $m = 1$ or $m = \infty$ Tresca criterion is obtained. It is mentioned in [20] that when $2 < m < 4$ the yield surface lies outside the Mises circular cylinder. When $1 < m < 2$ and $m > 4$ the yield surface lies between Tresca and Von-Mises. Hence, the criterion has a lower bound (which is Tresca criterion).

In order to obtain an upper bound, a more generalised version was introduced by Karafillis et al. [107]. The proposed criterion is given by:

$$\frac{1-c}{2}\Phi_1 - c\,\frac{3^{2k}}{2^{2k}+2}\Phi_2 = \sigma_{lim}^{2k}, \tag{1.14}$$

where,

$$\Phi_1 = |s_1 - s_2|^{2k} + |s_2 - s_3|^{2k} + |s_3 - s_1|^{2k} \quad \text{and} \quad \Phi_2 = |s_1|^{2k} + |s_2|^{2k} + |s_3|^{2k}. \tag{1.15}$$

s_1, s_2 and s_3 are the principal values of $\underset{\sim}{s}$, $(2k)$ have the same meaning as m and $c \in [0, 1]$ is a constant. The criterion is a combination of two threshold functions Φ_1 and Φ_2. Therefore, varying k and c gives more flexibility on the threshold surface and also adds an upper bound (comparing to Hershey/Hosford, see figure 1.5). The new upper bound is related to the Mohr-Coulomb maximum shear stress [94]. All this work comes following Mendelson [125] in which he demonstrated the existence of bounds in an isotropic yield (threshold) surface.

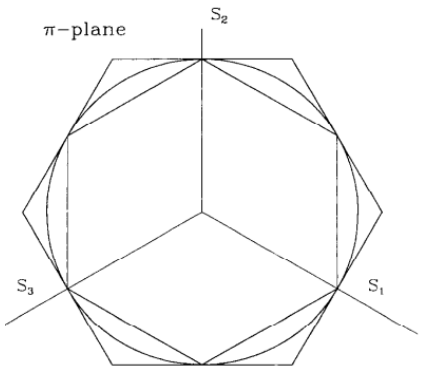

Figure 1.5: The upper bound, the lower bound (Tresca) and the von Mises yield surface in the deviatoric plane (π plane) [107]

Drucker 1949 (3D)

Drucker [62] proposed an isotropic criterion expressed in function of the two invariants J_2 and J_3 of $\underset{\sim}{s}$. In order to represent data located between [20] Tresca and Von Mises threshold surface he proposed the following criterion:

$$27\,(J_2^3 - cJ_3^2) = \sigma_{lim}^6, \tag{1.16}$$

where,

$$J_2 = \frac{1}{2} s_{ij} s_{ij} \quad ; \quad J_3 = (\frac{1}{3}) s_{ij} s_{jk} s_{ki}, \tag{1.17}$$

where c is a material parameter, its value is based on experimental data.

Bartlat and Richmond 1986 (2D)

Hosford attempted [28, 95] to express his criterion in function of the 3 components $\{\sigma_{11}, \sigma_{22}, \sigma_{12}\}$ of $\underset{\sim}{\sigma}$ (assuming planar stress). The intention is to make the criterion more suitable for sheet forming applications where plane stress is assumed. Hosford was unsuccessful because the new threshold function can not be expressed in function of the invariants of $\underset{\sim}{\sigma}$ (hence, it is not isotropic). Barlat et al. [26] managed to it do by assuming plane stress state $\sigma_3 = 0$, calculating the principle stresses σ_1 and σ_2 in function $\sigma_{11}, \sigma_{22}, \sigma_{12}$ and by replacing then in equation (1.13). The resulting criterion:

$$|J_1 - J_2|^m + |J_1 + J_2|^m + |2J_2|^m = 2\sigma_{lim}^m, \tag{1.18}$$

where

$$J_1 = \frac{\sigma_{11} + \sigma_{22}}{2} \quad ; \quad J_2 = \sqrt{\left(\frac{\sigma_{11} - \sigma_{22}}{2}\right)^2 + \sigma_{12}}. \tag{1.19}$$

is an isotropic criterion which is a generalisation of Hosford's one (2D). If the principal directions of the stress tensor coincide with material orthotropic directions ($\sigma_{12} = 0$) and Hosford's criterion is found. It is shown [20] that the criterion works well with isotropic FCC metals and they meet excellently data found numerical with Hill-Bishop model for polycrystal deformation.

Concluding remarks

Most of mentioned examples of isotropic criteria come from plasticity studies. The majority of these criterion are homogeneous polynomial of up to degree 6 of $\underset{\sim}{\sigma}$. It was proven that all isotropic threshold surfaces has an upper and lower bound defined by Tresca and Mohr maximum shear stress. Lot authors tried to take into account this aspect.

1.1.2 Dissymmetric criteria

Some materials (e.g. concrete) can exhibit different behaviour when the loading (or the stress) stat changes from tension/compression (σ) to compression/tension ($-\sigma$). A criterion is said disymmetric when its threshold function verify:

$$F(\underset{\sim}{\sigma}) \neq F(-\underset{\sim}{\sigma}). \tag{1.20}$$

Mathematically, it means that the expression of $F(\underset{\sim}{\sigma})$ includes elements that are sensitive to the change of sign.

Cazacu 2004 (3D)

Cazacu et al. [46] introduced an interesting isotropic threshold function for isotropic materials exhibiting tension/compression dissymmetry. The proposed threshold function is given by:

$$(J_2)^{3/2} - cJ_3 = \sigma_{lim}^3. \tag{1.21}$$

where c is material parameter which is linked to dissymmetry tension/compression. This particular aspect comes from the presence of odd powers of J_2 and J_3 (sensitive to the sign of $\underset{\sim}{\sigma}$). The criterion fits very well with the results of polycrystal simulations obtained by Horsford.

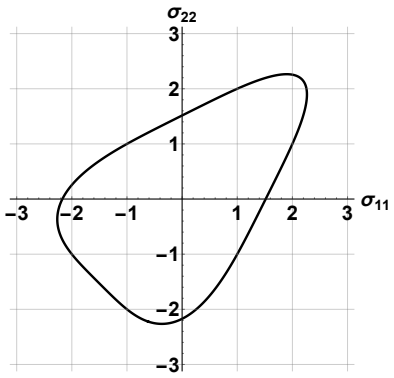

Figure 1.6: The contour of Cazacu's threshold surface in $(\sigma_{11}, \sigma_{22})$ plane [46].

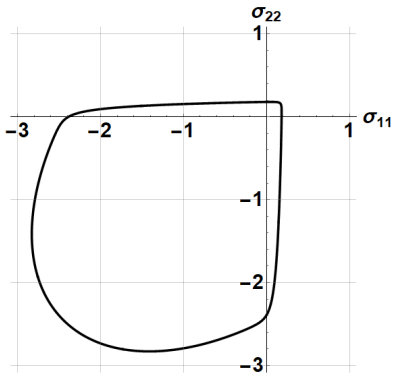

Figure 1.7: The contour of François's threshold surface in $(\sigma_{11}, \sigma_{22})$ plane [76].

François 2007 (3D)

Concrete is known to exhibit diffuse micro-cracking when exposed to high stress compressive stresses. It is also known to exhibit concentrated microcracking when subjected to low stress tension loading [76]. Francois et al. proposed the following criterion:

$$\begin{aligned}&\sqrt{\frac{(\sigma_2-\sigma_3)^2+(\sigma_3-\sigma_1)^2+(\sigma_1-\sigma_2)^2}{3}}\\&+\sigma_u\left(\sqrt{\exp\left(\frac{2\sigma_1}{\sigma_u}\right)+\exp\left(\frac{2\sigma_2}{\sigma_u}\right)+\exp\left(\frac{2\sigma_3}{\sigma_u}\right)-\sqrt{(3)}}\right)=\sigma_{lim},\end{aligned} \tag{1.22}$$

The constants σ_u and σ_{lim} are identified experimentally from uniaxial tension/compression tests. The proposed criterion is able to into account high tension/compression dissymmetry (see figure 1.7) it is driven by σ_0. It seems that the threshold is a sum of Von Mises function plus an exponential term that takes into account the loading dissymmetry.

1.2 Anisotropic criteria

Anisotropic material such as some metallic alloys and composites have a large variety of application. They posses privileged directions e.g. unidirectional carbon/epoxy has a very important difference in mechanical strength between rolling (longitudinal) and transversal direction. An associated criterion should take into account the anisotropic aspects of the material. A criterion is said to be anisotropic if:

$$F(\underset{\sim}{\mathbf{g}}^T\underset{\sim}{\sigma}\underset{\sim}{\mathbf{g}})=F(\underset{\sim}{\sigma}) \qquad \forall \underset{\sim}{\mathbf{g}}\in \mathrm{H}\subset \mathrm{O}(2), \tag{1.23}$$

H is a subgroup of O(2). The equation (1.23) means that the threshold function remains the same under a certain orthogonal transformations belonging to the group H. In this subsection, some examples of anisotropic criteria are given. Different approaches has been used to take into account the anisotropy of the material (mostly metal sheets forming applications).

1.2.1 Hill's Criteria

Hill 1948 (3D)

Hill [93] proposed the following criterion:

$$F\left(\sigma_{22}-\sigma_{33}\right)^2+G\left(\sigma_{33}-\sigma_{11}\right)^2+H\left(\sigma_{11}-\sigma_{22}\right)^2+2L\sigma_{23}^2+2M\sigma_{13}^2+2N\sigma_{12}^2=1, \tag{1.24}$$

where F, G, H, L, M and N are material parameters. If all the 6 are equal the Von Mises criterion is retrieved. Under plane stress assumption ($\sigma_{33}=\sigma_{13}=\sigma_{23}=0$), the criterion becomes:

$$(G+H)\sigma_{11}^2-2H\sigma_{11}\sigma_{22}+(H+F)\sigma_{22}^2+2N\sigma_{12}^2=1. \tag{1.25}$$

When the principal directions ($\sigma_{12}=0$) coincide with the orthotropy directions we have:

$$(G+H)\sigma_1^2-2H\sigma_1\sigma_2+(H+F)\sigma_2^2=1, \tag{1.26}$$

the criterion is widely used for orthotropic materials. It is also used for composite laminate [43]. The criterion is known to be user-friendly. It means that it meets the following requirements [92]:

- The derivative of threshold function is easy manipulate algebraically.
- It must contains a minimum number of parameters that are strictly necessary in technological applications.
- All parameters should be determinable by straightforward tests and without excessive computation.

All material parameters has proper physical meaning. However, it has limitation, it has poor prediction in case all the experimental data come from uniaxial tensile tests. It cannot also describe some materials presenting certain behaviours called *anomalous* and *second order anomalous*.

The *anomalous* behaviour was observed firstly in [193]. It consists of a noticeable disagreement between theoretical formulas (identification of the material parameters) and experimental observations in planar stress assumptions. The experimental data are:

1. r_θ the ratio of the transversal (width) strain and normal (thickness) one.
2. σ_θ is the threshold (tensile) stress.

Both quantities are measured for a cut specimen, which is inclined at an angle of θ from the rolling (longitudinal) direction. From the process of identification, it is found that:

$$\frac{\sigma_0}{\sigma_{90}} = \sqrt{\frac{r_0\,(1+r_{90})}{r_{90}\,(1+r_0)}}. \tag{1.27}$$

By replacing F, G, H, N with the experimental data in equation (1.26), it is found that:

$$\sigma_1^2 - \frac{2r_0}{1+r_0}\sigma_1\sigma_2 + \frac{r_0\,(1+r_{90})}{r_{90}\,(1+r_0)}\sigma_2^2 = \sigma_0^2. \tag{1.28}$$

In a particular case where $r_{90} = r_0 = r$ and $\sigma_{90} = \sigma_0$, the equation (1.28) becomes:

$$\sigma_1^2 - \frac{2r}{1+r}\sigma_1\sigma_2 + \sigma_2^2 = \sigma_u^2, \tag{1.29}$$

where σ_u is the uniaxial tensile stress. It is observed that when $r < 1$ the threshold surface stays inside the Von Mises one (or the reverse). Woodthrope et al. [193] observed (by doing biaxial tests) the opposite in some cases (in particular Aluminium alloys) hence this behaviour cannot be properly described by Hill 1948 criterion, therefore it is called *anomalous*.

The *second order anomalous* behaviour is found following the equation (1.27). It is noticed that when $\frac{r_0}{r_{90}} > 1$, $\frac{\sigma_0}{\sigma_{90}} > 1$. Experimentally, some opposite cases were found [90].

Hill 1979 (3D)

Researchers [20] agreed that higher degree polynomial functions are best candidates to address the problem (anomalous behaviour). Therefore, since 1970 several higher degree polynomial criteria were proposed. Since Hill 1948 cannot describe the anomalous behaviour, Hill et al. [90] introduced the following criterion:

$$\begin{aligned} &f\,|\sigma_2-\sigma_3|^m + g\,|\sigma_3-\sigma_1|^m + h\,|\sigma_1-\sigma_2|^m + a\,|2\sigma_1-\sigma_2-\sigma_3|^m + \\ &+ b\,|2\sigma_2-\sigma_1-\sigma_3|^m + c\,|\sigma_3-\sigma_1-\sigma_2|^m = \sigma_{lim}^m, \end{aligned} \tag{1.30}$$

where we have f, g, h, a, b and d are material parameters obtained from experimental data (r_θ and σ_θ), m is an non integer coefficient and it is numerically obtainable from a non-linear relationship (experimental data), m is not an integer thus, the threshold function in equation (1.30) is not polynomial.

In plane stress and under assumption of plane isotropy, the equation (1.30) can have 4 possible forms. The most widely used is called "case 4" and it's given by:

$$c\,|\sigma_1+\sigma_2|^m + h\,|\sigma_1-\sigma_2|^m = \sigma_{lim}^m. \tag{1.31}$$

This case corresponds to $a = b = f = g = 0$. It is shown by Banabic [20] that the criterion in equation (1.31) is similar to Bassani's one [29] given by:

$$\left|\frac{\sigma_1+\sigma_2}{2\sigma_b}\right|^n + \left|\frac{\sigma_1-\sigma_2}{2\tau}\right|^m - 1 = 0, \tag{1.32}$$

where σ_b is the biaxial tensile yield stress, τ is shear yield stress. The equation has a form similar to the equation (1.31) when $m = n$. The difference is in the way the material parameters are defined.

The advantages Hill 1979 is that it can describe anomalous behavior of some materials. The formulas are quiet simple in the identification process (except the part where it is needed to solve a non-linear equation to define m). One of the disadvantages is that the threshold function is expressed in function of the 3 principal stresses instead of the 6 components of $\underset{\sim}{\sigma}$ ($\{\sigma_{11}, \sigma_{22}, \sigma_{33}, \sigma_{23}, \sigma_{13}, \sigma_{12}\}$).

Hill 1990 (2D)

In order to include to the 3 components of $\underset{\sim}{\sigma}$ (assuming planar stress) when principal stress direction does not coincide with the orthotropy direction, Hill [91] introduced the following criterion:

$$\begin{aligned} &|\sigma_{11}+\sigma_{22}|^m + \left(\frac{\sigma_b}{\tau}\right)^m \left|(\sigma_{11}-\sigma_{22})^2 + 4\sigma_{12}^2\right|^{m/2} \\ &\quad + |\sigma_{11}^2+\sigma_{22}^2+2\sigma_{12}^2|^{(m/2)-1}\left(-2a\left(\sigma_{11}^2-\sigma_{22}^2\right)+b\left(\sigma_{11}-\sigma_{22}\right)^2\right) = (2\sigma_b)^m, \end{aligned} \tag{1.33}$$

where a, b, m are materials parameters, σ_b, τ are respectively biaxial tensile and pure shear yield stress. In principal stresses, the criterion is given by:

$$\begin{aligned} &|\sigma_1+\sigma_2|^m + \left(\frac{\sigma_b}{\tau}\right)^m |\sigma_1-\sigma_2|^m \\ &\quad + |\sigma_1^2+\sigma_2^2|^{m-\frac{1}{2}}\left[-2a\left(\sigma_1^2-\sigma_2^2\right)+b\left(\sigma_1-\sigma_2\right)^2\cos 2\theta\right]\cos 2\theta = (2\sigma_b)^m, \end{aligned} \tag{1.34}$$

where θ is the angle between the first principal direction and the rolling (longitudinal) direction. If $a = b = 0$ or $\theta = \frac{\pi}{4}$ we retrieve the "case 4" of Hill 1979. Hill 1990 conserve all advantages of Hill 1979. It is usable considering any physical basis in planar anisotropy. Liu et al. (2D) [120] proposed a more generalised form as follows:

$$\begin{aligned} &|\sigma_1+\sigma_2|^m + (1+2R)|\sigma_1-\sigma_2|^m \\ &\quad + |\sigma_1^2+\sigma_2^2|^{m-\frac{1}{2}}\cdot\left(-2a\left(|\sigma_1|^s-|\sigma_2|^s\right)+b|\sigma_1-\sigma_2|^s\cos 2\theta\right)\cos 2\theta = (2\sigma_b)^m, \end{aligned} \tag{1.35}$$

where s and R are material parameters. The "case 4" for Hill 1979 is found when $s = 2$ and $\theta = \frac{\pi}{4}$. We notice in equation (1.35) that the term in second line is not quadratic which can give more improvement comparing to Hill 1990 model.

Leacock (2D) [116] gave a more general version of Hill 1990. He proposed the following criterion:

$$\begin{aligned} &|\sigma_1+\sigma_2|^m + A^m|\sigma_1-\sigma_2|^m + |\sigma_1^2+\sigma_2^2|^{(m/2)-2}\left[\left(\sigma_1^2-\sigma_2^2\right)\right. \\ &\left(H\left(\sigma_1^2+\sigma_2^2\right)+I\left(\sigma_1^2-\sigma_2^2\right)\cos 2\theta\right)+\left(\sigma_1-\sigma_2\right)^2 \\ &\left.\left(J\left(\sigma_1^2+\sigma_2^2\right)+K\left(\sigma_1^2-\sigma_2^2\right)\cos 2\theta\right)\cos 2\theta\right] = (2\sigma_b)^m. \end{aligned} \tag{1.36}$$

where A, H, I, J, K and m are material parameters. The criterion is able describe the anomalous and second order anomalous behaviour. All the mentioned criteria are not user-friendly and require a lot of experimental data in the identification process.

1.2.2 Criteria based on linear transformation

The convexity remains one the main requirement for a criterion in order to be in plasticity studies. Establishing the convexity conditions could be difficult for certain threshold functions especially for anisotropic cases. One of the approaches to tackle this problem is using the *linear transformation*. It was introduced by Barlat [24] and Kraffilis [107]. In a brief manner, the concept of the approach is to consider an isotropic threshold function $F(\underset{\sim}{\sigma})$ and to create an anisotropic one by simply replacing the tensor $\underset{\sim}{\sigma}$ with a transformed one $\underset{\sim}{\Sigma}$ defined by:

$$\underset{\sim}{\Sigma} = \underset{\approx}{\mathrm{M}} : \underset{\sim}{\sigma}. \tag{1.37}$$

$\underset{\sim}{\Sigma}$ is the transformed stress tensor. $\underset{\approx}{\mathrm{M}}$ is a second order tensor which includes all material parameters. In this subsection we denote:

$$[\underset{\sim}{\mathrm{S}}] = \begin{bmatrix} S_{11} & S_{12} & S_{13} \\ S_{12} & S_{22} & S_{23} \\ S_{13} & S_{23} & S_{33} \end{bmatrix},$$

the deviatoric part of $\underset{\sim}{\Sigma}$ and $\{S_1, S_2, S_3\}$ its principal values (stresses). This approaches may not be user-friendly. The material parameters in $\underset{\approx}{\mathrm{M}}$ might not have an intuitive physical meanings. The main advantage is the guarantee of the convexity (required for plasticity). Lot of criteria that are based on linear transformation were proposed by Barlat. We briefly introduce the principal ones.

Yld91 (3D)

Barlat [24] proposed Yld91 which is a generalisation of his previous one [28]. The criterion is based on linear transformation where he picked the Hershy/Hosford isotropic criterion and applied the linear transformation on $\underset{\sim}{\sigma}$. The Yld91 [150] is given by:

$$|S_1 - S_2|^m + |S_3 - S_1|^m + |S_2 - S_3|^m = 2Y^m. \tag{1.38}$$

where

$$\begin{bmatrix} S_{11} \\ S_{22} \\ S_{33} \\ \sqrt{2}S_{23} \\ \sqrt{2}S_{13} \\ \sqrt{2}S_{12} \end{bmatrix} = \underbrace{\begin{bmatrix} \frac{c+b}{3} & \frac{-c}{3} & \frac{-b}{3} & 0 & 0 & 0 \\ \frac{-c}{3} & \frac{a+c}{3} & \frac{-a}{3} & 0 & 0 & 0 \\ \frac{-b}{3} & \frac{-a}{3} & \frac{a+b}{3} & 0 & 0 & 0 \\ 0 & 0 & 0 & \frac{f}{2} & 0 & 0 \\ 0 & 0 & 0 & 0 & \frac{g}{2} & 0 \\ 0 & 0 & 0 & 0 & 0 & \frac{h}{2} \end{bmatrix}}_{[\underset{\approx}{\mathrm{M}}]} \begin{bmatrix} \sigma_{11} \\ \sigma_{22} \\ \sigma_{33} \\ \sqrt{2}\sigma_{23} \\ \sqrt{2}\sigma_{13} \\ \sqrt{2}\sigma_{12} \end{bmatrix}, \tag{1.39}$$

where a, b, c, f, h and g are material parameters. The described material is orthotropic due to index symmetry and the form of $[\underset{\approx}{\mathrm{M}}]$. When $a = b = c = f = h = g = 1$, Hershy/Hosford isotropic criterion is obtained. Yld91 [20] has a good agreement with Taylor and Bishop and Hill polycrystal model and experimental data [96].

Karaffilis and Beyoce (3D)

Karaffilis et al. in their work [107] generalised framework of linear transformations. In their studies, they introduced the isotropic criterion showed in section 1.1.1. In order to generalise it to an anisotropic criterion, they replaced the stress tensor with a transformed one in the isotropic criterion. Karafillis et al. were the first to introduce linear transformation using a 4th order tensor as follows:

$$\underset{\sim}{\Sigma} = \underset{\approx}{\mathrm{M}} : \underset{\sim}{\sigma}. \tag{1.40}$$

where $\underset{\sim}{\Sigma}$ is the transformed stress tensor, $\underset{\approx}{\mathrm{M}}$ is an 4th order tensor which the same index symmetry as the elasticity tensor. Karafillis et al. in their paper spoke about the irreducible decomposition, a topic which we will extensively dwell on in chapter 3 and it is known as *harmonic decomposition*. They also established conditions for each the material symmetry (anisotropy) that can be described with tensor $\underset{\approx}{\mathrm{M}}$. The criterion has a lot advantages such as good agreement with Bishop and Hill Model [96] and experimental data. It has a simple numerical implementation. Though the only disadvantage is that the elements of $\underset{\approx}{\mathrm{M}}$ are obtainable via numerical process (not user-friendly).

Yld94 and Yld96 (3D)

It is shown in [25] that the Yld 91 has a poor prediction for on some samples of Aluminum-Magnesium alloys (fabricated differently). Barlat et al. proposed Yld94 as a generalisation of Yld91. The criterion is given by:

$$\alpha_3 |S_1 - S_2|^m + \alpha_2 |S_3 - S_1|^m + \alpha_1 |S_2 - S_3|^m = 2\sigma_{lim}^m \tag{1.41}$$

It is same one as Yld91 except that α_k are added as material parameters. If $\alpha_1 = \alpha_2 = \alpha_3 = 1$ the Yld91 is retrieved therefore, Yld94 is a more general criterion.

Yld94 is able to give an accurate prediction of Bishop and Hill model and has a good agreements with experimental data. Though, finite element simulations revealed some inaccuracies [20]. Barlat et al. improved the criterion and proposed Yld96 [25] by adding changes in the way α_k are defined. Yld96's has no proof of convexity hence its numerical implementation is complicated (plasticity).

Yld2000-2d (2D)

To overcome the convexity problem with Yld96, Barlat et al. proposed another criterion. It is mainly based on linear transformations from isotropic function (unlike Yld96). The reason is that linear transformation does not affect the convexity conditions. Barlat et al. had the idea to use two different linear transformations in order to add more material parameters [23]. The criterion is only available for planar stress, it's called Yld2000-2d and it's given by:

$$\phi'(\underset{\sim}{\mathrm{X}}') + \phi''(\underset{\sim}{\mathrm{X}}'') = 2\sigma_{lim}^a, \tag{1.42}$$

where a is material parameter, ϕ' and ϕ'' are isotropic functions:

$$\phi'(\underset{\sim}{X'}) = |X_1 - X_2|^a \quad \phi''(\underset{\sim}{X''}) = |2X_2'' + X_1''|^a + |2X_1'' + X_2''|^a\,, \tag{1.43}$$

X' and X'' are the linear transformed stress tensor. All material parameters are included as follows:

$$\begin{bmatrix} X'_{11} \\ X'_{22} \\ X'_{12} \end{bmatrix} = \begin{bmatrix} C'_{11} & C'_{12} & 0 \\ C'_{21} & C'_{22} & 0 \\ 0 & 0 & C'_{66} \end{bmatrix} \begin{bmatrix} s_{11} \\ s_{22} \\ s_{12} \end{bmatrix}, \quad ; \quad \begin{bmatrix} X''_{11} \\ X''_{22} \\ X''_{12} \end{bmatrix} = \begin{bmatrix} C''_{11} & C''_{12} & 0 \\ C''_{21} & C''_{22} & 0 \\ 0 & 0 & C''_{66} \end{bmatrix} \begin{bmatrix} s_{11} \\ s_{22} \\ s_{12} \end{bmatrix}, \tag{1.44}$$

where $\{s_{11}, s_{22}, s_{12}\}$ are elements of $\underset{\sim}{s}$ (not to be confused with $\underset{\sim}{S}$). Yld2000-2d appears to have a good agreement on both experimental data and polycrystal model. However, it is not easy to use because of the complexity of the process of identifying the material parameters.

Barlat et al. [21] extended Yld2000-2d to 3D. The criterion is called Yld2004-18p and it remains mainly based on linear transformation. This criterion has a great agreement with different experimental data [21] and it is recommended for highly anisotropic metals [150]. Barlat et al. also proposed Yld2004-13p [22]. It is simplified version of Yld2004-18p where 13 material parameters are considered (hence less amount of experimental data).

Cazacu 2004 (3D, anisotropic)

Cazacu et al. continued their work after proposing the dissymmetric isotropic criterion mentioned in subsection 1.1.2. She established an extension to orthotropic criterion (with dissymmetry) by the mean of *theory of representation*. She replaced the second and third invariant (J_2, J_3) by (J_2^0, J_3^0) where:

$$\begin{aligned}
J_2^0 &= \frac{a_1}{6}\left(\sigma_{11}-\sigma_{22}\right)^2 + \frac{a_2}{6}\left(\sigma_{11}-\sigma_{22}\right)^2 + \frac{a_3}{6}\left(\sigma_{11}-\sigma_{22}\right)^2 + a_4\sigma_{12}^2 + a_5\sigma_{13}^2 + a_6\sigma_{23}^2, \\
J_3^0 &= \frac{1}{27}\left(b_1+b_2\right)\sigma_{11}^3 + \frac{1}{27}\left(b_3+b_4\right)\sigma_{22}^3 + \frac{1}{27}\left[2\left(b_1+b_4\right)-b_2-b_3\right]\sigma_{33}^3 \\
&\quad + 2b_{11}\sigma_{12}\sigma_{13}\sigma_{23} + \frac{2}{9}\left(b_1+b_2\right)\sigma_{11}\sigma_{33}\sigma_{22} - \frac{1}{9}\left(b_1\sigma_{22}+b_2\sigma_{33}\right)\sigma_{11}^2 \\
&\quad - \frac{1}{9}\left(b_3\sigma_{33}+b_2\sigma_{11}\right)\sigma_{22}^2 - \frac{1}{9}\left[\left(b_1-b_2+b_4\right)\sigma_{11} + \left(b_1+b_3+b_4\right)\sigma_{22}\right]\sigma_{33}^2 \\
&\quad - \frac{\sigma_{23}^2}{3}\left[\left(b_6+b_7\right)\sigma_{11} - b_6\sigma_{22} - b_7\sigma_{33}\right] \\
&\quad - \frac{\sigma_{13}^2}{3}\left[2b_9\sigma_{22} - b_8\sigma_{33} - \left(2b_9-b_8\right)\sigma_{11}\right] - \frac{\sigma_{12}^2}{3}\left[2b_{10}\sigma_{33} - b_5\sigma_{22} - \left(2b_{10}-b_5\right)\sigma_{11}\right],
\end{aligned} \tag{1.45}$$

where all $a_i (i = 1, ..., 6)$ and $b_i (i = 1, ..., 11)$ are materials parameters. J_2^0, J_3^0 come from a generalisation of Drucker's criterion to orthotropy [44, 45] using *the theory of representation* (more details in section 2.4.3). The criterion show a very good agreements between theoretical and experimental data for different materials.

Polynomials criterion

Some authors introduced directly their criterion as polynomials of degree n. When the degree greater, the more important the number of material parameters therefore, taking into account the material anisotropy is more convenient and precise. In planar, a criterion is said to be orthotropic means that [166]:

$$F(\sigma_{11}, \sigma_{22}, -\sigma_{12}) = F(\sigma_{11}, \sigma_{22}, \sigma_{12}). \tag{1.46}$$

This condition is only valid when the orthotropy axes coincide with the axes of the chosen base reference. The main disadvantages is that convexity conditions (required for plasticity) must be established and considered in the identification process.

Hill 1950 (2D)

Hill in 1950 proposed an homogeneous polynomial criterion [89] in an attempt to improve the quadratic one (cf. section 1.2.1). The criterion function is defined as follows:

$$\sum_{i+j+2k=n} a_{ijk}\sigma_{11}^i\sigma_{22}^j\sigma_{12}^{2k} = \sigma_{lim}^n, \tag{1.47}$$

where a_{ijk} are material parameter. i, j and k are non-negative integers. The threshold function is independent of the sign of σ_{12} hence, the criterion is orthotropic.

Gotoh 1977 (2D)

Gotoh [84] proposed a 4th degree polynomial criterion as follows:

$$\begin{aligned} &A_0\left(\sigma_{11}+\sigma_{22}\right)^2+[A_1\sigma_{11}^4+A_2\sigma_{11}^3\sigma_{22}+A_3\sigma_{11}^2\sigma_{22}^2+A_4\sigma_{11}\sigma_{22}^3+A_5\sigma_{22}^4+\\ &\left(A_6\sigma_{11}^2+A_7\sigma_{11}\sigma_{22}+A_8\sigma_{22}^2\right)\sigma_{12}^2+A_9\sigma_{12}^4]=Y^4 \end{aligned} \tag{1.48}$$

Where all $A_i, i=0,...,9$ are material parameters. The first term is meant to add dependency on the hydrostatic pressure to the criterion. Gotoh in his paper established conditions (for A_i) for which the criterion describes planar isotropy (2D) and isotropy (3D). The criterion is capable of modelling the anomalous behaviour however, it has problems with predicting directional yield stress and with the convexity [167].

Soare's criteria

Soare et al. [167] [171] proposed three criteria "Poly4", "Poly6" and "Poly8". They are all homogeneous polynomials of degree $4, 6$ and 8 respectively and they are given by:

$$\begin{aligned} &a_1\sigma_{11}^4+a_2\sigma_{11}^3\sigma_{22}+a_3\sigma_{11}^2\sigma_{22}^2+a_4\sigma_{11}\sigma_{22}^3+a_5\sigma_{22}^4+\\ &\quad\left(a_6\sigma_{11}^2+a_7\sigma_{11}\sigma_{22}+a_8\sigma_{22}^2\right)\sigma_{12}^2+a_9\sigma_{12}^4\ =1,\\ &a_1\sigma_{11}^6+a_2\sigma_{11}^5\sigma_{22}+a_3\sigma_{11}^4\sigma_{22}^2+a_4\sigma_{11}^3\sigma_{22}^3+a_5\sigma_{11}^2\sigma_{22}^4+a_6\sigma_{11}\sigma_{22}^5+a_7\sigma_{22}^6+\\ &\quad\left(a_8\sigma_{11}^4+a_9\sigma_{11}^3\sigma_{22}+a_{10}\sigma_{11}^2\sigma_{22}^2+a_{11}\sigma_{11}\sigma_{22}^3+a_{12}\sigma_{22}^4\right)\sigma_{12}^2+\\ &\quad\left(a_{13}\sigma_{11}^2+a_{14}\sigma_{11}\sigma_{22}+a_{15}\sigma_{22}^2\right)\sigma_{12}^4+a_{16}\sigma_{12}^2=1,\\ &a_1\sigma_{11}^8+a_2\sigma_{11}^7\sigma_{22}+a_3\sigma_{11}^6\sigma_{22}^2+a_4\sigma_{11}^5\sigma_{22}^3+a_5\sigma_{11}^4\sigma_{22}^4+a_6\sigma_{11}^3\sigma_{22}^5+a_7\sigma_{11}^2\sigma_{22}^6+a_8\sigma_{11}\sigma_{22}^7+a_9\sigma_{22}^8+\\ &\quad\left(a_{10}\sigma_{11}^6+a_{11}\sigma_{11}^5\sigma_{22}+a_{12}\sigma_{11}^4\sigma_{22}^2+a_{13}\sigma_{11}^3\sigma_{22}^3+a_{14}\sigma_{11}^2\sigma_{22}^4+a_{15}\sigma_{11}\sigma_{22}^5+a_{16}\sigma_{22}^6\right)\sigma_{12}^2+\\ &\quad\left(a_{17}\sigma_{11}^4+a_{18}\sigma_{11}^3\sigma_{22}+a_{19}\sigma_{11}^2\sigma_{22}^2+a_{20}\sigma_{11}\sigma_{22}^3+a_{21}\sigma_{22}^4\right)\sigma_{12}^4+\\ &\quad\left(a_{22}\sigma_{11}^2+a_{23}\sigma_{11}\sigma_{22}+a_{24}\sigma_{22}^2\right)\sigma_{12}^6+a_{25}\sigma_{12}^2=1, \end{aligned} \tag{1.49}$$

where a_i are material parameters and they are in total $8, 16, 25$ for Poly4, Poly6, Poly8 respectively. The Poly4 is an improvement of Gotoh's criterion where Soare added changes to the identification process in order to solve the convexity issue and to have a good agreement with experimental results. For Poly6 and Poly8 the convexity conditions are also taken into account in the identification process. In his applications for sheet metal forming, he observed that the higher the degree of the polynomial, the greater the accuracy of the material model (when compared to experimental data).

1.3 Threshold criteria for Lattice

When it comes to lattice (or architectured) materials, defining a threshold functions is not that easy. Having a discontinuous unit cell with different geometries (like a truss system) leads to additional non linear phenomenons. For example when lattice is exposed to stresses, two phenomenons are observed [79] buckling and plasticity. Lot of authors managed [127, 68, 202, 201, 103, 188] to give a threshold surface for some lattice materials with numerically validation. Most of them reduce the study to one unit cell (different geometries) assuming the periodicity of the material. Most of them also used beam theory to establish an analytical criterion considering plasticity and buckling. It is important to point out that all these studies classified lattice materials into two main categories [58] *stretching dominated* and *bending dominated*. Under different loading conditions and for stretching dominated lattices, the unit cell tends to behave a rigid truss structure. This means that the structural elements (of the unit cell) are subjected to axial stresses in a dominant manner (no bending nor shearing). For bending dominated lattices, the unit cell tends to behave like a mechanisms [188] under plane loading. This means that structural elements are subjected mainly to bending or shearing (near joints) [172]. From experimental point of view, things are complicated specially with manufacturing defects [66]. We give example of the of work of Köhnen et al. [114], they did an experimental comparison between stretching and bending dominated lattices by doing tensile/compression and fatigue tests. Deshpande et al. [59] conducted an analytical and a numerical study of the octet-truss lattice. In their model they considered certain imperfections. A comparison between experimental, theoretical and numerical results has been done.

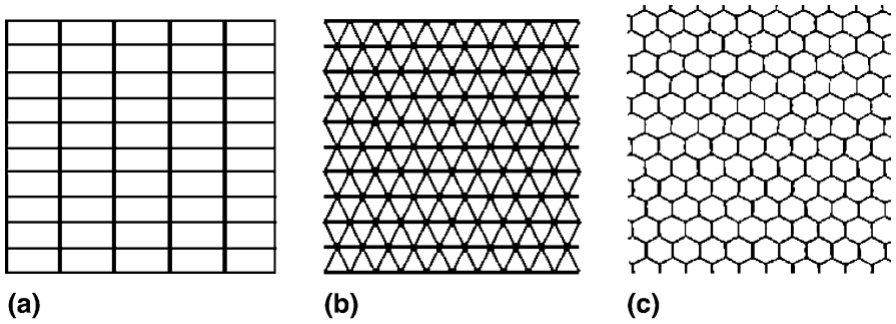

Figure 1.8: Different 2D periodic lattice materials showing their unit-cells : (a) rectangular,(b) triangular and (c) hexagonal [188]

In this section we give examples of some established threshold functions for 2D lattice materials. The first example is the work of Wang et al. [188]. Using simple beam theory, they managed to establish a threshold function for different lattice in planar stress considering only plasticity (no buckling). Different geometries are studied such as triangular, rectangular and hexagonal. We also give the example of Jeanneau et al. [103]. They established threshold surface numerically for equilateral triangular 2D lattice considering the plasticity and buckling instabilities.

For a lattice materials the relative density ρ is defined [79] as the ratio of the density of the lattice ρ^* divided that of the solid ρ_s:

$$\rho = \frac{\rho^*}{\rho^s}. \tag{1.50}$$

An example is given with equilateral triangular 2D lattice where the beam length is l and the wall thickness is t. ρ^* is evaluated as the surface occupied, divided by the surface of the triangle, multiplied by ρ_s.

$$\rho^* = \frac{3tl}{\frac{\sqrt{3}}{2}l^2}\rho_s = 2\sqrt{3}\frac{t}{l}\rho_s,$$

hence, the relative density if equilateral triangular lattice is:

$$\rho = \frac{2\sqrt{3}\frac{t}{l}\rho_s}{\rho_s} = 2\sqrt{3}\frac{t}{l}.$$

1.3.1 Rectangular lattice

A 2D lattice with a rectangular unit cell is exposed to axial stresses σ_{11} and σ_{22} and to a shear stress σ_{12} as illustrated in figure 1.9 ($\sigma_{11} = \sigma_1$, $\sigma_{22} = \sigma_2$, $\sigma_{12} = \tau$). Due to periodicity, the study is reduced to the unit cell. The lattice here is considered to be bending dominated [188]. It means that plasticity occurs when the maximum bending moment, calculated in each beam, is reached. The criterion is given by:

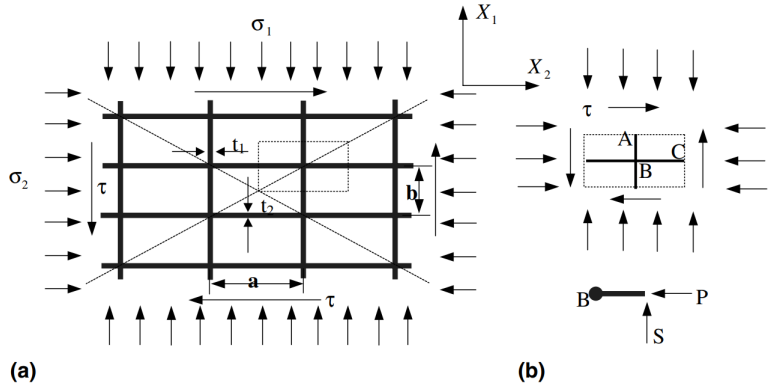

Figure 1.9: 2D lattice with rectangular unit cell under plane stresses : (a) periodic material, (b) the studied unit cell [188]

$$\max\left\{\left[\frac{b}{a}\left(\frac{\sigma_2}{\sigma_{lim}}\right)^2+2\frac{|\sigma_{12}|}{\sigma_{lim}}-\frac{(t_2)^2}{ab}\right],\left[\frac{a}{b}\left(\frac{\sigma_1}{\sigma_{lim}}\right)^2+2\frac{|\sigma_{12}|}{\sigma_{lim}}-\frac{(t_1)^2}{ab}\right]\right\}=0, \tag{1.51}$$

where σ_{lim} is the tensile stress of constituent solid, ρ relative density defined by:

$$\rho=\frac{at_2+bt_1}{ab}, \tag{1.52}$$

where (a,b) and (t_1,t_2) are lengths and thicknesses of the walls of the unit cell. The figure 1.10 shows the threshold surface defined by criterion (1.51).

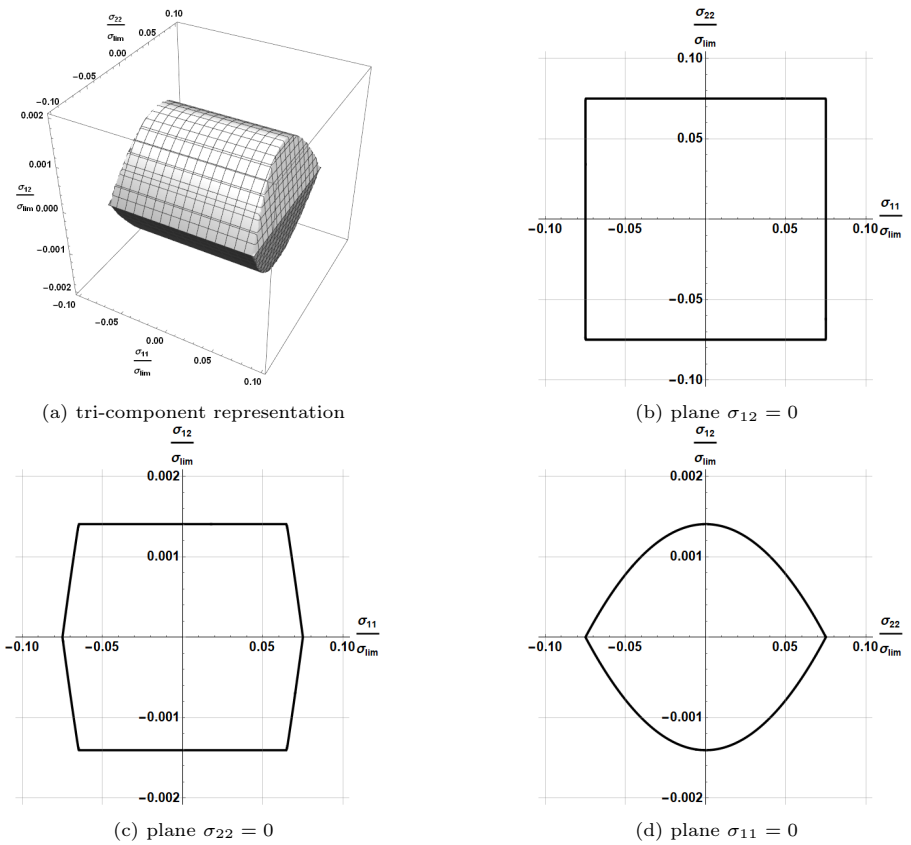

(a) tri-component representation

(b) plane $\sigma_{12}=0$

(c) plane $\sigma_{22}=0$

(d) plane $\sigma_{11}=0$

Figure 1.10: The plasticity threshold surface in the stress space for rectangular lattice [188].

1.3.2 Equilateral triangular lattice

A 2D lattice with a equilateral triangular unit cell is considered. As in previous case, the material is exposed to axial stresses σ_{11} and σ_{22} and to a shear stress σ_{12} depicted in figure 1.11. The lattice is considered to be stretching dominated [188] this means that we look for maximum axial stress in each beam. The criterion is given by:

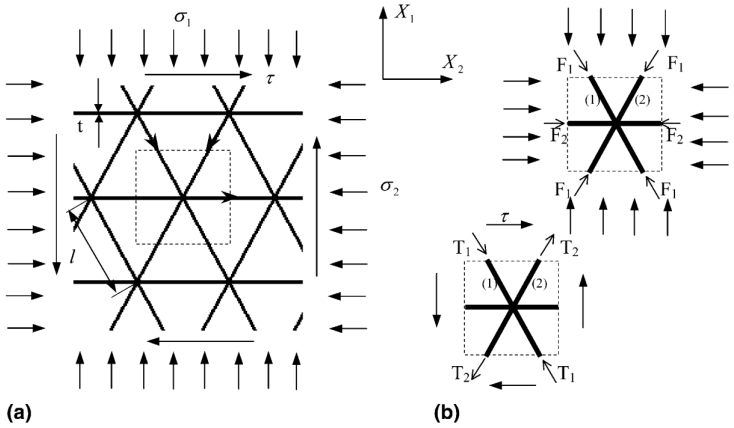

Figure 1.11: 2D lattice with triangular unit cell under plane stresses : (a) periodic material, (b) the studied unit cell [188].

$$\max\left\{\left|\frac{\sigma_{11}}{\sigma_{lim}}-\frac{\sqrt{3}\sigma_{12}}{\sigma_{lim}}\right|,\left|\frac{\sigma_{11}}{\sigma_{lim}}+\frac{\sqrt{3}_{12}}{\sigma_{lim}}\right|,\left|\frac{3}{2}\frac{\sigma_{22}}{\sigma_{lim}}-\frac{\sigma_{11}}{2\sigma_{lim}}\right|\right\}=\frac{1}{2}\rho, \tag{1.53}$$

where ρ, in this case, is given by:

$$\rho=2\sqrt{3}\,\frac{t}{l}, \tag{1.54}$$

where l and t are length and thickness of walls of the unit cell. The figure 1.12 shows the corresponding threshold surface.

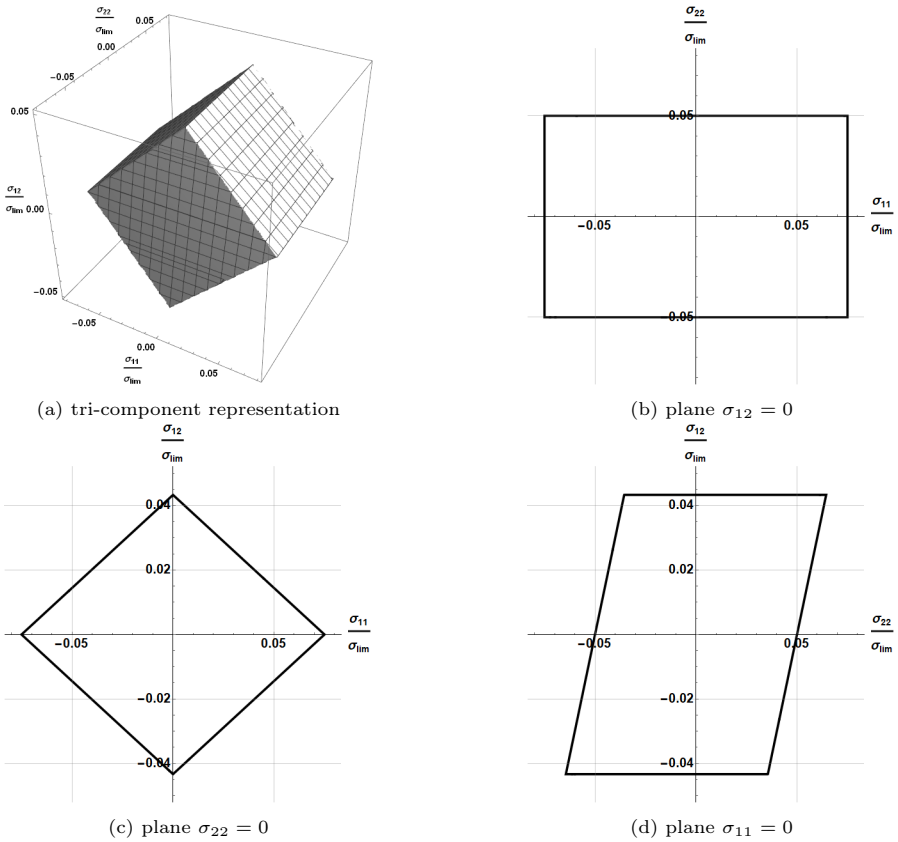

(a) tri-component representation

(b) plane $\sigma_{12}=0$

(c) plane $\sigma_{22}=0$

(d) plane $\sigma_{11}=0$

Figure 1.12: The plasticity threshold surface in the stress space for equilateral triangular lattice [188].

1.3.3 Hexagonal lattice

A 2D lattice with a hexagonal unit cell is considered. As in the previous cases, the materials is exposed to axial stresses σ_{11} and σ_{22} and to a shear stress σ_{12} depicted in figure 1.13. The honeycomb is considered to be bending dominated [188]. It means that plasticity occurs when the maximum bending moment, calculated in each beam, is reached. The criterion is given by:

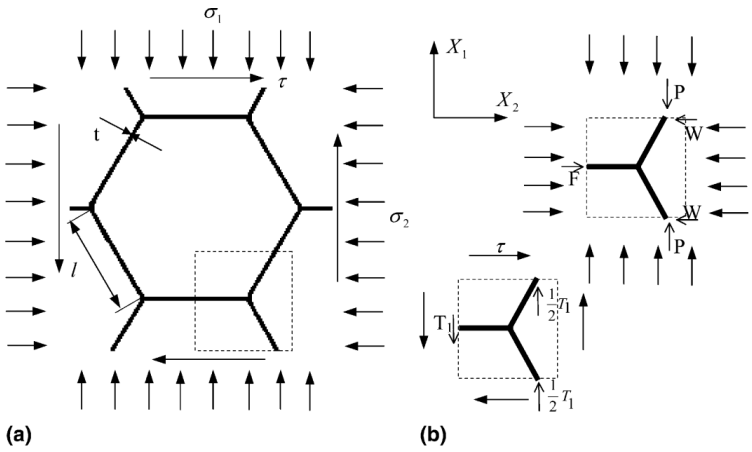

Figure 1.13: 2D lattice with a hexagonal unit cell under plane stresses : (a) periodic material, (b) the studied unit cell [188]

$$\max\left\{\left[\frac{3\left(3\left(\sigma_{11}+\sigma_{12}\right)+\sigma_{22}\right)^2}{16\left(\sigma_{lim}\right)^2}+\frac{3\left|\sigma_{22}-\left(\sigma_{11}+\sigma_{12}\right)\right|}{2\sigma_{lim}}-\frac{3}{4}\rho^2\right],\left[3\left(\frac{\sigma_{22}}{\sigma_{lim}}\right)^2+2\sqrt{3}\frac{|\sigma_{12}|}{\sigma_{lim}}-\frac{3}{4}\rho^2\right]\right\}=0 \quad (1.55)$$

the relative density is given by:

$$\rho=2\sqrt{3}\,\frac{t}{l}, \quad (1.56)$$

where l and t are length and thickness of walls of the unit cell. The figure 1.14 shows the corresponding surface.

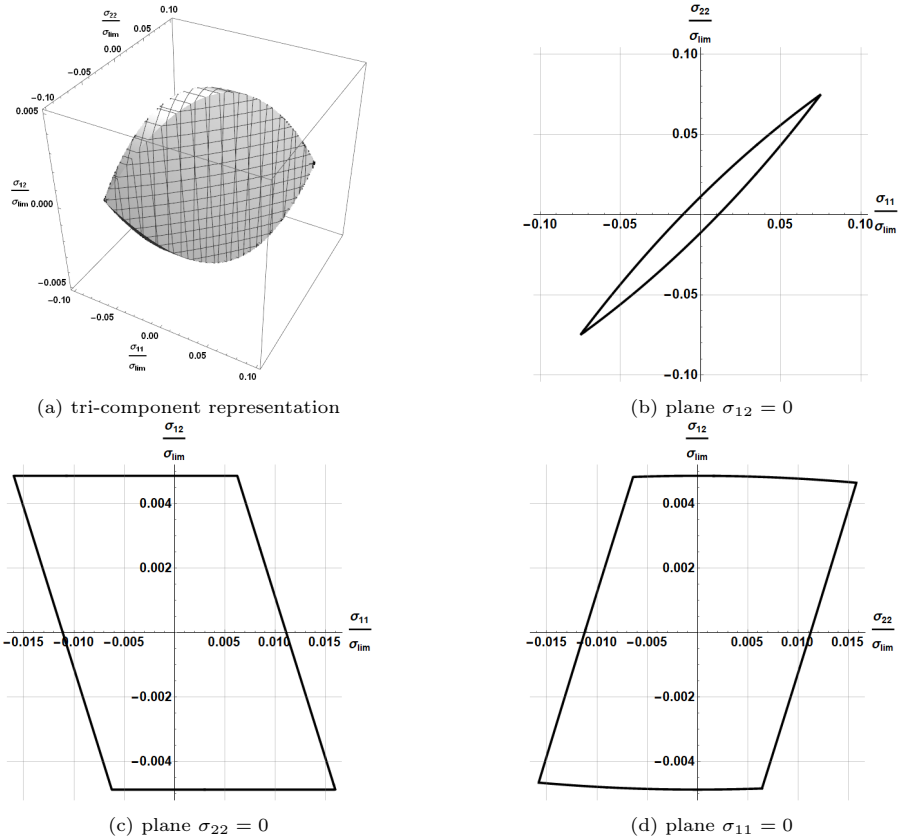

(a) tri-component representation

(b) plane $\sigma_{12}=0$

(c) plane $\sigma_{22}=0$

(d) plane $\sigma_{11}=0$

Figure 1.14: The plasticity threshold surface in the stress space for hexagonal lattice [188].

1.3.4 Jeanneau's threshold surface for equilateral triangular 2D lattice

In the strain stress, a threshold surface is established numerically by Jeanneau et al. [103] for equilateral triangular 2D lattice considering plasticity and buckling instabilities. It is the same studied unit cell as the one in section 1.3.2. The lattice is stretching dominated therefore the plasticity limit is established analytically. For the local buckling, the threshold surface is established numerically. A semi-analytical technique is used, which

combines Bloch wave theory and a finite element model of the unit cell [54]. Therefore, the buckling surface is given by points in the strain space (green points in figure 1.15). The threshold surface is the intersection of plasticity (in grey) and buckling (in red) surfaces and it is illustrated in figure 1.15.

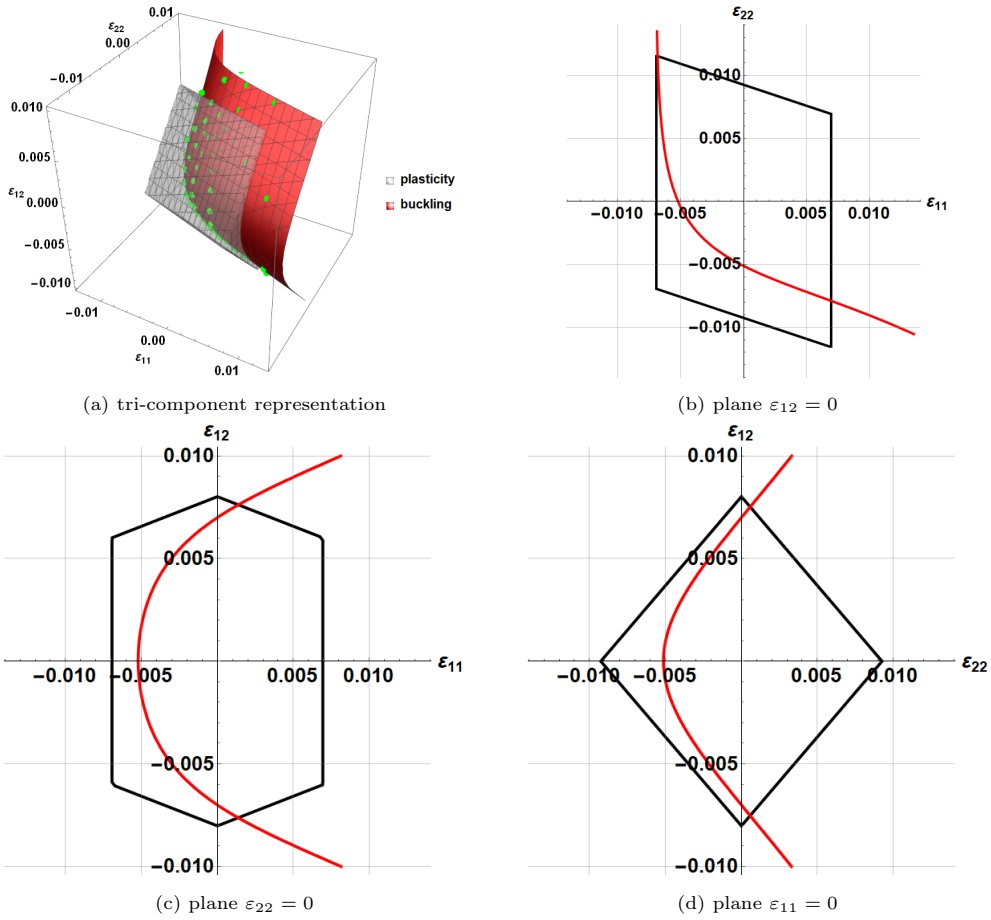

(a) tri-component representation

(b) plane $\varepsilon_{12} = 0$

(c) plane $\varepsilon_{22} = 0$

(d) plane $\varepsilon_{11} = 0$

Figure 1.15: The intersection the buckling (red) and the plasticity (black/grey) surface in the strain space. The green points represent the buckling limit obtained numerically [103].

1.4 Conclusion

In this chapter, an overview is provided of some established criteria for both bulk and lattice materials. Some isotropic criteria were introduced in the first step. For plasticity applications, it is proved [125] that all isotropic threshold surfaces has an upper and lower bound defined by Tresca and Mohr maximum shear stress. Lot authors tried to take into account this aspects hence, various isotropic criterion where proposed such as Hershey/Hosford [87] and Barlat and Richmond [26]. Some authors proposed tension/compression dissymmetric criteria. To include the dissymmetry aspect, they rely on adding terms that are sensitive to the change of sign of $\underset{\sim}{\sigma}$ such as odd degree polynomial terms for Cazacu criterion [46] and an exponential function for Francois criterion [76].

Lot of anisotropic criteria were proposed. An important work was done specially in sheet metal forming applications (plasticity) where orthotropic metal alloys were used. One of the first and known criterion is Hill 1948 [93]. Some theoretical (e.g. convexity) and experimental difficulties (e.g. anomalous behaviour) were encountered hence lot of anisotropic criteria where proposed. To address these difficulties lot of approaches are used: (i) The first approach of them is to add weight coefficients as material parameters [89, 91]. (ii) The second approach is to use linear transformations [27], it has an advantage of adding material parameters without need to prove the convexity. The third approach is the use of high degree polynomial functions. A number of orthotropic homogenous polynomial criteria were proposed. It is observed [166] that the higher the degree (more material parameters) the greater the accuracy. However, the convexity conditions need to be established [168]. For dissymmetric anisotropic criteria, only Cazacu's [46] is mentioned. Cazacu's et al generalised their dissymmetric isotropic criterion to orthotropy [44] using theory of representation (not spoken a lot in this chapter, see section 2.4.3 for more details).

Speaking of lattice materials, lot of authors [59, 127, 103] established criteria theoretically (beam theory) and numerically (finite elements) considering plasticity and buckling. Assuming the periodicity, the study is

always reduced to an unit cell and they are classified into two main categories *stretching* and *bending* dominated. From Wang's examples [188] (only plasticity), it is noticed that stretching dominated lattices resists to shear loading better than bending dominated lattices. All criteria are anisotropic and visually can be seen in their representation in the stress space. The threshold surfaces are not smooth due the fact the threshold functions are max functions (looking for maximum stress in each beam), this may cause issues for the numerical implementation. All featured examples show anisotropic, non-smooth and pressure dependant (dissymmetric is case of buckling) threshold surfaces.

From all the reviewed criteria coming from plasticity, most of them are polynomials functions. With high degree polynomial threshold functions, complicated shapes of threshold surfaces can be generated. We have seen that the theory of representation [44] can be used to generate polynomial threshold function which are invariant under a known material symmetry. When it comes to tension/compression dissymmetry odd degree polynomials also can be used. We conclude that in order to theoretically define a threshold function for lattice material polynomials meet all the requirements and can be a good enough to generate at least an approximate smooth threshold surfaces for lattice materials.

Chapter 2

A geometric approach of threshold surfaces

Contents

Physical field theories, such as solid continuum mechanics, relies on specific relations that link primal (kinematic) variables to dual (static) ones. Those relations, which are called constitutive laws, are not canonical and depend both on the physical nature of the material and on external parameters. Despite their great diversity, at room temperature, constitutive laws of solid materials generally have a linear regime for low intensity loading. This operating regime is called linear elasticity. This domain is finite since the constitutive law will become non-linear for higher loading. The nature of these non-linearities are very diverse: plasticity, instability, fracture,... and strongly depends on the material and on the modelling situation. In most engineering situations, to ensure their integrity, structures are designed to work within their linear regime. To meet this exigence, the domain of loading for which the behaviour is linear should be 1) experimentally defined , 2) mathematically characterised. This domain is a hypervolume in the loading space (which is generally the stress space) bounded by a hypersurface. The hypersurface enclosing the domain of elastic regime has different names according to the physical context: plasticity surface, yield surface, failure surface... . Its form is very dependant on the nature of material and two aspects are generally distinguished:

- anisotropy, it consist on how is the form the hyperspace changes in the stress space when the material is rotated with respect a fixed reference. There has been a lot of work on describing different phenomenons specially in plasticity for sheet metals (metal forming application [19]).
- loading state, some material can behave differently when the loading changes. Generally, it concerns tension/compression states. An example of a studied lattice material is given in section 1.3.3 where it is observed that plasticity occurs under tension loading, while buckling instabilities occur under compressive loading.

In the following, the terminology of *threshold surface* (instead of the hypersurface) will be adopted. Furthermore, it is important to point out that the evolution of surface during the loading process and the associated dissipative process will not be modelled. This chapter gives theoretical framework to well understand and analyse the threshold functions and their associated threshold surfaces. It begins from describing the state variable (Cauchy stress tensor), defining threshold function, describing anisotropy and giving some examples.

This chapter is organised as follows. In a first time in section 2.1 basic notions on material and physical symmetries are provided. Because of its importance for the sequel, the O(2) orthogonal group is introduced and some of its properties are detailed. The notion of group action is then used in section 2.2 to investigate the geometry of the stress space. This geometry is first analysed with stress-tensor considered as a second-order order tensor in $\mathbb{R}^2$, then as a vector in $\mathbb{R}^3$. This section brings together some very classic concepts, but in a way that we do not believe is standard. With all this material at our disposal, the next section 2.3 is devoted to a geometric description of the criterion functions as surfaces in $\mathbb{R}^3$. Different properties of surface symmetries are highlighted and a link is made with the physics of the problem under consideration. A set of characteristic surfaces identified in chapter 1 is reanalysed using the tools introduced in this chapter. In the last section 2.4, a quick overview of the representation theory of groups is proposed in order to make the geometrical approach of the previous section effective. In the context of polynomial criteria, we look at the minimum degree of the polynomial in $\underset{\sim}{\sigma}$ to be considered in order to take explicit account of material anisotropy. This point is important for the modelling of criterion functions for architectured lattices.

2.1 From material invariance to physical symmetry

The mechanical properties of a material are usually determined by its microstructure.

Let Ω be a $\mathbb{R}^3$ domain supposed to describe a solid continuum. At this scale, Ω is a continuous collection of material points. The material point is a richer physical concept than the geometric point since it also includes information about the organisation of matter at scales smaller than that used to establish the continuous model.

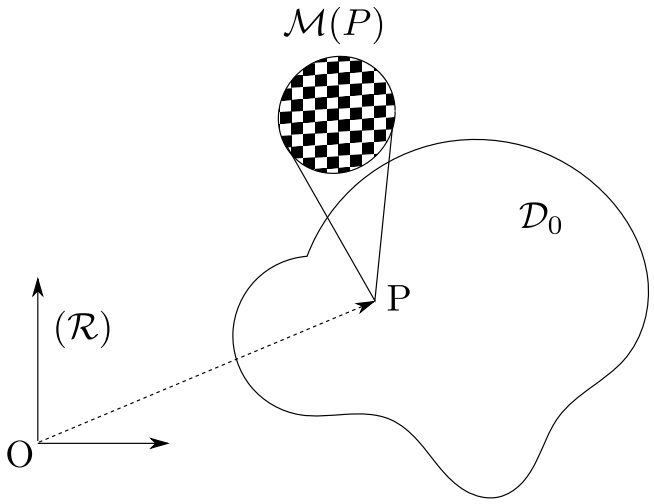

Figure 2.1: The description of the continuum solid Ω.

In the case of a multi-scale model, the connection between scales is explicit and the processes of homogenisation and localisation allow for transit between scales. But such an explicit description is not mandatory and we generally do not have a precise description of the organisation of matter at microscopic scales. What is generally retained at the material point of the microscopic organisation is its symmetry group, i.e. the set of operations that leave the microstructure invariant. A general principle is that a transformation that leaves the microstructure invariant leaves the physical properties, defined at the same point in the material, invariant.

Let us place ourselves at a material point, and let begin by introducing the notions of material symmetries. We will then introduce the concept of physical symmetries and the link between these two concepts. This section will end with a subsection devoted to the O(2)-orthogonal group and its subgroups. The language of symmetry groups will allow us to be more precise in the discussion of invariance properties.

2.1.1 Material and physical symmetry group

In what follows, attention is limited to what happens at a given material point P, and we do not look at how the microstructure and physical properties evolve in the Ω domain.

Therefore, let us denote the microstructure at a given material point P by $\mathcal{M}(\mathrm{P})$. In the case of a continuum with a periodic microstructure, $\mathcal{M}(\mathrm{P})$ can generally be reduced to a primitive unit cell. Let us now consider the set of rigid transformations letting P unchanged, in $\mathbb{R}^2$ this corresponds to the group of linear isometries $\mathrm{O}(2)$. This set will be discussed in more detail later, but it includes rotational symmetries and mirror symmetries.

To fix the idea, consider the periodic lattice materials which unit cells are depicted in figure 2.2. In this case $\mathcal{M}(\mathrm{P})$ corresponds to the unit cell.

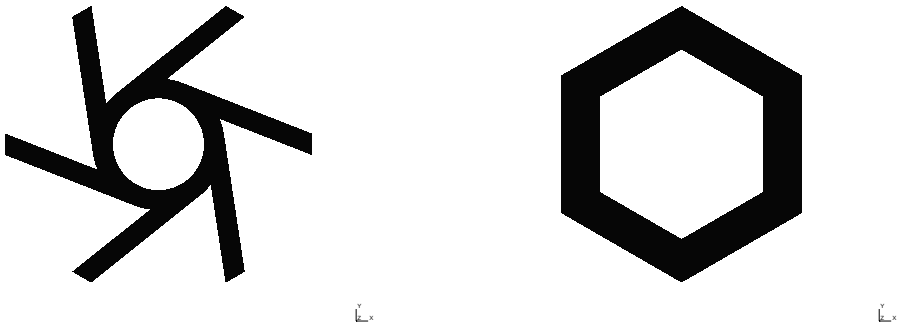

(a) A hexachiral unit-cell (b) A hexagonal unit-cell

Figure 2.2: Two examples of unit-cell.

As appear clearly on this figure $\mathcal{M}(\mathrm{P})$ can possess geometrical symmetries, i.e can be invariant with respect to orthogonal transformations. To keep track of this information, let us define $\mathrm{G}_{\mathcal{M}(\mathrm{P})}$ the set of operations that leave the microstructure invariant:

$$\mathrm{G}_{\mathcal{M}(\mathrm{P})} := \{\mathbf{g} \in \mathrm{O}(2) \mid \mathbf{g} \star \mathcal{M} = \mathcal{M}\}\,. \tag{2.1}$$

At the macroscopic scale, the behaviour is described by physical property fields on Ω. These fields define at each point P of Ω the values of the physical properties: elastic stiffnesses, thermal properties, damage state, etc. of the model. For the present discussion, let us consider that the physical properties are described by a n-th order tensor field on Ω.

Let denote by $\mathbf{T}(P) \in \mathbb{T}^n$, the tensor that describes a physical property at the material point P. This tensor can posses some invariance with respect to orthogonal transformations, hence it is natural to introduce $\mathrm{G}_{\mathbf{T}(P)}$, *the physical symmetry group* which is the group of transformations that preserves the tensor $\mathbf{T}(P)$. We write:

$$\mathrm{G}_{\mathbf{T}(P)} := \{\mathbf{g} \in \mathrm{O}(2) \mid \mathbf{g} \star \mathbf{T}(P) = \mathbf{T}(P)\}\,. \tag{2.2}$$

in which $\star$ is the classical tensorial action, i.e. $\mathrm{O}(2)$ acts on $\mathbb{T}^n$ as

$$\begin{aligned} \star : \mathrm{O}(2) \times \mathbb{T}^n &\to \mathbb{T}^n & (2.3)\\ (\mathbf{g}, \mathbf{T}) &\mapsto \mathbf{g} \star \mathbf{T} := g_{i_1 j_1} g_{i_2 j_2} \dots g_{i_n j_n} T_{j_1 j_2 \cdots j_n}. & (2.4) \end{aligned}$$

Since the constitutive tensor is defined at a material point P of Ω, the material symmetry group $\mathrm{G}_{\mathcal{M}(P)}$ and the physical symmetry group $\mathrm{G}_{\mathbf{T}(P)}$, must be related in some way. This link is provided by the Curie-Neumann principle.

Principle 2.1.1 (Curie-Neumann's Principle)**.** *At each material point $P \in \mathcal{M}$ with a physical property described by $T(P) \in \mathbb{T}^n$, every material symmetry is a physical symmetry, i.e :*

$$\mathrm{G}_{\mathcal{M}(P)} \subset \mathrm{G}_{\mathbf{T}(P)}.$$

It is important to note that this is only an inclusion, indicating that the physical properties emerging from a microstructure may be more symmetrical than this one. This principle state that the material symmetry group is always a subgroup of the physical symmetry group.

In the case of tensor properties, Hermann's theorems give sufficient conditions for having hemitropic and isotropic physical properties.

2.1.2 The orthogonal group $\mathrm{O}(2)$

The group of invertible linear transformations of $\mathbb{R}^2$ is denoted $\mathrm{GL}(2)$

Definition 2.1.2 (Linear Group)**.** *The linear group in* $\mathbb{R}^2$ *is defined as*

$$\mathrm{GL}(2) = \{\mathbf{g} \mid \det \mathbf{g} \neq 0\} \tag{2.5}$$

Let consider O(2) the subset of invertible transformations $\mathbf{g}$ of $\mathbb{R}^2$ satisfying $\mathbf{g}^{-1} = \mathbf{g}^T$, i.e.

$$\mathrm{O}(2) := \{\mathbf{g} \in \mathrm{GL}(2), \mathbf{g}^T = \mathbf{g}^{-1}\}$$

This set equipped with the classical product has the algebraic structure of a group, that is

Definition 2.1.3. *A* group *is a set* G *together with a multiplication on* G *which satisfies four axioms [11]:*

1. *(Closed) Multiplication of any ordered pair* $\mathbf{g}, \mathbf{h}$ *of elements from the set* G *imply a unique "product"* $\mathbf{g} \cdot \mathbf{h}$ *which also lies in the set* G*.*
2. *(Associative)* $\mathbf{g} \cdot (\mathbf{h} \cdot \mathbf{k}) = (\mathbf{g} \cdot \mathbf{h}) \cdot \mathbf{k}$ *for any three (not necessarily distinct) elements from* G*.*
3. *(Existence of an identity element) there is an element* $\mathbf{e} \in$ G*, called an identity element, such that* $\mathbf{g} \cdot \mathbf{e} = \mathbf{e} \cdot \mathbf{g} = \mathbf{g}$ *for* $\forall \mathbf{g} \in$ G*.*
4. *(Existence of an inverse) each element* $\mathbf{g} \in$ G *has a (so called) inverse* $\mathbf{g}^{-1}$ *which belongs to the set* G *and satisfies* $\mathbf{g}^{-1} \cdot \mathbf{g} = \mathbf{e} = \mathbf{g} \cdot \mathbf{g}^{-1}$*.*

O(2) is called the orthogonal group and is the set of vectorial isometries. This is a non commutative group of dimension 1 generated by:

- $\mathbf{r}(\theta)$ is the rotation by an angle θ;
- $\boldsymbol{\pi}(\underline{\mathrm{n}})$, in which $\boldsymbol{\pi}(\underline{\mathrm{n}})$ is the reflection across the line normal to $\underline{\mathrm{n}}$:

$$\boldsymbol{\pi}(\underline{\mathrm{n}}) := \underset{\sim}{\mathrm{I}} - 2\underline{\mathrm{n}} \otimes \underline{\mathrm{n}}, \quad \|\underline{\mathrm{n}}\| = 1,$$

  with $\underset{\sim}{\mathrm{I}}$ the second order identity tensor.

Those generators satisfy the presentation relation

$$\boldsymbol{\pi}(\underline{\mathrm{n}})\mathbf{r}(\theta) = \mathbf{r}(-\theta)\boldsymbol{\pi}(\underline{\mathrm{n}})$$

In terms of matrix we have,

$$\mathbf{r}(\theta) = \begin{pmatrix} \cos\theta & -\sin\theta \\ \sin\theta & \cos\theta \end{pmatrix} \quad \text{with } 0 \leq \theta < 2\pi \quad \text{and} \quad \boldsymbol{\pi}(\underline{\mathrm{e}}_2) = \begin{pmatrix} 1 & 0 \\ 0 & -1 \end{pmatrix}.$$

As a special transformation we mention the inversion $\mathbf{i}_2 = -\underset{\sim}{\mathrm{I}}$, with in $\mathbb{R}^2$ $\mathbf{i}_2 = \mathbf{r}(\pi)$, and which matrix representation is

$$\mathbf{i}_2 = \begin{pmatrix} -1 & 0 \\ 0 & -1 \end{pmatrix}$$

Among O(2) we can identify an infinite collection of closed subgroups [11]:

- Id is the identity group;
- $\mathrm{Z}_2^{\boldsymbol{\pi}(\underline{\mathrm{n}})}$ is the cyclic group[1] with 2 elements, generated by $\boldsymbol{\pi}(\underline{\mathrm{n}})$;
- $\mathrm{Z}_k (k \geq 2)$ the cyclic group with k elements, generated by $\mathbf{r}(2\pi/k)$;
- $\mathrm{D}_k^{\underline{\mathrm{n}}}$ $(k \geq 2)$ is dihedral group[2] with $2k$ elements generated by $\mathbf{r}(2\pi/k)$ and a mirror through an axis $\underline{\mathrm{n}}$;
- SO(2): the special orthogonal group generated by $\mathbf{r}(\theta)$, it can be viewed as the infinite cyclic group when $k \to \infty$;
- O(2): the full orthogonal group, which can be viewed as the infinite dihedral group when $k \to \infty$.

[1] A group is said to be cyclic if it is *monogene* and *finite*, meaning it is generated by an unique element q satisfying $q^k = e$ for a given k.

[2] A group is said to be dihedral if it is *finite* and generated by two elements q and s verifying the following relation $q^k = s^2 = (qs)^2 = e$.

In the notion of a group, the orientation of the symmetry elements is important. Among O(2) subgroups, this point is particularly important for $D_k^{\underline{n}}$ dihedral groups because, for a given k, $D_k^{\underline{n}_1}$ and $D_k^{\underline{n}_2}$ can have non-coincident mirror symmetry lines. An example of such a situation is depicted on figure 2.3. The subfigure 2.3a depicts a geometry which is invariant with respect to $D_4^{\underline{e}_2}$, while the subfigure 2.3*b* is let invariant with respect with $D_4^{\underline{n}}$, with $\underline{n} \neq \mathbf{r}(\frac{k\pi}{2}) \cdot \underline{e}_2$, $k \in \mathbb{Z}$.

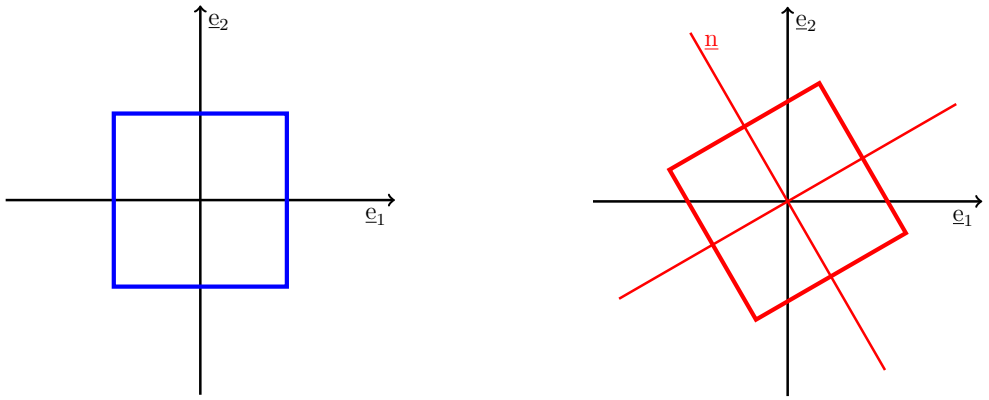

(a) $D_4^{\underline{e}_2}$ (b) $D_4^{\underline{n}}$

Figure 2.3: An example showing the difference between $D_4^{\underline{n}}$ and $D_4^{\underline{e}_2}$ symmetries.

In this situation the two groups $D_4^{\underline{e}_2}$ and $D_4^{\underline{n}}$ are different but are of the same type, they are said to be *conjugate*. The general definition is as follows

Definition 2.1.4. *Two subgroups* H_1 *and* H_2 *of a group* G *are said to be conjugate if* $\exists \mathbf{g} \in G$ *such that* $\mathbf{g}H_1\mathbf{g}^{-1} = H_2$

From this idea, we can define the conjugacy class of subgroup $H < G$, denoted [H] as the collection of subgroups of G that are conjugate to G:

$$[H] := \{H^* = \mathbf{g}H\mathbf{g}^T \in G, \mathbf{g} \in G\}, \tag{2.6}$$

This notion of conjugacy class will be important for future discussions as it allows us to characterise the type of symmetry an object has, rather than the specific symmetries it has about a given orientation.

Theorem 2.1.5. *The conjugacy classes of* O(2)*-closed subgroups are*

$$\{[\mathbb{1}], [Z_2^{\pi}], [Z_k], [D_k], [SO(2)], [O(2)]\}_{k>1}$$

in which Z_2^{π} *and* D_k *stands for* $Z_2^{\pi(\underline{e}_2)}$ *and* $D_k^{\underline{e}_2}$.

Chirality and non-centrosymmetry

O(2)-subgroups and their classes have been introduced in terms of the nature of their generators, before closing this section it is interesting to look at their geometric content. To that aim we will consider geometric figures that are left fixed by each kind of group and look at their symmetry properties. Consider the following figure

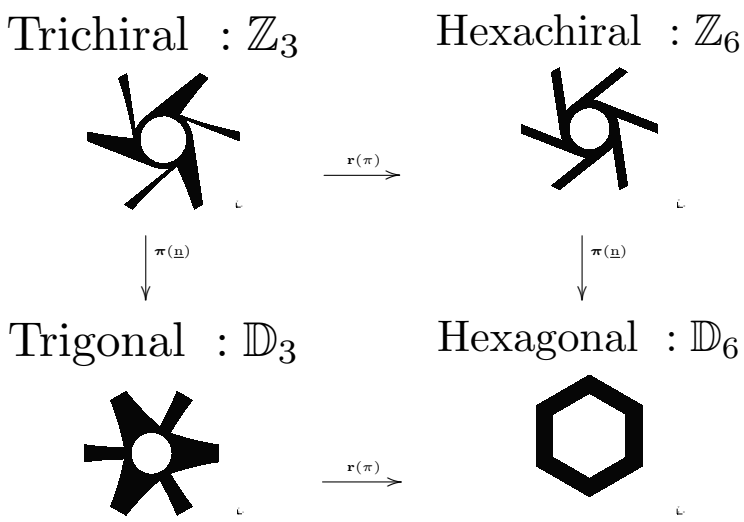

Figure 2.4: Examples of geometries showing the differences between trichiral, hexachiral, trigonal and hexagonal symmetries.

It appears that the Z_3- and Z_6-invariant figures do not possess mirror invariance and can therefore turn left or right. As such, they will be called *chiral*. It can be observed that Z_6- and D_6-invariant figures are centro symmetric, meaning that they are invariant under the transformation $\mathbf{i}_2$ which correspond, in $\mathbb{R}^2$ to $\mathbf{r}(\pi)$, this properties is clearly not satisfied by the Z_3- and D_3-invariant figures. Hence from this example introduce the notions of *chirality* and *centrosymmetry*. These concepts are very important for the intended physical applications. For a more formal defintion:

Definition 2.1.6. *A subgroup of* O(2) *will be said to be:*

- centrosymmetric *(denoted by* $\mathbf{I}$*) if it contains the inversion* $\mathbf{r}(\pi)$*, and* non-centrosymmetric *(*$\bar{\mathbf{I}}$*) otherwise;*
- chiral *(noted* $\mathbf{c}$*) if it only contains rotations, and* achiral *(noted* $\bar{\mathbf{c}}$*) otherwise (i.e. if it contains reflections).*

O(2)-closed subgroups can be divided into four subsets according to the nature of their generators. The different situations are reported in the following table:

	$\mathbf{I}$	$\bar{\mathbf{I}}$
$\bar{\mathbf{c}}$	D_{2k}	D_{2k+1}
$\mathbf{c}$	Z_{2k}	Z_{2k+1}

Theorem 2.1.7 (Hermann Theorem)**.** *Consider* $\mathcal{M}$ *be a microstructure and* $\mathbf{T} \in \mathbb{T}^n$ *a non-degenerate nth-order tensor describing a physical property emerging from* $\mathcal{M}$*.*

$$\begin{cases} Z_{n+1} \subset G_{\mathcal{M}} \Rightarrow G_{\mathbf{T}} \supset SO(2) \\ D_{n+1} \subset G_{\mathcal{M}} \Rightarrow G_{\mathbf{T}} = O(2) \end{cases}$$

The figure 2.5 is an illustration of the Hermann theorem in linear elasticity. The geometry of a honeycomb material is D_6 (left hand side figure), the effective elastic properties of such a material are described by a fourth-order elastic tensor. As a consequence of Hermann theorem in $\mathbb{R}^2$, the effective elasticity must be isotropic. The figure on the right illustrates the propagation of a wave from a point source in the effective continuum, the propagation being isotropic.

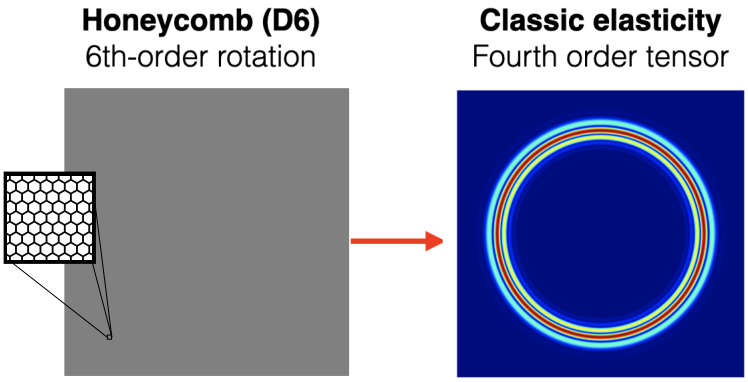

Figure 2.5: Wave propagation in an effective elastic continuum having hexagonal microstructure [148].

2.2 The geometry of the stress space

In the literature, threshold surfaces are most often expressed as surfaces in stress space. We will follow this approach here, and the stress tensor will therefore be the central variable in our study. Because of this central role, we will devote this section to recalling the basic properties of this tensor and of the space to which it belongs. The emphasis will be on the geometry of this space and on the way in which a tensor transforms under the action of the group of isometries. It is important to have a clear vision of this geometry in order to construct threshold surfaces and understand their physical content.

2.2.1 The stress tensor (2D)

Let define, within the two-dimensional Euclidean space $\mathcal{E}^2$, a reference frame associated to a point O and an orthonormal basis $\mathcal{B} = \{\underline{e}_1, \underline{e}_2\}$. This permits to identify $\mathcal{E}^2$ with the vector space $\mathbb{R}^2$ and to labelled any point P by it position vector $\underline{x} = \underline{OP}$. Consider a domain $\Omega \in \mathbb{R}^2$ as shown in figure 2.6

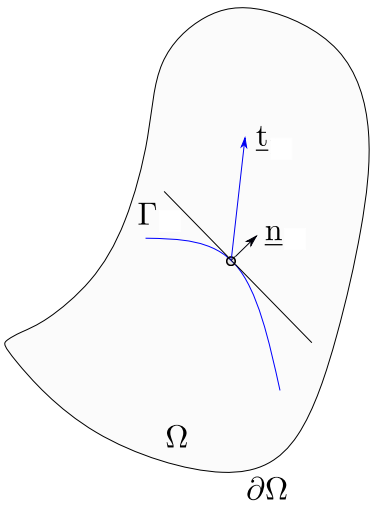

Figure 2.6: Stress vector exerted on a point of material surface Γ of Ω

Consider a *surface* $\Gamma \in \mathbb{R}$ embedded within Ω. Let $\underline{n}(\underline{x})$ be the normal vector to Γ at point $\underline{x}$, we denote by $\underline{t}(\underline{x}, \underline{n})$ the traction vector exerted at $\underline{x}$ on the infinitesimal surface $\gamma \in \mathbb{R}$ tangent to Γ. According to Cauchy's fundamental theorem [73], there exists a second order tensor field $\underset{\sim}{\sigma}$ such as

$$\underline{t}(\underline{x}, \underline{n}) = \underset{\sim}{\sigma}(\underline{x}) \cdot \underline{n}, \quad \underline{n} \in \Gamma \tag{2.7}$$

At a point $\underline{x}$ we can look at the stress vector exerted on the facet of normal $\underline{e}_i$, let us denote $\underline{t}(\underline{x}, \underline{e}_i)$ the resulting vector. This vector can be decomposed with respect to $\mathcal{B}$, the associated matrix expression condenses this

information into a table :

$$[\underset{\sim}{\sigma}] = \begin{pmatrix} \underline{t}(\underline{e}_1).\underline{e}_1 & \underline{t}(\underline{e}_2).\underline{e}_1 \\ \underline{t}(\underline{e}_1).\underline{e}_2 & \underline{t}(\underline{e}_2).\underline{e}_2 \end{pmatrix}_{\mathcal{B}} = \begin{pmatrix} \sigma_{11} & \sigma_{12} \\ \sigma_{21} & \sigma_{22} \end{pmatrix}_{\mathcal{B}}, \tag{2.8}$$

where σ_{ii} are normal stresses and $\sigma_{ij}, i \neq j$ are shear stresses. The components of $\underset{\sim}{\sigma}$ can be interpreted as follows

$$\sigma_{ij} = \underline{t}(\underline{e}_i).\underline{e}_j$$

meaning that σ_{ij} is the projection along $\underline{e}_j$ of the traction vector acting on the facet of normal $\underline{e}_i$. The first index i indicates that the stress acts on a plane normal to $\underline{e}_i$, while the second index j indicates the direction in which the stress acts.

The local angular momentum equation reads in 2D

$$\underset{\sim}{\epsilon} : \underset{\sim}{\sigma} = m$$

with m the volumic density of torque, and $\underset{\sim}{\epsilon}$ the Levi-Civita symbol in $\mathbb{R}^2$ which is defined as

$$[\underset{\sim}{\epsilon}] = \begin{pmatrix} 0 & 1 \\ -1 & 0 \end{pmatrix}$$

In $\mathbb{R}^2$ this quantity is a pseudo-scalar. This equation expresses that the antisymmetric part of $\underset{\sim}{\sigma}$ equilibrates m. In most of classical situations [73, 78] $m = 0$, leading to a symmetric stress tensor. This hypothesis will always be considered in the following. As a consequence, the space of stress tensors corresponds to

$$\underset{\sim}{\sigma} \in \mathcal{L}^s(\mathbb{R}^2, \mathbb{R}^2) \simeq S^2(\mathbb{R}^2), \tag{2.9}$$

in which $\mathcal{L}^s(\mathbb{R}^2, \mathbb{R}^2)$ denotes the space of linear symmetric applications of $\mathbb{R}^2$ and $S^2(\mathbb{R}^2)$ is the space of symmetric second-order tensors on $\mathbb{R}^2$.

2.2.2 O(2)-action on $S^2(\mathbb{R}^2)$

As well-known, any stress tensor can be decomposed into a deviatoric part $\underset{\sim}{\sigma}^{(2)}$ and a spherical part $\underset{\sim}{\sigma}^{(0)}$ as follows:

$$\underset{\sim}{\sigma} = \underset{\sim}{\sigma}^{(2)} + \underset{\sim}{\sigma}^{(0)}, \quad \text{with} \begin{cases} \underset{\sim}{\sigma}^{(0)} = \dfrac{1}{2}\operatorname{tr}(\underset{\sim}{\sigma})\underset{\sim}{\mathrm{I}}, \\ \underset{\sim}{\sigma}^{(2)} = \underset{\sim}{\sigma} - \underset{\sim}{\sigma}^{(0)}. \end{cases} \tag{2.10}$$

This decomposition can be expressed in terms of projectors as follows

$$\underset{\sim}{\sigma}^{(2)} = \underset{\approx}{\mathrm{P}}^2 : \underset{\sim}{\sigma}, \quad \underset{\sim}{\sigma}^{(0)} = \underset{\approx}{\mathrm{P}}^0 : \underset{\sim}{\sigma}.$$

in which $\underset{\approx}{\mathrm{P}}^2$ and $\underset{\approx}{\mathrm{P}}^0$ are, respectively, the deviatoric and spherical projectors. They are defined as follows:

$$\underset{\approx}{\mathrm{P}}^0 = \frac{1}{2}\underset{\sim}{\mathrm{I}} \otimes \underset{\sim}{\mathrm{I}} \qquad ; \qquad \underset{\approx}{\mathrm{P}}^2 = \underset{\approx}{\mathrm{I}} - \underset{\approx}{\mathrm{P}}^0. \tag{2.11}$$

with $\underset{\sim}{\mathrm{I}}$ and $\underset{\approx}{\mathrm{I}}$ the second and fourth order identity tensors. In this notation

1. the exponent 0 is associated with spherical part because it depends on one scalar;
2. the exponent 2 is associated with deviatoric part because it is a second-order tensor.

The following table ($\underset{\approx}{0}$ is 4th order null tensor) indicates that the projectors are orthogonal

:	$\underset{\approx}{\mathrm{P}}^2$	$\underset{\approx}{\mathrm{P}}^0$
$\underset{\approx}{\mathrm{P}}^2$	$\underset{\approx}{\mathrm{P}}^2$	$\underset{\approx}{0}$
$\underset{\approx}{\mathrm{P}}^0$	$\underset{\approx}{0}$	$\underset{\approx}{\mathrm{P}}^0$

Table 2.1: The orthogonality of the projectors $\underset{\approx}{\mathrm{P}}^2$ and $\underset{\approx}{\mathrm{P}}^0$.

It results that the space $S^2(\mathbb{R}^2)$ can be decomposed orthogonally as follows:

$$S^2(\mathbb{R}^2) \simeq \mathbb{K}^0 \oplus \mathbb{K}^2$$

in which $\mathbb{K}^2$ denotes the space of traceless second-order symmetric tensors and $\mathbb{K}^0$ the space of spherical tensors. This decomposition is also called [13, 60] *harmonic decomposition* (or O(2)-irreducible decomposition). A concept on which we will dwell in the next chapter 3.

Principal stresses and Invariants (2D)

Since $\underset{\sim}{\sigma}$ is a symmetric tensor, its matrix can be diagonalized. Let us denote by σ_1 and σ_2 the eigenvalues of $\underset{\sim}{\sigma}$ called the principal stresses in the present physical context. In the basis $\mathcal{P}$ of its eigenvectors,

$$[\underset{\sim}{\sigma}] = \begin{pmatrix} \sigma_1 & 0 \\ 0 & \sigma_2 \end{pmatrix}_{\mathcal{P}}, \quad \text{with } \sigma_1 \geq \sigma_2 \tag{2.12}$$

The principal stresses σ_1, σ_2 are the solutions of the equation:

$$\det(\underset{\sim}{\sigma} - \lambda \underset{\sim}{\mathrm{I}}) = \lambda^2 - I_1\lambda + I_2 = 0, \text{i.e. } \sigma_{1,2} = \frac{I_1 \pm \sqrt{I_1^2 - 4I_2}}{2} \tag{2.13}$$

in which I_1 and I_2 are symmetric polynomials in σ_1 and σ_2 of $\underset{\sim}{\sigma}$:

$$I_1 = \mathrm{tr}(\underset{\sim}{\sigma}) = \sigma_1 + \sigma_2 \qquad ; \qquad I_2 = \det(\underset{\sim}{\sigma}) = \sigma_1\sigma_2. \tag{2.14}$$

Those quantities are invariant with respect to the action of O(2). Since $\underset{\sim}{\sigma}$ can be decomposed as follows:

$$[\underset{\sim}{\sigma}] = [\underset{\sim}{\sigma}^{(2)}] + [\underset{\sim}{\sigma}^{(0)}] = \frac{\sigma_1 - \sigma_2}{2}\begin{pmatrix} 1 & 0 \\ 0 & -1 \end{pmatrix}_{\mathcal{P}} + \frac{\sigma_1 + \sigma_2}{2}\begin{pmatrix} 1 & 0 \\ 0 & 1 \end{pmatrix}_{\mathcal{P}},$$

it is obvious that in the case $\sigma_1 = \sigma_2$, the deviatoric part vanishes and $\underset{\sim}{\sigma}$ reduces to its spherical part

$$[\underset{\sim}{\sigma}] = \sigma_1 \begin{pmatrix} 1 & 0 \\ 0 & 1 \end{pmatrix}_{\mathcal{P}}.$$

The polynomial invariants of $\underset{\sim}{\sigma}^{(2)}$ are as follows:

$$J_1 = \mathrm{tr}(\underset{\sim}{\sigma}^{(2)}) = 0 \qquad ; \qquad J_2 = \underset{\sim}{\sigma}^{(2)} : \underset{\sim}{\sigma}^{(2)} = \frac{1}{2}(\sigma_1 - \sigma_2)^2. \tag{2.15}$$

It can be observed that

$$J_2 = \frac{1}{2}\left(I_1^2 - 4I_2\right) = \frac{\Delta}{2},$$

which correspond to the discriminant Δ of the characteristic polynomial. (I_1, I_2) constitutes a polynomial basis that allows to write any invariant polynomial in $\underset{\sim}{\sigma}$ as a polynomial with respect to (I_1, I_2). Polynomial invariants are labelled according to the following convention: their index indicates the degree of the associated polynomial, i.e. I_k is an homogeneous polynomial of degree k in the components of $\underset{\sim}{\sigma}$. Using results from [204, 61] we obtain

Proposition 2.2.1. *A minimal integrity basis for the invariant algebras* $\mathbf{Inv}(S^2(\mathbb{R}^2), \mathrm{SO}(2))$ *and* $\mathbf{Inv}(S^2(\mathbb{R}^2), \mathrm{O}(2))$ *is given by*

$$\{I_1 = \mathrm{tr}\,\underset{\sim}{\sigma},\ J_2 = \underset{\sim}{\sigma}^{(2)} : \underset{\sim}{\sigma}^{(2)}\}$$

in which $\mathbf{Inv}(\mathbb{V}, \mathrm{G}) = \mathbb{R}[\mathbb{V}]^{\mathrm{G}}$ is the algebra of G-invariant polynomials on $\mathbb{V}$.

The orbit of stress tensor

The O(2)-action on $S^2(\mathbb{R}^2)$, is the classical tensorial action, i.e.

$$(\underset{\sim}{\sigma}^*)_{ij} = (\mathbf{g} \star \underset{\sim}{\sigma})_{ij} = g_{ik}g_{jl}\sigma_{kl}. \tag{2.16}$$

This is particular case of the general formula (2.3). In this definition, we retain the active interpretation of transformations, this is an important point that deserves being discussed. This means that the transformation

of an object gives rise to a new object which is usually different from the original object. This interpretation has to be distinguished from the *passive interpretation* in which the object is unchanged but the basis used for its description is transformed. The difference between of point of view is illustrated in figure 2.7.

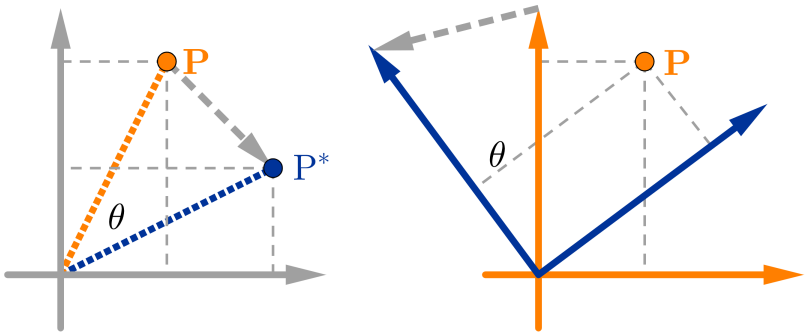

Figure 2.7: **Active transformation** on the left figure: a new vector is obtained; **Passive transformation** on the right figure, in which only the basis is changed

Starting from this, we can define the O(2)-orbit of a stress tensor $\underset{\sim}{\sigma}$ as the set of stress tensors resulting from all applied transformations O(2) on $\underset{\sim}{\sigma}$

$$\mathrm{Orb}(\underset{\sim}{\sigma}) = \left\{ \underset{\sim}{\sigma}^* \in S^2(\mathbb{R}^2) | \underset{\sim}{\sigma}^* = \mathbf{g} \star \underset{\sim}{\sigma},\ \forall \mathbf{g} \in \mathrm{O}(2) \right\}. \tag{2.17}$$

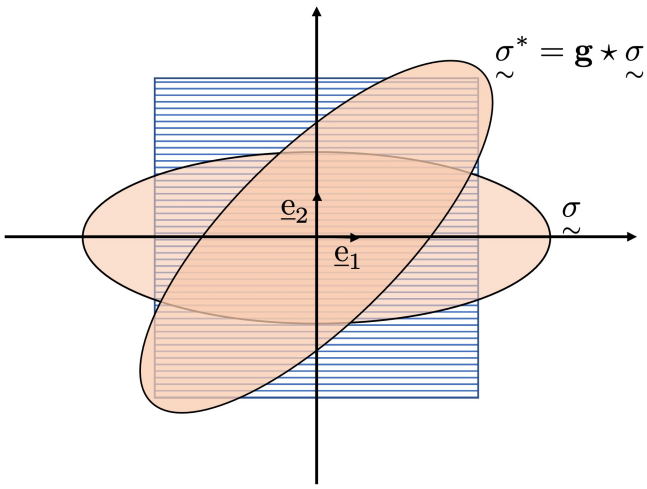

Figure 2.8: The SO(2)-orbit of a stress tensor $\underset{\sim}{\sigma}$ corresponds to the set of all the rotated states of stress. In the figure, the orange ellipsoids represent the stress states, while the material, with its preferred directions, is shown in blue.

This definition can be restricted to a subgroup H of O(2), and we define the H-orbit of the stress tensor $\mathrm{Orb}(\underset{\sim}{\sigma}, \mathrm{H})$ as

$$\mathrm{Orb}(\underset{\sim}{\sigma}, \mathrm{H}) = \left\{ \underset{\sim}{\sigma}^* = \mathbf{g} \star \underset{\sim}{\sigma},\ \forall \mathbf{g} \in \mathrm{H} \right\}. \tag{2.18}$$

The following result is demonstrated in appendix ii.3

Proposition 2.2.2. *For* $\underset{\sim}{\sigma} \in S^2(\mathbb{R}^2)$, $\mathrm{Orb}(\underset{\sim}{\sigma}, \mathrm{O}(2)) = \mathrm{Orb}(\underset{\sim}{\sigma}, \mathrm{SO}(2))$

This result is not generic and depends on the specific nature of the vector space under consideration; for more generic spaces, the orbits with respect to SO(2) and O(2) would be distinct. For instance, in the case of an asymmetric stress tensor, the orbits will be different depending on the considered group. In our case, this property can be read from theorem 2.2.1. Since the integrity bases, with respect to SO(2) or O(2), are identical, the orbits are also identical. More details can be found in appendix ii.

Since the orbits are identical, the study can be restricted to SO(2)-action, considering $\mathbf{r} \in \mathrm{SO}(2)$ instead of general $\mathbf{g} \in \mathrm{O}(2)$. Hence, considering any $\underset{\sim}{\sigma}^* \in S^2(\mathbb{R}^2)$, any point in $\mathrm{Orb}(\underset{\sim}{\sigma}^*)$ is parameterised by $\theta \in [0, \pi[$:

$$\underset{\sim}{\sigma}(\theta) = \mathbf{r}(\theta) \star \underset{\sim}{\sigma}^{(0)}.$$

The function $\underset{\sim}{\sigma}(.)$ is a π-periodic. Since every orbit intersects the space Span $(\underline{e}_1 \otimes \underline{e}_1, \underline{e}_2 \otimes \underline{e}_2)$ the diagonal form is a natural choice for parameterising the orbits. This geometric picture of the stress orbit will be further detailed in the next subsection.

With this image in mind, we can see that there are two types of orbit for a stress tensor, either

- $\sigma_1 = \sigma_2$, the stress tensor is spherical and therefore isotropic. Its orbit is reduced to a single point;
- $\sigma_1 \neq \sigma_2$, the stress tensor is orthotropic, its orbit is a circle since

$$\|\underset{\sim}{\sigma}(\theta)\| = \|\underset{\sim}{\sigma}^{(0)}\|, \ \forall\theta$$

2.2.3 Geometric representation in $\mathbb{R}^3$

Upon the choice of a basis $\mathbb{V} = S^2(\mathbb{R}^2)$ can be identified with $\mathbb{R}^3$. It results that stress tensors can be represented as points in $\mathbb{R}^3$. We will take advantage of this particular situation[3] to construct a geometric picture of the stress space in $\mathbb{R}^2$.

A first natural basis of $\mathbb{V}$ is given by the orthonormal *Kelvin basis* $\mathcal{K} = \{\underline{\hat{e}}_1, \underline{\hat{e}}_2, \underline{\hat{e}}_3\}$ defined by:

$$\underset{\sim_1}{\hat{e}} = \underline{e}_1 \otimes \underline{e}_1, \ \underset{\sim_2}{\hat{e}} = \underline{e}_2 \otimes \underline{e}_2, \ \underset{\sim_3}{\hat{e}} = \frac{1}{\sqrt{2}}(\underline{e}_1 \otimes \underline{e}_2 + \underline{e}_2 \otimes \underline{e}_1).$$

$\underset{\sim}{\sigma}$ can be pictured as a vector with respect to $\mathcal{K}$:

$$\{\underset{\sim}{\sigma}\}_{\mathcal{K}} = \begin{pmatrix} \sigma_{11} \\ \sigma_{22} \\ \sqrt{2}\sigma_{12} \end{pmatrix}_{\mathcal{K}}. \tag{2.19}$$

Associated to this picture of $\mathbb{V}$, we consider the group O(3), which is the set of linear isometries acting of $S^2(\mathbb{R}^2) \simeq \mathbb{R}^3$. Its action on an element $\underset{\sim}{\sigma}$ of $\mathbb{V}$ gives a new element $\underset{\sim}{\sigma}^\sharp$ of $\mathbb{V}$,

$$\underset{\sim}{\sigma}^\sharp = \mathbf{G} \cdot \underset{\sim}{\sigma}, \quad \mathbf{G} \in \mathrm{O}(3),$$

O(3) contains as a subgroup the group of physical transformations $\mathrm{O}(2)^{\underline{k}}$, in which $\underline{k}$ denotes in $\mathbb{R}^3$ the axis of physical rotations. But in O(3) there are also additional transformations, whose physical content will be studied later. The notion of O(3)-orbit can be defined

$$\mathrm{Orb}(\underset{\sim}{\sigma}, \mathrm{O}(3)) = \left\{\underset{\sim}{\sigma}^\sharp \in \mathbb{V}, \underset{\sim}{\sigma}^\sharp = \mathbf{G} \cdot \underset{\sim}{\sigma}, \ \forall \mathbf{G} \in \mathrm{O}(3)\right\}. \tag{2.20}$$

It can be demonstrated that[4]

Lemma 2.2.3. *The action of* O(3) *on* $\mathbb{R}^3$ *can be reduced to* SO(3).

It results that the definition of the orbit can be restricted to $\mathrm{Orb}(\underset{\sim}{\sigma}, \mathrm{SO}(3))$, and we have the obvious relationship

$$\mathrm{Orb}(\underset{\sim}{\sigma}, \mathrm{SO}(2)^{\underline{k}}) \subset \mathrm{Orb}(\underset{\sim}{\sigma}, \mathrm{SO}(3)),$$

when $\underset{\sim}{\sigma} = 0$ the orbits are reduced to a point and are therefore coincident, in the general case the inclusion is strict.

[3] In $\mathbb{R}^3$ the situation is far more complex since $S^2(\mathbb{R}^3)$ should now be embedded in $\mathbb{R}^6$.

[4] A proof is provided in Appendix iii.1.

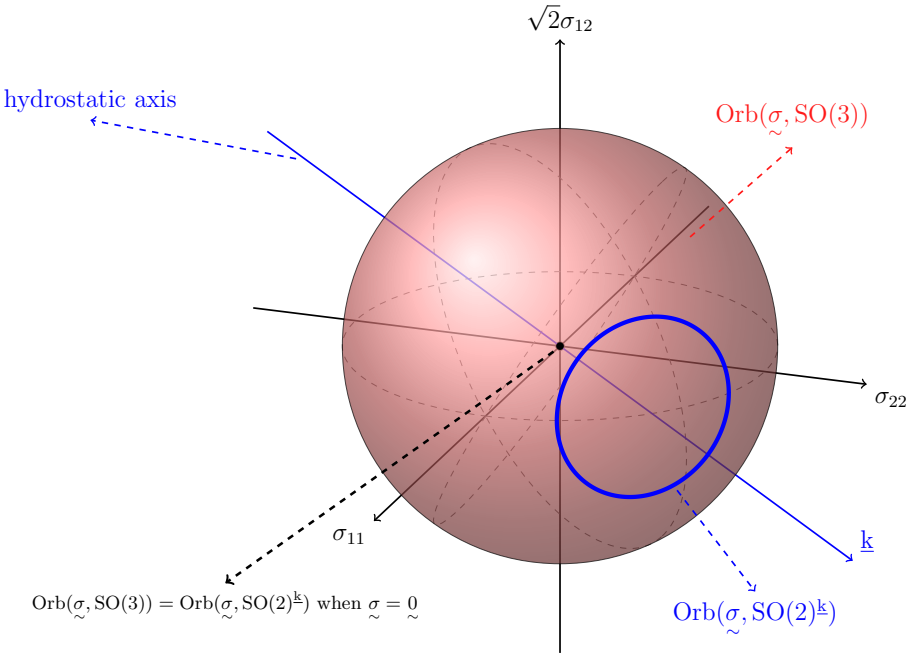

Figure 2.9: The inclusion of $\mathrm{Orb}(\underset{\sim}{\sigma}, \mathrm{SO}(2)^{\underline{\mathrm{k}}})$ in $\mathrm{Orb}(\underset{\sim}{\sigma}, \mathrm{SO}(3))$ in the stress space.

Polar parameterisation of stress tensor

Let us get back to the parameterisation of the stress tensors from an original diagonal one, i.e. $\underset{\sim}{\sigma}^* = \mathbf{r}(\theta) \star \underset{\sim}{\sigma}^0$. The vector form of $\underset{\sim}{\sigma}^*$ with respect to $\mathcal{K}$ is

$$\{\underset{\sim}{\sigma}^*\} = \begin{pmatrix} \sigma^*_{11} \\ \sigma^*_{22} \\ \sqrt{2}\sigma^*_{12} \end{pmatrix}_{\mathcal{K}} = \begin{pmatrix} \frac{1}{2}(\sigma_1 + \sigma_2 + (\sigma_1 - \sigma_2)\cos(2\theta)) \\ \frac{1}{2}(\sigma_1 + \sigma_2 - (\sigma_1 - \sigma_2)\cos(2\theta)) \\ \frac{\sqrt{2}}{2}(\sigma_1 - \sigma_2)\sin(2\theta) \end{pmatrix}_{\mathcal{K}}, \tag{2.21}$$

and we observe that for $\theta = 0$, the original diagonal form is retrieved. The orbit parameterisation can be expressed as

$$\{\underset{\sim}{\sigma}^*\} = \begin{pmatrix} \sigma_m + \sigma_{eq}\cos(2\theta) \\ \sigma_m - \sigma_{eq}\cos(2\theta) \\ \sqrt{2}\sigma_{eq}\sin(2\theta) \end{pmatrix}_{\mathcal{K}}. \tag{2.22}$$

where

$$\sigma_m = \frac{1}{2}(\sigma_1 + \sigma_2) = \frac{1}{2}I_1 \quad ; \quad \sigma_{eq} = \frac{1}{2}(\sigma_1 - \sigma_2) = \sqrt{\frac{J_2}{2}} \tag{2.23}$$

In this parametrisation $\theta \in [0, \pi[$ represents the orientation of $\underset{\sim}{\sigma}^*$ with respect to $\underset{\sim}{\sigma}$ in the diagonal form. It can be seen that σ_m and σ_{eq} are O(2)-invariants related to the spherical and deviatoric part of the stress tensor. The form given by equation (2.22) is known as the *polar parametrisation* of $\underset{\sim}{\sigma}$ [43, 184].

Geometrically, in the stress space, consider a point C which coordinates with respect to Kelvin basis are $(\sigma^*_{11}, \sigma^*_{22}, \sqrt{2}\sigma^*_{12})$. The polar parametrisation of $\underset{\sim}{\sigma}^*$ has the geometric content depicted in figure 2.10. The coefficient σ_m is related to the length of the segment $[OB] = \sqrt{2}\sigma_m$ along the hydrostatic axis (red line) defined by the direction $(1, 1, 0)$. $\sqrt{2}\sigma_{eq}$ is the radius of the blue circle in the plane $(\mathbf{D})$ normal to the hydrostatic axis. The parameter 2θ represents the angle $\langle \widehat{\underline{\mathrm{BD}}, \underline{\mathrm{BC}}} \rangle$. The blue circle thus, represents the orbit of the stress tensor. In the orbit, we have two particular cases. When the value of θ is $k\pi$ and $\frac{\pi}{2} + k\pi$ $(k \in \{0, 1\})$, the point C touches the plane $\sigma_{12} = 0$. This indicates that we are in the diagonal form since no shear stress is present. Both cases represent a permutation of the principal stresses, this phenomenon is known as monodromy [17].

This representation evidences two interesting points:

- (i) when the orientation is changed by θ, we have a rotation of an angle of 2θ along the hydrostatic axis;
- (ii) in the stress space the hydrostatic axis and the deviatoric plane (the $\mathbf{D}$ plane) are perpendicular. It results an interesting basis (which we call harmonic basis) in which the deviatoric and spherical (or

hydrostatic) part of the stress tensor are orthogonal. This splitting is useful for parameterising threshold functions.

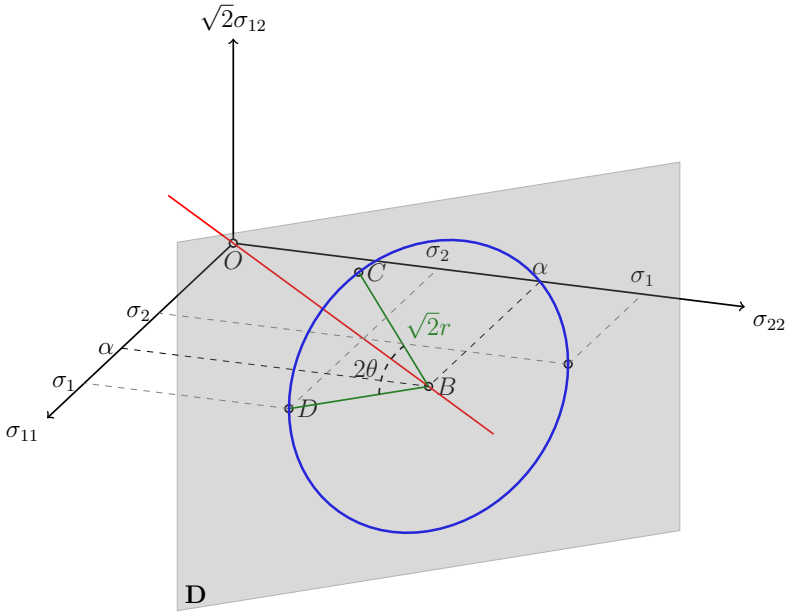

Figure 2.10: The geometric signification of polar parameterisation in the stress tensor space.

Harmonic basis

As a consequence of the previous observation, it is interesting to change the basis to a system compatible with the harmonic decomposition of $\underset{\sim}{\sigma}$. For this purpose we consider the orthonormal basis $\mathcal{H} = \{\hat{\underline{f}}_1, \hat{\underline{f}}_2, \hat{\underline{f}}_3\}$ defined as follows

$$\hat{\underline{f}}_1 = \frac{1}{\sqrt{2}}(\hat{\underline{e}}_1 - \hat{\underline{e}}_2) \quad ; \quad \hat{\underline{f}}_2 = \hat{\underline{e}}_3 \quad ; \quad \hat{\underline{f}}_3 = \frac{1}{\sqrt{2}}(\hat{\underline{e}}_1 + \hat{\underline{e}}_2). \tag{2.24}$$

with the following properties:

$$\mathbb{K}^2 = \text{span}\{\hat{\underline{f}}_1, \hat{\underline{f}}_2\}, \quad \mathbb{K}^0 = \text{span}\{\hat{\underline{f}}_3\}.$$

The change of basis results from the change of variables $(\sigma_{11}, \sigma_{22}, \sigma_{12}) \rightarrow (\sigma_{d_1}, \sigma_{d_2}, \sigma_h)$

$$\begin{cases} \sigma_{d_1} = \dfrac{\sigma_{11} - \sigma_{22}}{\sqrt{2}}, \\ \sigma_{d_2} = \sqrt{2}\sigma_{12}, \\ \sigma_h = \dfrac{\sigma_{11} + \sigma_{22}}{\sqrt{2}}. \end{cases}$$

leading to the passage matrix

$$[\mathrm{M}] = \begin{pmatrix} \frac{1}{\sqrt{2}} & -\frac{1}{\sqrt{2}} & 0 \\ 0 & 0 & 1 \\ \frac{1}{\sqrt{2}} & \frac{1}{\sqrt{2}} & 0 \end{pmatrix},$$

such as

$$\{\underset{\sim}{\sigma}\}_{\mathcal{H}} = [\mathrm{M}]\{\underset{\sim}{\sigma}\}_{\mathcal{B}}, \tag{2.25}$$

with

$$\{\underset{\sim}{\sigma}\}_{\mathcal{H}} = \begin{pmatrix} \sigma_{d_1} \\ \sigma_{d_2} \\ \sigma_h \end{pmatrix}_{\mathcal{H}}. \tag{2.26}$$

The harmonic basis is depicted in figure 2.11. In the harmonic basis, the orthogonality of the deviatoric part and the spherical part of the stress tensor is clear. Indeed, σ_h is directly related to σ_m (equation (2.10))

and σ_{d_1} and σ_{d_2} are the components of $\underset{\sim}{\sigma}^{(2)}$.

$$\{\underset{\sim}{\sigma}\} = \begin{pmatrix} \sigma_{d_1} \\ \sigma_{d_2} \\ \sigma_h \end{pmatrix}_{\mathcal{H}} = \begin{pmatrix} \sigma_{eq}\cos(2\theta) \\ \sigma_{eq}\sin(2\theta) \\ \sqrt{2}\sigma_m \end{pmatrix}_{\mathcal{H}}.$$

The polar parameterisation expressed in the harmonic basis corresponds to cylindrical coordinates:

$$\underset{\sim}{\sigma} = \sigma_{eq}\underbrace{\left(\cos(\Theta)\hat{\underline{f}}_1 + \sin(\Theta)\hat{\underline{f}}_2\right)}_{\hat{\underline{f}}_\Theta} + \sigma_h\hat{\underline{f}}_3 = \sigma_{eq}\hat{\underline{f}}_\Theta + \sigma_h\hat{\underline{f}}_3,$$

with $\Theta = 2\theta$. Any change in the orientation of the stress tensor means a rotation along $\hat{\underline{f}}_3$. It is clear that the subgroup of $\mathrm{O}(3)$ which corresponds to the physical transformations of $\mathbb{R}^2$ is $\mathrm{O}(2)^{\hat{\underline{f}}_3}$.

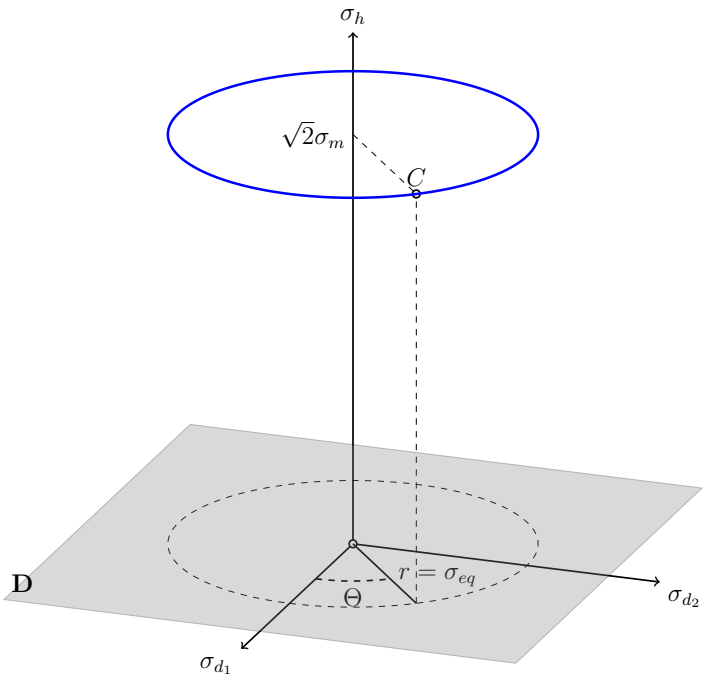

Figure 2.11: Representation of the orbit of $\underset{\sim}{\sigma}$ in harmonic cylindrical coordinates.

In this picture, the orbits with respect to the physical transformation are either points when the constraint is purely hydrostatic, or circles in the generic cases. The altitude of the orbit indicates the level of hydrostatic stress. Changing the sign of the hydrostatic stress is equivalent to taking the symmetric of the orbit with respect to the deviatoric plane.

This observation leads us to extend the set of transformations to include generalised transformations acting on the loading parameters. To that aim, introduce ρ the intensity of the loading. This quantity is the norm of $\underset{\sim}{\sigma}$ and correspond to the length of the stress vector in the $\mathbb{R}^3$ picture. In terms of $\mathrm{O}(2)$ invariants, we have $\rho = \frac{1}{2}\sqrt{I_1^2 + 2J_2}$. Introducing the loading angle φ defines as follows

$$\varphi = \arctan\frac{\sigma_h}{\sigma_{eq}},$$

the stress state is parameterised as follows

$$\begin{pmatrix} \sigma_{d_1} \\ \sigma_{d_2} \\ \sigma_h \end{pmatrix}_{\mathcal{H}} = \begin{pmatrix} \rho\sin(\varphi)\cos(2\theta) \\ \rho\sin(\varphi)\sin(2\theta) \\ \rho\cos(\varphi) \end{pmatrix}_{\mathcal{H}}. \tag{2.27}$$

It can be observed that

$$\underset{\sim}{\sigma} = \rho\left(\sin(\varphi)\cos(\Theta)\hat{\underline{f}}_1 + \sin(\varphi)\sin(\Theta)\hat{\underline{f}}_2 + \cos(\varphi)\hat{\underline{f}}_3\right) = \rho\hat{\underline{f}}_\rho.$$

In other words, it amounts to introducing spherical coordinates. The harmonic spherical coordinate system is illustrated in figure 2.12. Compared to the harmonic cylindrical coordinates (and to polar parametrisation), we have added another rotation in the stress space. The group of transformations on a vector in $\mathbb{R}^3$ is now the full orthogonal group[5] O(3). But its action can be reduced according to SO(3) according to the lemma 2.2.3.

In the present context, it is the set of transformations that lead from one state of stress to another state of equal intensity.

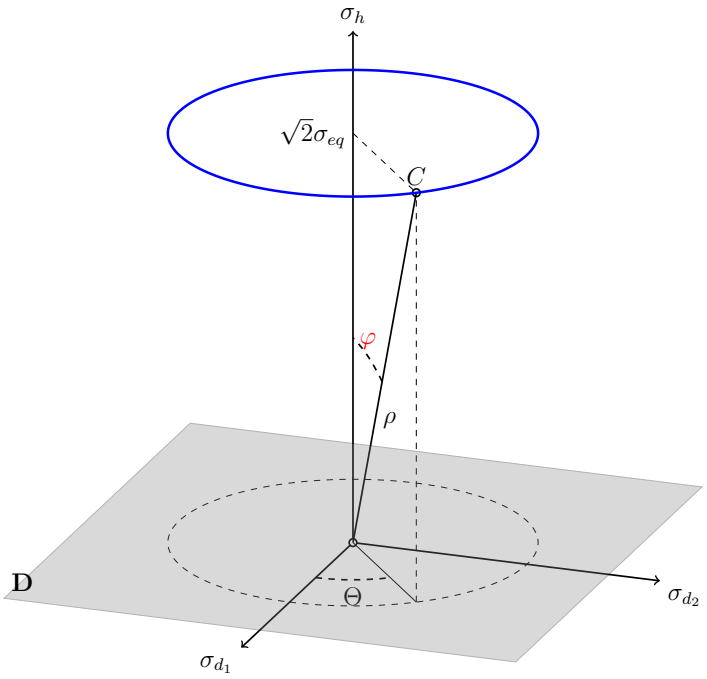

Figure 2.12: Representation of the harmonic basis (spherical coordinates).

Synthesis :
In the spherical parametrisation of $\underset{\sim}{\sigma}$ provided by equation (2.27):

- θ is associated to the physical orientation of the stress tensor;
- φ is the ratio of the hydrostatic stress to the shear stress
  - $\varphi = 0$: purely positive hydrostatic stress;
  - $\varphi = \dfrac{\pi}{2}$: purely deviatoric
  - $\varphi = \pi$: purely compressive hydrostatic state.

Remark 2.2.4. *The operation*

$$\underset{\sim}{\sigma} \to -\underset{\sim}{\sigma},$$

which corresponds to the inversion in $\mathbb{R}^3$ *is obtained by rotation of* π

$$\underset{\sim}{\sigma}(\theta, \phi) \to \underset{\sim}{\sigma}(\theta, \phi + \pi).$$

[5] In fact, it can be demonstrated that this action can be reduced to SO(3).

2.3 Threshold criterion theory in a nutshell

The transition of the behaviour of a material from elasticity to anelasticity occurs when the stress level reaches a critical state in the stress space[6]. The threshold point is mostly determined experimentally (tensile tests). The set of threshold points defines in $S^2(\mathbb{R}^2) \simeq \mathbb{R}^3$ a surface that will be denoted $\mathcal{S}$ and called the *threshold surface*.

2.3.1 Threshold surface

Consider $\mathcal{S}$ as a geometric object in $\mathbb{R}^3$, and denote by $\mathcal{P}(h)$ the intersection of $\mathcal{S}$ with the affine plane of equation $\sigma_h = h$. The symmetry group of the slice $\mathcal{P}(h)$ will be denoted $\mathcal{G}^{2D}_{\mathcal{P}(h)}$, it is conjugate to a subgroup of $\mathrm{O}(2)$. For $\mathcal{S}$, its symmetry group will be noted $\mathcal{G}_{\mathcal{S}}$, generally speaking

$$\mathcal{G}_{\mathcal{S}} := \{\mathbf{g} \in \mathrm{GL}(3) |\ \mathbf{g} \cdot \mathcal{S} = \mathcal{S}\}.$$

Physical information of various kinds is contained in $\mathcal{G}_{\mathcal{S}}$. From it we can obtain $\mathcal{G}^{3D}_{\mathcal{S}} = \mathcal{G}_{\mathcal{S}} \cap \mathrm{O}(3)$, which is the group of linear isometric transformations leaving the 3D surface invariant. It includes rotations, mirror symmetries, inversion and their products. As such $\mathcal{G}^{3D}_{\mathcal{S}}$ is conjugate to a closed subgroup of $\mathrm{O}(3)$.

This group characterises the overall symmetry of the surface, which includes both spatial anisotropy and load sensitivity. To study the spatial anisotropy of the criterion, cross-sections by planes parallel $\mathcal{P}(h)$ to the deviatoric plane need to be made. In this notation h indicates the value of the hydrostatic stress. Two notions will here be introduced and considered,

- $\mathcal{G}^{2D}_{\mathcal{P}(h)}$, it is the symmetry group (in $\mathbb{R}^2$) of the restriction of the threshold surface to the plane $\mathcal{P}(h)$. It characterises the spatial anisotropy associated to a certain level of hydrostatic stress.
- $\mathcal{G}^{2D}_{\mathcal{S}} = \bigcap_h \mathcal{G}^{2D}_{\mathcal{P}(h)}$, it is the intersection of the symmetry group of all the cross section of $\mathcal{S}$ by parallel deviatoric planes. It characterises the global anisotropy of the criterion. This group can also be characterises by the restriction to $\mathrm{O}(2) \in \mathbb{R}^2$ of
$$\mathcal{G}_{\mathcal{S}} \cap \mathrm{O}(2)^{(-,\hat{\underline{\mathrm{f}}}_3)},$$
and will be called the column symmetry group of $\mathcal{S}$.

The intensity of the stress is evaluated through a function F defined as follows:

$$\begin{aligned} F : S^2(\mathbb{R}^2) &\longrightarrow \mathbb{R}^+, \\ \underset{\sim}{\sigma} &\longrightarrow F(\underset{\sim}{\sigma}), \end{aligned} \tag{2.28}$$

F is the *equivalent stress function*[7]. Let us denote by $\sigma_{lim} \in \mathbb{R}^*_+$ the *threshold stress*. The surface $\mathcal{S}$ in the stress space is the level set $F^{-1}(\sigma_{lim})$:

$$\mathcal{S} = \left\{ \underset{\sim}{\sigma} \in S^2(\mathbb{R}^2), F(\underset{\sim}{\sigma}) - \sigma_{lim} = 0 \right\}.$$

As long as $F < \sigma_{lim}$ the material is in its elasticity domain, when $F = 0$ the system is at the boundary of its elasticity domain and we have a transition to another behaviour such us plasticity, damage, buckling ... etc.

Depending on the experimental observations, one can specify different additional properties to be satisfied by F:

- insensitivity to hydrostatic pressure:
$$\frac{\partial F}{\partial \sigma_h} = 0,$$
in such a case the transformation
$$\mathbf{g} = \mathbf{I} + \lambda \hat{\underline{\mathrm{f}}}_3 \otimes \hat{\underline{\mathrm{f}}}_3,$$
for $\lambda \neq 0$ belongs to $\mathcal{G}_{\mathcal{S}}$. The surface $\mathcal{S}$ is a cylinder along $\hat{\underline{\mathrm{f}}}_3$.
- symmetry with respect to the reversal of the load :
$$F(-\underset{\sim}{\sigma}) = F(\underset{\sim}{\sigma}), \forall \underset{\sim}{\sigma} \in S^2(\mathbb{R}^2).$$

[6] It should be noted that most of the examples come from work on plasticity. Interesting reviews related to plasticity can be found in [20, 150]. In the context of plasticity additional constraints can be placed on the threshold functions, notably convexity criteria. These restrictions will not be considered in the following discussion.

[7] It should be noted that the equivalent constraint function as defined is not a norm. A norm should verify the property that $\|\underset{\sim}{\sigma}\| = 0 \Rightarrow \underset{\sim}{\sigma} = 0$. This property is not verified by, for example, the equivalent Von-Mises constraint function.

In such a case the transformation[8] $\mathbf{i}_3$ belongs to $\mathcal{G}_\mathcal{S}$. The surface $\mathcal{S}$ is centrosymmetric.

- the maximum order of discrete rotational invariance which can be described as anisotropic by F.

The previous examples illustrate 3 types of invariance of different nature. The first one concerns the choice of the model, the second one concerns the invariance with respect to the loading while the last one concerns the anisotropy of the material. We will not go back to the first type of invariance here, and before looking in detail at the anisotropy we will characterise the invariances associated with mechanical loading.

2.3.2 Relation with the material symmetry group

It is important to observe that, even if related to the anisotropy of the material, the symmetry group $\mathcal{G}^{2D}_{\mathcal{P}(h)}$ of a slice of $\mathcal{S}$ is not the physical symmetry group $\mathrm{G}_\mathcal{P}$.

Indeed the azimuthal angle Θ of the surface is twice the physical angle θ, parameterised with respect to this angle the surface covers only the angular sector $[0, \pi]$. To obtain the complete surface, and to read the anisotropy of physical properties, it is necessary to add the angular sector $[\pi, 2\pi]$, that is to consider two periods instead of one. This is illustrated graphically in figure 2.13. In fact any symmetry of order n observed on any slice corresponds to a physical invariance of $2n$.

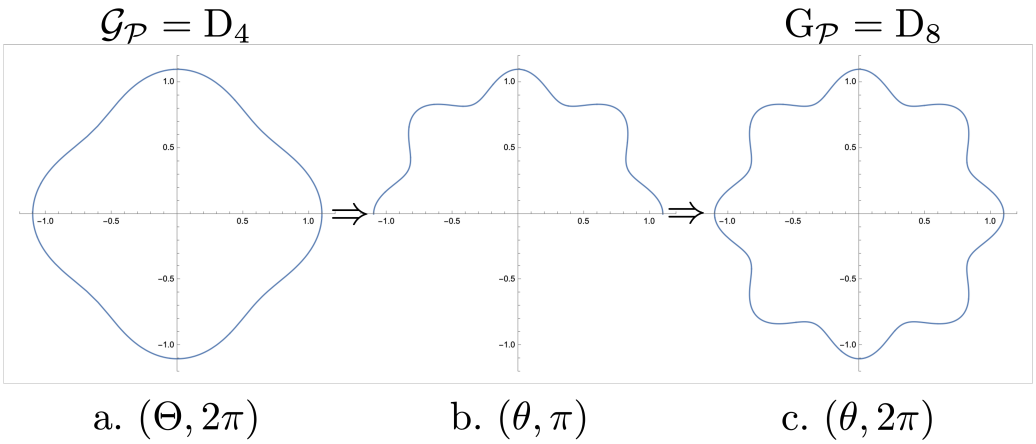

Figure 2.13: The symmetry group of the slice is half the symmetry group of the physical property

The symmetry group of the material and the symmetry group of a cross-section are related by the Currie-Neumann principle, which states that :

$$\mathrm{G}_\mathcal{M} \subset \mathrm{G}_\mathcal{P}.$$

To be more precise, we have the following property

$$\mathrm{Z}_n \subset \mathrm{G}_\mathcal{M} \Rightarrow \begin{cases} \mathrm{Z}_{n/2} \subset \mathcal{G}_\mathcal{P}, \ n = 2p \\ \mathrm{Z}_n \subset \mathcal{G}_\mathcal{P}, \ n = 2p+1 \end{cases}$$

This means, for example, that a material with hexagonal symmetry will have a threshold surface with an axis of invariance in rotation of order 3. Note that a material with 3rd order rotational symmetry will also have a surface with a 3rd order rotational invariance axis.

2.3.3 Invariance with respect to $\mathrm{O}(3)$

$$\mathcal{G}^{3D}_\mathcal{S} := \{\mathbf{g} \in \mathrm{O}(3) | \ \mathbf{g} \cdot \mathcal{S} = \mathcal{S}\}.$$

It is the group of linear isometries of $\mathcal{S}$. It includes rotations, mirror symmetries, inversion and their products. As such $\mathcal{G}^{3D}_\mathcal{S}$ is conjugate to a closed subgroup of $\mathrm{O}(3)$.

To characterise the geometry of the threshold surface, the following transformations are important

1. For the anisotropy

[8] $\mathbf{i}_3$ denotes the inverssion in $\mathbb{R}^3$, i.e. the transformation which matrix representation is

$$[\mathbf{i}_3] = \begin{pmatrix} -1 & 0 & 0 \\ 0 & -1 & 0 \\ 0 & 0 & -1 \end{pmatrix}.$$

(a) $\mathbf{i}_2 = \mathbf{r}(\pi, \hat{\underset{\sim}{\mathrm{f}}}_3)$, the in-plane inversion[9];

(b) $\boldsymbol{\pi}(\hat{\underset{\sim}{\mathrm{f}}}_2)$, in-plane miror symmetry;

2. For the loading

(a) $\boldsymbol{\pi}(\hat{\underset{\sim}{\mathrm{f}}}_3)$, the mirror symmetry with respect to the deviatoric plane, i.e. the operation that changes the sign of the hydrostatic stress:

$$(\underset{\sim}{\sigma}^{(2)}, \sigma_h) \to (\underset{\sim}{\sigma}^{(2)}, -\sigma_h),$$

(b) $\mathbf{i}_3$, the inversion, i.e. the operation that change the sign of $\underset{\sim}{\sigma}$:

$$\underset{\sim}{\sigma} \to -\underset{\sim}{\sigma}.$$

The inversion can result from the combination of the in-plane centro symmetry and $\boldsymbol{\pi}(\hat{\underset{\sim}{\mathrm{f}}}_3)$.

To be more specific we should now introduce definitions relative to the closed subgroups of O(3). Classification of O(3)-closed subgroups is classical [100, 176]. Following Golubitsky and al. [83], O(3)–closed subgroups can be described using *three types of subgroups*. These subgroups are defined as follows, where $\mathbf{e}$ is the neutral element in O(3):

Type I (Chiral) A subgroup Γ is of type I if it is a subgroup of SO(3). Type I subgroups are also said to be *chiral* subgroups;

Type II (Centrosymmetric) A subgroup Γ is of type II if $\mathbf{i} \in \Gamma$. In that case, $\Gamma = K \otimes \mathrm{Z}_2^c$ where K is some SO(3) closed subgroup and $\mathrm{Z}_2^c := \{\mathbf{e}, \mathbf{i}\}$. Type II subgroups are also said to be *centrosymmetric*

Type III A subgroup Γ is of type III if $\mathbf{i} \notin \Gamma$ and Γ is not a subgroup of SO(3).

To have a geometrical picture of these groups some illustrations are provided. In figures 2.15, 2.16 and 2.17, the geometries are invariant with respect to groups of type I, II and II are provided. On these figures:

- the rotational order of the invariance is indicated on the rotation axis (depicted with an arrow);
- symmetry planes are indicated in solid lines and without arrow;
- arrows drawn on the figures indicate the *spin* of the object. The presence of spin is due to chirality.

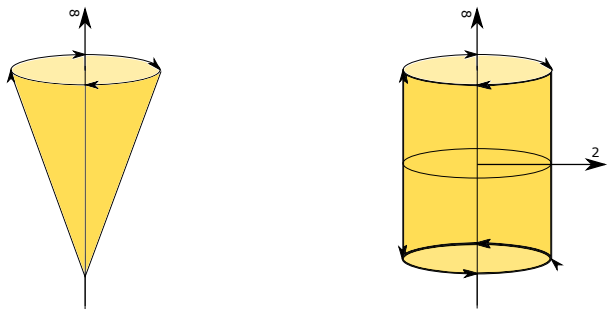

(a) a (b) b

Figure 2.14: Type I invariant figures: (A) is SO(2)-invariant, while (B) is O(2)-invariant.

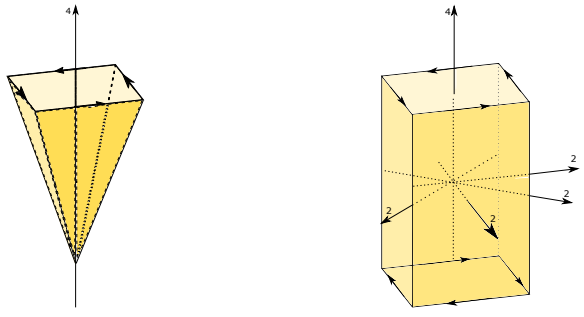

(a) (b)

Figure 2.15: Type I invariant figures: (A) non regular oriented tetrahedron, Z_4-invariant (Chiral and Polar), while (B) non cubic twisted rectangular parallelepiped, D_4-invariant (Chiral).

[9] Attention due to the doubling of the angle, the in-plane centro-symmetry corresponds to a rotation of angle $2\theta = \pi$, thus to material invariance by rotation of $\theta = \frac{\pi}{2}$

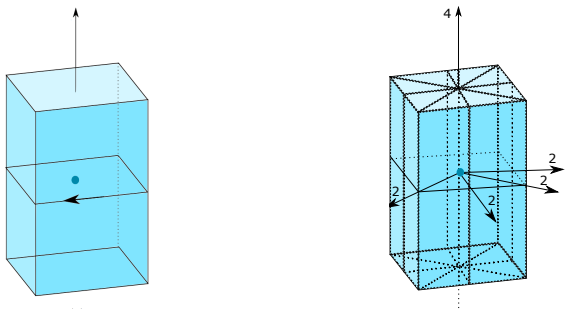

(a) (b)

Figure 2.16: Different invariant figures of Type II: (A) is $Z_4 \otimes Z_2^c$-invariant, while (B) is $D_4 \otimes Z_2^c$-invariant. The central inversion is indicated by a dot.

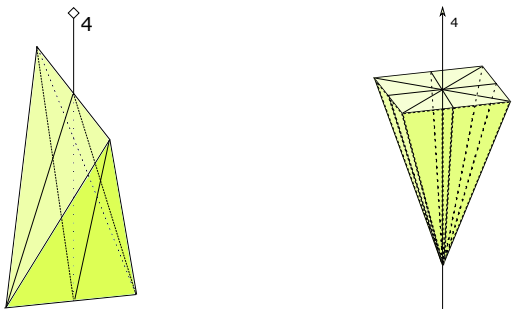

(a) (b)

Figure 2.17: Type III invariant figures: (A) non regular tetrahedron, Z_4^--invariant, while (B) is D_4^v-invariant (Polar). The diamond shape indicates an axis of rotoinversion.

From a physical point of view:

Type I (Chiral) The surface $\mathcal{S}$ does not posses mirror symmetries, nor centrosymmetry. The threshold surface is asymmetric in traction compression. No type I threshold surface seems to have been identified in the literature so far;

Type II (Centrosymmetric) The surface $\mathcal{S}$ is centrosymmetric but may not necessary possess symmetry planes. The threshold surface is symmetric in traction compression; classical symmetric threshold functions always possess a type II symmetry group;

Type III The surface $\mathcal{S}$ is not centrosymmetric but possess symmetry planes. The threshold surface is asymmetric in traction compression; classical asymmetric threshold functions are of type III.

Let us consider some examples.

2.3.4 Geometric analysis of some criteria

Cazacu isotropic criterion

Let us take up the isotropic criterion of Cazacu as it has been introduced section 1.1.2.

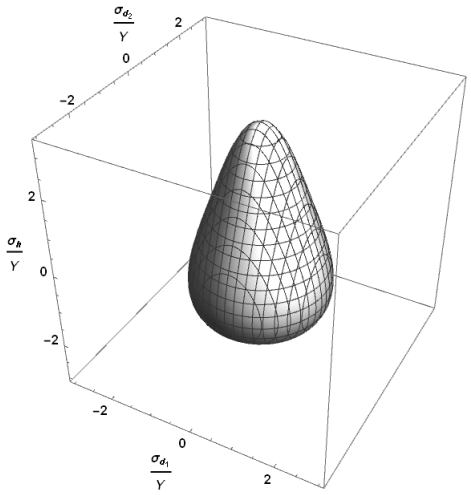

Figure 2.18: Threshold surface defined an example of cazacu's criterion

The criterion is isotropic as can be observed in figure 2.19 on any cut of the surface by plane

$$\sigma_h = k.$$

Hence, for all k, $\mathcal{G}^{2D}_{\mathcal{P}(k)} = \mathrm{O}(2)$ and $\mathcal{G}^{2D}_{S} = \mathrm{O}(2)$.

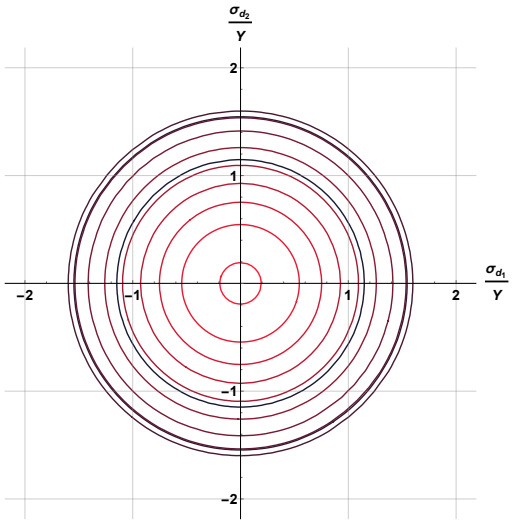

Figure 2.19: The projections of Cazacu's threshold surface on the deviatoric plane from bottom (black) to the above level (red).

Other cuts of the surface are given on the following figure:

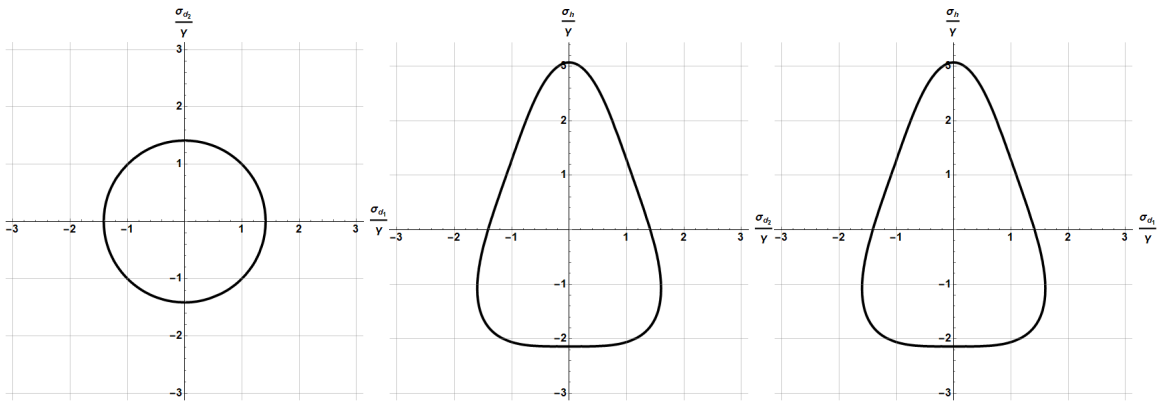

(a) The plane $\sigma_h = 0$. (b) The plane $\sigma_{d_1} = 0$. (c) The plane $\sigma_{d_2} = 0$.

Figure 2.20: Cut of the Cazacu's surface along different relevant planes

As the criterion is asymmetric, the surface is not centro-symmetric, but it has vertical planes of symmetry (the criterion is achiral). The symmetry group of the surface is therefore type III, more precisely

$$\mathcal{G}_S^{3D} = \mathrm{O}(2)^-.$$

A precise description of this group and its generators can be found in the section iii of appendix A.

Soare's Poly4 anisotropic criterion

Consider now a the symmetric anisotropic fourth-order polynomial criterion introduced in chapter 1 section 1.2.2. Consider the threshold surface (yield surface) corresponding to the AA2090-T3 alloy [166]:

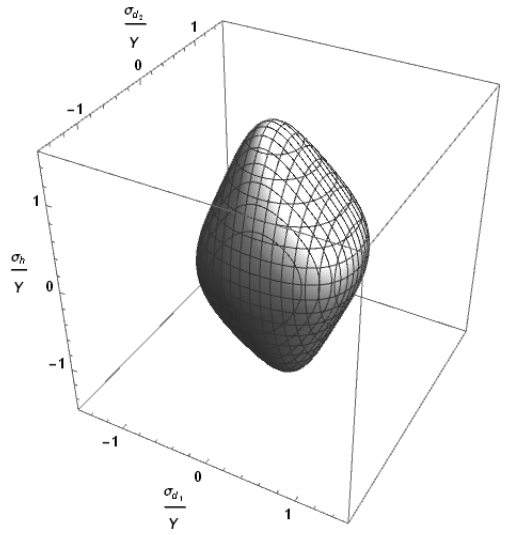

Figure 2.21: The threshold surface corresponding to Poly4 criterion for AA2090-T3 alloy [166].

The different sections of $\mathcal{S}$ by parallel planes are drawn on the figure below

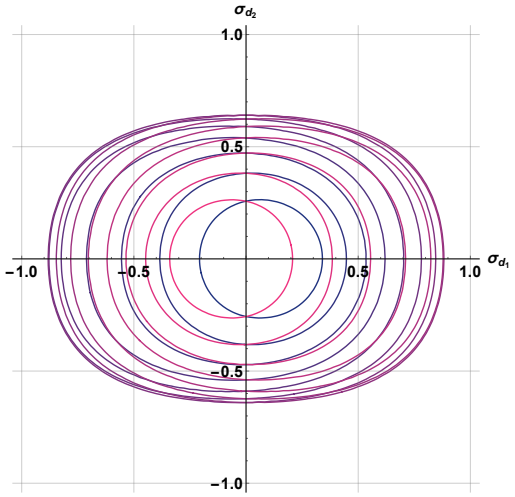

Figure 2.22: The projections of Poly4 threshold surface on the deviatoric plane from bottom (black) to the above level (red).

The symmetry groups of the different slices are

$$\mathcal{G}_{\mathcal{P}(k)}^{2D} = \begin{cases} \mathrm{Z}_2^{\pi}, & k \neq 0; \\ \mathrm{D}_2, & k = 0. \end{cases}$$

Hence $\mathcal{G}_S^{2D} = \mathrm{Z}_2^{\pi}$. The rotation order of the physical invariance being twice the rotation order of $\mathcal{G}^{2D}$ the criterion is globally orthotropic. For $\sigma_h = 0$, the situation is degenerated and the criterion appears as tetragonal for this loading. This situation is clear on the following slices:

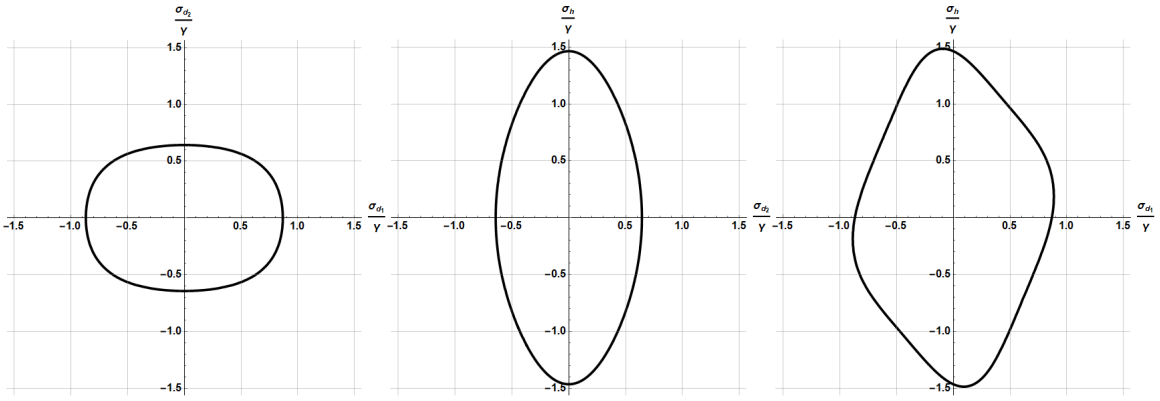

(a) The plane $\sigma_h = 0$. (b) The plane $\sigma_{d_1} = 0$. (c) The plane $\sigma_{d_2} = 0$.

Figure 2.23: The cuts of the threshold surface corresponding to Poly4 criterion for AA2090-T3 alloy along different relevant planes.

The criterion is symmetric, the surface is centro-symmetric and possess a vertical plane of symmetry (the criterion is achiral). The symmetry group of the surface is therefore of type II, more precisely

$$\mathcal{G}_S^{3D} = \mathrm{D}_2 \otimes \mathrm{Z}_2^c.$$

A precise description of this group and its generators can be found in the section iii of appendix A.

Wang's anisotropic criterion

Consider the Wang criterion for equilateral triangular 2D lattice as introduced in section 1.3.2. The following surface is obtained for a relative density of 0.15.

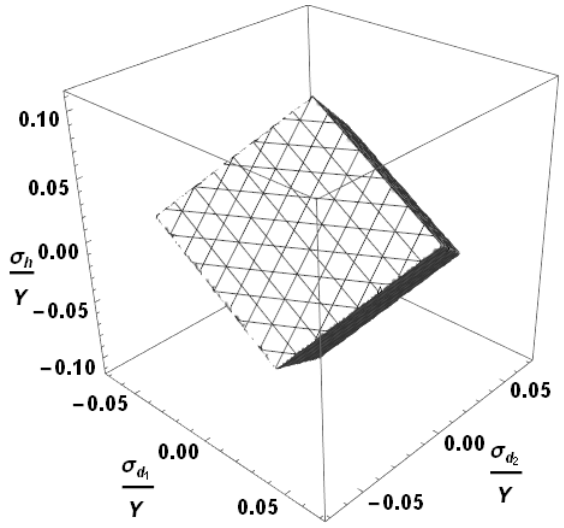

Figure 2.24: The threshold surface of equilateral triangular 2D lattice [188].

The different sections of $\mathcal{S}$ by parallel planes are drawn on the figure below

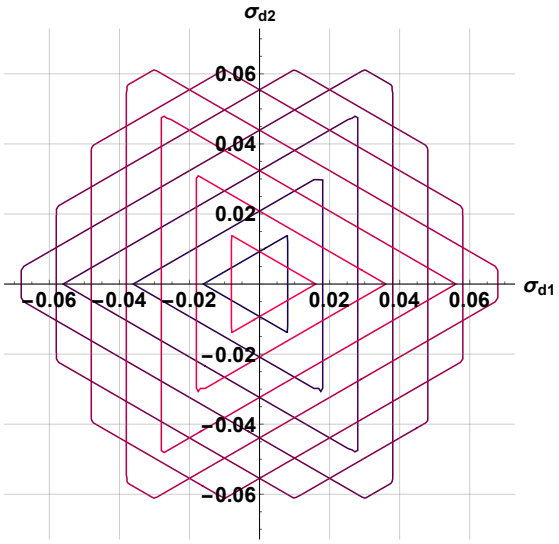

Figure 2.25: The projections of Wang et al. threshold surface on the deviatoric plane from bottom (black) to the above level (red).

The symmetry groups of the different slices are

$$\mathcal{G}^{2D}_{\mathcal{P}(k)} = \begin{cases} \mathrm{D}_3, & k \neq 0; \\ \mathrm{D}_6, & k = 0. \end{cases}$$

Hence $\mathcal{G}^{2D}_S = \mathrm{D}_3$. The rotation order of the physical invariance being twice the rotation order of $\mathcal{G}^{2D}$ the criterion is globally D_6. For $\sigma_h = 0$, the situation is degenerate and the criterion appears as D_{12} for this loading. This situation is clear on the following slices:

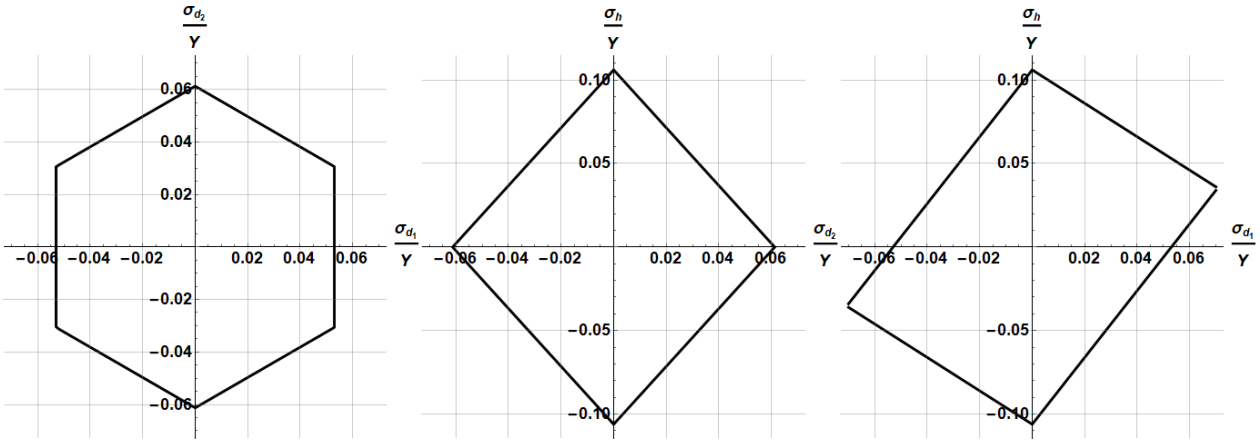

(a) The plane $\sigma_h = 0$. (b) The plane $\sigma_{d_1} = 0$. (c) The plane $\sigma_{d_2} = 0$.

Figure 2.26: The cuts of the threshold surface of equilateral triangular 2D lattice [188] along different relevant planes.

The criterion is symmetric, the surface is centro-symmetric and possess a vertical plane of symmetry (the criterion is achiral). The symmetry group of the surface is therefore of type II, more precisely

$$\mathcal{G}^{3D}_S = \mathrm{D}_3 \otimes \mathrm{Z}^c_2.$$

A precise description of this group and its generators can be found in the section iii of appendix A.

Remark 2.3.1. *These examples reveal an interesting general property. Surfaces whose symmetry group is of the type* $\mathrm{Z}_{2p+1} \otimes \mathrm{Z}^c_2$ *or* $\mathrm{D}_{2p+1} \otimes \mathrm{Z}^c_2$ *have a column symmetry group* $\mathcal{G}^{2D}_S$ *of type* Z_{2p+1} *or* D_{2p+1}*. However the section with* $\sigma_h = 0$ *has a symmetry group for which the rotation order is double i.e.* $\mathcal{G}_{\mathcal{P}(0)} = \mathrm{Z}_{2(2p+1)}$ *or* $\mathrm{D}_{2(2p+1)}$*. We see this phenomenon in the case of Soare's Poly4 criterion (cf. fig.3.17.(a)) as well as Wang's (cf. fig.3.18.(a)). The reason for this is simple, the restriction of the inversion* $\mathbf{i}_3$ *to the plane* $\sigma_h = 0$ *is the rotation of order 2 in this plane. This invariance applied to a figure which is non-centro symmetric in the plane, will double the order of its rotation. This is particularly noticeable on the Wang surface, whose cross-section is generally triangular, with the exception of the* $k = 0$ *cross-section, for which the intersection is hexagonal.*

Jeanneau's anisotropic criterion

Consider the Jeanneau criterion for equilateral triangular 2D lattice introduced section 1.3.4 for which insatiability in compression has been considered. The lattice is made of aluminium with of walls of length $l = 10mm$ and thickness $t = 1mm$. The obtained threshold surface (in the strain space) is illustrated in the following figure.

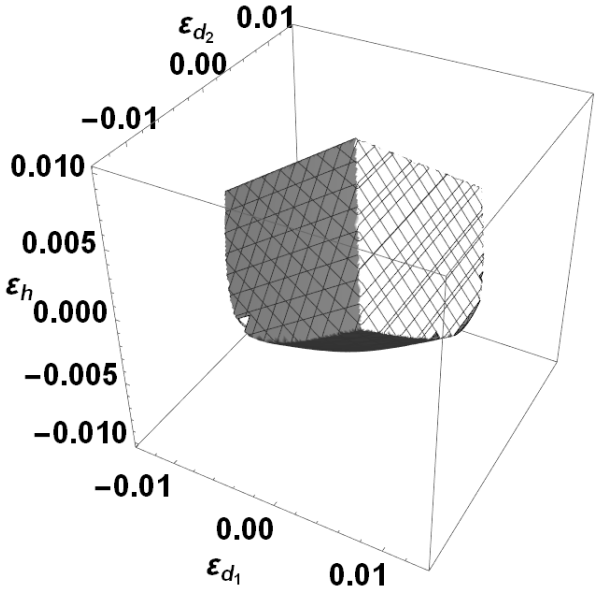

Figure 2.27: The threshold surface of the a equilateral triangular lattice considering the buckling [103].

The different sections of $\mathcal{S}$ by parallel planes are drawn on the figure below

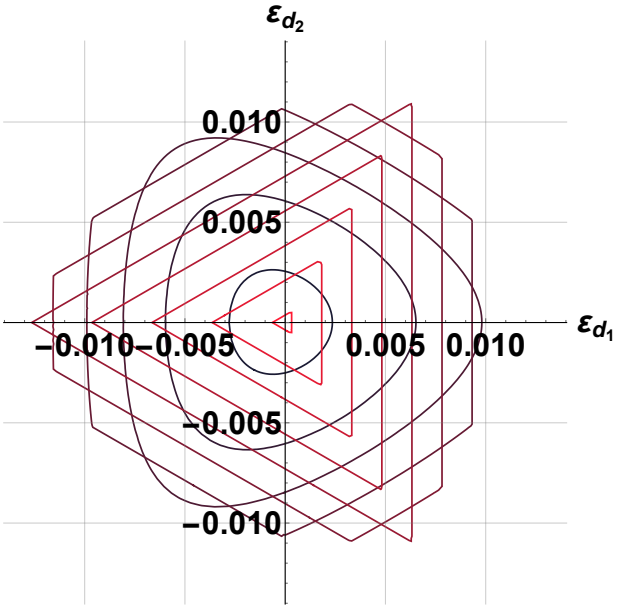

Figure 2.28: The projections og the threshold surface of the a triangular lattice on the deviatoric plane from bottom (green) to the above level (orange). [103].

This shows that the central symmetry is broken by the change of failure mechanism in tension and compression. The symmetry groups $\mathcal{G}^{2D}_{\mathcal{P}(k)}$ of the different slices are D_3. The symmetry group of the $\sigma_h = 0$ slice, i.e. $\mathcal{G}_{\mathcal{P}(0)}$, does not present any particularity for the current surface. Different cuts are represented on the figure below:

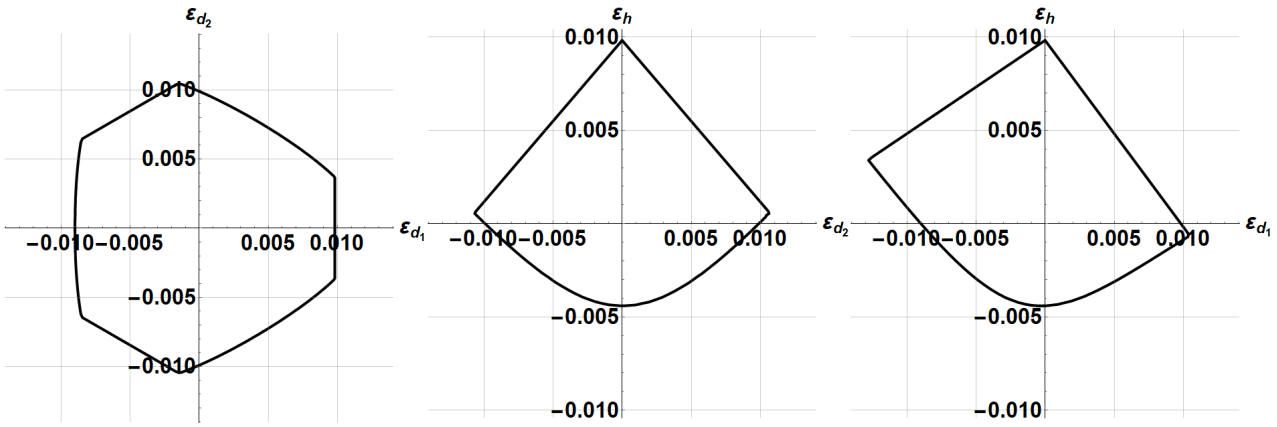

(a) The plane $\epsilon_h = 0$. (b) The plane $\epsilon_{d_1} = 0$. (c) The plane $\epsilon_{d_2} = 0$.

Figure 2.29: The cut threshold surface of the equilateral triangular 2D lattice [103] in the relevant planes.

The criterion is asymmetric, the surface possess three vertical planes of symmetry (the criterion is achiral). The symmetry group of the surface is therefore of type III, more precisely

$$\mathcal{G}_S^{3D} = \mathrm{D}_3^v.$$

A precise description of this group and its generators can be found in the section iii of appendix A.

2.4 Anisotropic threshold function

This last subsection is devoted to the explicit modelling of an anisotropic polynomial threshold criterion. In a first time the central notion of G−equivariant map will be introduced [83]. This notion is also known as the *Principle of Isotropic of Space* [33] or *Principle of Material Indifference* [182]. We will first particularised this notion to the case of isotropic functions to retrieve the classical results. We will move, in a second time, to the case of anisotropic functions which motivate our study. The different strategies used in the literature to model anisotropic functions will be reviewed and compared. It will be shown that in the case of polynomial function F, the order of anisotropy to consider fixes the minimal degree of the polynomial in $\underset{\sim}{\sigma}$.

2.4.1 G−equivariant map

Let $\mathbb{V}$ and $\mathbb{W}$ two vector spaces on which the group G acts and consider a map ϕ between these spaces [137]:

$$\begin{aligned} \phi\colon \mathbb{V} &\longrightarrow \mathbb{W} \\ \mathbf{u} &\longmapsto \mathbf{v} = \phi(\mathbf{u}) \end{aligned}$$

The map ϕ is said G−equivariant if[10]

$$\forall \mathbf{g} \in \mathrm{G},\ \phi(\mathbf{g} \overset{\mathbb{V}}{\star} \mathbf{u}) = \mathbf{g} \overset{\mathbb{W}}{\star} \phi(\mathbf{u})$$

which means that the following diagram commutes $\forall \mathbf{g} \in \mathrm{G}$,

$$\begin{array}{ccc} \mathbf{u} \in \mathbb{V} & \xrightarrow{\phi} & \mathbf{v} \in \mathbb{W} \\ \Big\downarrow{\scriptstyle \mathbf{g}} & & \Big\downarrow{\scriptstyle \mathbf{g}} \\ \overline{\mathbf{u}} & \xrightarrow{\phi} & \overline{\mathbf{v}} \end{array}$$

when obvious from the context the notation $\overset{\mathbb{W}}{\star}$ is simplified as $\star$.

Particular case $\mathbb{W} = \mathbb{R}$

A particular interest is the situation for which $\mathbb{W} = \mathbb{R}$, in this case the action $\overset{\mathbb{W}}{\star}$ reduces to the identity and the equiavriance property G is expressed by

$$\forall \mathbf{g} \in \mathrm{G},\ \phi(\mathbf{g} \star \mathbf{u}) = \phi(\mathbf{u})$$

In the context of mechanics the function ϕ is said to be G-invariant for $\mathrm{G} < \mathrm{O}(2)$, and simply invariant or isotropic if $\mathrm{G} = \mathrm{O}(2)$.

[10] The notation $\overset{\mathbb{U}}{\star}$ underlines the fact that the action depends on the space considered.

Principle of Isotropy of Space

This principle can be formulated as follows. The ambient space being isotropic, the mechanical fields resulting from an experiment do not intrinsically depends on the specific orientation of the experiment setting in space.

We consider a tensor-valued function $\mathbf{T}$ depending on 2 arguments, the first argument indicating the value of a field $\mathbf{A}$, the second describing the orientation of the material $\mathbf{M}$.

$$\mathbf{T} = \phi(\mathbf{A}, \mathbf{M})$$

The principle of isotropy of space indicates that this function is O(2)-equivariant.

$$\forall \mathbf{g} \in \mathrm{O}(2),\ \phi(\mathbf{g} \star \mathbf{A}, \mathbf{g} \star \mathbf{M}) = \mathbf{g} \star \mathbf{T}$$

That is, if the argument tensor and the material are rotated, the resulting tensor will be rotated in a concordant manner

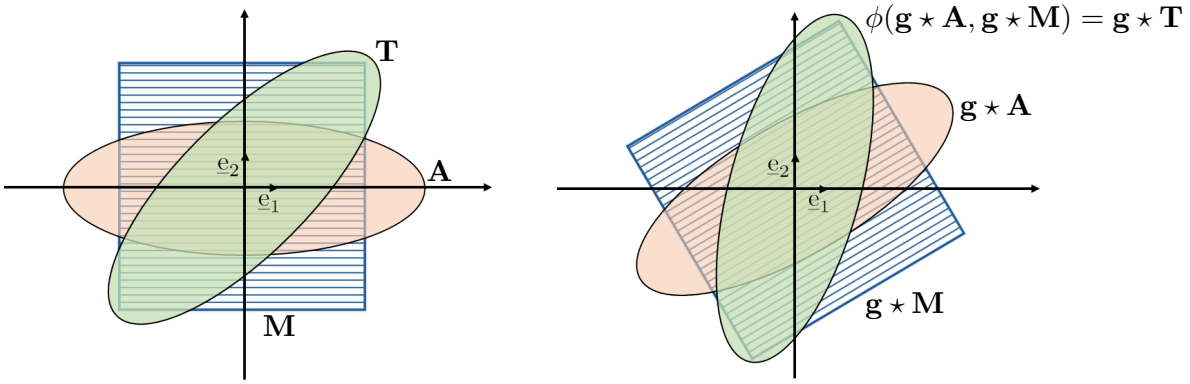

Figure 2.30: Isotropy of space, transforming both the material (in blue) and the physical source field (in red) in the same way transform the physical response field (in green) by the same transformation.

Anisotropy

When studying the anisotropy of a physical property, we are interested in the variation of $\mathbf{T}$ when either

- $\mathbf{M}$ is transformed relatively to $\mathbf{A}$, i.e.
$$\overline{\mathbf{T}} = \phi(\mathbf{g} \star \mathbf{A}, \mathbf{M})$$
- $\mathbf{A}$ is transformed relatively to $\mathbf{M}$, i.e.
$$\overline{\mathbf{T}} = \phi(\mathbf{A}, \mathbf{g} \star \mathbf{M})$$

The choice of one transformation over the other is a matter of point of view, what is important is that is testing the consequence of the transformation of one field relatively to the others.

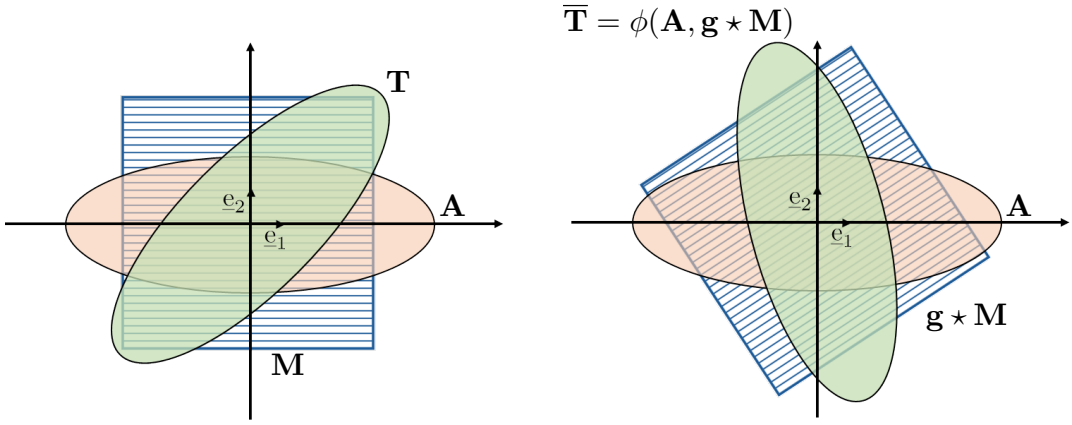

Figure 2.31: Anisotropy, on fixe chargement on tourne materiau

2.4.2 Isotropic threshold criterion

In the context of threshold functions $\mathbb{V} = S^2(\mathbb{R}^2)$ and $\mathbb{W} = \mathbb{R}$. The definition of an isotropic threshold function F is:

$$\forall g \in \mathrm{O}(2), \quad F(\mathbf{g} \star \underset{\sim}{\sigma}) = F(\underset{\sim}{\sigma}). \tag{2.29}$$

Isotropic threshold functions are generally used for elastically isotropic materials. But basically nothing prevents an elastically isotropic material from having an anisotropic plasticity limit. Only experiments can determine this. Referring to the geometric framework introduced in section 2.2.2, equation (2.29) means that isotropic functions are constant on O(2)-orbits. Since, as depicted on figure 2.10, generic orbit intersects the vector space of symmetric matrices in two points, F depends on the eigenvalues of $\underset{\sim}{\sigma}$ through elementary symmetric polynomials[11]

$$F(\underset{\sim}{\sigma}) = f(I_1, I_2)$$

with $I_1 = \sigma_1 + \sigma_2$, and $I_2 = \sigma_1\sigma_2$. Further, since being able to separate the orbit of $S^2(\mathbb{R}^2)$, any integrity basis is also a functional basis and can serve as a basis for constructing non-polynomial invariant functions [33, 147].

2.4.3 Anisotropic threshold criterion

Let us consider now the case of an anisotropic threshold function. Anisotropic functions are H-invariant functions for H a closed subgroup of O(2), i.e

$$\forall \mathbf{g} \in H, \quad F(\mathbf{g} \star \underset{\sim}{\sigma}) = F(\underset{\sim}{\sigma}). \tag{2.30}$$

From a physical point of view, the group H correspond to $\mathrm{G}_{\mathcal{M}}$ the material symmetry group[12]. Unlike isotropic functions, anisotropic functions depend on the orientation of $\underset{\sim}{\sigma}$ with respect to specific material directions. The function F is no more constant over the orbits but is still π-periodic.

In the literature, different strategies are used to model anisotropic threshold functions, we can mention :

1. Representation theorems [33, 204];
2. Tensor polynomial functions [167].
3. Linear transformations [27];

The the first two approaches are closely related and will be presented and discussed below. The third approach will not be discussed further, and we refer the interested reader to the references already mentioned. The results of this section will form the basis for the modelling choices made and developed in the next chapter.

It should be noted that most of the examples come from work on plasticity. Interesting reviews related to plasticity can be found in [20, 150]. In the context of plasticity additional constraints can be placed on the threshold functions, notably convexity criteria. These restrictions will not be considered in the following discussion.

Group representation theorems

The most rigorous and versatile approach to anisotropic threshold function is to use group representation theory [33, 204].

Consider an anisotropic material which material symmetry group $\mathrm{G}_{\mathcal{M}} = \mathrm{H}$, with $\mathrm{H} < \mathrm{O}(2)$. Consider also a collection of tensors $\mathbf{M}_k$ such as $\bigcap_k \mathrm{G}_{\mathbf{M}_k} = \mathrm{H}$. The tensors $\mathbf{M}_k$ belonging to this collection are referred to as *Structure Tensors* [204].

The key property is the following one based on the equivariance properties discussed above.

Proposition 2.4.1. *Any* H*-invariant function*

$$\forall \mathbf{g} \in \mathrm{H}, \quad F(\mathbf{g} \star \underset{\sim}{\sigma}) = F(\underset{\sim}{\sigma}). \tag{2.31}$$

can be reformulated as an O(2)*-invariant function using a collection of tensors* $\mathbf{M}_k$ *such that* $\bigcap_k \mathrm{G}_{\mathbf{M}_k} = \mathrm{H}$ *and satisfying*

$$\forall \mathbf{g} \in \mathrm{O}(2), \quad \hat{F}(\mathbf{g} \star \underset{\sim}{\sigma}, \mathbf{g} \star \mathbf{M}_k) = \hat{F}(\underset{\sim}{\sigma}, \mathbf{M}_k). \tag{2.32}$$

[11] Obviously, any integrity basis equivalent to (I_1, I_2) can be used, for instance the basis (I_1, J_2).

[12] The material is supposed to be homogeneous and hence the symmetry group do not depend on the choice of particular point.

Proof. The equivalence is as follows. When studying anisotropy of F amounts to transforms the stress field while keeping the material unchanged.

$$F(\underset{\sim}{\sigma}, \mathbf{M}) \to F(\mathbf{g} \star \underset{\sim}{\sigma}, \mathbf{M})$$

If F is H-invariant,

$$\forall \mathbf{g} \in \mathrm{H}, \quad F(\mathbf{g} \star \underset{\sim}{\sigma}, \mathbf{M}) = F(\underset{\sim}{\sigma}, \mathbf{M})$$

Since $\mathrm{G}_{\mathbf{M}} = \mathrm{H}$, the last relation is equivalent to

$$\forall \mathbf{g} \in \mathrm{H}, \quad F(\mathbf{g} \star \underset{\sim}{\sigma}, \mathbf{g} \star \mathbf{M}) = F(\underset{\sim}{\sigma}, \mathbf{M})$$

which holds for any $\mathbf{g} \in \mathrm{O}(2)$ thanks to the *Isotropy of Space*.

Conversely consider the *Principle of Isotropy of Space*, for $\mathbf{g} \in \mathrm{G}_{\mathbf{M}} = \mathrm{H}$

$$\mathbf{g} \star \mathbf{M} = \mathbf{M}$$

and we obtain

$$\forall \mathbf{g} \in \mathrm{H}, \quad F(\mathbf{g} \star \underset{\sim}{\sigma}, \mathbf{M}) = F(\underset{\sim}{\sigma}, \mathbf{M})$$

□

Hence any anisotropic function of $\underset{\sim}{\sigma}$ can be reformulated as an isotropic function of $\underset{\sim}{\sigma}$ and structure tensors.

The next step is the use of representation theorems, that will be formulated here in the framework of polynomial invariant functions.

Theorem 2.4.2. *Let $\mathbb{V}$ be a real vector space, there exists a finite set $\mathcal{IB} = \{I_k\}$ of $\mathrm{O}(2)$-invariant polynomials, such that any $\mathrm{O}(2)$-invariant polynomial P on $\mathbb{V}$, is a polynomial with respect to the elements of $\mathcal{IB}$. The set $\mathcal{IB}$ is the* integrity basis *of $\mathbb{V}$ for the $\mathrm{O}(2)$-action.*

Let us sketch out a general methodology:

1. Consider a collection of tensors $\mathbf{M}_k$ such that $\bigcap_k \mathrm{G}_{\mathbf{M}_k} = \mathrm{H}$ and denote by $\mathbb{K}$ the space to which they belong;
2. The space $\mathbb{V}$ is then $\mathbb{V} = S^2(\mathbb{R}^2) \oplus \mathbb{K}$;
3. Compute the $\mathrm{O}(2)$-integrity basis $\mathcal{IB}$ of $\mathbb{V}$. In $\mathbb{R}^2$, we have a general algorithm to determine such a basis [61];
4. A H-invariant polynomial of degree n is a linear combination of monomials of degree n obtained from the elements of $\mathcal{IB}$.

One last point before closing this theoretical section and considering explicit examples, how to choose the collection of structure tensors $\mathbf{M}_k$ associated to a subgroup H of anisotropy ? In $\mathbb{R}^2$, the simplest choice will be to choose structure tensors as *harmonic tensors*.

Harmonic tensors

Harmonic tensors are the elementary building block of anisotropic tensors. For a more thorough introduction of harmonic tensor in $\mathbb{R}^2$, we refer to [16]. Their definition is as follows:

Definition 2.4.3. *Let $\mathbb{K}^n$ be the space of nth-order harmonic tensors in 2D, its elements are:*

1. *n-th order tensors: $K_{i_1 i_2 \dots i_n}$*
2. *symmetric with respect to the permutation of all the indices: $K_{(i_1 i_2 \dots i_n)}$*
3. *traceless*[13]*: $K_{(i_1 i_2 \dots i_p i_p)} = 0$*

[13] Since being completely symmetric all the traces of $\mathbf{K}$ are equivalent.

Harmonic tensor are the nth-order generalisation to the notion of a deviatoric tensor. Harmonic tensors have multiple interesting properties. Regarding their dimension, we have in $\mathbb{R}^2$

$$\dim \mathbb{K}^n = \begin{cases} 2, & n \geq 1; \\ 1, & n = \{0, -1\}. \end{cases}$$

O(2)-representation on harmonic tensors is very simple, for all $n \geq 1$, O(2)-action on $\mathbb{K}^n$ is given by ρ_n:

$$\rho_n(\mathbf{r}(\theta)) := \begin{pmatrix} \cos n\theta & -\sin n\theta \\ \sin n\theta & \cos n\theta \end{pmatrix}, \quad \rho_n(\boldsymbol{\pi}(\underset{\sim}{\mathrm{e}}_2)) := \begin{pmatrix} 1 & 0 \\ 0 & -1 \end{pmatrix}.$$

The O(2)-action on $\mathbb{K}^0$ is the identity and the O(2)-action on $\mathbb{K}^{-1}$ is given by the determinant of the transformation:

$$\rho_0(\mathbf{Q}) := 1, \qquad \rho_{-1}(\mathbf{Q}) := \det \mathbf{Q}. \tag{2.33}$$

Hence submitted to a rotation of θ, a harmonic tensor in $\mathbb{K}^{n>0}$ will turn at $n\theta$. Its results from this, the following results concerning the symmetry classes of harmonic tensors:

Theorem 2.4.4. *Let $\mathfrak{I}(\mathbb{K}^n)$ denotes the set of all isotropy classes associated to $\mathbb{K}^n$. The symmetry classes of $\mathbb{K}^n$ are:*

$$\mathfrak{I}(\mathbb{K}^n) = \begin{cases} n \geq 1, & \{[\mathrm{D}_n], [\mathrm{O}(2)]\} \\ n = -1, & \{[\mathrm{SO}(2)], [\mathrm{O}(2)]\} \\ n = 0, & \{[\mathrm{O}(2)]\} \end{cases}.$$

with the convention that $\mathrm{D}_1 = \mathrm{Z}_2^{\sigma_x}$.

This theorem is essential for our purposes. From it we can obtain the following result that define the needed collection of structure tensors $\mathbf{M}_k$ to describe any H-invariant function as an O(2)-invariant one:

Proposition 2.4.5. H *being a subgroup of* O(2)*, it is either of type* Z_n *or* D_n*. The space* $\mathbb{V}$ *to consider for computing the integrity basis of a* H*-invariant polynomial is*

- $\mathbb{V} = S^2(\mathbb{R}^2) \oplus \mathbb{K}^n$ *if* $\mathrm{H} = \mathrm{D}_n$*;*
- $\mathbb{V} = S^2(\mathbb{R}^2) \oplus \mathbb{K}^n \oplus \mathbb{K}^{-1}$ *if* $\mathrm{H} = \mathrm{Z}_n$*.*

Practical examples

Rather than being abstract, let's look at practical examples of how to apply the method. In the following example the notation $(\mathbf{T})_0$ stands for the generalised deviatoric part [61] of $\mathbf{T}$, i.e.

$$(\cdot)_0 : \mathbb{T}^n \mapsto \mathbb{K}^n$$

Example 1: Orthotropic threshold functions In $\mathbb{R}^2$, the group $\mathrm{D}_2^{\underline{\mathrm{n}}}$ can be characterised by the following structure tensor $\underset{\sim}{\mathrm{K}} = (\underline{\mathrm{n}} \otimes \underline{\mathrm{n}})_0 \in \mathbb{K}^2$. Without loss of generality, we will consider the case $\underline{\mathrm{n}} = \underline{\mathrm{e}}_1$ in what follows. In this case

$$\underset{\sim}{\mathrm{K}} \propto (\underline{\mathrm{e}}_1 \otimes \underline{\mathrm{e}}_1)_0 \propto \underline{\mathrm{e}}_1 \otimes \underline{\mathrm{e}}_1 - \underline{\mathrm{e}}_2 \otimes \underline{\mathrm{e}}_2$$

in which $\propto$ means *proportional to*. Following the equation (2.31), a D_2-invariant function F:

$$\forall \mathbf{g} \in \mathrm{D}_2, \quad \mathbf{F}(\mathbf{g} \star \underset{\sim}{\sigma}) = \mathbf{F}(\underset{\sim}{\sigma})$$

can be reformulated as an isotropic function:

$$\forall \mathbf{g} \in \mathrm{O}(2), \quad \mathbf{F}(\mathbf{g} \star \underset{\sim}{\sigma}, \mathbf{g} \star \underset{\sim}{\mathrm{K}}) = \mathbf{F}(\underset{\sim}{\sigma}, \underset{\sim}{\mathrm{K}})$$

The O(2)-integrity basis of a pair of symmetric second order tensors is a well known result [204]. In $\mathbb{R}^2$ it consists of the following set of five polynomials (or any equivalent combinations):

$$\mathcal{IB} = \{\mathrm{tr}(\underset{\sim}{\sigma}),\ \mathrm{tr}(\underset{\sim}{\mathrm{K}}),\ \underset{\sim}{\sigma} : \underset{\sim}{\sigma},\ \underset{\sim}{\sigma} : \underset{\sim}{\mathrm{K}},\ \underset{\sim}{\mathrm{K}} : \underset{\sim}{\mathrm{K}}\}$$

This integrity base can be reduced by

- dropping the invariants $\mathrm{tr}(\underset{\sim}{\mathrm{K}})$ and $\underset{\sim}{\mathrm{K}} : \underset{\sim}{\mathrm{K}}$ which are constant with respect to $\underset{\sim}{\sigma}$;
- decomposing $\underset{\sim}{\sigma}$ into σ_m and $\underset{\sim}{\sigma}^{(2)}$.

A the end we obtain 3 elementary invariant monomials:

$$\mathcal{IB} = \{I_1 = \sigma_m,\ J_1 = \underset{\sim}{\sigma}^{(2)} : \underset{\sim}{\mathrm{K}},\ J_2 = \underset{\sim}{\sigma}^{(2)} : \underset{\sim}{\sigma}^{(2)}\}$$

Any orthotropic polynomial function of $\underset{\sim}{\sigma}$ is a polynomial in (I_1, J_1, J_2). In this basis we retrieve (I_1, J_2) which are the classical O(2)-invariants of $\underset{\sim}{\sigma}$, already introduced in section 2.2. Alongside these isotropic invariants appears J_1 which is characteristic of the considered anisotropy. It can be seen that this is a linear invariant, so the anisotropy will manifest itself as a polynomial function from degree 1 in $\underset{\sim}{\sigma}$.

The collection of monomials generating orthotropic invariant homogeneous polynomials is provided in the table below up to degree four. In this table, anisotropic monomials are shown in red.

Degree	Monomials	Dimension
1	$I_1,\ J_1$	2
2	$I_1^2,\ I_1J_1,\ J_I^2,\ J_2$	4
3	$I_1^3,\ I_1^2J_1,\ I_1J_1^2,\ J_I^3,\ I_1J_2,\ J_1J_2$	6
4	$I_1^4,\ I_1^3J_1^2,\ I_1^2J_1^2,\ I_1J_1^3,\ J_I^4,\ I_1^2J_2,\ J_1^2J_2,\ I_1J_1J_2,\ J_2^2$	9

As a result, and for the example, a general homogeneous polynomial of degree two has the following expression[14] :

$$\begin{aligned} F(\underset{\sim}{\sigma}, \underset{\sim}{\mathrm{K}}) &= \alpha_1 I_1^2 + \alpha_2 I_1 J_1 + \alpha_3 J_2 + \alpha_4 J_I^2 \\ &= \alpha_1(\sigma_m)^2 + \alpha_2\sigma_m\left(\underset{\sim}{\sigma}^{(2)} : (\underline{\mathrm{e}}_1 \otimes \underline{\mathrm{e}}_1)\right) + \alpha_3\underset{\sim}{\sigma}^{(2)} : \underset{\sim}{\sigma}^{(2)} + \alpha_4\left(\underset{\sim}{\sigma}^{(2)} : (\underline{\mathrm{e}}_1 \otimes \underline{\mathrm{e}}_1)\right)^2 \end{aligned}$$

with $\alpha_k \in \mathbb{R}$.

It is interesting to compare what has been obtained using representation theorems with Tsai-Hill criterion. The Tsai-Hill criterion can be written as

$$F(\underset{\sim}{\sigma}) = \underset{\sim}{\sigma} : \underset{\approx}{\mathrm{F}} : \underset{\sim}{\sigma}.$$

where $\underset{\approx}{\mathrm{F}}$ is a fourth-order tensor whose index symmetries are identical to those of the elasticity tensor. As such, results from elasticity can be used to decompose[15] and parameterise it [60, 13]:

$$\underset{\approx}{\mathrm{F}} = \alpha\underset{\approx}{\mathrm{J}} + \beta\underset{\approx}{\mathrm{K}} + \frac{1}{2}(\underset{\sim}{\mathrm{I}} \otimes \underset{\sim}{\mathrm{h}} + \underset{\sim}{\mathrm{h}} \otimes \underset{\sim}{\mathrm{I}}) + \underset{\approx}{\mathrm{H}}$$

in which $\underset{\sim}{\mathrm{h}} \in \mathbb{K}^2$ and $\underset{\approx}{\mathrm{H}} \in \mathbb{K}^4$. This decomposition can be interpreted as follows:

$$F(\underset{\sim}{\sigma}) = \begin{pmatrix} \underset{\sim}{\sigma}^{(2)} \\ \underset{\sim}{\sigma}^{(0)} \end{pmatrix} \begin{pmatrix} \underset{\approx}{\mathrm{H}} + \alpha\underset{\approx}{\mathrm{J}} & \frac{1}{2}\underset{\sim}{\mathrm{h}} \otimes \underset{\sim}{\mathrm{I}} \\ \frac{1}{2}\underset{\sim}{\mathrm{I}} \otimes \underset{\sim}{\mathrm{h}} & \beta\underset{\approx}{\mathrm{K}} \end{pmatrix} \begin{pmatrix} \underset{\sim}{\sigma}^{(2)} \\ \underset{\sim}{\sigma}^{(0)} \end{pmatrix}$$

This allows to express the polynomial criterion with respect to the stress tensor decomposed into its deviatoric and its spherical part, i.e.

$$F(\underset{\sim}{\sigma}) = \beta(\sigma_m)^2 + 2(\underset{\sim}{\sigma}^{(2)} : \underset{\sim}{\mathrm{h}})\sigma_m + \alpha\underset{\sim}{\sigma}^{(2)} : \underset{\sim}{\sigma}^{(2)} + \underset{\sim}{\sigma}^{(2)} : \underset{\approx}{\mathrm{H}} : \underset{\sim}{\sigma}^{(2)} \tag{2.34}$$

It can be observed that setting β and $\underset{\sim}{\mathrm{h}}$ to zero, the Hill criterion is retrieved.

The previous polynomial is generic and corresponds to a Z_2-invariant function, not to an orthotropic one. The condition of being D_2-invariant imposes a relation between $\underset{\approx}{\mathrm{H}}$ and $\underset{\sim}{\mathrm{h}}$ [130]:

[14] In the present case we have

$$J_1 = \underset{\sim}{\sigma}^{(2)} : \underset{\sim}{\mathrm{K}} = \underset{\sim}{\sigma}^{(2)} : (\underline{\mathrm{e}}_1 \otimes \underline{\mathrm{e}}_1)_0 = \underset{\sim}{\sigma}^{(2)} : (\underline{\mathrm{e}}_1 \otimes \underline{\mathrm{e}}_1)$$

the last equality holds since $\mathbb{K}^2$ is a subspace of $S^2(\mathbb{R}^2)$.

[15] The concept behind this decomposition will be fully detailed in the chapter 3.

Lemma 2.4.6. $\underset{\approx}{\mathrm{F}}$ *is orthotropic if and only if* $\underset{\approx}{\mathrm{H}} \propto (\underset{\sim}{\mathrm{h}} \otimes \underset{\sim}{\mathrm{h}})_0$.

Since $\underset{\sim}{\mathrm{h}} = \lambda(\underline{\mathrm{e}}_1 \otimes \underline{\mathrm{e}}_1)_0$, we have $\underset{\approx}{\mathrm{H}} = \mu(\underline{\mathrm{e}}_1 \otimes \underline{\mathrm{e}}_1 \otimes \underline{\mathrm{e}}_1 \otimes \underline{\mathrm{e}}_1)_0$. As a result, the developed expression for the orthotropic Tsai-Hill criterion gives

$$F(\underset{\sim}{\sigma}) = \beta(\sigma_m)^2 + \lambda(\underset{\sim}{\sigma}^{(2)} : (\underline{\mathrm{e}}_1 \otimes \underline{\mathrm{e}}_1))\sigma_m + \alpha \underset{\sim}{\sigma}^{(2)} : \underset{\sim}{\sigma}^{(2)} + \mu(\underset{\sim}{\sigma}^{(2)} : (\underline{\mathrm{e}}_1 \otimes \underline{\mathrm{e}}_1))^2$$

and we retrieve the expression provided by the group representation theory.

The computation of the last term should be a bit detailed, we need to compute

$$\underset{\sim}{\sigma}^{(2)} : \underset{\approx}{\mathrm{H}} : \underset{\sim}{\sigma}^{(2)} = \mu \underset{\sim}{\sigma}^{(2)} : (\underline{\mathrm{e}}_1 \otimes \underline{\mathrm{e}}_1 \otimes \underline{\mathrm{e}}_1 \otimes \underline{\mathrm{e}}_1)_0 : \underset{\sim}{\sigma}^{(2)}$$

From the definition of the harmonic product [15], the term $(\underline{\mathrm{e}}_1 \otimes \underline{\mathrm{e}}_1 \otimes \underline{\mathrm{e}}_1 \otimes \underline{\mathrm{e}}_1)_0$ can be computed as

$$(\underline{\mathrm{e}}_1 \otimes \underline{\mathrm{e}}_1 \otimes \underline{\mathrm{e}}_1 \otimes \underline{\mathrm{e}}_1)_0 = (\underline{\mathrm{e}}_1 \otimes \underline{\mathrm{e}}_1 \otimes \underline{\mathrm{e}}_1 \otimes \underline{\mathrm{e}}_1) - \frac{1}{2}\underset{\approx}{\mathrm{I}}$$

It results that

$$\underset{\sim}{\sigma}^{(2)} : \underset{\approx}{\mathrm{H}} : \underset{\sim}{\sigma}^{(2)} = \mu(\underset{\sim}{\sigma}^{(2)} : (\underline{\mathrm{e}}_1 \otimes \underline{\mathrm{e}}_1))^2 - \frac{\mu}{2}\underset{\sim}{\sigma}^{(2)} : \underset{\sim}{\sigma}^{(2)}$$

Injecting this expression into equation (2.34) we obtain

$$F(\underset{\sim}{\sigma}) = \beta(\sigma_m)^2 + 2\lambda\sigma_m(\underset{\sim}{\sigma}^{(2)} : (\underline{\mathrm{e}}_1 \otimes \underline{\mathrm{e}}_1)) + (\alpha - \frac{\mu}{2})\underset{\sim}{\sigma}^{(2)} : \underset{\sim}{\sigma}^{(2)} + \mu(\underset{\sim}{\sigma}^{(2)} : (\underline{\mathrm{e}}_1 \otimes \underline{\mathrm{e}}_1))^2$$

As a side result, it provides the following explicit link between the structure tensor $\underset{\sim}{\mathrm{N}} = (\underline{\mathrm{n}} \otimes \underline{\mathrm{n}})_0$ and the harmonic decomposition of $\underset{\approx}{\mathrm{F}}$ in the orthotropic case:

$$\underset{\approx}{\mathrm{F}} = \alpha \underset{\approx}{\mathrm{J}} + \beta \underset{\approx}{\mathrm{K}} + \frac{\lambda}{2}(\underset{\sim}{\mathrm{I}} \otimes \underset{\sim}{\mathrm{N}} + \underset{\sim}{\mathrm{N}} \otimes \underset{\sim}{\mathrm{I}}) + \gamma(\underset{\sim}{\mathrm{N}} \otimes \underset{\sim}{\mathrm{N}})_0$$

Example 2: Hexatropic threshold functions

Let us now define the general shape of a polynomial function invariant with respect to the group D_6. In $\mathbb{R}^2$, this group can be characterised by the structure tensor $\underset{\approx\approx\approx}{\mathrm{K}} = (\underline{\mathrm{n}}^{\otimes 6})_0 \in \mathbb{K}^6$. As for the previous example the case $\underline{\mathrm{n}} = \underline{\mathrm{e}}_1$ is considered. In this case [204, 61]:

$$\underset{\approx\approx\approx}{\mathrm{K}} \propto \underline{\mathrm{e}}_1^{\otimes 6} - 15\left(\underline{\mathrm{e}}_1^{\otimes 4} \otimes \underline{\mathrm{e}}_2^{\otimes 2}\right)^s + 15\left(\underline{\mathrm{e}}_1^{\otimes 2} \otimes \underline{\mathrm{e}}_2^{\otimes 4}\right)^s - \underline{\mathrm{e}}_2^{\otimes 6}$$

in which $\mathbf{T}^s$ denotes the total symmetrisation (over all subscripts) of $\mathbf{T}$, i.e is a projector from $\mathbb{T}^n(\mathbb{R}^2)$ onto $\mathbb{S}^n(\mathbb{R}^2)$.

Following (2.31), a D_6-invariant function F:

$$\forall \mathbf{g} \in \mathrm{D}_6^{\mathrm{n}}, \quad \mathbf{F}(\mathbf{g} \star \underset{\sim}{\sigma}) = \mathbf{F}(\underset{\sim}{\sigma})$$

can be reformulated as an isotropic function:

$$\forall \mathbf{g} \in \mathrm{O}(2), \quad \mathbf{F}(\mathbf{g} \star \underset{\sim}{\sigma}, \mathbf{g} \star \underset{\approx\approx\approx}{\mathrm{K}}) = \mathbf{F}(\underset{\sim}{\sigma}, \underset{\approx\approx\approx}{\mathrm{K}})$$

for a $\underset{\approx\approx\approx}{\mathrm{K}} \in \mathbb{K}^6$ such as $\mathrm{G}_{\underset{\approx\approx\approx}{\mathrm{K}}} = \mathrm{D}_6$.

Direct construction of the integrity basis, using for instance the algorithm provided in [61], provides the following integrity basis:

$$\mathcal{IB} = \{I_1 = \sigma_m,\ I_2 = \underset{\sim}{\sigma}^{(2)} : \underset{\sim}{\sigma}^{(2)}, I_3 = \underset{\approx\approx\approx}{\mathrm{K}} \cdot^6 \left(\underset{\sim}{\sigma}^{(2)} \otimes \underset{\sim}{\sigma}^{(2)} \otimes \underset{\sim}{\sigma}^{(2)}\right)_0\}$$

It should be noted here that the invariant characterising the anisotropy is of degree 3 with respect to $\underset{\sim}{\sigma}^{(2)}$. By way of comparison, in the orthotropic case, the anisotropic invariant was of degree 1. Let us examine the consequences of this for generating monomials up to degree 4.

Degree	Monomials	Dimension
1	I_1	1
2	$I_1^2,\ I_2$	2
3	$I_1^3,\ I_1 I_2,\ I_3$	3
4	$I_1^4,\ I_1^2 I_2,\ I_1 I_3,\ I_2^2$	4

Two interesting observations can directly be made reading this table:

- hexatropic quadratic homogeneous polynomials are in fact completely isotropic since anisotropy can only manifest itself from a cubic polynomial. Translated into the language of tensor criteria, this means that a tensor of order at least six is needed to capture this anisotropic feature;
- while at degree 3 the hexatropic term is purely deviatoric, at degree 4 it encodes a coupling between deviatoric and spherical stress. As such, it will vanish for purely deviatoric criteria at this degree, such as the generalized Hill criterion.

For instance, a general homogeneous polynomial of degree four has the following expression:

$$\begin{aligned} F(\underset{\sim}{\sigma}, \underset{\approx}{\underset{\approx}{\mathrm{K}}}) &= \alpha_1 I_1^4 + \alpha_2 I_1^2 I_2 + \alpha_3 I_1 I_3 + \alpha_4 I_2^2 \\ &= \alpha_1 \sigma_m^4 + \alpha_2 \sigma_m^2 \left(\underset{\sim}{\sigma}^{(2)} : \underset{\sim}{\sigma}^{(2)}\right) + \alpha_3 \sigma_m \left(\underset{\approx}{\underset{\approx}{\mathrm{K}}} \overset{6}{\cdot} (\underset{\sim}{\sigma}^{(2)} \otimes \underset{\sim}{\sigma}^{(2)} \otimes \underset{\sim}{\sigma}^{(2)})\right) + \alpha_4 \left(\underset{\sim}{\sigma}^{(2)} : \underset{\sim}{\sigma}^{(2)}\right)^2 \end{aligned}$$

Such function corresponds to a tensorial criterion having the following shape

$$F(\underset{\sim}{\sigma}) = \underset{\approx}{\underset{\approx}{\mathrm{A}}} \overset{8}{\cdot} (\underset{\sim}{\sigma} \otimes \underset{\sim}{\sigma} \otimes \underset{\sim}{\sigma} \otimes \underset{\sim}{\sigma})$$

with $\mathrm{G}_{\underset{\approx}{\underset{\approx}{\mathrm{A}}}} = \mathrm{D}_6$.

Example 3: Trichiral threshold function

Let us now define the general shape of a polynomial function invariant with respect to the group Z_3. In $\mathbb{R}^2$, this group can be characterised by two structure tensors

- $\underset{\simeq}{\mathrm{K}} = (\underline{\mathrm{n}}^{\otimes 3})_0 \in \mathbb{K}^3$, for the D_3-invariance;
- $\xi \in \mathbb{K}^{-1}$ to impose the chiral dependency.

In the case $\underline{\mathrm{n}} = \underline{\mathrm{e}}_1$:

$$\underset{\simeq}{\mathrm{K}} \propto \underline{\mathrm{e}}_1 \otimes \underline{\mathrm{e}}_1 \otimes \underline{\mathrm{e}}_1 - 3\,(\underline{\mathrm{e}}_1 \otimes \underline{\mathrm{e}}_2 \otimes \underline{\mathrm{e}}_2)^s$$

As usual now, the Z_3-equivariance properties:

$$\forall \mathbf{g} \in \mathrm{Z}_3, \quad \mathbf{F}(\mathbf{g} \star \underset{\sim}{\sigma}) = \mathbf{F}(\underset{\sim}{\sigma})$$

can be reformulated as the $\mathrm{O}(2)$-equivariance one:

$$\forall \mathbf{g} \in \mathrm{O}(2), \quad \mathbf{F}(\mathbf{g} \star \underset{\sim}{\sigma}, \mathbf{g} \star \underset{\simeq}{\mathrm{K}}, \det(\mathbf{g})\xi) = \mathbf{F}(\underset{\sim}{\sigma}, \underset{\simeq}{\mathrm{K}}, \xi)$$

The associated integrity base is

$$\begin{aligned} \mathcal{IB}(\mathrm{Z}_3, \mathrm{O}(2)) = \Big\{ & I_1 = \sigma_m,\ I_2 = \xi^2,\ J_2 = \underset{\sim}{\sigma}^{(2)} : \underset{\sim}{\sigma}^{(2)}, I_3 = \left(\underset{\simeq}{\mathrm{K}} \otimes \underset{\simeq}{\mathrm{K}}\right)_0 \overset{6}{\cdot} \left(\underset{\sim}{\sigma}^{(2)} \otimes \underset{\sim}{\sigma}^{(2)} \otimes \underset{\sim}{\sigma}^{(2)}\right)_0, \\ & J_3 = \xi \left((\underset{\sim}{\mathrm{I}} \times \underset{\simeq}{\mathrm{K}}) \otimes \underset{\simeq}{\mathrm{K}}\right)_0 \overset{6}{\cdot} \left(\underset{\sim}{\sigma}^{(2)} \otimes \underset{\sim}{\sigma}^{(2)} \otimes \underset{\sim}{\sigma}^{(2)}\right)_0 \Big\} \end{aligned} \tag{2.35}$$

and can be reduced for trigonal functions (i.e. with ξ=0) to

$$\mathcal{IB}(\mathrm{D}_3, \mathrm{O}(2)) = \{I_1 = \sigma_m,\ J_2 = \underset{\sim}{\sigma}^{(2)} : \underset{\sim}{\sigma}^{(2)}, I_3 = \left(\underset{\simeq}{\mathrm{K}} \otimes \underset{\simeq}{\mathrm{K}}\right)_0 \overset{6}{\cdot} \left(\underset{\sim}{\sigma}^{(2)} \otimes \underset{\sim}{\sigma}^{(2)} \otimes \underset{\sim}{\sigma}^{(2)}\right)_0\}.$$

If we forget chirality sensitivity, what we should observe here is that there is no difference between $IB(\mathrm{D}_3, \mathrm{O}(2))$ and $IB(\mathrm{D}_6, \mathrm{O}(2))$. Associated to $\underset{\sim}{\sigma}^{(2)}$ the structure tensor viewed by the system is not $\underset{\simeq}{\mathrm{K}} \in \mathbb{K}^3$ but its image in $\mathbb{K}^6$, as a result[16]

$$\mathbb{R}[S^2(\mathbb{R}^2)]^{\mathrm{D}_3} = \mathbb{R}[S^2(\mathbb{R}^2)]^{\mathrm{D}_6}$$

This result can be checked here up to degree four:

Degree	Monomials	Dimension
1	I_1	1
2	$I_1^2,\ I_2$	2
3	$I_1^3,\ I_1 I_2,\ I_3,\ J_3$	4
4	$I_1^4,\ I_1^2 I_2,\ I_1 I_3,\ I_1 J_3,\ I_2^2$	5

A general homogeneous polynomial of degree four has the following expression

$$\begin{aligned} F(\underset{\sim}{\sigma}, \underset{\simeq}{\mathrm{K}}) &= \alpha_1 I_1^4 + \alpha_2 I_1^2 I_2 + \alpha_3 I_1 I_3 + \alpha_4 I_1 J_3 + \alpha_5 I_2^2, \\ &= \alpha_1 \sigma_m^4 + \alpha_2 \sigma_m^2 \left(\underset{\sim}{\sigma}^{(2)} : \underset{\sim}{\sigma}^{(2)}\right) + \alpha_3 \sigma_m \left(\underset{\simeq}{\mathrm{K}} \otimes \underset{\simeq}{\mathrm{K}}\right)_0 \overset{6}{\cdot} \left(\underset{\sim}{\sigma}^{(2)} \otimes \underset{\sim}{\sigma}^{(2)} \otimes \underset{\sim}{\sigma}^{(2)}\right)_0, \\ &= +\alpha_4 \sigma_m \xi \left((\underset{\sim}{\mathrm{I}} \times \underset{\simeq}{\mathrm{K}}) \otimes \underset{\simeq}{\mathrm{K}}\right)_0 \overset{6}{\cdot} \left(\underset{\sim}{\sigma}^{(2)} \otimes \underset{\sim}{\sigma}^{(2)} \otimes \underset{\sim}{\sigma}^{(2)}\right)_0 + \alpha_5 \left(\underset{\sim}{\sigma}^{(2)} : \underset{\sim}{\sigma}^{(2)}\right)^2. \end{aligned}$$

[16] In fact, the following result can be conjectured

$$\mathbb{R}[S^2(\mathbb{R}^2)]^{\mathrm{D}_{2p+1}} = \mathbb{R}[S^2(\mathbb{R}^2)]^{\mathrm{D}_{2(2p+1)}}$$

2.5 Synthesis

In this section we have detailed the links between writing H-invariant functions:

1. from group representation theory and integrity basis computation;
2. from a tensor polynomial of a given order;

More precisely we have seen how 1) $\Rightarrow$ 2) and how to obtain a H-invariant tensor polynomial from a suitable structure tensor.

This approach allows us to state the following properties:

Proposition 2.5.1. *A rotational symmetry of order $2p$ is perceived as anisotropic for a polynomial whose minimal degree in $\underset{\sim}{\sigma}$ is p.*

Proposition 2.5.2. *A rotational symmetry of order $2p+1$ is perceived as a rotational symmetry of order $2(2p+1)$ and is perceived as anisotropic for a polynomial of minimal degree $2p+1$ in $\underset{\sim}{\sigma}$.*

These properties can be reformulated in terms of tensor polynomials as follows:

Proposition 2.5.3. *A rotational symmetry of order $2p$ is perceived as anisotropic for a tensor of minimal order $2p$;*

Proposition 2.5.4. *A rotational symmetry of order $2p+1$ is seen as a rotational symmetry of order $2(2p+1)$ is seen as anisotropic for a tensor of minimal order $2(2p+1)$.*

It follows from this that if we wish to establish a threshold allowing to describe in the same formalism the different surfaces presented in this chapter, i.e.

- Cazacu's isotropic asymmetric surface;
- Soare's Poly4 orthotropic surface;
- Wang's hexatropic symmetric surface;
- Jeanneau's hexatropic asymmetric surface

the criterion must be at least of degree 4 in $\underset{\sim}{\sigma}$ and contains odd powers in order to allow for compression asymmetry. The function is a generalised case of the Tsai-Wu function, so we call it "Tsai-Wu4" and it is given by:

$$F(\underset{\sim}{\sigma}) = \underset{\approx\approx\approx}{\mathrm{A}} \overset{8}{\cdot} (\underset{\sim}{\sigma} \otimes \underset{\sim}{\sigma} \otimes \underset{\sim}{\sigma} \otimes \underset{\sim}{\sigma}) + \underset{\approx\approx\approx}{\mathrm{B}} \overset{6}{\cdot} (\underset{\sim}{\sigma} \otimes \underset{\sim}{\sigma} \otimes \underset{\sim}{\sigma}) + \underset{\approx}{\mathrm{C}} :: (\underset{\sim}{\sigma} \otimes \underset{\sim}{\sigma}) + \underset{\sim}{\mathrm{D}} : \underset{\sim}{\sigma}. \tag{2.36}$$

Note that in the case of Wang's criterion a tensor of order 12 would be needed to describe the anisotropy of the deviatoric plane. In our case the order of the dominant tensor being of order 8, we will only see a circle in this plane.

The study of this criterion is the subject of the next chapter.

Chapter 3

Quartic polynomial threshold criterion

Contents

It is concluded in chapter 1, that polynomial function is the best candidate that meets all the requirements to establish a threshold criterion for architectured materials. This because polynomial function has been very effective to it comes to modelling anisotropy and the asymmetry in traction/compression.

In chapter 2, a methodology based on group representation theory has been introduced to construct, on a case-by-case basis, H-invariant polynomials. Using this approach some general principles have been put forward. The most important one is that to model an anisotropy of order n, a tensor of order n is needed in the criterion.

We will adopt here a different point of view from the one considered in the previous chapter by choosing a polynomial criterion and by looking at the set of situations that it can describe. Our aim is to determine a unified framework to describe threshold function for architectured materials. These materials are known to be anisotropic and known for an asymmetric failure modes depending on the the stress state (plasticity/brittleness in tension and plasticity/buckling compression). The proposed threshold function includes the contribution of all polynomial terms from 1st to 4th degree.

This idea is not new and has a history. Gol'denblat et al. [82] seems to be the first to have introduced a threshold function of the following form:

$$F(\underset{\sim}{\sigma}) = \left(\underset{\sim}{\mathrm{D}} : \underset{\sim}{\sigma}\right)^{\alpha} + \left(\underset{\approx}{\mathrm{C}} :: (\underset{\sim}{\sigma} \otimes \underset{\sim}{\sigma})\right)^{\beta} + \left(\underset{\approx\approx}{\mathrm{B}} \overset{6}{\cdot} (\underset{\sim}{\sigma} \otimes \underset{\sim}{\sigma} \otimes \underset{\sim}{\sigma})\right)^{\gamma} + \dots ,$$

in which $\underset{\sim}{\mathrm{D}}$, $\underset{\approx}{\mathrm{C}}$ and $\underset{\approx\approx}{\mathrm{B}}$ are, respectively, 2nd, 4th and 6th order strength tensors. α, β and γ are coefficients. In the cited paper, Gol'denblat et al. studied the case of in-plane stress (2D) with $\alpha = 1, \beta = \frac{1}{2}$ and $\gamma = -\infty$. Tsai et al. considered the 3D situation and simplified the formulation by getting rid of the square roots, they obtained the function which has since become known as the Tsai-Wu criterion:

$$F(\underset{\sim}{\sigma}) = \underset{\sim}{\mathrm{D}} : \underset{\sim}{\sigma} + \underset{\approx}{\mathrm{C}} :: (\underset{\sim}{\sigma} \otimes \underset{\sim}{\sigma}).$$

They justify ignoring higher degree terms for two reasons

1. the number of parameter woulds be too large, and their physical content unclear;
2. badly chosen parameter leads to non-closed surfaces.

As illustrated in the previous chapter, in the case of achitectured materials higher degree terms are required to model higher-order anisotropy. These materials also have asymmetrical failure modes depending on the state of stress (plasticity/fragility in tension and plasticity/stress in compression). The proposed threshold function is the contribution of all polynomial terms for 1st degree to 4th are considered. The function is a more generalised case of the Tsai-Wu function, so we call it *Tsai-Wu 4* (TW4) and it is given by:

$$F(\underset{\sim}{\sigma}) = \underset{\approx\approx\approx}{\mathrm{A}} \overset{8}{\cdot} (\underset{\sim}{\sigma} \otimes \underset{\sim}{\sigma} \otimes \underset{\sim}{\sigma} \otimes \underset{\sim}{\sigma}) + \underset{\approx\approx}{\mathrm{B}} \overset{6}{\cdot} (\underset{\sim}{\sigma} \otimes \underset{\sim}{\sigma} \otimes \underset{\sim}{\sigma}) + \underset{\approx}{\mathrm{C}} :: (\underset{\sim}{\sigma} \otimes \underset{\sim}{\sigma}) + \underset{\sim}{\mathrm{D}} : \underset{\sim}{\sigma}. \tag{3.1}$$

All $\underset{\approx\approx\approx}{\mathrm{A}}$, $\underset{\approx\approx}{\mathrm{B}}$, $\underset{\approx}{\mathrm{C}}$ and $\underset{\sim}{\mathrm{D}}$ are respectively 8th, 6th, 4th and 2nd order tensors which include all material parameters. By adding higher degree we have higher order tensors which will certainly be much richer when it comes to anisotropy. With polynomial terms of even degree, we can only generate symmetric surfaces [170] verifying $F(-\underset{\sim}{\sigma}) = F(\underset{\sim}{\sigma})$. On the other hand, with odd terms, we can generate asymmetric surfaces. Tsai-Wu4 is a very general form of quartic polynomial function: this means that it encompasses a significant number of existing functions in the literature (e.g. [167, 158]) as special cases. It is important to notice that the proposed form is already present in some papers. We find the work of Bower et al. [37] where he proposed the same function (3D case) and established all convexity conditions. We also find Sanya et al. [155]. He studied the multiaxial yielding behaviour of human trabecular bone. He concluded that the function proposed in his study, can be extended to the form we have in the equation (3.1). Hence, it is a more appropriate form for generating boxlike shaped threshold surfaces that are often found with foams.

As mentioned before, the expression of our threshold function is in a general. It is worth simplifying according to the anisotropy of the described material. In order to do so, the so-called the *harmonic decomposition* [16] is applied. In a nutshell, it is a generalisation of deviatoric and spheric decomposition of the stress tensor for higher order tensors. It is suitable for harmonic basis where distinguish anisotropy and loading symmetry is more practical.

This chapter is organised as follows. The section 3.1 is devoted to introduce the concept of harmonic decomposition. The harmonic space structure of the material tensors of TW4 is provided in section 3.2. The section 3.3 is devoted the explicit algebraic decomposition of all material tensors. In section 3.4 we analyse the geometry of threshold surface of TW4 under the effect of the harmonic parameters (elements of harmonic tensors). Lastly, in section 3.5 approximations of some of selected threshold criteria from chapter 1. Simplifications with respect to the anisotropy are considered in the approximation process.

3.1 Harmonic decomposition: concept and methodology

When a material is rotated[1] its physical nature is not affected but, with respect to a fixed reference, material tensors are transformed[2]. Since material tensors are usually of order greater than 2, the way they transform is not simple and their different parts transform differently: some components are left fixed while others *turn* at different speeds.

3.1.1 Concept of harmonic decomposition

In mathematics, when facing a sophisticated object, a general strategy consists in decomposing it into a collection of elementary parts, whose behaviour is easier to understand. This is the idea of harmonic decomposition. This concept, which exists in $\mathbb{R}^d$, will be used for $d = 2$ and 3. For this reason, it will be introduced in all generality before being particularised to the specific dimensions.

[1] Here *rotated* is understood in the broad sense of a full orthogonal transformation.

[2] By material tensor, we mean tensors that translate physical properties (in the broadest sense) resulting from the arrangement of matter.

Consider a general tensor space $\mathbb{T}^n$ and denote by $\mathbf{T}$ one of its element. To study the way $\mathbf{T}$ transforms under $\mathrm{O}(d)$-action, the idea is to decompose $\mathbf{T}$ into elementary pieces:

$$\mathbf{T} = \phi\left(\mathbf{H}_{i_1}, \ldots, \mathbf{H}_{i_n}\right), \text{ with } \left(\mathbf{H}_{i_1}, \ldots, \mathbf{H}_{i_n}\right) \in \mathbb{H}(\mathbb{R}^d)^{i_1} \times \ldots \times \mathbb{H}(\mathbb{R}^d)^{i_n}.$$

in such way that:

$$\forall g \in \mathrm{O}(d),\ \mathbf{g} \star \phi\left(\mathbf{H}_{i_1}, \ldots, \mathbf{H}_{i_n}\right) = \phi\left(\mathbf{g} \star \mathbf{H}_{i_1}, \ldots, \mathbf{g} \star \mathbf{H}_{i_n}\right)$$

i.e.

$$\begin{array}{ccc} \mathbf{T} & \xrightarrow{\phi} & \left(\mathbf{H}_{i_1}, \ldots, \mathbf{H}_{i_n}\right) \\ \Big\downarrow{\scriptstyle \mathbf{g}} & & \Big\downarrow{\scriptstyle \mathbf{g}} \\ \mathbf{g} \star \mathbf{T} & \xrightarrow{\phi} & \left(\mathbf{H}'_{i_1}, \ldots, \mathbf{H}_{i_n}\right) \end{array}$$

This $\mathrm{O}(d)$-equivariance property expresses the idea that it is the same to decompose $\mathbf{T}$ and then transform the elements of its decomposition, or to first turn $\mathbf{T}$ and then decompose it. In this decomposition:

- $\mathbf{H}_{i_k}$ is a harmonic tensor;
- $\mathbb{H}(\mathbb{R}^d)^{i_1} \times \ldots \times \mathbb{H}(\mathbb{R}^d)^{i_n}$ is the harmonic structure of $\mathbb{T}^n$;
- ϕ is an explicit harmonic decomposition.

Harmonic tensors have been introduced in chapter 2 (cf. Definition 2.4.3), in the case $d = 2$. Their defining properties are the same for $d = 2, 3$, i.e. the space of harmonic tensors are $\mathrm{O}(d)$-irreducible, i.e

1. $\mathrm{O}(d)$-*invariant* (i.e., $\mathbf{g} \star \mathrm{T} \in \mathbb{H}(\mathbb{R}^d)^k$ for all $\mathbf{g} \in \mathrm{O}(d)$ and $\mathrm{T} \in \mathbb{H}(\mathbb{R}^d)^k$);
2. its only invariant subspaces are itself and the null space. It is known that $\mathrm{O}(2)$-reducible spaces are isomorphic to a direct sum of harmonic tensor spaces $\mathbb{H}(\mathbb{R}^d)^n$ [83, 16].

In the following, the classical convention will be used:

- $d = 2$, $\mathbb{H}(\mathbb{R}^2)^k$ will be denoted $\mathbb{K}^k$;
- $d = 3$, $\mathbb{H}(\mathbb{R}^3)^k$ will be denoted $\mathbb{H}^k$;

The harmonic decomposition consists in decomposing a finite-dimensional vector space into a direct sum of $\mathrm{O}(d)$-*irreducible subspaces*. Associated with harmonic decomposition we can distinguish two different but closely related objects

- **Harmonic structure:** the harmonic structure only concerns the structure of the tensor space, i.e. the number and type of harmonic tensor spaces it contains.
- **Explicit harmonic decomposition:** it is an explicit formula detailing the decomposition. The explicit harmonic decomposition is, in general, not unique.

The rest of the section is devoted to the harmonic structure of the tensor spaces involved in the threshold function, with respect to $\mathbb{R}^2$ and $\mathbb{R}^3$ respectively. The harmonic structure with respect to $\mathbb{R}^2$ allows us to understand the role of material anisotropy, while that with respect to $\mathbb{R}^3$ allows us to take loading into account and to characterise the symmetry of the threshold surface in the stress space. These harmonic structures will first be established before constructing, in section 3.3, the explicit harmonic decomposition in the case $\mathbb{R}^2$.

3.1.2 Clebsch-Gordan formula

The harmonic structure of tensor space $\mathbb{T}$ is its expression as a direct sum of harmonic spaces,

$$\mathbb{T}^n = \bigoplus_k \alpha_k \mathbb{H}(\mathbb{R}^d)^k. \tag{3.2}$$

where α_k stands for the multiplicity of $\mathbb{H}(\mathbb{R}^d)^k$ in the decomposition. Many significant information is encoded by the harmonic structure

- the set of symmetry classes;
- the structure of the integrity basis;
- ...

further it is a precious guideline when it comes to determining an explicit isomorphism.

Interestingly, the harmonic structure of a tensor space can be determined without making heavy computations by using *Clebsch-Gordan formula*. These formula indicate how the tensor product of two irreducible spaces decomposes into a direct sum of irreducible spaces:

$$\mathbb{H}(\mathbb{R}^d)^k_1 \otimes \mathbb{H}(\mathbb{R}^d)^k_2 = \bigoplus_j \mathbb{H}(\mathbb{R}^d)^j$$

These formula are known both for $d = 2$ and $d = 3$.

Clebsch-Gordan formula in $\mathbb{R}^2$

For the determination of the harmonic structure, we use the following result, the proof of which is found in [16].

Lemma 3.1.1 (Clebsch-Gordan formula)**.** *The tensor product of two* O(2)*-irreducible spaces is reducible and decomposes according to:*

$\otimes$	$\mathbb{K}^n$	$\mathbb{K}^0$	$\mathbb{K}^{-1}$
$\mathbb{K}^m$	$\begin{cases} \mathbb{K}^{m+n} \oplus \mathbb{K}^{\lvert m-n\rvert}, & m \neq n \\ \mathbb{K}^{2n} \oplus \mathbb{K}^0 \oplus \mathbb{K}^{-1}, & m = n \end{cases}$	$\mathbb{K}^m$	$\mathbb{K}^m$
$\mathbb{K}^0$	$\mathbb{K}^n$	$\mathbb{K}^0$	$\mathbb{K}^{-1}$
$\mathbb{K}^{-1}$	$\mathbb{K}^n$	$\mathbb{K}^{-1}$	$\mathbb{K}^0$

In the case where the spaces are identical, the tensor product can be decomposed into S^2 and Λ^2. This represents, respectively, the symmetrized product and the anti-symmetrized product[3]:

$$\forall n \geq 1, \mathbb{K}^n \otimes \mathbb{K}^n = S^2\left(\mathbb{K}^n\right) \oplus \Lambda^2\left(\mathbb{K}^n\right)$$

Therefore, Lemma 3.1.1 is completed by the following lemma:

Lemma 3.1.2 (Clebsch-Gordan formula)**.** *For all $n \geq 1$, we have the following isotropic decompositions, in which meaningless products are indicated by $\times$:*

S^2	$\mathbb{K}^n$	$\mathbb{K}^0$	$\mathbb{K}^{-1}$
$\mathbb{K}^n$	$\mathbb{K}^{2n} \oplus \mathbb{K}^0$	$\times$	$\times$
$\mathbb{K}^0$	$\times$	$\mathbb{K}^0$	$\times$
$\mathbb{K}^{-1}$	$\times$	$\times$	$\mathbb{K}^0$

Λ^2	$\mathbb{K}^n$	$\mathbb{K}^0$	$\mathbb{K}^{-1}$
$\mathbb{K}^n$	$\mathbb{K}^{-1}$	$\times$	$\times$
$\mathbb{K}^0$	$\times$	0	$\times$
$\mathbb{K}^{-1}$	$\times$	$\times$	0

Clebsch-Gordan formula in $\mathbb{R}^3$

In $\mathbb{R}^3$ the formula are slightly different [105]:

Lemma 3.1.3. *The tensor product of 2 harmonic spaces is reducible and decomposes into:*

$$\mathbb{H}^i \otimes \mathbb{H}^j = \bigoplus_{k=|i-j|}^{i+j} \mathbb{H}^k.$$

In the case where the spaces are identical, the tensor product can be decomposed into S^2 and Λ^2, represent respectively, a symmetrized product and an anti-symmetrized product

$$\forall n \geq 1, \mathbb{H}^n \otimes \mathbb{H}^n = S^2\left(\mathbb{H}^n\right) \oplus \Lambda^2\left(\mathbb{H}^n\right)$$

Therefore, Lemma 3.1.1 is completed by the following lemma:

Lemma 3.1.4. *For all $n \geq 1$, we have the following Clebsch-Gordan formulas [105, 134]:*

$$S^2\left(\mathbb{H}^n\right) = \bigoplus_{k=0}^{n} \mathbb{H}^{2k} \quad ; \quad \Lambda^2\left(\mathbb{H}^n\right) = \bigoplus_{k=1}^{n} \mathbb{H}^{2k-1}.$$

[3] Let $\mathbb{V}$ a vector space of dimension d, and $\underline{\mathrm{v_i}}$ the basis of $\mathbb{V}$, thus the basis of $\mathbb{V} \otimes \mathbb{V}$ is defined by: $\mathcal{B}(\mathbb{V} \otimes \mathbb{V}) = \underline{\mathrm{v_i}} \otimes \underline{\mathrm{v_j}}$, we have:

$$\mathcal{B}(S^2(\mathbb{V})) = \frac{1}{2}(\underline{\mathrm{v_i}} \otimes \underline{\mathrm{v_j}} + \underline{\mathrm{v_j}} \otimes \underline{\mathrm{v_i}}) \quad \mathcal{B}(\Lambda^2(\mathbb{V})) = \frac{1}{2}(\underline{\mathrm{v_i}} \otimes \underline{\mathrm{v_j}} - \underline{\mathrm{v_j}} \otimes \underline{\mathrm{v_i}})$$

3.2 Harmonic structures of TW4

The considered threshold function is as follows:

$$F(\underset{\sim}{\sigma}) = \underset{\approx\approx\approx}{\mathrm{A}} \overset{8}{\cdot} (\underset{\sim}{\sigma} \otimes \underset{\sim}{\sigma} \otimes \underset{\sim}{\sigma} \otimes \underset{\sim}{\sigma}) + \underset{\approx\approx}{\mathrm{B}} \overset{6}{\cdot} (\underset{\sim}{\sigma} \otimes \underset{\sim}{\sigma} \otimes \underset{\sim}{\sigma}) + \underset{\approx}{\mathrm{C}} :: (\underset{\sim}{\sigma} \otimes \underset{\sim}{\sigma}) + \underset{\sim}{\mathrm{D}} : \underset{\sim}{\sigma}, \tag{3.3}$$

in this expression the 4 tensors are $\underset{\approx\approx\approx}{\mathrm{A}}$, $\underset{\approx\approx}{\mathrm{B}}$, $\underset{\approx}{\mathrm{C}}$ and $\underset{\sim}{\mathrm{D}}$ are respectively 8th, 6th, 4th and 2nd order tensors which contain all material parameters. Let us begin by introducing some definitions.

Definition 3.2.1. *Let us denote by $\mathbb{W}_n$ the space of tensors of order $2n$ which works with $\underset{\sim}{\sigma}^{\otimes^n}$. Such tensors will be referred to as nth-order* Wu *tensors.*

Definition 3.2.2. *Let $\mathbb{TW}_n$ the space of nth order Tsai-Wu criterion, defined as*

$$\mathbb{TW}_n = \bigoplus_{i=1}^{n} \mathbb{W}_i$$

in which $\mathbb{W}_i = S^i(S^2(\mathbb{R}^2))$ denotes the space of ith order Wu tensors.

3.2.1 Harmonic structure with respect to $\mathbb{R}^2$

In order to determine the $\mathbb{R}^2$-harmonic structure of the $\mathbb{TW}_n$ tensor spaces, the first step is to identify the space to which they belong. The index symmetries of the elements of $\mathbb{W}_n$ correspond those of the tensor $\underset{\sim}{\sigma}^{\otimes^n}$, i.e. the space $\mathbb{W}_n$ has the structure $S^n(S^2(\mathbb{R}^2))$. Let us denote by $\mathbb{G}(\mathbf{T})$ the index symmetry group of $\mathbf{T} \in \mathbb{W}_n$. $\mathbb{G}(\mathbf{T})$ is given by[4]:

$$\mathbb{G}(\mathbf{T}) = \mathfrak{S}_n \otimes \mathrm{Z}_2$$

in which

1. $\mathfrak{S}_n$ corresponds to the permutation of the n terms $\underset{\sim}{\sigma}$;
2. Z_2 corresponds to the transposition $\underset{\sim}{\sigma} \to \underset{\sim}{\sigma}^T$ of each term.

In the present case:

$$\underset{\approx\approx\approx}{\mathrm{A}} \in \mathbb{W}_4 = S^4(S^2(\mathbb{R}^2)), \quad \underset{\approx\approx}{\mathrm{B}} \in \mathbb{W}_3 = S^3(S^2(\mathbb{R}^2)), \quad \underset{\approx}{\mathrm{C}} \in \mathbb{W}_2 = S^2(S^2(\mathbb{R}^2)), \quad \underset{\sim}{\mathrm{D}} \in \mathbb{W}_1 = S^2(\mathbb{R}^2)$$

The results available in the literature, and summarised in the subsection above, allow us to deal directly with the case of $\underset{\approx}{\mathrm{C}}$ and $\underset{\sim}{\mathrm{D}}$. To consider the other cases we had to establish the following results

Lemma 3.2.3. *The isotypic decomposition of $S^n(\mathbb{K}^2 \oplus \mathbb{K}^0)$ $(n \geq 1)$ are given by:*

$$S^n(\mathbb{K}^2 \oplus \mathbb{K}^0) \simeq \bigoplus_{k=0}^{n} S^k(\mathbb{K}^2) \tag{3.4}$$

in which $S^1(\mathbb{K}^2) = \mathbb{K}^2$ and $S^0(\mathbb{K}^2) = \mathbb{K}^0$.

Lemma 3.2.4. *The isotypic decomposition of $S^{2n}(\mathbb{K}^p)$ and $S^{2n+1}(\mathbb{K}^p)$ $(n \geq 1)$ are given by:*

$$\begin{cases} S^{2n}(\mathbb{K}^p) \simeq \bigoplus_{k=0}^{n} \mathbb{K}^{2kp}, \\ S^{2n+1}(\mathbb{K}^p) \simeq \bigoplus_{k=0}^{n} \mathbb{K}^{(2k+1)p}. \end{cases}$$

[4] This group contains $n!2^n$ elements.

Generic harmonic structure

Using these results, we obtain the following harmonic structures for the tensor spaces of $\mathbb{TW}_4$

Proposition 3.2.5. *The harmonic structure of tensor spaces of* $\mathbb{TW}_4$ *are as follows:*

$$\begin{array}{l|l}
\underset{\sim}{\mathrm{D}} \in \mathbb{W}_1 \simeq \mathbb{K}^2 \oplus \mathbb{K}^0, & \dim(\mathbb{W}_1) = 3, \\
\underset{\approx}{\mathrm{C}} \in \mathbb{W}_2 \simeq \mathbb{K}^4 \oplus \mathbb{K}^2 \oplus 2\mathbb{K}^0, & \dim(\mathbb{W}_2) = 6, \\
\underset{\approx\approx}{\mathrm{B}} \in \mathbb{W}_3 \simeq \mathbb{K}^6 \oplus \mathbb{K}^4 \oplus 2\mathbb{K}^2 \oplus 2\mathbb{K}^0, & \dim(\mathbb{W}_3) = 10, \\
\underset{\approx\approx}{\mathrm{A}} \in \mathbb{W}_4 \simeq \mathbb{K}^8 \oplus \mathbb{K}^6 \oplus 2\mathbb{K}^4 \oplus 2\mathbb{K}^2 \oplus 3\mathbb{K}^0, & \dim(\mathbb{W}_4) = 15.
\end{array}$$

As a result, the number of coefficients required in the most generic situation is

$$\dim(\mathbb{TW}_4) = 34$$

This number of parameters is quite large, but corresponds to a situation with no symmetry, either material or physical. As will be seen, as soon as symmetries come into play, the number of parameters decreases. But, even in the most generic situation, many interesting properties can be read directly from the harmonic structure. First of all, note that:

1. the harmonic structure of $\mathbb{W}_2$ corresponds to the structure of the Hill tensor as detailed in section 2.4.3. The result is retrieved here using Clebsch-Gordan formula;
2. the harmonic structures of $\mathbb{W}_3$ and $\mathbb{W}_4$ correspond to the structures of the cubic and quartic polynomials discussed in the same subsection.

Anisotropic properties

To derive properties associated to material symmetries, we need first to introduced the following notion. The *generalised cross product* for two symmetric tensors defined is defined as follows [61]

$$\mathbf{S}_1 \times \mathbf{S}_2 := (\mathbf{S}_1 \cdot \underset{\sim}{\epsilon} \cdot \mathbf{S}_2)^s$$

the result is a totally symmetric tensor of order $n_1 + n_2 - 2$. It can further be demonstrated that if $\mathbf{K}_1$ and $\mathbf{K}_2$ are harmonic tensors of order n_1 and n_2, respectively, the result is an harmonic tensor of order $|n_1 - n_2|$ embedded in a symmetric tensor of order $n_1 + n_2 - 2$. We can now enunciate the following proposition [74, 14]

Proposition 3.2.6. *Let* $\mathbf{T} \in \mathbb{T}^n$, $\mathrm{G}_\mathbf{T}$ *its symmetry group and denote by* ϕ *its harmonic decomposition*

$$\mathbf{T} = \phi\left(\mathbf{K}_{i_1}, \ldots, \mathbf{K}_{i_n}\right), \text{ with } \left(\mathbf{K}_{i_1}, \ldots, \mathbf{K}_{i_n}\right) \in \mathbb{H}^{i_1} \times \ldots \times \mathbb{H}^{i_n}.$$

- *If* $\mathrm{Z}_p \subset \mathrm{G}_\mathbf{T}$, $\mathbf{K}_i \notin \mathbb{K}^{\alpha p} = 0$, $\alpha \in \mathbb{N}$,
- *If* $\mathrm{Z}_2^\pi \subset \mathrm{G}_\mathbf{T}$, $\forall i, j$ $\mathbf{K}_i \times \mathbf{K}_j = 0$,
- *If* $\mathrm{D}_p \subset \mathrm{G}_\mathbf{T}$, *the two previous conditions are combined.*

To say the same thing in words, if a tensor $\mathbf{T}$ is Z_p-invariant all harmonics belonging to spaces whose order is not an integer multiple of p are zero. The second property says that if $\mathbf{T}$ is invariant with respect to at least a symmetry line, then all its harmonics are co-linear (in a general sense cf. [61]). The last condition, that is, to be D_p-invariant, is obtained by combining the two previous requirements.

Other observations can be made from this result:

- harmonic structure of $\mathbb{TW}_4$ only contains even-order harmonic spaces, its results that
  1. $\mathbb{TW}_4$ is always at least Z_2-invariants, which means centrosymmetric in $\mathbb{R}^2$;
  2. $\mathbb{TW}_4$ can not see material rotational symmetry of odd-order $2p+1$, the rotation perceived by the tensor will be of twice order, i.e. $2(2p+1)$. This explains why a D_3-invariant material is modelled as a D_6-invariant one.

- in the case of a D_6-invariant polynomial the harmonic structure reduces to[5]

$$\begin{array}{ll} \underset{\sim}{D} \in \mathbb{W}_1 \simeq \mathbb{K}^0, & \dim(\mathbb{W}_1) = 1, \\ \underset{\approx}{C} \in \mathbb{W}_2 \simeq 2\mathbb{K}^0, & \dim(\mathbb{W}_2) = 2, \\ \underset{\approx\approx}{B} \in \mathbb{W}_3 \simeq \mathbb{K}^6 \oplus 2\mathbb{K}^0, & \dim(\mathbb{W}_3) = 3, \\ \underset{\approx\approx}{A} \in \mathbb{W}_4 \simeq \mathbb{K}^6 \oplus 3\mathbb{K}^0, & \dim(\mathbb{W}_4) = 4. \end{array}$$

  This result should be compared with the table obtained in section 2.4.3

Degree	Monomials	Dimension
1	I_1	1
2	$I_1^2,\ I_2$	2
3	$I_1^3,\ I_1 I_2,\ I_3$	3
4	$I_1^4,\ I_1^2 I_2,\ I_1 I_3,\ I_2^2$	4

  This highlights the link between the representation theorem approach and the harmonic decomposition approach. It reveals that the structure tensor we introduced in the previous chapter corresponds exactly to the harmonic tensor of the harmonic decomposition of $\mathbb{W}_3$ and $\mathbb{W}_4$.

- The last point amounts to compare the structure we obtain for a D_2-invariant polynomial and the harmonic decomposition in the same case. The harmonic structure reads

$$\mathbb{F}\mathrm{ix}(\mathbb{W}_4, D_2) \simeq \mathbb{K}^8 \oplus \mathbb{K}^6 \oplus 2\mathbb{K}^4 \oplus 2\mathbb{K}^2 \oplus 3\mathbb{K}^0$$

  Being orthotropic, the harmonic tensors of the decomposition are all collinear (in a generalised sense). Hence up to a rotation each harmonic component is defined by a unique parameter, it results that

$$\dim \mathbb{F}\mathrm{ix}(\mathbb{W}_4, D_2) = 8$$

  in which $\mathbb{F}\mathrm{ix}(\mathbb{V}, G)$ indicates the vector subspace of elements that are at least G-invariant.

  Consider now the monomials generating the quartic polynomial

$$\{I_1^4,\ I_1^3 J_1^2,\ I_1^2 J_1^2,\ I_1 J_1^3,\ J_I^4,\ I_1^2 J_2,\ J_1^2 J_2,\ I_1 J_1 J_2,\ J_2^2\}$$

  These monomials can be seen as polynomials in J_1, if we list these polynomials with respect to the degree in J_1

4	3	2	1	0
J_1^4	$I_1 J_1^3$	$I_1^2 J_1^2,\ J_2 J_1^2$	$I_1 J_2 J_1,\ I_1^3 J_1$	$I_1^4,\ J_2^2,\ I_1^2 J_2$

  The powers of J_1^k can be mapped to the harmonic tensor elements of $\mathbb{K}^{2k}$ appearing in the harmonic structure.

As we have just shown, the harmonic structure under $\mathbb{R}^2$ provides a good understanding of the link between the material symmetries and the independent components of the threshold function.

3.2.2 Harmonic structure with respect to $\mathbb{R}^3$

As discussed in the previous chapter, it is interesting to look at a threshold function as a surface in the stress space, i.e. in $\mathbb{R}^3$. This point of view makes it possible to include in the approach the *extended symmetry* of the material with respect to the loading. In fact, we will adopt this generalised point of view in the following sub-section.

Exceptionally we will note, in this section, $\underline{\sigma}$ the stress tensor considered as a vector of $\mathbb{R}^3$. The threshold function has the following shape

$$F(\underline{\sigma}) = \underset{\approx}{\hat{A}} :: (\underline{\sigma} \otimes \underline{\sigma} \otimes \underline{\sigma} \otimes \underline{\sigma}) + \underset{\approx}{\hat{B}} \vdots (\underline{\sigma} \otimes \underline{\sigma} \otimes \underline{\sigma}) + \underset{\sim}{\hat{C}} : (\underline{\sigma} \otimes \underline{\sigma}) + \underline{\hat{D}} \cdot \underline{\sigma},$$

[5] The notation is a little abusive, and the dimensions are given up to one rotation, which reduces the number of parameters for anisotropic spaces by one.

the 4 tensors are $\hat{\underset{\approx}{A}}, \hat{\underset{\simeq}{B}}, \hat{\underset{\sim}{C}}$ and $\hat{\underline{D}}$ are respectively 4th, 3rd, 2nd and 1st order tensors which contain all material parameters. In the present situation, each tensor of the threshold function is completely symmetric, i.e. belongs to $\mathbb{S}^n(\mathbb{R}^3)$. To continue, we need to introduce the notion of harmonic tensors in $\mathbb{R}^3$.

Definition 3.2.7. *Let $\mathbb{H}^n$ be the space of nth-order harmonic tensors in $\mathbb{R}^3$, its elements are:*

1. *n-th order tensors: $H_{i_1 i_2 \dots i_n}$*
2. *symmetric with respect to the permutation of all the indices: $H_{(i_1 i_2 \dots i_n)}$*
3. *traceless: $H_{(i_1 i_2 \dots i_p i_p)} = 0$*

As for $\mathbb{R}^2$, harmonic tensors in $\mathbb{R}^3$ are the nth-order generalisation to the notion of a deviatoric tensor. Regarding the dimension of these spaces we have:

$$\dim \mathbb{H}^n = 2n + 1$$

We have in $\mathbb{R}^3$ the following property: [105, 136]

Lemma 3.2.8. *In $\mathbb{R}^3$, the spaces of completely symmetric nth order tensors have the following harmonic structures*

$$\mathbb{S}^n = \begin{cases} \bigoplus_0^p \mathbb{H}^{2i}, \text{ if } n = 2p, \\ \bigoplus_0^p \mathbb{H}^{2i+1}, \text{ if } n = 2p+1. \end{cases}$$

Proposition 3.2.9. *The harmonic structure of tensor spaces of $\mathbb{TW}_4$ with respect to $\mathrm{SO}(3)$ are:*

$$\begin{array}{l|l} \underline{D} \in \mathbb{S}_1 \simeq \mathbb{H}^1, & \dim(\mathbb{S}_1) = 3, \\ \underset{\sim}{C} \in \mathbb{S}_2 \simeq \mathbb{H}^2 \oplus \mathbb{H}^0, & \dim(\mathbb{S}_2) = 6, \\ \underset{\simeq}{B} \in \mathbb{S}_3 \simeq \mathbb{H}^3 \oplus \mathbb{H}^1, & \dim(\mathbb{S}_3) = 10, \\ \underset{\approx}{A} \in \mathbb{S}_4 \simeq \mathbb{H}^4 \oplus \mathbb{H}^2 \oplus \mathbb{H}^0, & \dim(\mathbb{S}_4) = 15. \end{array}$$

It can be observed that $\dim(\mathbb{TW}_4) = 34$, since, of course, the change of decomposition does not affect the dimension of the space.

Threshold functions that are invariant with respect to $\underset{\sim}{\sigma} \to -\underset{\sim}{\sigma}$ are centro symmetric in $\mathbb{R}^3$. It results that odd-order harmonic tensors are null for such functions. As a result $\underline{D}$ and $\underset{\simeq}{B}$ are null for symmetric criteria and are necessary to model disymmetric ones.

3.2.3 Symmetry classes of the threshold surface

The main interest of deriving the $\mathbb{R}^3$ harmonic structure, is that it allows to obtain the exhaustive set of symmetry classes that the threshold surface can have. Indeed, the symmetry classes of harmonic spaces are known [100] and we have a tool, called *clips product*, to combine them [134, 135, 18] in order to obtain the symmetry classes of a direct sum of harmonic spaces. This approach will not be detailed here, we refer the interested reader to the above mentioned references, only the main results will be given without proof.

Proposition 3.2.10. *The $\mathrm{O}(3)$-symmetry classes of each tensor of the $\mathbb{TW}_4$ threshold function*

$$\begin{aligned} \mathfrak{I}(\mathbb{S}_1) &= \{[\mathrm{O}(2)^-], [\mathrm{O}(3)]\} \\ \mathfrak{I}(\mathbb{S}_2) &= \{[\mathrm{D}_2 \otimes \mathrm{Z}_2^c], [\mathrm{O}(2) \otimes \mathrm{Z}_2^c], [\mathrm{SO}(3) \otimes \mathrm{Z}_2^c]\} \\ \mathfrak{I}(\mathbb{S}_3) &= \{[\mathbb{1}], [\mathrm{Z}_2^-], [\mathrm{D}_2^v], [\mathrm{D}_3^v], [\mathrm{D}_6^h], [\mathcal{O}^-], [\mathrm{O}(2)^-], [\mathrm{O}(3)]\} \\ \mathfrak{I}(\mathbb{S}_4) &= \{[\mathrm{Z}_2^c], [\mathrm{Z}_2 \otimes \mathrm{Z}_2^c], [\mathrm{D}_2 \otimes \mathrm{Z}_2^c], [\mathrm{D}_3 \otimes \mathrm{Z}_2^c], [\mathrm{D}_4 \otimes \mathrm{Z}_2^c], [\mathcal{O} \otimes \mathrm{Z}_2^c], [\mathrm{O}(2) \otimes \mathrm{Z}_2^c], [\mathrm{SO}(3) \otimes \mathrm{Z}_2^c]\} \end{aligned}$$

As a trivial observation, the symmetry classes of even-order tensor spaces are centro-symmetric (Type II,), while the symmetry classes of odd-order tensor spaces are not centro-symmetric (Type I and III). For definitions of surface types, see the section 2.3.3.

A first result is that we can characterise the symmetry classes of the threshold surfaces that can be modelled using the classical Tsai-Wu criterion:

Proposition 3.2.11. *The symmetry classes of $\mathbb{TW}_2$ are*

$$\mathfrak{I}(\mathbb{TW}_2) = \{[\mathbb{1}], [\mathrm{D}_2 \otimes \mathrm{Z}_2^c], [\mathrm{O}(2) \otimes \mathrm{Z}_2^c], [\mathrm{Z}_2^-], [\mathrm{D}_2^v], [\mathrm{O}(2)^-], [\mathrm{O}(3)]\}$$

In this collection the centro symmetric classes are indicated in red, while the chiral one is in blue and the type III ones in purple. It can be observed on this result that the symmetric criteria that can be described by the model are of three types: $[\mathrm{D}_2 \otimes \mathrm{Z}_2^c]$, $[\mathrm{O}(2) \otimes \mathrm{Z}_2^c]$ and $[\mathrm{O}(3)]$.

The physical content of this result is a little subtle and we need to be careful about relating it to material anisotropy. For instance, it says that the symmetry symmetry class of the most generic surface that can be described by the model is $[\mathrm{D}_2 \otimes \mathrm{Z}_2^c]$. This result only indicates that the shape of the surface in the stress space is a generic ellipsoid: $\lambda_1 \neq \lambda_2 \neq \lambda_3 > 0$, and it does not specify the anisotropy of the material. Material anisotropy, which can be read in the deviatoric plane, is a property of invariance with respect to the specific axis $\hat{\underline{\mathrm{f}}}_3$ axis. Consider the harmonic basis $\mathcal{H} = \{\hat{\underline{\mathrm{f}}}_1, \hat{\underline{\mathrm{f}}}_2, \hat{\underline{\mathrm{f}}}_3\}$ together with $\mathcal{V} = \{\underline{\mathrm{v}}_1, \underline{\mathrm{v}}_2, \underline{\mathrm{v}}_3\}$ the direct orthonormal basis consisting of the principal axes of the ellipsoid:

- if $\hat{\underline{\mathrm{f}}}_3 = \underline{\mathrm{v}}_i$ for some i, the surface is $\mathrm{D}_2 \otimes \mathrm{Z}_2^c$ along this axis, and due to the doubling of the angle the criterion is D_4.
- if there is no i such as $\hat{\underline{\mathrm{f}}}_3 = \underline{\mathrm{v}}_i$, but a $\underline{\mathrm{v}}_i$ is in the deviatoric plane the surface is Z_2^π due to the doubling of the angle the criterion is D_2, i.e. orthotropic.
- if there is no i such as $\hat{\underline{\mathrm{f}}}_3 = \underline{\mathrm{v}}_i$, and no $\underline{\mathrm{v}}_i$ in the deviatoric plane the surface is $\mathbb{1}$ hence, due to the doubling of the angle, the criterion is Z_2, i.e. biclinic.

As such the expected $\mathbb{R}^2$ symmetry classes are retrieved.

The addition of higher-order tensors extends the capabilities of the model by allowing it to describe a richer set of surfaces. The descriptive capabilities of $\mathbb{TW}_4$ are given by the following result:

Proposition 3.2.12. *The symmetry classes of* $\mathbb{TW}_4$ *are*

$$\begin{aligned}\mathfrak{I}(\mathbb{TW}_4) \quad = \quad & \{[\mathbb{1}], [\mathrm{Z}_2], [\mathrm{Z}_3], [\mathrm{D}_2], [\mathrm{D}_3], \dots \\ & , [\mathrm{Z}_2^c], [\mathrm{Z}_2 \otimes \mathrm{Z}_2^c], [\mathrm{D}_2 \otimes \mathrm{Z}_2^c], [\mathrm{D}_3 \otimes \mathrm{Z}_2^c], [\mathrm{D}_4 \otimes \mathrm{Z}_2^c], [\mathcal{O} \otimes \mathrm{Z}_2^c], [\mathrm{O}(2) \otimes \mathrm{Z}_2^c], [\mathrm{O}(3)] \\ & , [\mathrm{Z}_2^-], [\mathrm{Z}_4^-], [\mathrm{D}_2^v], [\mathrm{D}_3^v], [\mathrm{D}_4^v], [\mathrm{D}_2^h], [\mathrm{D}_4^h], [\mathrm{D}_6^h], [\mathcal{O}^-], [\mathrm{O}(2)^-]\}\end{aligned}$$

Some immediate observations can be made:

- 23 different symmetry classes can be seen by the model instead of 7 in the case of $\mathbb{TW}_2$;
- the criterion has a greater ability to describe anisotropy. For instance, its ability to see the $[\mathrm{D}_3 \oplus \mathrm{Z}_2^c]$ class indicates that the criterion is capable of qualitatively describing the anisotropy of the Wang criterion, and the presence of the $[\mathrm{D}_3^v]$ class allows the Jeanneau surface to be modelled.
- we can also note the appearance of chiral classes (in blue) which were not really present in the standard model. These classes may be of interest for materials with chiral architecture.
- finally, the criteria can model some non crystallographic symmetry class, for instance a surface of class $[\mathrm{D}_4 \otimes \mathrm{Z}_2^c]$ can be described. This would correspond to a material with 8-fold invariance, such as the Ammann-Benker quasi-periodic lattice (cf. figure 3.1). Such an approach would therefore be of interest for quasi-periodic architectured materials.

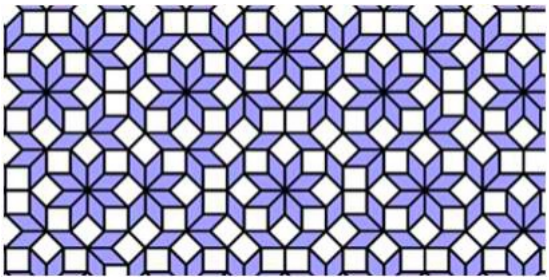

Figure 3.1: Quasi-periodic Amman-Beenker tilling "has" 8-fold symmetry.

3.3 Explicit Harmonic Decomposition

In the previous section we have seen, thanks to the harmonic structure of the different constitutive tensors, what physical information is contained in the model: anisotropy classes, asymmetry with respect to the loading,... This analysis has highlighted the role of the different harmonic tensors in the shape of the threshold surface.

However, at this stage we have no explicit parametrisation for this decomposition. Such a parametrisation is necessary to

1. to study the model in more detail using graphs, and thus better understand the specific contribution of each term;
2. provide an explicit threshold function for a given material;
3. fit an existing surface via our criterion.

The objective of the present section is to construct such a parametrisation. This involves constructing an explicit harmonic decomposition for each tensor in the criterion. A few points need to be made before we begin

- the harmonic decomposition of a tensor is, in general, not uniquely defined. So choices have to be made, which ideally should be made based on the physics of the problem under consideration. This simplifies the interpretation of the results as well as their use for optimisation.
- in the literature, few results are available concerning the harmonic decomposition of tensors of order greater than 4. In our case, we need to go up to order 8.

Consequently, the explicit decomposition of the 6th and 8th tensors of the model are new results that we had to establish. To do this, we adapted the Clebsch-Gordan approach to the harmonic decomposition introduced by Auffray et al. in [13].

The section is organised as follows. First, the available results concerning the explicit harmonic decomposition of the tensors $\underset{\approx}{\mathrm{C}}$ and $\underset{\sim}{\mathrm{D}}$ will be presented. Then, the general method to obtain the new result is introduced following the formalism used in [13]. The next subsection illustrates how to adapt this method to the 6th order tensor $\underset{\approx\approx\approx}{\mathrm{B}}$. Finally, results for the 8th-order tensor $\underset{\approx\approx\approx}{\mathrm{A}}$ are provided, while the explicit construction has been deferred to section i.

3.3.1 Explicit harmonic decompositions available

The explicit harmonic decomposition of the tensors $\underset{\approx}{\mathrm{C}}$ and $\underset{\sim}{\mathrm{D}}$ has already been done in [13]. We summarise the associated propositions here:

Proposition 3.3.1. *The tensor $\underset{\sim}{\mathrm{D}} \in S^2(\mathbb{R}^2)$ admits the uniquely defined Clebsch-Gordan Harmonic decomposition defined as follows:*

$$\underset{\sim}{\mathrm{D}} = \underset{\sim}{\mathrm{h}}^{2,1} + \alpha^{2,0}\underset{\sim}{\mathrm{I}}.$$

$\underset{\sim}{\mathrm{I}}$ is the identity second order tensor. $(\underset{\sim}{\mathrm{h}}^{2,1}, \alpha^{2,0})$ are elements of $\mathbb{K}^2 \times \mathbb{K}^0$ defined from $\underset{\sim}{\mathrm{D}}$ as follows:

$$\underset{\sim}{\mathrm{h}}^{2,1} = \underset{\approx}{\mathrm{P}}^{(2)} : \underset{\sim}{\mathrm{D}} \qquad ; \qquad \alpha^{2,0}\underset{\sim}{\mathrm{I}} = \underset{\approx}{\mathrm{P}}^{(0)} : \underset{\sim}{\mathrm{D}} = \frac{1}{2}(\mathrm{tr}\,\underset{\sim}{\mathrm{D}})\underset{\sim}{\mathrm{I}},$$

where $\underset{\approx}{\mathrm{P}}^{(2)}$ and $\underset{\approx}{\mathrm{P}}^{(0)}$ are the deviatoric and the spherical projectors.

Proposition 3.3.2. *The tensor $\underset{\approx}{\mathrm{C}} \in S^2(S^2(\mathbb{R}^2))$ admits the uniquely defined Clebsch-Gordan Harmonic Decomposition defined as follows::*

$$\underset{\approx}{\mathrm{C}} = \underset{\approx}{\mathrm{H}}^{4,1} + \frac{\alpha^{4,2}}{2}\underset{\approx}{\mathrm{P}}^{(2)} + \underset{\sim}{\mathrm{h}}^{4,1} \otimes \underset{\sim}{\mathrm{I}} + \underset{\sim}{\mathrm{I}} \otimes \underset{\sim}{\mathrm{h}}^{4,1} + 2\alpha^{4,0}\underset{\approx}{\mathrm{P}}^{(0)}, \tag{3.5}$$

$\underset{\sim}{\mathrm{I}}$ is the identity second order tensor. $(\underset{\approx}{\mathrm{H}}^{4,2}, \underset{\sim}{\mathrm{h}}^{4,1}, \alpha^{4,2}, \alpha^{4,0})$ are elements of $\mathbb{K}^4 \times \mathbb{K}^2 \times \mathbb{K}^0 \times \mathbb{K}^0$ defined from $\underset{\approx}{\mathrm{C}}$ as follows:

$\mathbb{K}^0$	$\mathbb{K}^2$	$\mathbb{K}^4$
$\alpha^{4,0} = \underset{\approx}{\mathrm{P}}^{(2)} :: \underset{\approx}{\mathrm{C}}$	$\underset{\sim}{\mathrm{h}}^{4,1} = \underset{\approx}{\mathrm{P}}^{(2)} : \underset{\approx}{\mathrm{C}}$	
$\alpha^{4,2} = \underset{\approx}{\mathrm{C}}^{2,2} :: \underset{\approx}{\mathrm{P}}^{(2)}$		$\underset{\approx}{\mathrm{H}}^{4,2} = \underset{\approx}{\mathrm{C}}^{2,2} - \frac{\alpha^{4,0}}{2}\underset{\approx}{\mathrm{P}}^{(2)}$

where $\underset{\approx}{\mathrm{C}}^{2,2} = \underset{\approx}{\mathrm{P}}^{(2)} : \underset{\approx}{\mathrm{C}} : \underset{\approx}{\mathrm{P}}^{(2)}$.

The remaining two harmonic decompositions are not yet available in the literature and have therefore been explicitly derived during this PhD. the next section, the three-step method introduced in [13] is presented as defined in the original article. This method will then be adapted to the current situation.

3.3.2 The original three-step methodology

Consider two spaces of state tensors denoted by $\mathbb{E}$ and $\mathbb{F}$. The (linear) constitutive law is an element $\mathbf{T} \in \mathcal{L}(\mathbb{E}, \mathbb{F})$. In the present context, $\mathbf{T}$ represents the constitutive tensor of which we want to obtain the harmonic decomposition. The construction of a Clebsch-Gordan Harmonic Decomposition (in abbreviated form CGHD) of $\mathbf{T}$ is obtained using the following procedure:

1) State Tensor Harmonic Decomposition (STHD) Choose and compute a harmonic decomposition for elements $\mathbf{v} \in \mathbb{E}$ and $\mathbf{w} \in \mathbb{F}$. This decomposition implies the definition of *harmonic embedding* operators. From these operators, we get a family of orthogonal projectors that will be used to decompose $\mathbf{T}$;

2) Intermediate Block Decomposition (IBD) Consider an element $\mathbf{T} \in \mathcal{L}(\mathbb{E}, \mathbb{F})$ which represents the constitutive tensor of which we want to obtain the harmonic decomposition. The choice of a STHD and the use of the associated projectors induce a decomposition of $\mathcal{L}(\mathbb{E}, \mathbb{F})$ into *blocks*. This decomposition, that will be referred to as the *Intermediate Block Decomposition*, is not irreducible;

3) Clebsch-Gordan Harmonic Decomposition (CGHD) Each elementary block of the *Intermediate Block Decomposition* belongs to a space $\mathbb{K}^p \otimes \mathbb{K}^q$, the harmonic structure of which is known by the Clebsch-Gordan formula. The use of harmonic embeddings allows us to break down each block into irreducible tensors.

The combination of the last two steps provides the Clebsch-Gordan Harmonic Decomposition of $\mathbf{T} \in \mathcal{L}(\mathbb{E}, \mathbb{F})$. The resulting decomposition is a particular explicit harmonic decomposition of $\mathbf{T}$ which is compatible with the harmonic decompositions of $\mathbf{v}$ and $\mathbf{w}$. This decomposition is uniquely defined by the choice of a particular form of the harmonic decompositions for the spaces $\mathbb{E}$ and $\mathbb{F}$. It has to be noted that different choices for the decompositions of $\mathbb{E}$ and $\mathbb{F}$ will lead to different decompositions of $\mathbf{T}$.

3.3.3 The CGHD of $\mathbb{W}_3$

The previous method will be adapted to the current situation. The associated changes are minor and will be illustrated below. But first, let's define some of the notations that will be used.

Step 0: General settings

First let us introduce the notation:

$$\underset{\approx}{\mathrm{B}} \overset{6}{\cdot} (\underset{\sim}{\sigma} \otimes \underset{\sim}{\tau} \otimes \underset{\sim}{\eta}) = (\underset{\sim}{\sigma} : \underset{\approx}{\mathrm{B}} : \underset{\sim}{\eta}) : \underset{\sim}{\tau} \tag{3.6}$$

which reads, in components,

$$B_{(ij)(kl)(mn)} \sigma_{(ij)} \tau_{(kl)} \eta_{(mn)}$$

Here, only the case $\underset{\sim}{\sigma} = \underset{\sim}{\tau} = \underset{\sim}{\eta}$ will be considered, hence

$$B_{\underline{(ij)}\ \underline{(kl)}\ \underline{(mn)}} \sigma_{(ij)} \sigma_{(kl)} \sigma_{(mn)} \tag{3.7}$$

The coefficients of the third-order polynomial in $\underset{\sim}{\sigma}$ are contained in the 6th-order tensor $\underset{\approx}{\mathrm{B}} \in \mathbb{W}_3$. We recall that this space has the following structure $\mathbb{W}_3 = S^3(S^2(\mathbb{R}^2))$. The index symmetry group of $\underset{\approx}{\mathrm{B}}$ is

$$\mathbb{G}(\underset{\approx}{\mathrm{B}}) = \mathfrak{S}_3 \otimes \mathrm{Z}_2.$$

where $\mathfrak{S}_3$ is the symmetric group on 3 elements and corresponds to the permutation of the underlined blocks appearing in equation (3.6). The group Z_2 corresponds to the index symmetry of σ indicated by parentheses in equation (3.6). The resulting number of index symmetries of $\underset{\approx}{\mathrm{B}}$ is $\#\mathbb{G}(\underset{\approx}{\mathrm{B}}) = 3!2^3 = 48$ and a set of generators of $\mathbb{G}(\underset{\approx}{\mathrm{B}})$ is given by:

$$\mathrm{Gen}\left(\mathbb{G}(\underset{\approx}{\mathrm{B}})\right) = \{(12), (13)(24), (15)(26)\}.$$

Knowing $\mathbb{G}(\underset{\approx}{\mathrm{B}})$, let us establish the harmonic decomposition of $\underset{\approx}{\mathrm{B}}$.

Let us adapt the algorithm introduced in section 3.3.2 to the current situation

Step 1: Decomposition of the state tensor

In this case there is a unique state tensor space $\mathbb{E}$ which is the stress tensor space $S^2(\mathbb{R}^2)$. The harmonic decomposition of $\underset{\sim}{\sigma}$ has been introduced in section 2.2.2, we have:

$$\underset{\sim}{\sigma} = \underset{\sim}{\sigma}^{(2)} + \underset{\sim}{\sigma}^{(0)}, \quad (\underset{\sim}{\sigma}^{(2)}, \underset{\sim}{\sigma}^{(0)}) \in \mathbb{K}^2 \times \mathbb{K}^0$$

This decomposition can be obtained using the deviatoric $\underset{\approx}{\mathrm{P}}^{(2)}$ and the spherical projector $\underset{\approx}{\mathrm{P}}^{(0)}$

$$\underset{\sim}{\sigma}^{(2)} = \underset{\approx}{\mathrm{P}}^{(2)} : \underset{\sim}{\sigma}, \qquad \underset{\sim}{\sigma}^{(0)} = \underset{\approx}{\mathrm{P}}^{(0)} : \underset{\sim}{\sigma},$$

and, for the next step, we recall the following properties of the projection operator:

$$\underset{\approx}{\mathrm{P}}^{i} : \underset{\approx}{\mathrm{P}}^{i} = \underset{\approx}{\mathrm{P}}^{i}, \qquad \underset{\approx}{\mathrm{P}}^{i} : \underset{\sim}{\sigma} = \underset{\sim}{\sigma} : \underset{\approx}{\mathrm{P}}^{i} \quad \text{for } i \in \{0, 2\}. \tag{3.8}$$

Step 2: Intermediate block decomposition

The introduction of the decomposition $\underset{\sim}{\sigma}$ in equation (3.7) induces the following partition

$$\begin{aligned}
(\underset{\sim}{\sigma} : \underset{\approx\approx}{\mathrm{B}} : \underset{\sim}{\sigma}) : \underset{\sim}{\sigma} &= \left[(\underset{\sim}{\sigma}^{(2)} + \underset{\sim}{\sigma}^{(0)}) : \underset{\approx\approx}{\mathrm{B}} : (\underset{\sim}{\sigma}^{(2)} + \underset{\sim}{\sigma}^{(0)})\right] : (\underset{\sim}{\sigma}^{(2)} + \underset{\sim}{\sigma}^{(0)}), \\
&= (\underset{\sim}{\sigma}^{(2)} : \underset{\approx\approx}{\mathrm{B}} : \underset{\sim}{\sigma}^{(2)}) : \underset{\sim}{\sigma}^{(2)} + (\underset{\sim}{\sigma}^{(2)} : \underset{\approx\approx}{\mathrm{B}} : \underset{\sim}{\sigma}^{(2)}) : \underset{\sim}{\sigma}^{(0)} + (\underset{\sim}{\sigma}^{(2)} : \underset{\approx\approx}{\mathrm{B}} : \underset{\sim}{\sigma}^{(0)}) : \underset{\sim}{\sigma}^{(2)} + (\underset{\sim}{\sigma}^{(0)} : \underset{\approx\approx}{\mathrm{B}} : \underset{\sim}{\sigma}^{(2)}) : \underset{\sim}{\sigma}^{(2)} \\
&+ (\underset{\sim}{\sigma}^{(0)} : \underset{\approx\approx}{\mathrm{B}} : \underset{\sim}{\sigma}^{(0)}) : \underset{\sim}{\sigma}^{(2)} + (\underset{\sim}{\sigma}^{(0)} : \underset{\approx\approx}{\mathrm{B}} : \underset{\sim}{\sigma}^{(2)}) : \underset{\sim}{\sigma}^{(0)} + (\underset{\sim}{\sigma}^{(2)} : \underset{\approx\approx}{\mathrm{B}} : \underset{\sim}{\sigma}^{(0)}) : \underset{\sim}{\sigma}^{(0)} + (\underset{\sim}{\sigma}^{(0)} : \underset{\approx\approx}{\mathrm{B}} : \underset{\sim}{\sigma}^{(0)}) : \underset{\sim}{\sigma}^{(0)}.
\end{aligned} \tag{3.9}$$

This expression can be reformulated from the following property

$$(\underset{\sim}{\sigma}^{(p)} : \underset{\approx\approx}{\mathrm{B}} : \underset{\sim}{\sigma}^{(q)}) : \underset{\sim}{\sigma}^{(r)} = (\underset{\sim}{\sigma}^{(p)} : \underset{\approx\approx}{\mathrm{B}}^{p,q,r} : \underset{\sim}{\sigma}^{(q)}) : \underset{\sim}{\sigma}^{(r)}, \qquad \forall p, q, r \in \{0, 2\}.$$

in which

$$\underset{\approx\approx}{\mathrm{B}}^{p,q,r} = \underset{\approx\approx}{\mathrm{B}} \overset{6}{\circ} (\underset{\approx}{\mathrm{P}}^{p} \otimes \underset{\approx}{\mathrm{P}}^{q} \otimes \underset{\approx}{\mathrm{P}}^{r}) \tag{3.10}$$

with the definition

$$\left(\underset{\approx\approx}{\mathrm{B}} \overset{6}{\circ} (\underset{\approx}{\mathrm{P}} \otimes \underset{\approx}{\mathrm{Q}} \otimes \underset{\approx}{\mathrm{R}})\right)_{ijklmn} = B_{pqrstu} P_{pqij} Q_{rskl} R_{tumn}.$$

To see why consider a term from (B.3) (the table 2.1 is useful):

$$\begin{aligned}
(\underset{\sim}{\sigma}^{(2)} : \underset{\approx\approx}{\mathrm{B}} : \underset{\sim}{\sigma}^{(2)}) : \underset{\sim}{\sigma}^{(0)} &= \left[(\underset{\approx}{\mathrm{P}}^{(2)} : \underset{\sim}{\sigma}) : \underset{\approx\approx}{\mathrm{B}} : (\underset{\approx}{\mathrm{P}}^{(2)} : \underset{\sim}{\sigma})\right] : (\underset{\approx}{\mathrm{P}}^{(0)} : \underset{\sim}{\sigma}), \\
&= B_{ijklmn} P^2_{ijop} \sigma_{op} P^2_{mnqr} \sigma_{qr} P^0_{klst} \sigma_{st}, \\
&= B_{ijklmn} P^2_{ijop} P^2_{mnqr} P^0_{klst} \sigma_{op} \sigma_{qr} \sigma_{st}, \\
&= \underbrace{B_{ijklmn} P^2_{ijuv} P^2_{klyz} P^0_{mnwx}}_{\underset{\approx\approx}{\mathrm{B}} \overset{6}{\circ} (\underset{\approx}{\mathrm{P}}^{(2)} \otimes \underset{\approx}{\mathrm{P}}^{(2)} \otimes \underset{\approx}{\mathrm{P}}^{(0)})} \underbrace{P^2_{uvop} \sigma_{op}}_{\underset{\approx}{\mathrm{P}}^{(2)} : \underset{\sim}{\sigma}} \underbrace{P^2_{yzst} \sigma_{st}}_{\underset{\approx}{\mathrm{P}}^{(2)} : \underset{\sim}{\sigma}} \underbrace{P^0_{wxqr} \sigma_{qr}}_{\underset{\approx}{\mathrm{P}}^{(0)} : \underset{\sim}{\sigma}}, \\
&= \left[(\underset{\approx}{\mathrm{P}}^{(2)} : \underset{\sim}{\sigma}) : \left[\underset{\approx\approx}{\mathrm{B}} \overset{6}{\circ} (\underset{\approx}{\mathrm{P}}^{(2)} \otimes \underset{\approx}{\mathrm{P}}^{(2)} \otimes \underset{\approx}{\mathrm{P}}^{(0)})\right] : (\underset{\approx}{\mathrm{P}}^{(0)} : \underset{\sim}{\sigma})\right] : (\underset{\approx}{\mathrm{P}}^{(2)} : \underset{\sim}{\sigma}), \\
&= (\underset{\sim}{\sigma}^{(2)} : \underbrace{\left[\underset{\approx\approx}{\mathrm{B}} \overset{6}{\circ} (\underset{\approx}{\mathrm{P}}^{(0)} \otimes \underset{\approx}{\mathrm{P}}^{(2)} \otimes \underset{\approx}{\mathrm{P}}^{(0)})\right]}_{\underset{\approx\approx}{\mathrm{B}}^{2,2,0}} : \underset{\sim}{\sigma}^{(0)}) : \underset{\sim}{\sigma}^{(2)}.
\end{aligned} \tag{3.11}$$

It follows that $\underset{\approx\approx}{\mathrm{B}}$ can be split into

$$\underset{\approx\approx}{\mathrm{B}} = \underset{\approx\approx}{\mathrm{B}}^{2,2,2} + \underset{\approx\approx}{\mathrm{B}}^{2,2,0} + \underset{\approx\approx}{\mathrm{B}}^{2,0,2} + \underset{\approx\approx}{\mathrm{B}}^{0,2,2} + \underset{\approx\approx}{\mathrm{B}}^{2,0,0} + \underset{\approx\approx}{\mathrm{B}}^{0,2,0} + \underset{\approx\approx}{\mathrm{B}}^{0,0,2} + \underset{\approx\approx}{\mathrm{B}}^{0,0,0}$$

in which, because of equation (3.10), all the blocks are orthogonal to each other with respect to the complete contraction.

On this decomposition it can be observed that only the terms $\underset{\approx}{\mathrm{B}}^{2,2,2}$ and $\underset{\approx}{\mathrm{B}}^{0,0,0}$ have the same index symmetry as $\underset{\approx}{\mathrm{B}}$, i.e. belongs to $\mathbb{W}_3$, being $\mathfrak{S}_3$ symmetric, these blocks will henceforth be denoted $\underset{\approx}{\mathrm{B}}^{(222)}$ and $\underset{\approx}{\mathrm{B}}^{(000)}$. This is not the case for the remaining blocks taken individually, but if we group them as follows

$$\begin{aligned}\underset{\approx}{\mathrm{B}}^{(220)} &= \underset{\approx}{\mathrm{B}}^{2,2,0}+\underset{\approx}{\mathrm{B}}^{2,0,2}+\underset{\approx}{\mathrm{B}}^{0,2,2}\\ \underset{\approx}{\mathrm{B}}^{(200)} &= \underset{\approx}{\mathrm{B}}^{2,0,0}+\underset{\approx}{\mathrm{B}}^{0,2,0}+\underset{\approx}{\mathrm{B}}^{0,0,2}\end{aligned}$$

$\underset{\approx}{\mathrm{B}}^{(220)}$ and $\underset{\approx}{\mathrm{B}}^{(220)}$ are elements of $\mathbb{W}_3$ and the mismatch is solved. At the end,

$$\underset{\approx}{\mathrm{B}}=\underset{\approx}{\mathrm{B}}^{(222)}+\underset{\approx}{\mathrm{B}}^{(220)}+\underset{\approx}{\mathrm{B}}^{(200)}+\underset{\approx}{\mathrm{B}}^{(000)}$$

which means that $\mathbb{W}_3$ has been split into 4 orthogonal subspaces, i.e

$$\mathbb{W}_3=\mathbb{W}_3^3\oplus\mathbb{W}_3^2\oplus\mathbb{W}_3^1\oplus\mathbb{W}_3^0,\qquad(\underset{\approx}{\mathrm{B}}^{(222)},\underset{\approx}{\mathrm{B}}^{(220)},\underset{\approx}{\mathrm{B}}^{(200)},\underset{\approx}{\mathrm{B}}^{(000)})\in(\mathbb{W}_3^3\times\mathbb{W}_3^2\times\mathbb{W}_3^1\times\mathbb{W}_3^0)\tag{3.12}$$

in which the number k in $\mathbb{W}_3^k$ indicates the number of occurrences of the space $\mathbb{K}^2$ in the underlying tensor product. This decomposition should be compared with the expression given by the lemma 3.2.3, i.e.

$$\mathbb{W}_3\simeq S^3(\mathbb{K}^2)\oplus S^2(\mathbb{K}^2)\oplus\mathbb{K}^2\oplus\mathbb{K}^0\tag{3.13}$$

through the isomorphism

$$\mathbb{W}_3^k\simeq S^k(\mathbb{K}^2)$$

.

Step 3: Clebsch-Gordan harmonic decomposition

The blocks $\underset{\approx}{\mathrm{B}}^{(pqr)}$ we have obtained are not O(2)-irreducible and should therefore be decomposed further. The first step to compute their explicit harmonic decomposition is to determine their harmonic structure. This structure is a consequence of equation (3.12) and equation (3.13). For $\mathbb{W}_3^1$ and $\mathbb{W}_3^0$, the results are straightforward,

$$\mathbb{W}_3^1\simeq\mathbb{K}^2,\ \mathbb{W}_3^0\simeq\mathbb{K}^0$$

whereas for the other two spaces, they are obtained by applying the formula of the lemma 3.2.4

$$\mathbb{W}_3^3\simeq\mathbb{K}^6\oplus\mathbb{K}^2,\ \mathbb{W}_3^2\simeq\mathbb{K}^4\oplus\mathbb{K}^0$$

It results that the harmonic structure of $\mathbb{W}_3$ is:

$$\mathbb{W}_3\simeq\mathbb{K}^6\oplus\mathbb{K}^4\oplus2\mathbb{K}^2\oplus2\mathbb{K}^0,\quad\dim(\mathbb{W}_3)=10$$

as already known from proposition 3.2.5 but, now, we know explicitly in which elementary block each harmonic tensor is located.

Using this information, we can now carry out an explicit decomposition, block by block. The cornerstone of the procedure is the expression of $\underset{\approx}{\mathrm{P}}^{(0)}$, which for the record is

$$\underset{\approx}{\mathrm{P}}^{(0)}=\frac{1}{2}\underset{\sim}{\mathrm{I}}\otimes\underset{\sim}{\mathrm{I}},$$

and which will be injected into the definition of each block. The different problems will be dealt with in order of increasing complexity.

a) The space $\mathbb{W}_3^0$ Since $\underset{\approx}{\mathrm{B}}^{(000)}\in\mathbb{W}_3^0\simeq\mathbb{K}^0$ this term is isotropic and reduces to a unique scalar that will be denoted[6] $\alpha^{6,0}$. Let us insert the expression of $\underset{\approx}{\mathrm{P}}^{(0)}$ into the definition of $\underset{\approx}{\mathrm{B}}^{(000)}$

$$\begin{aligned}\underset{\approx}{\mathrm{B}}^{(000)} &= \underset{\approx}{\mathrm{B}}\overset{6}{\circ}(\underset{\approx}{\mathrm{P}}^{(0)}\otimes\underset{\approx}{\mathrm{P}}^{(0)}\otimes\underset{\approx}{\mathrm{P}}^{(0)})=\frac{1}{8}\underset{\approx}{\mathrm{B}}\overset{6}{\circ}\left[(\underset{\sim}{\mathrm{I}}\otimes\underset{\sim}{\mathrm{I}})\otimes(\underset{\sim}{\mathrm{I}}\otimes\underset{\sim}{\mathrm{I}})\otimes(\underset{\sim}{\mathrm{I}}\otimes\underset{\sim}{\mathrm{I}})\right]\\ &= \frac{1}{8}\underbrace{\left(\underset{\approx}{\mathrm{B}}\overset{6}{\circ}\left[\underset{\sim}{\mathrm{I}}\otimes\underset{\sim}{\mathrm{I}}\otimes\underset{\sim}{\mathrm{I}}\right]\right)}_{\alpha^{6,0}}\underset{\sim}{\mathrm{I}}\otimes\underset{\sim}{\mathrm{I}}\otimes\underset{\sim}{\mathrm{I}}\end{aligned}$$

[6] In the notation $\alpha^{p,q}$, p denotes the order of the tensor and q the degree in $\mathbb{K}^2$. Here $q=0$ since $\underset{\approx}{\mathrm{B}}^{(000)}$ is purely hydrostatic.

$$\begin{aligned}
\underset{\approx\approx}{\mathrm{B}}^{(000)} &= \underset{\approx\approx}{\mathrm{B}} \overset{6}{\circ} (\underset{\approx}{\mathrm{P}}^{(0)} \otimes \underset{\approx}{\mathrm{P}}^{(0)} \otimes \underset{\approx}{\mathrm{P}}^{(0)}) = \frac{1}{8}\underset{\approx\approx}{\mathrm{B}} \overset{6}{\circ} \left[(\underset{\sim}{\mathrm{I}} \otimes \underset{\sim}{\mathrm{I}}) \otimes (\underset{\sim}{\mathrm{I}} \otimes \underset{\sim}{\mathrm{I}}) \otimes (\underset{\sim}{\mathrm{I}} \otimes \underset{\sim}{\mathrm{I}})\right] \\
&= \frac{1}{8}\left(\underset{\approx\approx}{\mathrm{B}} \overset{6}{\circ} \left[\underset{\sim}{\mathrm{I}} \otimes \underset{\sim}{\mathrm{I}} \otimes \underset{\sim}{\mathrm{I}}\right]\right) \underset{\sim}{\mathrm{I}} \otimes \underset{\sim}{\mathrm{I}} \otimes \underset{\sim}{\mathrm{I}} \\
&= \frac{1}{8}\alpha^{6,0}\underset{\sim}{\mathrm{I}} \otimes \underset{\sim}{\mathrm{I}} \otimes \underset{\sim}{\mathrm{I}} \\
&= \frac{1}{4}\alpha^{6,0}\underset{\sim}{\mathrm{I}} \otimes \underset{\approx}{\mathrm{P}}^{(0)}
\end{aligned}$$

Hence the following parameterisation is obtained

$$\underset{\approx\approx}{\mathrm{B}}^{(000)} = \frac{1}{4}\alpha^{6,0}(\underset{\sim}{\mathrm{I}} \otimes \underset{\approx}{\mathrm{P}}^{(0)}),$$

and conversely the scalar we are looking for is determined as

$$\alpha^{6,0} = (\underset{\sim}{\mathrm{I}} : \underset{\approx\approx}{\mathrm{B}} : \underset{\sim}{\mathrm{I}}) : \underset{\sim}{\mathrm{I}} = \mathrm{tr}_{12}\left(\mathrm{tr}_{12}\left(\mathrm{tr}_{12}(\underset{\approx\approx}{\mathrm{B}})\right)\right) = \mathrm{tr}_{12}^{(3)}(\underset{\approx\approx}{\mathrm{B}})$$

in which $\mathrm{tr}_{ab}^{(n)}$ stands for the nth-order iterated trace on the index ab, and should not be confused with the n-th power of tr_{ab}.

b) The space $\mathbb{W}_3^1$ The term $\underset{\approx\approx}{\mathrm{B}}^{(200)} \in \mathbb{W}_3^1$ will be treated in two stages. First the harmonic term $\underset{\approx\approx}{\mathrm{B}}^{2,0,0}$ will be proceed, and then its expression symmetrised to obtained $\underset{\approx\approx}{\mathrm{B}}^{(200)}$.

From its harmonic structure, we know that $\underset{\approx\approx}{\mathrm{B}}^{2,0,0}$ is parameterised by a second order harmonic tensor $\mathrm{h}^{6,1} \in \mathbb{K}^2$. As in the previous paragraph, let's start by inserting the expression for $\underset{\approx}{\mathrm{P}}^{(0)}$ into the definition of $\underset{\approx\approx}{\tilde{\mathrm{B}}}^{2,0,0}$.

$$\begin{aligned}
\underset{\approx\approx}{\mathrm{B}}^{2,0,0} &= \underset{\approx\approx}{\mathrm{B}} \overset{6}{\circ} (\underset{\approx}{\mathrm{P}}^{(2)} \otimes \underset{\approx}{\mathrm{P}}^{(0)} \otimes \underset{\approx}{\mathrm{P}}^{(0)}) = \frac{1}{4}\underset{\approx\approx}{\mathrm{B}} \overset{6}{\circ} \left[\underset{\approx}{\mathrm{P}}^{(2)} \otimes (\underset{\sim}{\mathrm{I}} \otimes \underset{\sim}{\mathrm{I}}) \otimes (\underset{\sim}{\mathrm{I}} \otimes \underset{\sim}{\mathrm{I}})\right] \\
&= \frac{1}{4}\left(\underset{\approx\approx}{\mathrm{B}} \overset{6}{\circ} \left[\underset{\approx}{\mathrm{P}}^{(2)} \otimes \underset{\sim}{\mathrm{I}} \otimes \underset{\sim}{\mathrm{I}}\right]\right) \underset{\sim}{\mathrm{I}} \otimes \underset{\sim}{\mathrm{I}} \\
&= \frac{1}{4}\underset{\sim}{\mathrm{h}}^{6,1} \otimes \underset{\sim}{\mathrm{I}} \otimes \underset{\sim}{\mathrm{I}} \\
&= \frac{1}{2}\underset{\sim}{\mathrm{h}}^{6,1} \otimes \underset{\approx}{\mathrm{P}}^{(0)}
\end{aligned}$$

Hence the following parameterisation is obtained

$$\underset{\approx\approx}{\mathrm{B}}^{2,0,0} = \frac{1}{2}\underset{\sim}{\mathrm{h}}^{6,1} \otimes \underset{\approx}{\mathrm{P}}^{(0)},$$

and conversely the harmonic tensor we are looking for is determined as

$$\underset{\sim}{\mathrm{h}}^{6,1} = \underset{\approx}{\mathrm{P}}^{(2)} : (\underset{\sim}{\mathrm{I}} : \underset{\approx\approx}{\mathrm{B}} : \underset{\sim}{\mathrm{I}}) = \underset{\approx}{\mathrm{P}}^{(2)} : \left(\mathrm{tr}_{12}^{(2)}(\underset{\approx\approx}{\mathrm{B}})\right).$$

The parameterisation of $\underset{\approx\approx}{\mathrm{B}}^{(200)}$ can now be obtained by symmetrisation

$$\begin{aligned}
\underset{\approx\approx}{\mathrm{B}}^{(200)} &= \underset{\approx\approx}{\mathrm{B}}^{2,0,0} + \underset{\approx\approx}{\mathrm{B}}^{0,2,0} + \underset{\approx\approx}{\mathrm{B}}^{0,0,2} \\
&= \underbrace{(\varsigma_{(e)} + \varsigma_{(13)(24)} + \varsigma_{(15)(26)})}_{\tau_3} \star \underset{\approx\approx}{\mathrm{B}}^{2,0,0}
\end{aligned}$$

in which τ_3 is the symmetrisation operator from $\mathbb{K}^2 \otimes S^2(\mathbb{R}^2)$ to $\mathbb{W}_3^1$.

c) The space $\mathbb{W}_3^2$ As for the previous situation, the term $\underset{\approx\approx}{\mathrm{B}}^{(220)} \in \mathbb{W}_3^2$ will be treated in two stages. First the harmonic term $\underset{\approx\approx}{\mathrm{B}}^{0,2,2}$ will be proceed, and then its expression symmetrised to obtained $\underset{\approx\approx}{\mathrm{B}}^{(220)}$. The harmonic structure of $\underset{\approx\approx}{\mathrm{B}}^{0,2,2}$ is a little more complex because it contains two terms $\underset{\approx}{\mathrm{H}}^{6,2} \in \mathbb{K}^4$ and $\alpha^{6,2} \in \mathbb{K}^0$. The insertion of $\underset{\approx}{\mathrm{P}}^{(0)}$ into the definition of $\underset{\approx\approx}{\mathrm{B}}^{0,2,2}$ allows to write

$$\begin{aligned}
\underset{\approx\approx}{\mathrm{B}}^{0,2,2} &= \underset{\approx\approx}{\mathrm{B}} \overset{6}{\circ} (\underset{\approx}{\mathrm{P}}^{(0)} \otimes \underset{\approx}{\mathrm{P}}^{(2)} \otimes \underset{\approx}{\mathrm{P}}^{(2)}) = \frac{1}{2}\underset{\approx\approx}{\mathrm{B}} \overset{6}{\circ} ((\underset{\sim}{\mathrm{I}} \otimes \underset{\sim}{\mathrm{I}}) \otimes \underset{\approx}{\mathrm{P}}^{(2)} \otimes \underset{\approx}{\mathrm{P}}^{(2)}) \\
&= \frac{1}{2}\underset{\sim}{\mathrm{I}} \otimes \left[\underset{\approx}{\mathrm{P}}^{(2)} : (\underset{\approx\approx}{\mathrm{B}} : \underset{\sim}{\mathrm{I}}) : \underset{\approx}{\mathrm{P}}^{(2)}\right] \\
&= \frac{1}{2}\underset{\sim}{\mathrm{I}} \otimes \underset{\approx}{\mathrm{Q}}^{6,2}
\end{aligned}$$

The sixth-order tensor $\underset{\approx\approx}{\mathrm{B}}^{0,2,2}$ can thus be reduced to a fourth-order one $\underset{\approx}{\mathrm{Q}}^{6,2}$ element of $S^2(\mathbb{K}^2)$, i.e.

$$\underset{\approx}{\mathrm{Q}}^{6,2} = \underset{\approx}{\mathrm{P}}^{(2)} : (\underset{\approx\approx}{\mathrm{B}} : \underset{\sim}{\mathrm{I}}) : \underset{\approx}{\mathrm{P}}^{(2)} = \underset{\approx}{\mathrm{P}}^{(2)} : \left(\mathrm{tr}_{12}(\underset{\approx\approx}{\mathrm{B}})\right) : \underset{\approx}{\mathrm{P}}^{(2)},$$

but, unlike the previous situations, this tensor is not O(2) -irreducible and must therefore be redecomposed. Using a procedure described in [13], and recalled in appendix ii, it can be demonstrated that

$$\underset{\approx}{\mathrm{Q}}^{6,2} = \underset{\approx}{\mathrm{H}}^{6,2} + \frac{\alpha^{6,2}}{2}\underset{\approx}{\mathrm{P}}^{(2)}, \quad \text{with } (\underset{\approx}{\mathrm{H}}^{6,2}, \alpha^{6,2}) \in \mathbb{K}^4 \times \mathbb{K}^0$$

with:

$$\alpha^{6,2} = \underset{\approx}{\mathrm{P}}^{(2)} :: \underset{\approx}{\mathrm{Q}}^{6,2}, \qquad \underset{\approx}{\mathrm{H}}^{6,2} = \underset{\approx}{\mathrm{Q}}^{6,2} - \frac{\alpha^{6,2}}{2}\underset{\approx}{\mathrm{P}}^{(2)},$$

hence, putting all the pieces together,

$$\underset{\approx\approx}{\mathrm{B}}^{0,2,2} = \frac{1}{2}\underset{\sim}{\mathrm{I}} \otimes \left(\underset{\approx}{\mathrm{H}}^{6,2} + \frac{\alpha^{6,2}}{2}\underset{\approx}{\mathrm{P}}^{(2)}\right)$$

The ultimate expression is obtained by symmetrising the last one

$$\underset{\approx\approx}{\mathrm{B}}^{(220)} = \tau_3 \star \underset{\approx\approx}{\mathrm{B}}^{0,2,2}$$

in which $\tau_3 = (\varsigma_{(e)} + \varsigma_{(13)(24)} + \varsigma_{(15)(26)})$ is the already introduced symmetrisation operator from $\mathbb{K}^2 \otimes S^2(\mathbb{R}^2)$ to $\mathbb{W}_3^2$.

d) The space $\mathbb{W}_3^3$ Unlike the other terms, $\underset{\approx\approx}{\mathrm{B}}^{(222)} \in \mathbb{W}_3^3$ cannot be reduced to a lower order tensor by contraction with $\underset{\approx}{\mathrm{P}}^{(0)}$. It is minimal for this aspect, although this does not make it O(2)-irreducible.

From the harmonic structure of $\mathbb{W}_3^3$, we know that the harmonic parameterisation is given by two harmonic tensors $\underset{\approx\approx}{\mathrm{S}}^{6,3} \in \mathbb{K}^6$ and $\underset{\sim}{\mathrm{h}}^{6,3} \in \mathbb{K}^2$ such as

$$\underset{\approx\approx}{\mathrm{B}}^{(222)} = \underset{\approx\approx}{\mathrm{S}}^{6,3} + \underset{\approx\approx\approx}{\Phi}^{6,3} : \underset{\sim}{\mathrm{h}}^{6,3},$$

in which $\underset{\approx\approx\approx}{\Phi}^{6,3} \in S^3(\mathbb{K}^2) \otimes \mathbb{K}^2$ is a $8th$-order tensor to be determined. Full details of how we find $\underset{\approx\approx\approx}{\Phi}^{6,3}$ are presented in appendix ii. At the end, the following formula is obtained

$$\underset{\approx\approx\approx}{\Phi}^{6,3} : \underset{\sim}{\mathrm{h}}^{6,3} = \frac{1}{3}\tau_3 \star \left[\underset{\sim}{\mathrm{h}}^{6,3} \otimes \underset{\approx}{\mathrm{P}}^{(2)}\right]. \tag{3.14}$$

Once $\underset{\approx\approx\approx}{\Phi}^{6,3}$ identified the converse formula are

$$\underset{\sim}{\mathrm{h}}^{6,3} = \mathrm{tr}_{23}^{(2)}(\underset{\approx\approx}{\mathrm{B}}^{(222)}), \quad \underset{\approx\approx}{\mathrm{S}}^{6,3} = \underset{\approx\approx}{\mathrm{B}}^{(222)} - \underset{\approx\approx\approx}{\Phi}^{6,3} : \underset{\sim}{\mathrm{h}}^{6,3}. \tag{3.15}$$

All this is summarised in the following proposition

Proposition 3.3.3. *The tensor* $\underset{\approx\approx}{\mathrm{B}}$ *admits the uniquely defined Clebsch-Gordan harmonic decomposition associated to the family projectors* $\left(\underset{\approx}{\mathrm{P}}^{(2)}, \underset{\approx}{\mathrm{P}}^{(0)}\right)$*:*

$$\underset{\approx\approx}{\mathrm{B}} = \underset{\approx\approx}{\mathrm{S}}^{6,3} + \frac{1}{2}\tau_3 \star \left[\frac{2}{3}\underset{\sim}{\mathrm{h}}^{6,3} \otimes \underset{\approx}{\mathrm{P}}^{(2)} + \underset{\sim}{\mathrm{I}} \otimes \left(\underset{\approx}{\mathrm{H}}^{6,2} + \frac{\alpha^{6,2}}{2}\underset{\approx}{\mathrm{P}}^{(2)}\right) + \underset{\sim}{\mathrm{h}}^{6,1} \otimes \underset{\approx}{\mathrm{P}}^{(0)}\right] + \frac{\alpha^{6,0}}{4}(\underset{\sim}{\mathrm{I}} \otimes \underset{\approx}{\mathrm{P}}^{(0)}),$$

where $\underset{\sim}{\mathrm{I}}$ *the identity second order tensor, and* $\tau_3 = (\varsigma_{(e)} + \varsigma_{(13)(24)} + \varsigma_{(15)(26)})$*. All tensors* $(\underset{\approx\approx}{\mathrm{S}}^{6,3}, \underset{\approx}{\mathrm{H}}^{6,2}, \underset{\sim}{\mathrm{h}}^{6,3}, \underset{\sim}{\mathrm{h}}^{6,1}, \alpha^{6,2}, \alpha^{6,0})$ *are elements of* $\mathbb{K}^6 \times \mathbb{K}^4 \times \mathbb{K}^2 \times \mathbb{K}^2 \times \mathbb{K}^0 \times \mathbb{K}^0$ *defined from* $\underset{\approx\approx}{\mathrm{B}}$ *as follows:*

$\mathbb{K}^0$	$\mathbb{K}^2$	$\mathbb{K}^4$	$\mathbb{K}^6$
$\alpha^{6,0} = \mathrm{tr}_{12}^{(3)}(\underset{\approx\approx}{\mathrm{B}})$	$\underset{\sim}{\mathrm{h}}^{6,1} = \mathrm{tr}_{12}^{(2)}(\underset{\approx\approx}{\mathrm{B}}) : \underset{\approx}{\mathrm{P}}^{(2)}$		
$\alpha^{6,2} = \underset{\approx}{\mathrm{Q}}^{6,2} :: \underset{\approx}{\mathrm{P}}^{(2)}$	$\underset{\sim}{\mathrm{h}}^{6,3} = \mathrm{tr}_{23}^{(2)}(\underset{\approx\approx}{\mathrm{B}}^{(222)})$	$\underset{\approx}{\mathrm{H}}^{6,2} = \underset{\approx}{\mathrm{Q}}^{6,2} - \frac{\alpha^{6,2}}{2}\underset{\approx}{\mathrm{P}}^{(2)}$	$\underset{\approx\approx}{\mathrm{S}}^{6,3} = \underset{\approx\approx}{\mathrm{B}}^{(222)} - \underset{\approx\approx}{\Phi}^{6,3} : \underset{\sim}{\mathrm{h}}^{6,3}$

where $\underset{\approx}{\mathrm{Q}}^{6,2} = \underset{\approx}{\mathrm{P}}^{(2)} : \mathrm{tr}_{12}(\underset{\approx\approx}{\mathrm{B}}) : \underset{\approx}{\mathrm{P}}^{(2)}$*. The projectors* $\underset{\approx}{\mathrm{P}}^{(2)}$*,* $\underset{\approx}{\mathrm{P}}^{(0)}$ *are defined by equation (2.11), the block* $\underset{\approx\approx}{\mathrm{B}}^{(222)}$ *by the equation (3.10) and* $\underset{\approx\approx}{\Phi}^{6,3} : \underset{\sim}{\mathrm{h}}^{6,3}$ *by equation (3.14).*

3.3.4 The CGHD of $\mathbb{W}_4$

This subsection will be limited to the statement of the main result concerning the explicit harmonic decomposition of $\underset{\approx\approx}{\mathrm{A}} \in \mathbb{W}_4$. Full details of the derivation are given in appendix i, and follow the lines of the method used in the previous section for $\mathbb{W}_3$.

Proposition 3.3.4. *The tensor* $\underset{\approx\approx}{\mathrm{A}}$ *admits the uniquely defined Clebsch-Gordan harmonic decomposition associated to the family projectors* $\left(\underset{\approx}{\mathrm{P}}^{(2)}, \underset{\approx}{\mathrm{P}}^{(0)}\right)$*:*

$$\begin{aligned}\underset{\approx\approx}{\mathrm{A}} \;=\; & \underset{\approx\approx}{\mathrm{E}}^{8,4} + \tau_2 \star \left(\underset{\approx}{\mathrm{H}}^{8,4} \otimes \underset{\approx}{\mathrm{P}}^{2}\right) + \frac{1}{2}\tau_4 \star \left[\underset{\sim}{\mathrm{I}} \otimes \left(\underset{\approx\approx}{\mathrm{S}}^{8,3} + \frac{1}{3}\tau_3 \star \left(\underset{\sim}{\mathrm{h}}^{8,3} \otimes \underset{\approx}{\mathrm{P}}^{(2)}\right)\right)\right] + \tau_{22} \star \left[\left(\underset{\approx}{\mathrm{H}}^{8,2} + \frac{\alpha^{8,2}}{2}\underset{\approx}{\mathrm{P}}^{(2)}\right) \otimes \underset{\approx}{\mathrm{P}}^{(0)}\right] \\ & + \frac{1}{4}\tau_4 \star \left[\underset{\sim}{\mathrm{h}}^{8,1} \otimes \underset{\sim}{\mathrm{I}} \otimes \underset{\approx}{\mathrm{P}}^{(0)}\right] + \frac{1}{4}\alpha^{8,0}\underset{\approx}{\mathrm{P}}^{(0)} \otimes \underset{\approx}{\mathrm{P}}^{(0)} + \alpha^{8,4}\tau_3^{\star} \star \left(\underset{\approx}{\mathrm{P}}^{2} \otimes \underset{\approx}{\mathrm{P}}^{2}\right),\end{aligned}$$

where $\underset{\sim}{\mathrm{I}}$ *is the identity second order tensor, and with the following symmetrizers:*

- $\tau_2 = \frac{1}{2}(\varsigma_{(e)} + \varsigma_{(13)(24)(35)(48))})$*;*
- $\tau_{22} = (\varsigma_{(e)} + \varsigma_{(35)(46)} + \varsigma_{(37)(48)} + \varsigma_{(15)(26)} + \varsigma_{(17)(28)} + \varsigma_{(15)(26)(37)(48)})$*;*
- $\tau_3 = (\varsigma_{(e)} + \varsigma_{(13)(24)} + \varsigma_{(15)(26)})$*;*
- $\tau_3^{\star} = \frac{1}{3}(\varsigma_{(e)} + \varsigma_{(35)(46)} + \varsigma_{(37)(48)})$*;*
- $\tau_4 = (\varsigma_{(e)} + \varsigma_{(13)(24)} + \varsigma_{(15)(26)} + \varsigma_{(17)(28)})$*;*

We have the tensors, $\underset{\approx\approx}{\mathrm{E}}^{8,4} \in \mathbb{K}^8$*,* $\underset{\approx\approx}{\mathrm{S}}^{8,3} \in \mathbb{K}^6$*,* $(\underset{\approx}{\mathrm{H}}^{8,4}, \underset{\approx}{\mathrm{H}}^{8,2}) \in (\mathbb{K}^4)^2$*,* $(\underset{\sim}{\mathrm{h}}^{8,3}, \underset{\sim}{\mathrm{h}}^{8,1}) \in (\mathbb{K}^2)^2$ $(\alpha^{8,4}, \alpha^{8,2}, \alpha^{8,0}) \in (\mathbb{K}^0)^3$*. Those elements are defined from* $\underset{\approx\approx}{\mathrm{A}}$ *as follows:*

$\mathbb{K}^0$	$\mathbb{K}^2$	$\mathbb{K}^4$
$\alpha^{8,0} = \mathrm{tr}^4_{12}(\underset{\approx\approx\approx}{\mathrm{A}})$	$\underset{\sim}{\mathrm{h}}^{8,1} = \underset{\approx}{\mathrm{P}}^{(2)} : (\mathrm{tr}^3_{12}(\underset{\approx\approx\approx}{\mathrm{A}}))$	
$\alpha^{8,2} = \underset{\approx}{\mathrm{Q}}^{8,2} :: \underset{\approx}{\mathrm{P}}^{(2)}$	$\underset{\sim}{\mathrm{h}}^{8,3} = \mathrm{tr}^2_{23}(\underset{\approx\approx\approx}{\mathrm{Q}}^{8,3})$	$\underset{\approx}{\mathrm{H}}^{8,2} = \underset{\approx}{\mathrm{Q}}^{8,2} - \dfrac{\alpha^{8,2}}{2}\underset{\approx}{\mathrm{P}}^{(2)}$
$\alpha^{8,4} = 2\,\mathrm{tr}_{12}(\mathrm{tr}^3_{23}(\underset{\approx\approx\approx}{\mathrm{A}}^{(2222)}))$		$\underset{\approx}{\mathrm{H}}^{8,4} = \mathrm{tr}_{13}(\mathrm{tr}_{12}(\underset{\approx\approx\approx}{\mathrm{A}}^{(2222)} - \alpha^{8,4}\underset{\approx\approx\approx}{\Theta}))$

$\mathbb{K}^6$	$\mathbb{K}^8$
$\underset{\approx\approx\approx}{\mathrm{S}}^{8,3} = \underset{\approx\approx\approx}{\mathrm{Q}}^{8,3} - \underset{\approx\approx\approx}{\Phi}^{6,3} : \underset{\sim}{\mathrm{h}}^{8,3}$	$\underset{\approx\approx\approx}{\mathrm{E}}^{8,4} = \underset{\approx\approx\approx}{\mathrm{A}}^{(2222)} - \underset{\approx\approx\approx}{\Phi}^{8,4} : \underset{\approx}{\mathrm{H}}^{8,4} - \alpha^{8,4}\underset{\approx\approx\approx}{\Theta}$

where $\underset{\approx}{\mathrm{Q}}^{8,2} = \underset{\approx}{\mathrm{P}}^{(2)} : (\underset{\approx\approx\approx}{\mathrm{A}} : \underset{\sim}{\mathrm{I}}) : \underset{\approx}{\mathrm{P}}^{(2)}$. $\underset{\approx}{\mathrm{Q}}^{8,3} = (\underset{\approx\approx\approx}{\mathrm{A}} : \underset{\sim}{\mathrm{I}}) \overset{6}{\circ} (\underset{\approx}{\mathrm{P}}^{(2)} \otimes \underset{\approx}{\mathrm{P}}^{(2)} \otimes \underset{\approx}{\mathrm{P}}^{(2)})$. *The projectors* $\underset{\approx}{\mathrm{P}}^{(2)}$, $\underset{\approx}{\mathrm{P}}^{(0)}$ *are defined by equation* (2.11). *All blocks* $\underset{\approx\approx\approx}{\mathrm{A}}^{p,q,r,s}$ *are defined by equation* (B.4). $\underset{\approx\approx\approx}{\Phi}^{6,4} : \underset{\approx}{\mathrm{H}}^{8,4}$ *and* $\underset{\approx\approx\approx}{\Theta}$ *are given equations* (B.11) *and* (B.12) *in the appendix i.*

3.3.5 Synthesis

At the end, the TW4 function can be parameterised as follows:

$$\begin{aligned} F(\underset{\sim}{\sigma}; \underset{\approx\approx\approx}{\mathrm{A}}, \underset{\approx}{\mathrm{B}}, \underset{\approx}{\mathrm{C}}, \underset{\sim}{\mathrm{D}}) \quad = \quad & F(\underset{\sim}{\sigma}; \underset{\approx\approx\approx}{\mathrm{E}}^{8,4}, \underset{\approx\approx\approx}{\mathrm{S}}^{8,3}, \underset{\approx\approx\approx}{\mathrm{S}}^{6,3}, \underset{\approx}{\mathrm{H}}^{8,4}, \underset{\approx}{\mathrm{H}}^{8,2}, \underset{\approx}{\mathrm{H}}^{6,2}, \underset{\approx}{\mathrm{H}}^{4,2}, \underset{\sim}{\mathrm{h}}^{8,3}, \underset{\sim}{\mathrm{h}}^{8,1}, \underset{\sim}{\mathrm{h}}^{6,3}, \underset{\sim}{\mathrm{h}}^{6,1}, \\ & \underset{\sim}{\mathrm{h}}^{4,1}, \underset{\sim}{\mathrm{h}}^{2,1}, \alpha^{8,4}, \alpha^{8,2}, \alpha^{8,0}, \alpha^{6,2}, \alpha^{6,0}, \alpha^{4,2}, \alpha^{4,0}, \alpha^{2,0}), \end{aligned}$$

where

Terms degree	$\mathbb{K}^8$	$\mathbb{K}^6$	$\mathbb{K}^4$	$\mathbb{K}^2$	$\mathbb{K}^0$
4	$\underset{\approx\approx\approx}{\mathrm{E}}^{8,4}$	$\underset{\approx\approx\approx}{\mathrm{S}}^{8,3}$	$\underset{\approx}{\mathrm{H}}^{8,4}$, $\underset{\approx}{\mathrm{H}}^{8,2}$	$\underset{\sim}{\mathrm{h}}^{8,3}$, $\underset{\sim}{\mathrm{h}}^{8,2}$	$\alpha^{8,4}, \alpha^{8,2}, \alpha^{8,0}$
3		$\underset{\approx\approx\approx}{\mathrm{S}}^{6,3}$	$\underset{\approx}{\mathrm{H}}^{6,2}$	$\underset{\sim}{\mathrm{h}}^{6,3}, \underset{\sim}{\mathrm{h}}^{6,2}$	$\alpha^{6,2}, \alpha^{6,0}$
2			$\underset{\approx}{\mathrm{H}}^{4,2}$	$\underset{\sim}{\mathrm{h}}^{4,1}$	$\alpha^{4,2}, \alpha^{4,0}$
1				$\underset{\sim}{\mathrm{h}}^{2,1}$	$\alpha^{2,0}$

As the decomposition process detailed above clearly shows, the harmonic elements are indexed according to the coupling they induce between the deviatoric part and the spherical part of the stress tensor. This coupling is clear from the couple of index used to designate harmonic tensors. For instance, $\mathbf{K}^{q,p} \in \mathbb{K}^n$ $(0 \leq n \leq q)$, the index q means that $\mathbf{K}$ parameterise a tensor of order q. Meanwhile, the index p indicate that the deviatoric part of stress tensor occurs p times in the coupling, and hence the spherical part occurs $\dfrac{q}{2} - p$ times. If $p = \dfrac{q}{2}$ or $p = 0$ there is no coupling between the two parts which allows to say that the harmonic tensor is purely deviatoric or spherical respectively.

From the general situation, some particular interesting cases can directly be derived.

Hexatropic Tsai-Wu The hexatropic symmetry is a non standard feature of threshold surface that may be of interest for architectured materials. In the following table, the terms for symmetrical criteria are shown in black, and the blue terms represent the contribution to be added in the case of an asymmetrical function.

Terms degree	$\mathbb{K}^8$	$\mathbb{K}^6$	$\mathbb{K}^4$	$\mathbb{K}^2$	$\mathbb{K}^0$
4		$\underset{\approx\approx\approx}{\mathrm{S}}^{8,3}$			$\alpha^{8,4}, \alpha^{8,2}, \alpha^{8,0}$
3		$\underset{\approx\approx\approx}{\mathrm{S}}^{6,3}$			$\alpha^{6,2}, \alpha^{6,0}$
2					$\alpha^{4,2}, \alpha^{4,0}$
1					$\alpha^{2,0}$

In the case of a symmetrical threshold function, the expressions of the tensors involved can be reduced to :

$$\begin{aligned}\underset{\approx\approx\approx}{\mathrm{A}} &= \frac{1}{2}\tau_4 \star \left[\underset{\sim}{\mathrm{I}} \otimes \underset{\approx\approx\approx}{\mathrm{S}}^{8,3}\right] + \alpha^{8,4}\tau_3^\star \star \left(\underset{\approx}{\mathrm{P}}^2 \otimes \underset{\approx}{\mathrm{P}}^2\right) + \frac{\alpha^{8,2}}{2}\tau_{22} \star \left[\underset{\approx}{\mathrm{P}}^{(2)} \otimes \underset{\approx}{\mathrm{P}}^{(0)}\right] + \frac{\alpha^{8,0}}{4}\underset{\approx}{\mathrm{P}}^{(0)} \otimes \underset{\approx}{\mathrm{P}}^{(0)} \\ \underset{\approx}{\mathrm{C}} &= \frac{\alpha^{4,2}}{2}\underset{\approx}{\mathrm{P}}^{(2)} + 2\alpha^{4,0}\underset{\approx}{\mathrm{P}}^{(0)},\end{aligned}$$

The general expression contains 6 material parameters to be identified. This result was anticipated using the representation theorems in the previous chapter, and is confirmed here using harmonic decomposition. The Wang criterion should be approximated with this expression.

If we want to consider Jeanneau's surface, the following terms should be added to the previous ones

$$\begin{aligned}\underset{\approx\approx\approx}{\mathrm{B}} &= \underset{\approx\approx\approx}{\mathrm{S}}^{6,3} + \frac{\alpha^{6,2}}{4}\tau_3 \star \left[\underset{\sim}{\mathrm{I}} \otimes \underset{\approx}{\mathrm{P}}^{(2)}\right] + \frac{\alpha^{6,0}}{4}(\underset{\sim}{\mathrm{I}} \otimes \underset{\approx}{\mathrm{P}}^{(0)}) \\ \underset{\sim}{\mathrm{D}} &= \alpha^{2,0}\underset{\sim}{\mathrm{I}}.\end{aligned}$$

and the complete criterion requires a maximum number of 10 material parameters.

Generalised Hill This criterion is purely deviatoric, hence all hydrostatic coupling are nil.

Terms degree	$\mathbb{K}^8$	$\mathbb{K}^6$	$\mathbb{K}^4$	$\mathbb{K}^2$	$\mathbb{K}^0$
4	$\underset{\approx\approx\approx}{\mathrm{E}}^{8,4}$		$\underset{\approx}{\mathrm{H}}^{8,4}$		$\alpha^{8,4}$
3		$\underset{\approx\approx\approx}{\mathrm{S}}^{6,3}$		$\underset{\sim}{\mathrm{h}}^{6,3}$	
2			$\underset{\approx}{\mathrm{H}}^{4,2}$		$\alpha^{4,2}$
1				$\underset{\sim}{\mathrm{h}}^{2,1}$	

In the case of a symmetrical threshold function, the expressions of the tensors involved can be reduced to :

$$\begin{aligned}\underset{\approx\approx\approx}{\mathrm{A}} &= \underset{\approx\approx\approx}{\mathrm{E}}^{8,4} + \tau_2 \star \left(\underset{\approx}{\mathrm{H}}^{8,4} \otimes \underset{\approx}{\mathrm{P}}^2\right) + \alpha^{8,4}\tau_3^\star \star \left(\underset{\approx}{\mathrm{P}}^2 \otimes \underset{\approx}{\mathrm{P}}^2\right) \\ \underset{\approx}{\mathrm{C}} &= \underset{\approx}{\mathrm{H}}^{4,1} + \frac{\alpha^{4,2}}{2}\underset{\approx}{\mathrm{P}}^{(2)}\end{aligned}$$

It can be seen from this expression that a generalised Hill criterion is unable to describe a 6-fold invariant anisotropic surface. Sensitivity to hydrostatic pressure is necessary to see such symmetries, at least using polynomial functions.

3.3.6 Polar parameterisation

Now that the threshold function has been decomposed, the question arises of how to parameterise its components. A good parameterisation that is easy to handle allows to design graphical representation tools that are simple to use.

In the case of $\mathbb{R}^2$, all non-trivial harmonic spaces are of dimension 2. Let $\mathcal{K}^n$ be an orthonormal basis of $\mathbb{K}^n$, $n > 0$. We refer to [15] for a systematic method for constructing $\mathcal{K}^n$.

A first possibility is to use Cartesian coordinates with respect to $\mathcal{K}^n$.

$$\{\mathbf{K}\} = K_1\mathbf{E}_1 + K_2\mathbf{E}_2,$$

but another possibility is to use polar coordinates [43, 75, 184]. In such a case, the vector $\mathbf{K}$ being parameterised by its norm $\|\mathbf{K}\| = \sqrt{K_1^2 + K_2^2}$ and its angle with respect to $\mathbf{E}_1$ (see figure 3.2)

$$\{\mathbf{K}\} = \|\mathbf{K}\|\left(\cos\theta_k\mathbf{E}_1 + \sin\theta_k\mathbf{E}_2\right) = \|\mathbf{K}\|\mathbf{E}_r \tag{3.16}$$

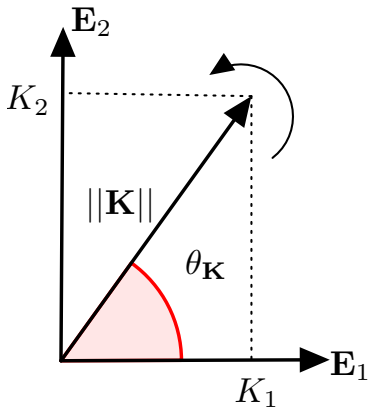

Figure 3.2: Polar parametrisation of n-th order harmonic tensor ($n \geq 1$).

The main interested is associated with the way harmonic tensors are transformed

$$\rho_n(\mathbf{r}(\theta)) := \begin{pmatrix} \cos n\theta & -\sin n\theta \\ \sin n\theta & \cos n\theta \end{pmatrix}, \qquad \rho_n(\boldsymbol{\pi}(\underline{e}_2)) := \begin{pmatrix} 1 & 0 \\ 0 & -1 \end{pmatrix} \quad \forall (n > 0).$$

Hence the rotation of θ angle of a harmonic tensor just changes its angle by $n\theta$ in polar coordinate without affecting its norm.

$$\mathbf{r}(\theta) \star \mathbf{K} \in \mathbb{K}^n \Longrightarrow (||\mathbf{K}||, \theta_{\mathbf{K}} + n\theta) \tag{3.17}$$

The harmonic decomposition of TW4 will therefore be parameterised using the polar representation of the components of the harmonic tensor. In this way, it will be fairly intuitive to manipulate the surfaces generated from the TW4 criterion.

3.4 Influence of harmonic components on the shape of surfaces

As TW4 has been parameterised by harmonic tensors, it is interesting to understand the role of these different contributions on the resulting threshold surface. This point will be addressed in this section by means of graphics.As TW4 is a versatile function, this section is not intended to be exhaustive and only a few relevant cases will be examined below.

All surfaces will be represented below with respect to the harmonic basis. As mentioned previously, the interest is that this representation naturally decouples anisotropy and charge. Consequently, the physical content is easier to grasp using this convention. In the following, the surface areas are taken from the TW4 criterion expressed as below:

$$F_{TW4}(\underset{\sim}{\sigma}) = 1.$$

The influence of the various harmonic components of the criterion will be considered in two steps. First, we will look only at the physical anisotropy. Secondly, the terms modelling the sensitivity to loading will be studied.

3.4.1 Invariance with respect to the material symmetry

In the harmonic basis, the material symmetry is indicated by the group $\mathcal{G}_{\mathcal{S}}^{2D}$ which characterises the symmetry of all slices of $\mathcal{S}$ with respect to the deviatoric plane. To simplify the following study we will consider the restriction of the criterion to that of a generalised Hill criterion as introduced above, that is:

$$\begin{aligned} \underset{\approx\approx\approx}{\mathrm{A}} &= \underset{\approx\approx\approx}{\mathrm{E}}^{8,4} + \tau_2 \star \left(\underset{\approx}{\mathrm{H}}^{8,4} \otimes \underset{\approx}{\mathrm{P}}^2 \right) + \alpha^{8,4} \tau_3^\star \star \left(\underset{\approx}{\mathrm{P}}^2 \otimes \underset{\approx}{\mathrm{P}}^2 \right) \\ \underset{\approx}{\mathrm{C}} &= \underset{\approx}{\mathrm{H}}^{4,1} + \frac{\alpha^{4,2}}{2} \underset{\approx}{\mathrm{P}}^{(2)} \end{aligned}$$

The influence of the asymmetry will be considered by adding the following contributions

$$\begin{aligned} \underset{\approx\approx}{\mathrm{B}} &= \underset{\approx\approx}{\mathrm{S}}^{6,3} + \frac{1}{2}\tau_3 \star \left[\frac{2}{3}\underset{\sim}{\mathrm{h}}^{6,3} \otimes \underset{\approx}{\mathrm{P}}^{(2)}\right] \\ \underset{\sim}{\mathrm{D}} &= \underset{\sim}{\mathrm{h}}^{2,1}. \end{aligned}$$

The advantage of having an exclusively deviatoric criterion is that the $\mathcal{S}$ surface will be invariant along the hydrostatic axis. In other words, $\mathcal{S}$ will be a cylinder which constant cross-section will be characteristic of spatial anisotropy.

Let's start by considering only the role of $\alpha^{8,4}$, with the other parameters set to zero. On the figure 3.3, $\mathcal{S}$ appears as cylinder with circular section. The criterion is obviously isotropic, $\mathcal{G}_{\mathcal{S}}^{2D} = \mathrm{O}(2)$, and the $\mathbb{R}^3$ symmetry class of $\mathcal{S}$ is $\mathcal{G}_{\mathcal{S}}^{3D} = \mathrm{O}(2) \otimes \mathrm{Z}_2^c$.

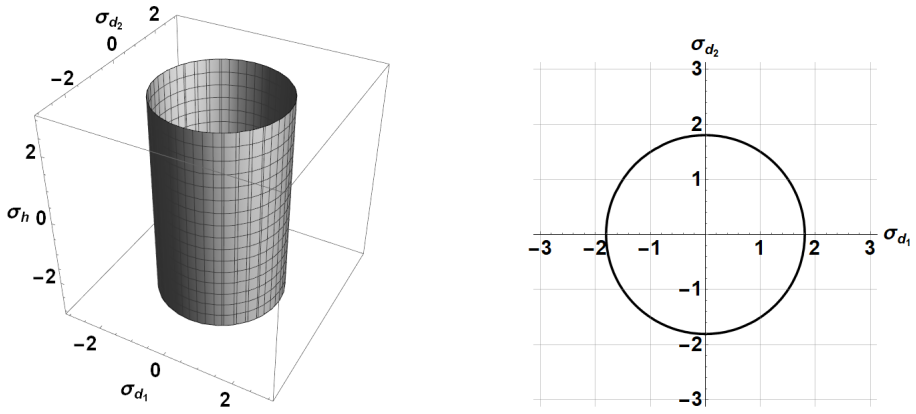

(a) Tri-component representation. (b) The plane $\sigma_h = 0$.

Figure 3.3: The TW4's surface with only $\alpha^{8,4} = 0.3$. The surface is $\mathcal{G}_{\mathcal{S}}^{3D} = \mathrm{O}(2) \otimes \mathrm{Z}_2^c$

Now let us add the contribution of $\underset{\approx\approx}{\mathrm{E}}^{8,4}$. As shown on Figure 3.4, this contribution changes the shape of the section of the cylinder which appears now to have square symmetry, ie. $\mathcal{G}_{\mathcal{S}}^{2D} = \mathrm{D}_4$. As discussed in subsection 2.3.2 of the previous chapter, this means the associated physical symmetry is $\mathrm{G}_{\mathcal{P}} = \mathrm{D}_8$. This is due to the 8th order harmonic tensor which is $\frac{2\pi}{8}$ periodic in spatial basis. The periodicity in the stress space, is halved because the angle Θ of the surface is twice the physical angle θ (look the subfigures (c) and (d)).

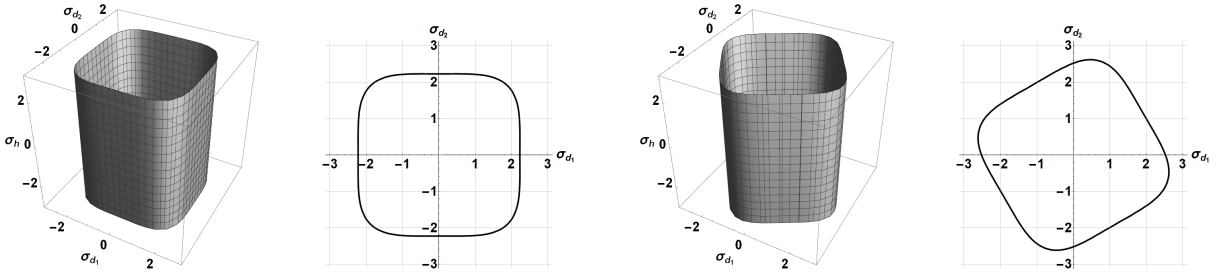

(a) Tri-component representation ($\theta = 0$). (b) The plane $\sigma_h = 0$ ($\theta = 0$). (c) Tri-component representation ($\theta = \frac{\pi}{3}$). (d) The plane $\sigma_h = 0$ ($\theta = \frac{\pi}{3}$).

Figure 3.4: The TW4's surface with only $||\underset{\approx\approx}{\mathrm{E}}^{8,4}|| = 0.3, \alpha^{8,4} = 0.8$. The surface is $\mathcal{G}_{\mathcal{S}}^{3D} = \mathrm{D}_4 \otimes \mathrm{Z}_2^c$

Let us now substitute $\underset{\approx\approx}{\mathrm{E}}^{8,4}$ with $\underset{\approx\approx}{\mathrm{E}}^{6,3}$, the resulting surface is pictured on Figure 3.5. In this case the shape of the section of the cylinder has now trigonal symmetry, ie. $\mathcal{G}_{\mathcal{S}}^{2D} = \mathrm{D}_3$, which means the associated physical symmetry is $\mathrm{G}_{\mathcal{P}} = \mathrm{D}_6$. The symmetry of the whole surface in $\mathbb{R}^3$ is $\mathcal{G}_{\mathcal{S}}^{3D} = \mathrm{D}_3^v$. What is interesting is that such a surface only appears in the case of asymmetric criteria, which is not necessarily intuitive at first sight. However, this is perfectly logical since this surface is not centrosymmetrical and therefore cannot correspond to a symmetrical criterion.

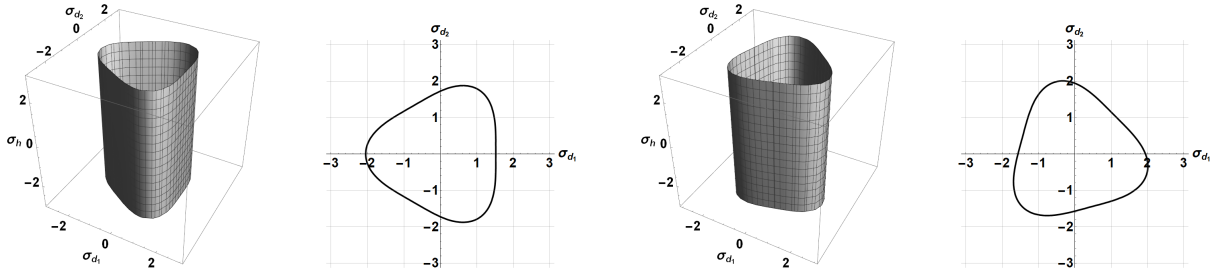

(a) Tri-component representation ($\theta = 0$). (b) The plane $\sigma_h = 0$ ($\theta = 0$). (c) Tri-component representation ($\theta = \frac{\pi}{8}$). (d) The plane $\sigma_h = 0$ ($\theta = \frac{\pi}{8}$).

Figure 3.5: The TW4's surface with only $||\underset{\approx\approx}{\mathrm{S}}^{6,3}|| = 0.23, \alpha^{8,4} = 0.3$. The surface is $\mathcal{G}_S^{3D} = \mathrm{D}_3^v$

To make the criterion sensitive to hexagonal symmetry, we could consider the term $\underset{\approx\approx}{\mathrm{S}}^{8,3}$ instead of $\underset{\approx\approx}{\mathrm{S}}^{6,3}$. It should be noted that this approach involves taking into account sensitivity to hydrostatic stress, since $\underset{\approx\approx}{\mathrm{S}}^{8,3}$ reflects a coupling between deviatoric stress and spherical stress. Since $\underset{\approx\approx}{\mathrm{S}}^{8,3}$ is contained in the tensor 8th order tensor $\underset{\approx\approx}{\mathrm{A}}$, the resulting surface, as pictured on Figure 3.6, is now centrosymmetric. It is twisted figure with varying sections, the symmetry group of which depends on the hydrostatic stress. From bottom to top, the symmetry of the section changes as follows[7]:

$$\mathcal{G}^{2D}_{\mathcal{P}(\sigma_h)} \begin{cases} \mathrm{D}_3, & \sigma_h \neq 0; \\ \mathrm{O}(2), & \sigma_h = 0. \end{cases}$$

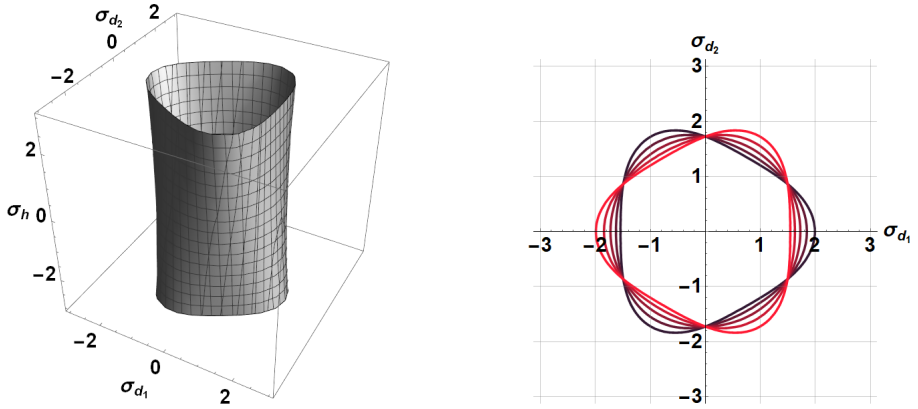

(a) The plane $\sigma_h = 0$. (b) Tri-component representation S83=0.023, a84=0.3

Figure 3.6: The TW4's surface with only $||\underset{\approx\approx}{\mathrm{S}}^{8,3}|| = 0.023, \alpha^{8,4} = 0.3$. The surface is $\mathcal{G}_S^{3D} = \mathrm{D}_3 \otimes \mathrm{Z}_2^c$

As a results the symmetry class of the criterion is $\mathcal{G}_S^{2D} = \mathrm{D}_3$ and hence the described physical symmetry is $\mathrm{G}_{\mathcal{P}} = \mathrm{D}_6$. The symmetry class of the surface with respect to $\mathbb{R}^3$ is $\mathcal{G}_S^{3D} = \mathrm{D}_3 \otimes \mathrm{Z}_2^c$.

It should be noted that if the sectional symmetry groups are indicated, the overall symmetry of the surface is different, since in this case it is centrosymmetrical. This difference is associated with the sensitivity of the criterion to loading, a point that will be dealt with in the next section.

3.4.2 Invariance with respect to the loading

The main elements for characterising invariance with respect to the loading are the following ones:

1. $\boldsymbol{\pi}(\hat{\underset{\sim}{\mathrm{f}}}_3)$, the mirror symmetry with respect to the deviatoric plane, i.e. the operation that changes the sign of the hydrostatic stress:

$$(\underset{\sim}{\sigma}^{(2)}, \sigma_h) \to (\underset{\sim}{\sigma}^{(2)}, -\sigma_h)$$

[7]It can be observed that symmetry of the cross-section for $\sigma_h = 0$ is O(2). This result can be understood as follows. As noted in remark (2.3.1) surface with symmetry group $\mathrm{D}_{2p+1} \otimes \mathrm{Z}_2^c$ have cross-section symmetry group $\mathcal{G}_{\mathcal{P}(0)} = \mathrm{D}_{2(2p+1)}$. In the present case, it means $\mathcal{G}_{\mathcal{P}(0)} = \mathrm{D}_6$. Due to Hermann theorem, a model should possess at least a 12-th order tensor to see such a symmetry. Since the higher-order tensor of the model is 8th order, this anisotropy can not be described by the TW4 criterion and hence conduct to an isotropic behaviour.

when present this symmetry will be indicated below as $\boldsymbol{\pi}$, ans when absent as $\overline{\boldsymbol{\pi}}$.

2. $\mathbf{i}_3$, the inversion[8], i.e. the operation that change the sign of $\underset{\sim}{\sigma}$:

$$\underset{\sim}{\sigma} \rightarrow -\underset{\sim}{\sigma}$$

when present this symmetry will be indicated below as $\mathbf{i}$, ans when absent as $\bar{\mathbf{i}}$.

These invariances translate into the following harmonic structure of TW4 :

- centro-symmetry: $\mathbf{K}^{p,q} = 0$ if $\frac{p}{2} \neq 2n$;
- hydrostatic invariance: $\mathbf{K}^{p,q} = 0$ if $\frac{p}{2} - q \neq 2n$;

As a result, threshold surfaces fall into one of the following 4 types:

	$\mathbf{i}$	$\bar{\mathbf{i}}$
$\boldsymbol{\pi}$	type 1	type 2
$\overline{\boldsymbol{\pi}}$	type 3	type 4

i.e.:

- type 1: surfaces are centrosymmetric and possess mirror symmetry with respect to the deviatoric plane. The associated TW4 harmonic structure is

Terms degree	$\mathbb{K}^8$	$\mathbb{K}^6$	$\mathbb{K}^4$	$\mathbb{K}^2$	$\mathbb{K}^0$
4	$\underset{\approx\approx\approx}{\mathrm{E}}^{8,4}$		$\underset{\approx}{\mathrm{H}}^{8,4}$, $\underset{\approx}{\mathrm{H}}^{8,2}$	$\underset{\sim}{\mathrm{h}}^{8,2}$	$\alpha^{8,4}, \alpha^{8,2}, \alpha^{8,0}$
3					
2			$\underset{\approx}{\mathrm{H}}^{4,2}$		$\alpha^{4,2}, \alpha^{4,0}$
1					

- type 2: surfaces are just centrosymmetric. The associated TW4 harmonic structure is

Terms degree	$\mathbb{K}^8$	$\mathbb{K}^6$	$\mathbb{K}^4$	$\mathbb{K}^2$	$\mathbb{K}^0$
4	$\underset{\approx\approx\approx}{\mathrm{E}}^{8,4}$	$\underset{\approx\approx\approx}{\mathrm{S}}^{8,3}$	$\underset{\approx}{\mathrm{H}}^{8,4}$, $\underset{\approx}{\mathrm{H}}^{8,2}$	$\underset{\sim}{\mathrm{h}}^{8,3}$, $\underset{\sim}{\mathrm{h}}^{8,2}$	$\alpha^{8,4}, \alpha^{8,2}, \alpha^{8,0}$
3					
2			$\underset{\approx}{\mathrm{H}}^{4,2}$	$\underset{\sim}{\mathrm{h}}^{4,1}$	$\alpha^{4,2}, \alpha^{4,0}$
1					

- type 3: surface a not centrosymmetric, the criterion is dysmetric but still invariant with respect to the reverse of σ_h The associated TW4 harmonic structure is

Terms degree	$\mathbb{K}^8$	$\mathbb{K}^6$	$\mathbb{K}^4$	$\mathbb{K}^2$	$\mathbb{K}^0$
4	$\underset{\approx\approx\approx}{\mathrm{E}}^{8,4}$		$\underset{\approx}{\mathrm{H}}^{8,4}$, $\underset{\approx}{\mathrm{H}}^{8,2}$	$\underset{\sim}{\mathrm{h}}^{8,2}$	$\alpha^{8,4}, \alpha^{8,2}, \alpha^{8,0}$
3		$\underset{\approx\approx\approx}{\mathrm{S}}^{6,3}$		$\underset{\sim}{\mathrm{h}}^{6,3}$	
2			$\underset{\approx}{\mathrm{H}}^{4,2}$		$\alpha^{4,2}, \alpha^{4,0}$
1					$\alpha^{2,0}$

- type 4: Completely asymmetric, the harmonic structure is generic.

For the sake of simplicity, let's consider the effect of these different terms on an isotropic criterion, i.e. one for which the harmonic decomposition reduces to the elements of $\mathbb{K}^0$.

Four different isotropic functions ($\mathcal{G}_{\mathcal{S}}^{2D} = \mathrm{O}(2)$), with an increasing number of terms in their harmonic structure are considered and their associated surfaces are plotted in figures 3.7, 3.8, 3.9 and 3.10 below.

[8]The inversion can result from the combination of the in-plane centro symmetry and $\boldsymbol{\pi}(\hat{\underset{\sim}{\mathrm{f}}}_3)$.

1. The first polynomial just contains $\alpha^{8,4}$. This is a purely deviatoric criterion, so the resulting surface is an unclosed cylinder. This surface is obviously of type 1.

2. The second polynomial now includes $\alpha^{8,0}$, which is a purely spherical term. The addition of this contribution closes the previous cylinder. The type of the surface is unchanged.

3. In the third polynomial (cf. figure 3.9); the term $\alpha^{8,2}$ is added, which correspond to a coupling between deviatoric and sphercial stress. The surface show now a strong dependence on the hydrostatic level, but is still of type 1.

4. In the last polynomial, the term $\alpha^{6,0}$ is added. This term is purely spherical and comes from a cubic polynomial in $\underset{\sim}{\sigma}$. As a result, the associated surface is not centrosymmetric (see figure 3.10). This characteristic models the tension/compression asymmetry. The surface is of type 4.

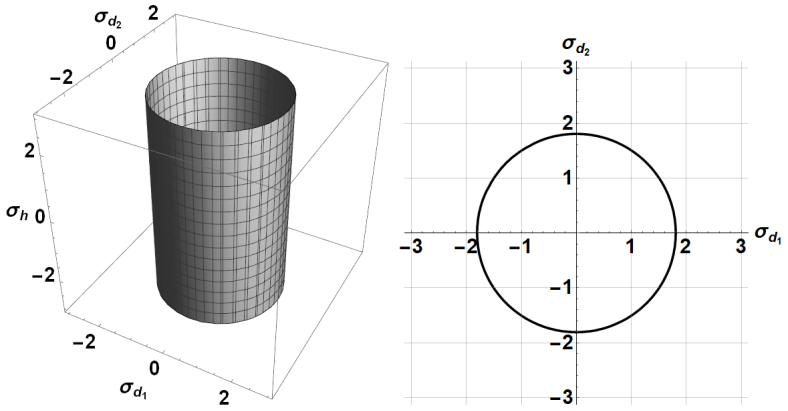

(a) Tri-component representation. (b) The plane $\sigma_h = 0$.

Figure 3.7: The TW4's surface with only $\alpha^{8,4} = 0.3$. The surface is $\mathcal{G}_S^{3D} = \mathrm{O}(2) \otimes \mathrm{Z}_2^c$

.

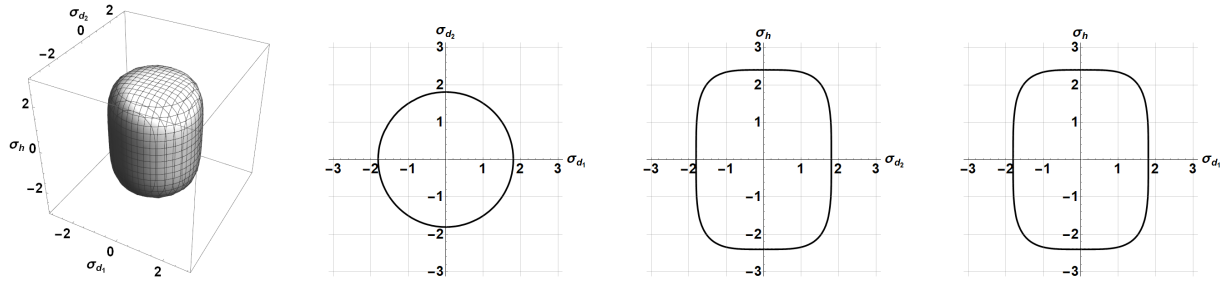

(a) tri-component representation. (b) The plane $\sigma_h = 0$. (c) The plane $\sigma_{d_2} = 0$. (d) The plane $\sigma_{d_1} = 0$.

Figure 3.8: The TW4's surface with only $\alpha^{8,4} = 0.25, \alpha^{8,0} = 0.12$.

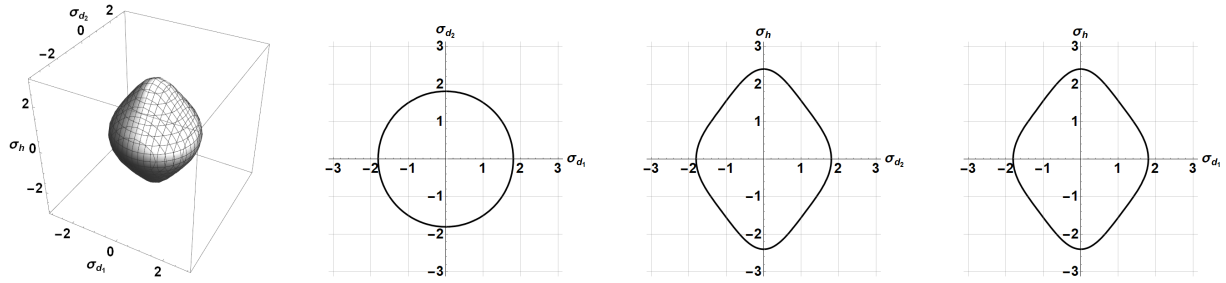

(a) tri-component representation. (b) The plane $\sigma_h = 0$. (c) The plane $\sigma_{d_2} = 0$. (d) The plane $\sigma_{d_1} = 0$.

Figure 3.9: The TW4's surface with only $\alpha^{8,4} = 0.25$, $\alpha^{8,2} = 0.2$ and $\alpha^{8,0} = 0.12$.

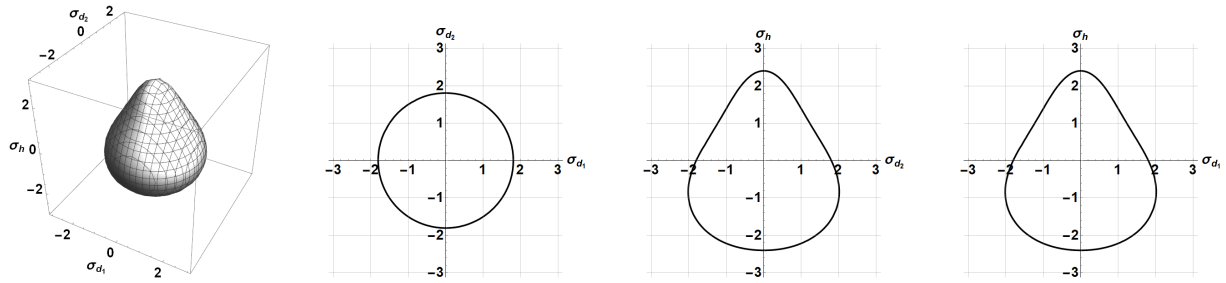

(a) tri-component representation (b) The plane $\sigma_h = 0$. (c) The plane $\sigma_{d_2} = 0$. (d) The plane $\sigma_{d_1} = 0$.

Figure 3.10: The TW4's surface with only $\alpha^{8,4} = 0.25$, $\alpha^{8,2} = 0.2$, $\alpha^{8,0} = 0.12$ and $\alpha^{6,0} = 0.3$.

The next two examples, now add anisotropic terms in the criterion:

1. Figure 3.11 shows an anisotropic surface which is shaped like a box. It is in fact similar to that of figure 3.4. The difference is due to the addition of $\underset{\approx}{\mathrm{H}}^{8,4}$ which has broken the D_4 (slice) symmetry into D_2. This is followed by $\alpha^{8,0}$ to close the surface at the top and bottom.

2. For the figure 3.12, the tensor $\underset{\approx}{\mathrm{H}}^{6,2}$ as been added, it results that the surface is of type 4. More specifically the surface has the following symmetry $\mathcal{G}_S^{3D} = \mathrm{Z}_4^-$

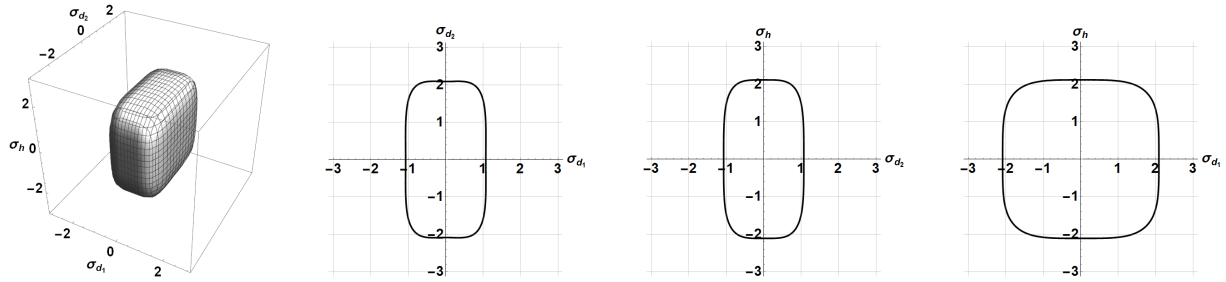

(a) tri-component representation. (b) The plane $\sigma_h = 0$. (c) The plane $\sigma_{d_1} = 0$. (d) The plane $\sigma_{d_2} = 0$.

Figure 3.11: The TW4's surface considering $||\underset{\approx\approx\approx}{\mathrm{E}}^{8,4}|| = 0.3$, $||\underset{\approx}{\mathrm{H}}^{8,4}|| = 0.5$, $\alpha^{8,4} = 0.8$ and $\alpha^{8,0} = 0.2$. The surface is $\mathcal{G}_S^{3D} = \mathrm{D}_2 \otimes \mathrm{Z}_2^c$

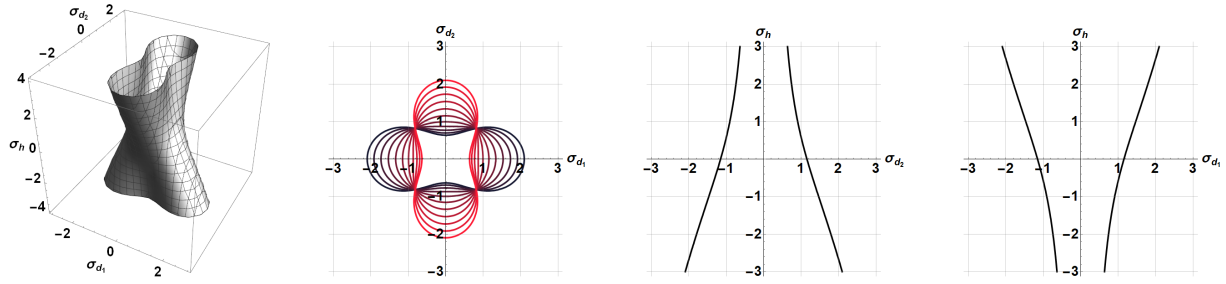

(a) H84=0.3, a84=0.8, $\theta = \pi/3$ (b) The plane $\sigma_h = 0$. (c) The plane $\sigma_{d_1} = 0$. (d) The projections on plane $\sigma_{d_2} = 0$.

Figure 3.12: The TW4's surface considering $||\underset{\approx}{\mathrm{H}}^{6,2}|| = 0.5$ and $\alpha^{8,4} = 1.5$. The surface is $\mathcal{G}_S^{3D} = \mathrm{Z}_4^-$.

3.5 Approximation of some existing threshold functions

As indicated in the first part of this chapter, the TW4 function has been taken into account as it seems to be able to encompass in its formalism many different threshold criteria that can be found in the literature.

The previous section gave us an idea of how the harmonic parameters influence the shape of the threshold surface. The goal of the present section is to retrieve with our model some of the four particular criteria we identified in the literature:

- Cazacau's isotropic threshold function [46];

- The anisotropic "Poly4" threshold model of Soare;
- the Wang hexagonal criterion for architectured material;
- the dissymetric Jeanneau threshold surface for architectured materials.

For details concerning these threshold functions we refer to chapter 1. The used process of identification is quite simple:

1. the first step consists of generating enough number of points from a given model ;
2. the second step, consist in identify harmonic parameters by using *Mathematica* standard fitting tools[9].

Each harmonic tensor is parameterised by its norm and orientation as detailed by equation (3.16) (polar parametrisation). As discussed above, the number of harmonic parameters can be considerably lowered depending on the anisotropy of material.

3.5.1 Cazacu 2004 (3D)

As a recall, the threshold function of Cazacu et al. [46] is given by:

$$F(\underset{\sim}{\sigma}) = (J_2)^{3/2} - cJ_3,$$

where c is a material parameter and J_2 and J_3 are the second and third invariant of the deviatoric part of the 3D stress tensor. The function is meant to be used for isotropic materials that present a traction/compression asymmetry in tensile yield stress. In the case of plane stress hypothesis, the function is given by:

$$\begin{aligned} F_{2D}(\underset{\sim}{\sigma}) &= \left[\frac{1}{3}\left(\sigma_1^2 - \sigma_1\sigma_2 + \sigma_2^2\right)\right]^{3/2} - \frac{c}{27}\left[2\sigma_1^3 + 2\sigma_2^3 - 3\left(\sigma_1 + \sigma_2\right)\sigma_1\sigma_2\right], \\ &= \left[\frac{1}{3}\left(I_1^2 - 3I_2\right)\right]^{3/2} - \frac{c}{27}\left(2I_1^3 - 9I_1I_2\right), \end{aligned} \tag{3.18}$$

where σ_1 and σ_2 are the principal stresses while I_1 and I_2 are the first and the second invariant of the stress tensor. The isotropy of the function is clear from its expression. It can be noticed that

1. the function is purely deviatoric in 3D but not in 2D;
2. the function is not polynomial.

The fact that the function is isotropic can be visualised in the stress space (cf. figure 3.13, since the projections of cross section of the surface on the deviatoric plane give a family of concentric circles.

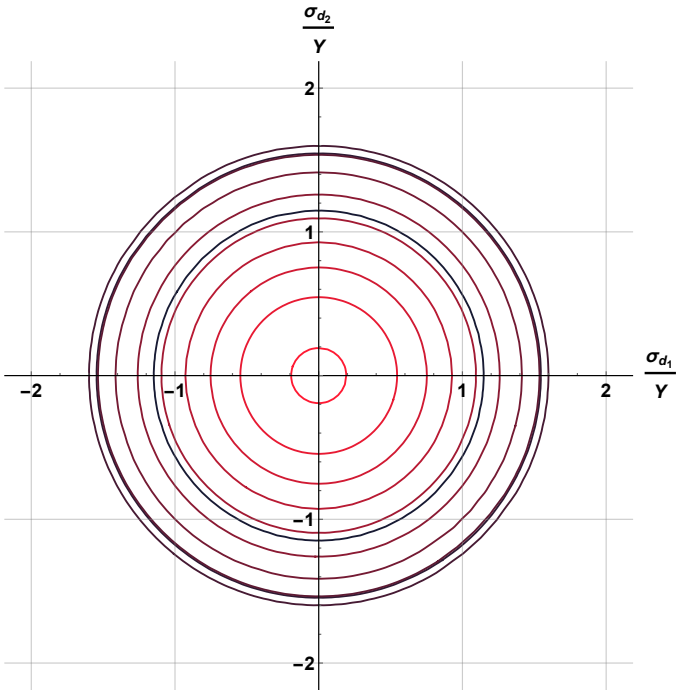

Figure 3.13: The projections of cazacau's threshold surface on the deviatoric plane from bottom (black) to the above level (red).

[9] As a fitting tool we use the *NonLinearModelFit* of the software. All options are set to defaults and no constraints are considered.

Knowing the symmetry of the threshold surface, the parametrisation of the function to be identified can be simplified. All harmonic tensors of order $n \geq 1$ are null and can be set to zero. As a result, the independent parameters of the problem that remain to be adjusted are as follows:

$$\{\alpha^{8,4}, \alpha^{8,2}, \alpha^{8,0}, \alpha^{6,2}, \alpha^{6,0}, \alpha^{4,2}, \alpha^{4,0}, \alpha^{2,0}\}. \tag{3.19}$$

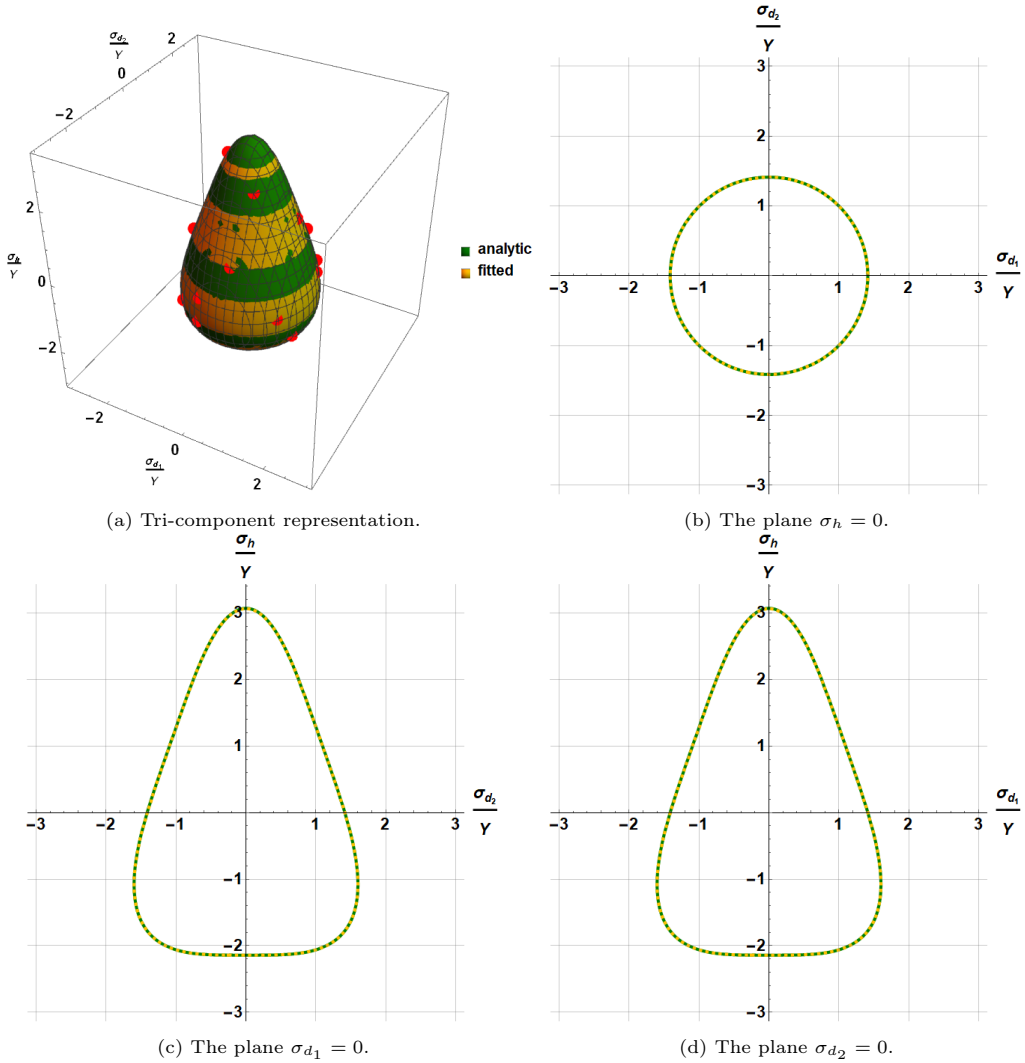

(a) Tri-component representation.

(b) The plane $\sigma_h = 0$.

(c) The plane $\sigma_{d_1} = 0$.

(d) The plane $\sigma_{d_2} = 0$.

Figure 3.14: The threshold surface and the fitted of Cazacu's function for $F(\underset{\sim}{\sigma}) = 1$. The green one is the analytical expression from equation (3.18). The orange one is the fitted one. The points are in red are the ones chosen in the identification process.

The identification results are shown in the figure 3.14. It shows that with the proposed threshold function, we manage identify the Cazacu's one with 20 chosen points (in red). We calculated the volume difference between both analytic and fitted surface and the relative error is valued of 0.01%. The values of the considered harmonic parameters (see equation (3.19)) in approximation process are given in the following table (for $F_{TW4}(\underset{\sim}{\sigma}) = 1$):

$\alpha^{8,4}$	$\alpha^{8,2}$	$\alpha^{8,0}$	$\alpha^{6,2}$	$\alpha^{6,0}$	$\alpha^{4,2}$	$\alpha^{4,0}$	$\alpha^{2,0}$
0.2070	0.0325	0.03575	0.2421	-0.09	0.06899	0.02303	0.0206

3.5.2 Poly4

The threshold function Poly4 of Soare [167] is given by:

$$F(\underset{\sim}{\sigma}) = a_1\sigma_{11}^4 + a_2\sigma_{11}^3\sigma_{22} + a_3\sigma_{11}^2\sigma_{22}^2 + a_4\sigma_{11}\sigma_{22}^3 + a_5\sigma_{22}^4 + \left(a_6\sigma_{11}^2 + a_7\sigma_{11}\sigma_{22} + a_8\sigma_{22}^2\right)\sigma_{12}^2 + a_9\sigma_{12}^4. \tag{3.20}$$

This function corresponds to the homogeneous polynomial function of degree 4 :

$$F(\underset{\sim}{\sigma}) = \underset{\approx\approx\approx}{\mathrm{A}} \overset{8}{\cdot} (\underset{\sim}{\sigma} \otimes \underset{\sim}{\sigma} \otimes \underset{\sim}{\sigma} \otimes \underset{\sim}{\sigma}) \tag{3.21}$$

In terms of parameters, the identification process concerns the following harmonic tensors:

$$\{\underset{\approx\approx\approx}{\mathrm{E}}^{8,4}, \underset{\approx\approx\approx}{\mathrm{S}}^{8,3}, \underset{\approx}{\mathrm{H}}^{8,4}, \underset{\approx}{\mathrm{H}}^{4,2}, \underset{\sim}{\mathrm{h}}^{8,3}, \underset{\sim}{\mathrm{h}}^{4,1}, \alpha^{8,4}, \alpha^{8,2}, \alpha^{8,0}\}.$$

which, without any further assumptions, correspond to a set of 15 parameters. The equation (3.20) corresponds to the specialisation of the general form to the orthotropic case. According to the proposition 3.2.6, the orthotropic symmetry condition requires all harmonic tensors to be "collinear" with each other in a generalised sense. This deceases the number of independent parameters to identify from 15 to 9. When the orthotropy axis coincides with the physical base axis, the orthotropy condition is expressed as follows

$$F(\sigma_{11}, \sigma_{22}, \sigma_{12}) = F(\sigma_{11}, \sigma_{22}, -\sigma_{12}) \tag{3.22}$$

this explains why monomials involving odd powers in σ_{12} are missing in the expression, and why 9 parameters appears in the Soare's Poly4 function. In stress space, cf figure 3.15, this condition means that the threshold surface is symmetric with respect to the plane (σ_{d_1}, σ_h).

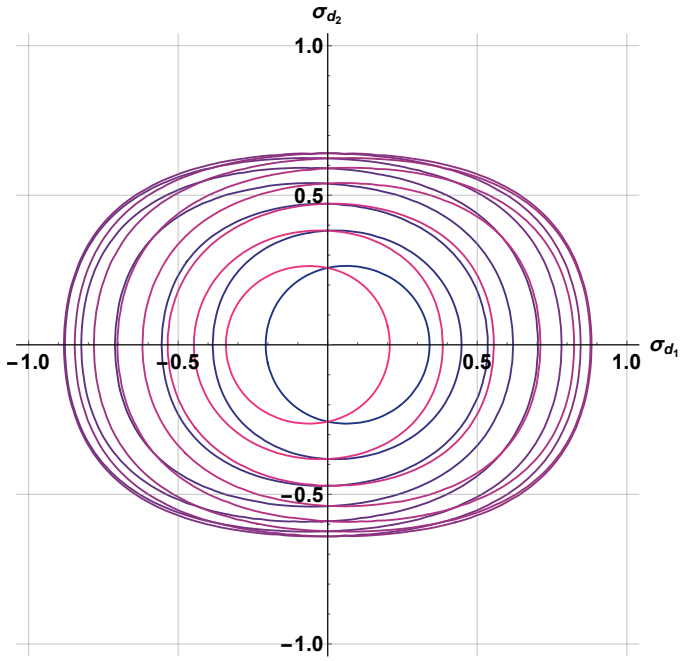

Figure 3.15: The projections of Poly4 threshold surface on the deviatoric plane from bottom (black) to the above level (red).

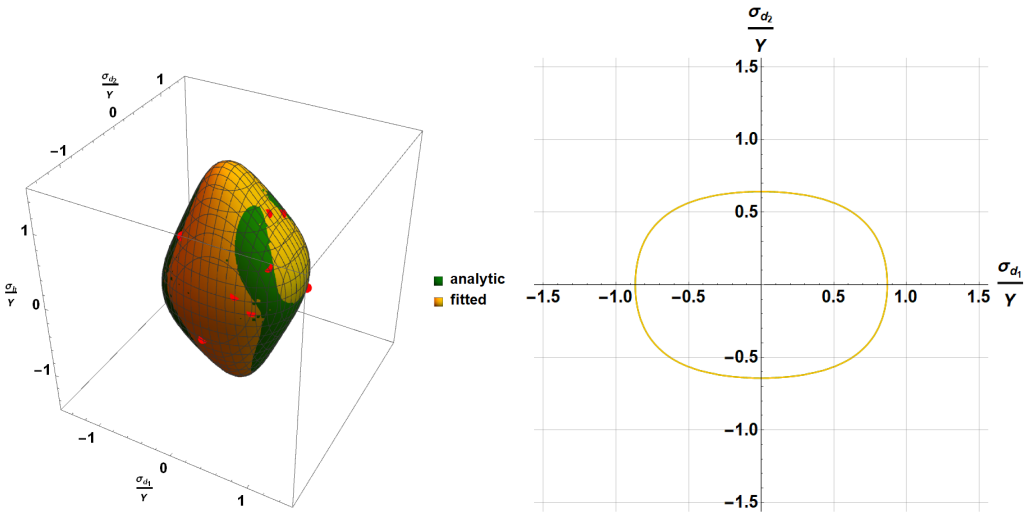

(a) Tri-component representation.

(b) The plane $\sigma_h = 0$.

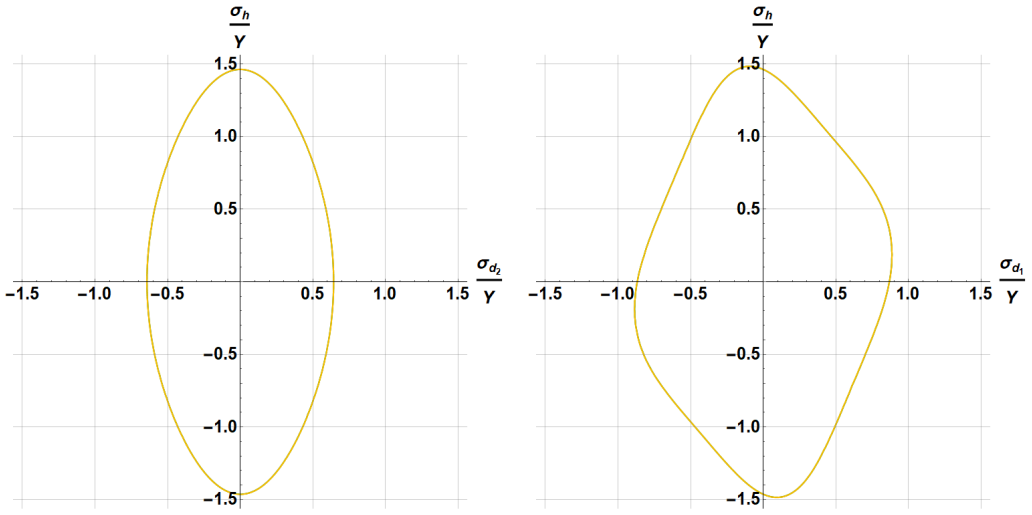

(c) The plane $\sigma_{d_1} = 0$.

(d) The plane $\sigma_{d_2} = 0$.

Figure 3.17: The threshold surface and the fitted of Soare's function for $F(\underset{\sim}{\sigma}) = 1$. The green one is the analytical expression from equation (3.20). The orange one is the fitted one. The points are in red are the ones chosen in the identification process.

The considered harmonic parameters (see equation (3.19)) in approximation process are (we remind that each harmonic tensor $\mathbf{K}$ of order $n \geq 1$ has 2 components (K_1 and K_2)):

$$\{E_1^{8,4}, S_1^{8,3}, H_1^{8,4}, H_1^{4,2}, h_1^{8,3}, h_1^{4,1}, \alpha^{8,4}, \alpha^{8,2}, \alpha^{8,0}\}, \tag{3.23}$$

Their values are given in the following table (for $F_{TW4}(\underset{\sim}{\sigma}) = 1$):

$E_1^{8,4}$	$S_1^{8,3}$	$H_1^{8,4}$	$H_1^{4,2}$	$h_1^{8,3}$	$h_1^{4,1}$	$\alpha^{8,4}$	$\alpha^{8,2}$	$\alpha^{8,0}$
0.1234	0.018	-1.0226	-0.0164	-0.4854	0.1931	8.8288	2.0272	0.8703

As mentioned in chapter 1, Poly4 is an improvement on Gotoh's criterion for which Soare has added new conditions in the identification process in order to resolve convexity problems. Gotoh, in his article [84], established the conditions for which Poly4 is isotropic in 2D (planar isotropy). The same conditions can be established by setting all harmonic tensors of order $n \geq 1$ to 0, i.e.

$$\|\underset{\approx\approx}{\mathrm{E}}^{8,4}\| = \|\underset{\approx\approx}{\mathrm{S}}^{8,3}\| = \|\underset{\approx}{\mathrm{H}}^{8,4}\| = \|\underset{\approx}{\mathrm{H}}^{4,2}\| = \|\underset{\sim}{\mathrm{h}}^{8,3}\| = \|\underset{\sim}{\mathrm{h}}^{4,1}\| = 0$$

This implies the following relations in the polynomial expression (3.20):

$$\begin{aligned} a_5 = a_1 \quad ; \quad a_4 = a_2 \quad ; \quad a_8 = a_6 \quad ; \quad a_2 + a_6 = 4a_1, \\ a_3 + a_7 + a_9 = 6a_1 \quad ; \quad 4a_1 + 2a_2 = 2a_3 + a_7 \end{aligned}$$

As shown in figure 3.17 we manage to identify the threshold function with 11 points. We compared the obtained values from the identification and the analytical ones, the error is valued 1%.

3.5.3 Triangular lattice (plasticity)

In their paper Wang et al. [188] established the threshold surface for equilateral triangular 2D lattice shown in figure 1.11. Assuming periodicity, they reduced their study to one unit cell and used beam theory the evaluate the stress. The Lattice is considered to be stretching dominated therefore, plasticity occurs the axial stresses, evaluated in each beam, reaches the threshold. The obtained threshold criterion is given by:

$$F(\underset{\sim}{\sigma}) = \max\left\{\left|\frac{\sigma_{11}}{Y} - \frac{\sqrt{3}\sigma_{12}}{Y}\right|, \left|\frac{\sigma_{11}}{Y} + \frac{\sqrt{3}\sigma_{12}}{Y}\right|, \left|\frac{3}{2}\frac{\sigma_{22}}{Y} - \frac{\sigma_{11}}{2Y}\right|\right\}, \tag{3.24}$$

where Y in the tensile stress of the constituent material. The threshold surface is defined by the equation $F(\underset{\sim}{\sigma}) = \dfrac{\bar{\rho}}{2}$ where $\bar{\rho}$ is the relative density. For $\bar{\rho} = 0.15$ the surface shown in figure 3.18 (harmonic basis) is obtained:

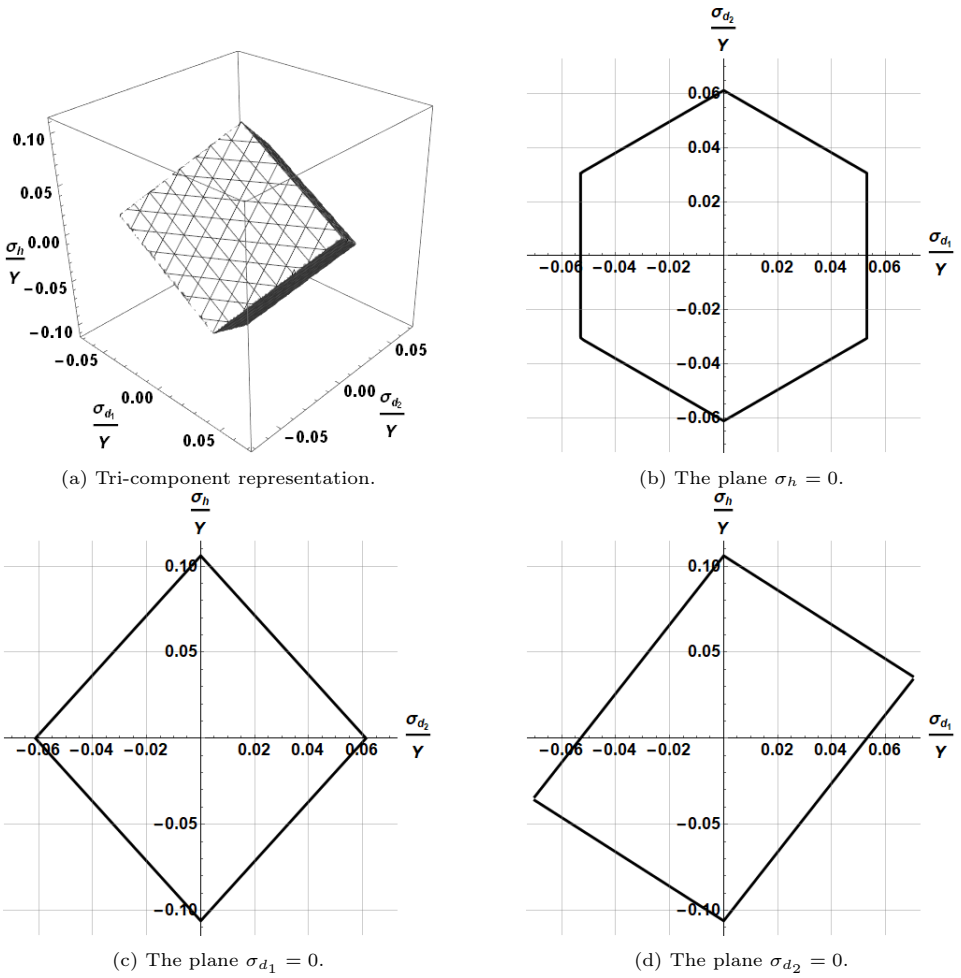

(a) Tri-component representation.

(b) The plane $\sigma_h = 0$.

(c) The plane $\sigma_{d_1} = 0$.

(d) The plane $\sigma_{d_2} = 0$.

Figure 3.18: The threshold surface of equilateral triangular 2D lattice for ($\bar{\rho} = 0.15$) [188].

As detailed in section 2.3.4, and illustrated on figure 3.19, the symmetry group of each cross section are

$$\mathcal{G}^{2D}_{\mathcal{P}(k)} = \begin{cases} \mathrm{D}_3, & k \neq 0; \\ \mathrm{D}_6, & k = 0. \end{cases}$$

Hence the resulting in-plane anisotropy of the surface is $\mathcal{G}^{2D}_{\mathcal{S}} = \mathrm{D}_3$, which is consistent with the symmetry of the unit cell which is D_6.

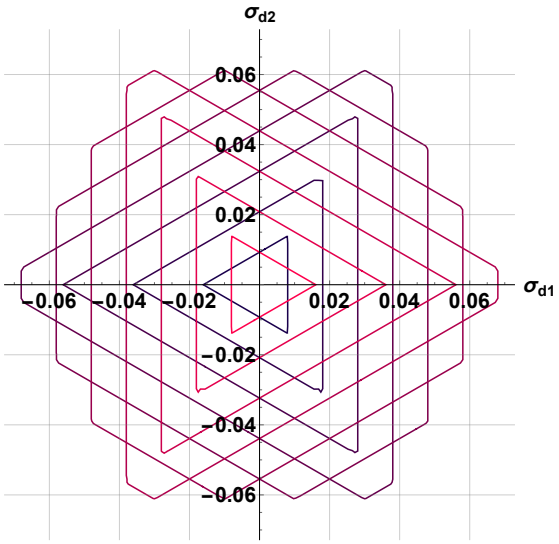

Figure 3.19: The projections of Wang et al. threshold surface on the deviatoric plane from bottom (black) to the above level (red).

Further, the surface is symmetric with respect to traction compression. The symmetry group of the surface is therefore of type II, more precisely

$$\mathcal{G}_S^{3D} = \mathrm{D}_3 \otimes \mathrm{Z}_2^c.$$

Hence, in the identification process, the non null components to be identified are

$$\{\underset{\approx}{\mathrm{S}}^{8,3}, \alpha^{8,4}, \alpha^{8,2}, \alpha^{8,0}, \alpha^{4,2}, \alpha^{4,0}\}.$$

which means that we have a total of 7 unknown parameters. Since the surface has a symmetry plane positioned at an angle $\theta = 0$, the number of parameter can be reduced to only 6:

$$\{S_1^{8,3}, \alpha^{8,4}, \alpha^{8,2}, \alpha^{8,0}, \alpha^{4,2}, \alpha^{4,0}\}.$$

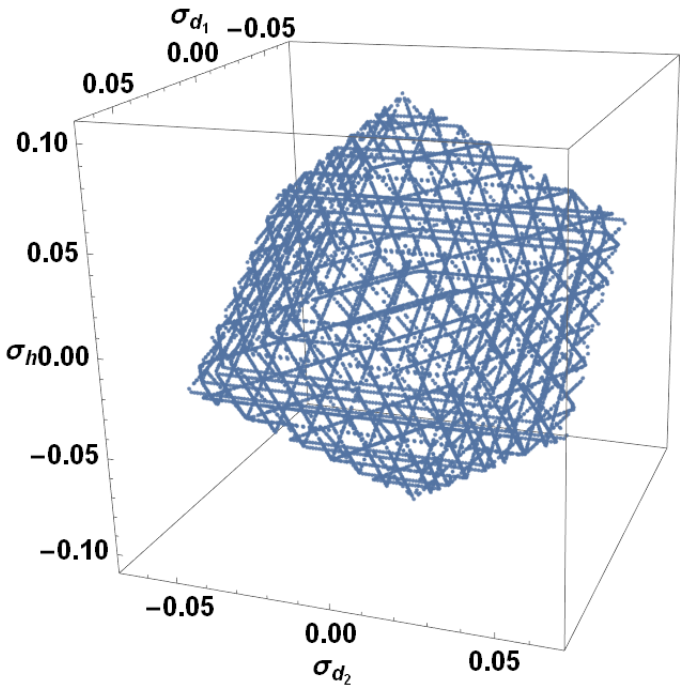

Figure 3.20: The chosen red points (25 in total) for identification process.

The results of the identification are shown in figure 3.21. The figure 3.20 shows the considered points[10] in the identification. It seems that the surface identified corresponds fairly well to the analytical surface, although there are some discrepancies. The fitted surface is open in certain areas and extends beyond the analytical surface. In addition, certain constraints must be added to make the surface convex (if necessary).

[10] We tried to consider the maximum of points in an attempt to obtain the best results.

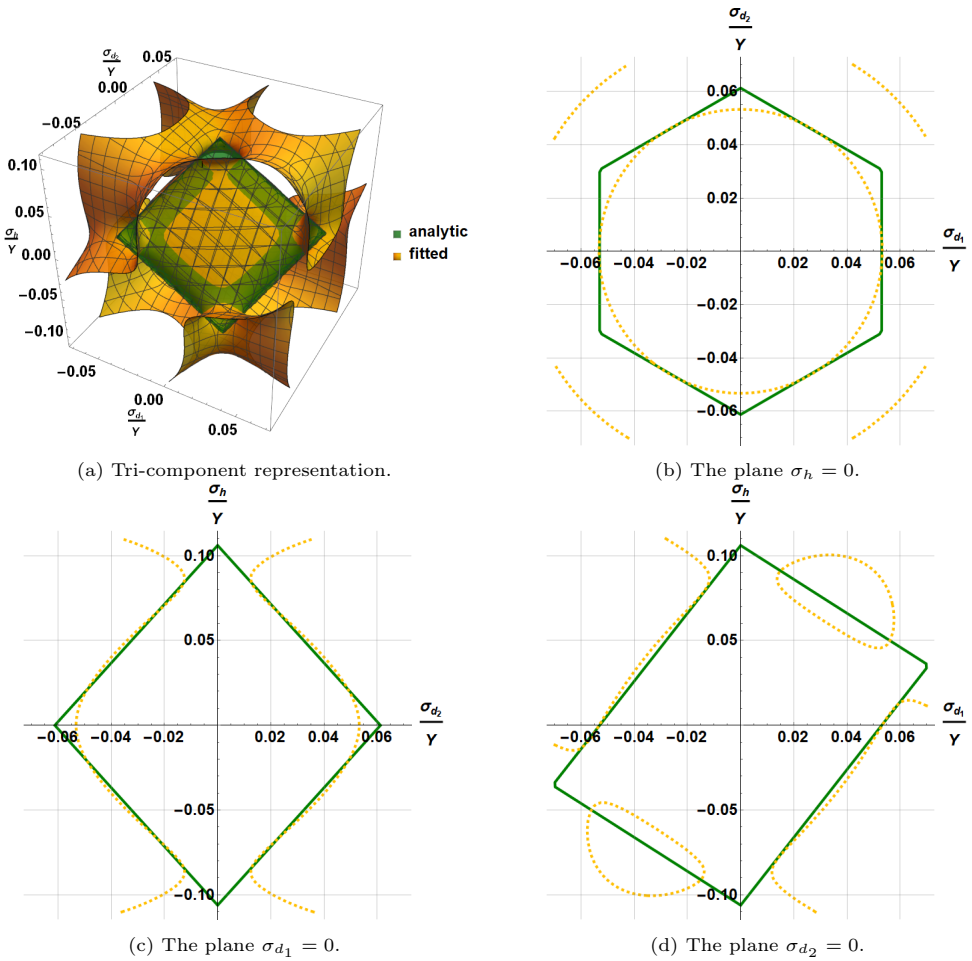

(a) Tri-component representation.

(b) The plane $\sigma_h = 0$.

(c) The plane $\sigma_{d_1} = 0$.

(d) The plane $\sigma_{d_2} = 0$.

Figure 3.21: The threshold surface and the fitted of Wang et al. function for $\bar{\rho} = 0.15$. The green one is the analytical expression from equation (3.18). The orange one is the fitted one.

All this is due to discontinuities in the corners, which are singularities and need to be smoothed out. One way of doing this is to smooth the max function. We have the following lemma:

Lemma 3.5.1. *For all $x_1, ..., x_n \in \mathbb{R}^n$ $(n\mathbb{N})$, we have the P-norm [186]:*

$$\|(x_1, \ldots, x_n)\|_p = (|x_1|^p + \cdots + |x_n|^p)^{1/p}$$

which converges to $\|(x_1, \ldots, x_n)\|_\infty = \max_{1 \le i \le n} |x_i|$ as $p \to \infty$.

The function $F(\underset{\sim}{\sigma})$ (3.24) can be approximated by the following function $\tilde{F}(\underset{\sim}{\sigma})$:

$$\tilde{F}(\underset{\sim}{\sigma}) = \left(\left| \frac{\sigma_{11}}{Y} - \frac{\sqrt{3}\sigma_{12}}{Y} \right|^p + \left| \frac{\sigma_{11}}{Y} + \frac{\sqrt{3}\sigma_{12}}{Y} \right|^p + \left| \frac{3}{2}\frac{\sigma_{22}}{Y} - \frac{\sigma_{11}}{2Y} \right|^p \right)^{\frac{1}{p}}, \tag{3.25}$$

The special case $p = 4$ is considered, which corresponds to a homogeneous polynomial function of degree 4. Hence, instead of identifying the surface coming from $F(\underset{\sim}{\sigma}) = \frac{\bar{\rho}}{2}$, we try this time to identify $\tilde{F}(\underset{\sim}{\sigma}) = \frac{\bar{\rho}}{2}$. The following 4 harmonic parameters are considered:

$$\{S_1^{8,3}, \alpha^{8,4}, \alpha^{8,2}, \alpha^{8,0}\}. \tag{3.26}$$

which are issued from the homogeneous polynomial of degree 4:

$$F(\underset{\sim}{\sigma}) = \underset{\approx}{\mathrm{A}}^{8} \cdot (\underset{\sim}{\sigma} \otimes \underset{\sim}{\sigma} \otimes \underset{\sim}{\sigma} \otimes \underset{\sim}{\sigma}) \tag{3.27}$$

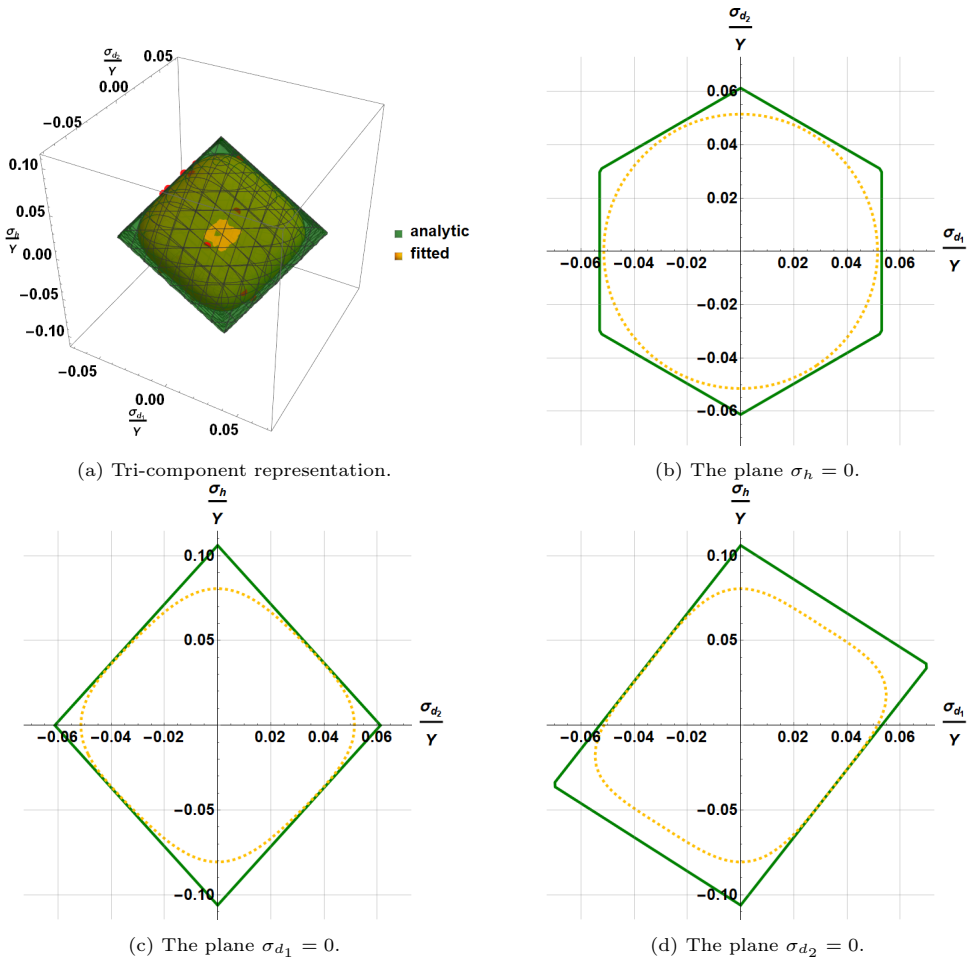

(a) Tri-component representation.

(b) The plane $\sigma_h = 0$.

(c) The plane $\sigma_{d_1} = 0$.

(d) The plane $\sigma_{d_2} = 0$.

Figure 3.22: The threshold surface and the fitted of Wang et al. for the smoothed function for $\bar{\rho} = 0.15$. The green one is the analytical expression from equation (3.24). The orange one is the fitted one. The points are in red are the ones chosen in the identification process.

The value of the considered harmonic parameters (see equation (3.19)) for the approximated threshold surface (fitted one) in figure 3.22 are given in the following table (for $F_{TW4}(\underset{\sim}{\sigma}) = \frac{1}{2}\rho$):

$S_1^{8,3}$	$\alpha^{8,4}$	$\alpha^{8,2}$	$\alpha^{8,0}$
-1775.32	28435.44	14208.75	7113.39

Using this approach, a polynomial approximation of the Wang threshold criterion is established, the result of the adjustment is plotted on the figure 3.22. Unlike the first approach, the fitted surface is closed, convex and does not extend beyond the analytical surface. Of course, in order to be more precise, one will need to add polynomial terms of higher degree as indicated by the lemma 3.5.1.

One can also try identifying the analytical surface $F(\underset{\sim}{\sigma}) = \dfrac{\bar{\rho}}{2}$, from the reduced set of parameters (3.26) and considering the points in figure 3.20. The result is shown in figure 3.24. The fitted surface, this time, is closed. comparing it to figure 3.22, the result is better, although convexity is not respected.

As for the failure of direct identification, this is probably due to the fact that we used too broad a set of parameters, which led to an unwanted solutions. By deduction, knowing a priori the presence of tension/compression symmetry, probably, only one homogeneous polynomial of even degree is needed. The choice of the degree of this polynomial obviously depends on the degree of anisotropy to be described. In our case, for example, the material symmetry is D_6 which cannot be described by a polynomial of degree 2.

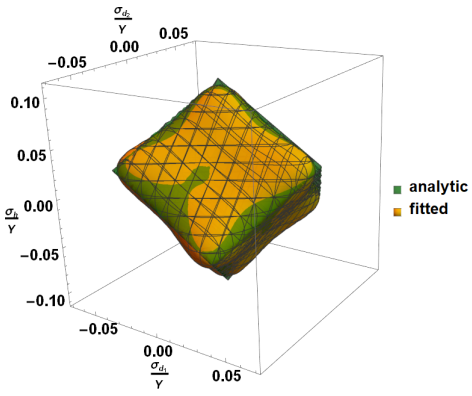

(a) Tri-component representation.

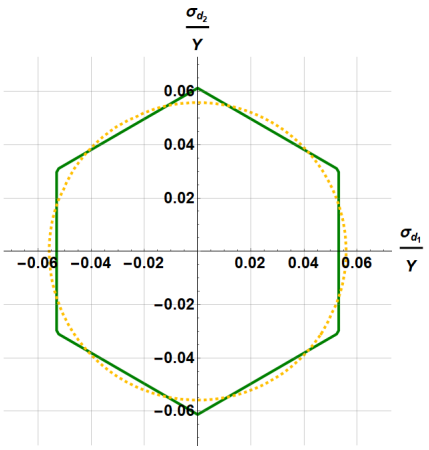

(b) The plane $\sigma_h = 0$.

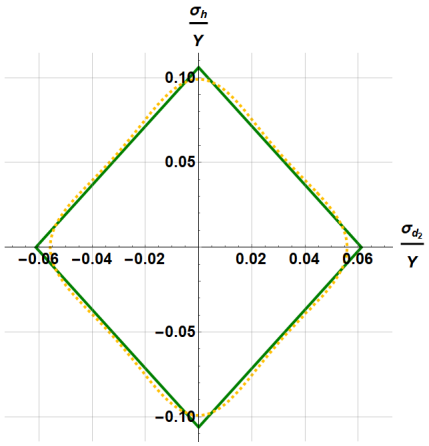

(c) The plane $\sigma_{d_1} = 0$.

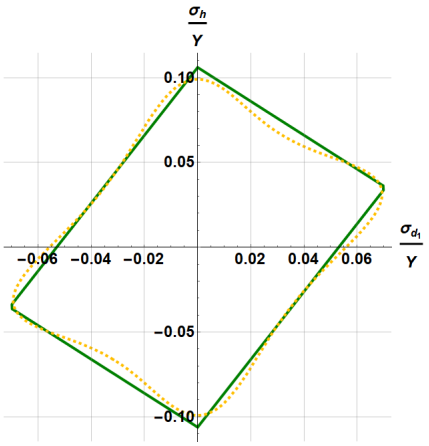

(d) The plane $\sigma_{d_2} = 0$.

Figure 3.24: The threshold surface and the fitted of Wang et al. for the analytical function for $\bar{\rho} = 0.15$. The green one is the analytical expression from equation (3.24). The orange one is the fitted one.

In figure 3.24 the value of the harmonic parameters, corresponding to the fitted surface, are given in the following table (for $F_{TW4}(\underset{\sim}{\sigma}) = \frac{1}{2}\rho$):

$S_1^{8,3}$	$\alpha^{8,4}$	$\alpha^{8,2}$	$\alpha^{8,0}$
-2386.48	21201.65	14669.1	3055.31

3.5.4 Triangular lattice (plasticity and buckling)

A threshold surface has been established numerically by V. Jeanneau [103] during his PhD for equilateral triangular 2D lattice by considering plasticity and buckling instabilities. The plasticity limit is established analytically by considering the following function F_p (p is referred plasticity):

$$F_p(\underset{\sim}{\varepsilon}) = \max\{|P_1|, |P_2|, |P_3|\}$$

where

$$\begin{aligned} P_1 &: (E\varepsilon_{11}) = 0 \\ P_2 &: \left(\frac{1}{4}E\left(\varepsilon_{11} + \sqrt{6}\varepsilon_{12} + 3\varepsilon_{22}\right)\right) = 0 \\ P_3 &: \left(\frac{1}{4}E\left(\varepsilon_{11} - \sqrt{6}\varepsilon_{12} + 3\varepsilon_{22}\right)\right) = 0 \end{aligned}$$

This time, the criterion is formulated in strain space, which makes no difference to the previous approach since the two spaces are identical ($S^2(\mathbb{R}^2)$). The parameters E is the Young's modulus of the solid constituent material

(the solid material used to make Lattice). The plasticity threshold surface is defined by the equation $F(\underset{\sim}{\varepsilon}) = Y$. In this example we have $E = 72000MPa$ and $Y = 500MPa$

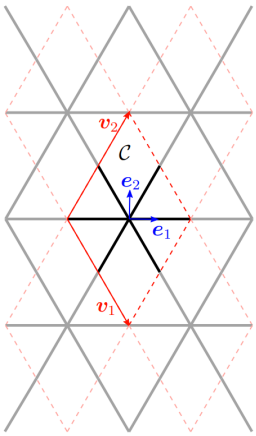

Figure 3.25: The triangular 2D lattice (grey line), unit cell $\mathcal{C}$ (red dashed line) and basis vectors (red arrows) [103].

To take account of the local buckling limit, the surface is established numerically. A semi-analytical technique is used, which combines Bloch wave theory and a finite element model of the 2D lattice unit cell [54]. The buckling surface is given by the red points in figure 3.26). A surface passing through most of the points is defined by the equation $P_b = Y$. In this expression P_b is obtained by directly fitting the proposed threshold function (see figure 3.26).

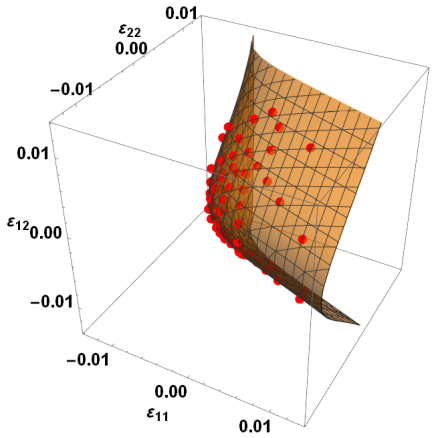

Figure 3.26: The buckling surface (spatial basis)).

to take into account the presence of plasticity and buckling at the same time, the following threshold function F_{pb} (pb refers to plasticity and buckling) is considered:

$$F_{pb}(\underset{\sim}{\varepsilon}) = \max\{P_1, P_2, P_3, P_b\}$$

The resulting threshold surface is plotted on figure 3.27 (harmonic basis). It is clear that the surface is dissymmetric in tension/compression. The 3 intersecting planes above the surface represent the plasticity limit, while the curved surface at the bottom represents the locus of buckling instabilities. It is noticed, in figure 3.28, that symmetry groups $\mathcal{G}^{2D}_{\mathcal{P}(k)}$ of the different cross sections are D_3. In addition, the surface has a plane of symmetry positioned at an angle $\theta = 0$. The symmetry class of the surface is D^v_3 which is a type III group.

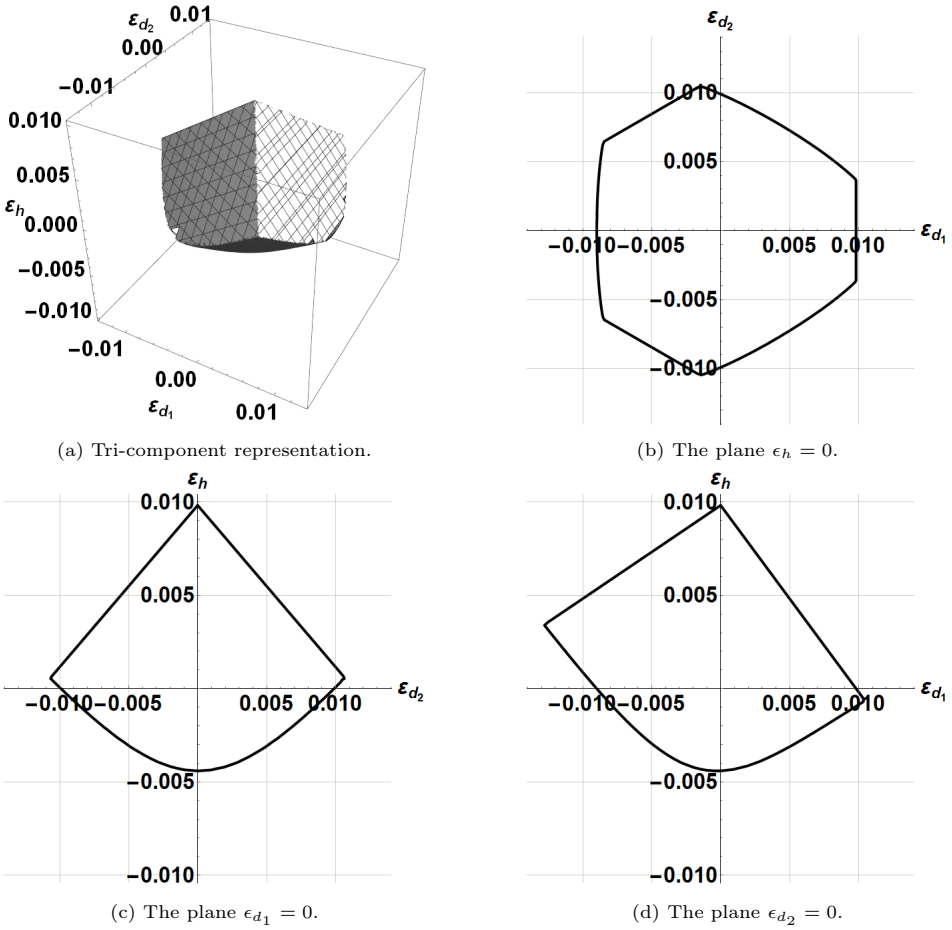

(a) Tri-component representation.

(b) The plane $\epsilon_h = 0$.

(c) The plane $\epsilon_{d_1} = 0$.

(d) The plane $\epsilon_{d_2} = 0$.

Figure 3.27: The threshold surface of the a triangular lattice considering the buckling.

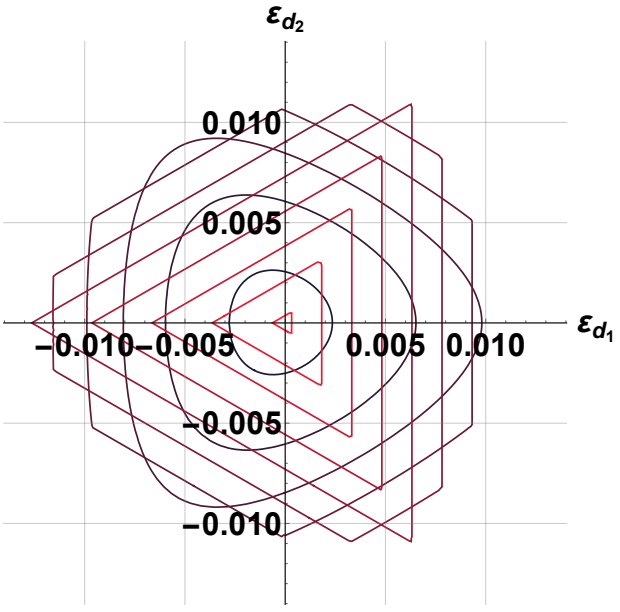

Figure 3.28: The projections og the threshold surface of the a triangular lattice on the deviatoric plane from bottom (green) to the above level (orange). [103].

Consequently, the independent parameters to be taken into account in the identification process can be reduced to the elements in the following list (10 in total):

$$\{S_1^{8,3}, S_2^{6,3}, \alpha^{8,4}, \alpha^{8,2}, \alpha^{8,0}, \alpha^{6,2}, \alpha^{6,0}, \alpha^{4,2}, \alpha^{4,0}, \alpha^{2,0}\}.$$

As before, it seems that the surface identified corresponds fairly well to the analytical surface, but a few problems have arisen. The fitted surface is open in certain areas and extends beyond the analytical surface. In addition,

certain constraints must be added to make the surface convex (if necessary). As in tre previous case, the max function need to be smoothed, but this time the P-norm approach is not usable because it can only admits positive values (the absolute value is not applied to P_b).

Instead, the so-called LSE (log-sum-exp) function.

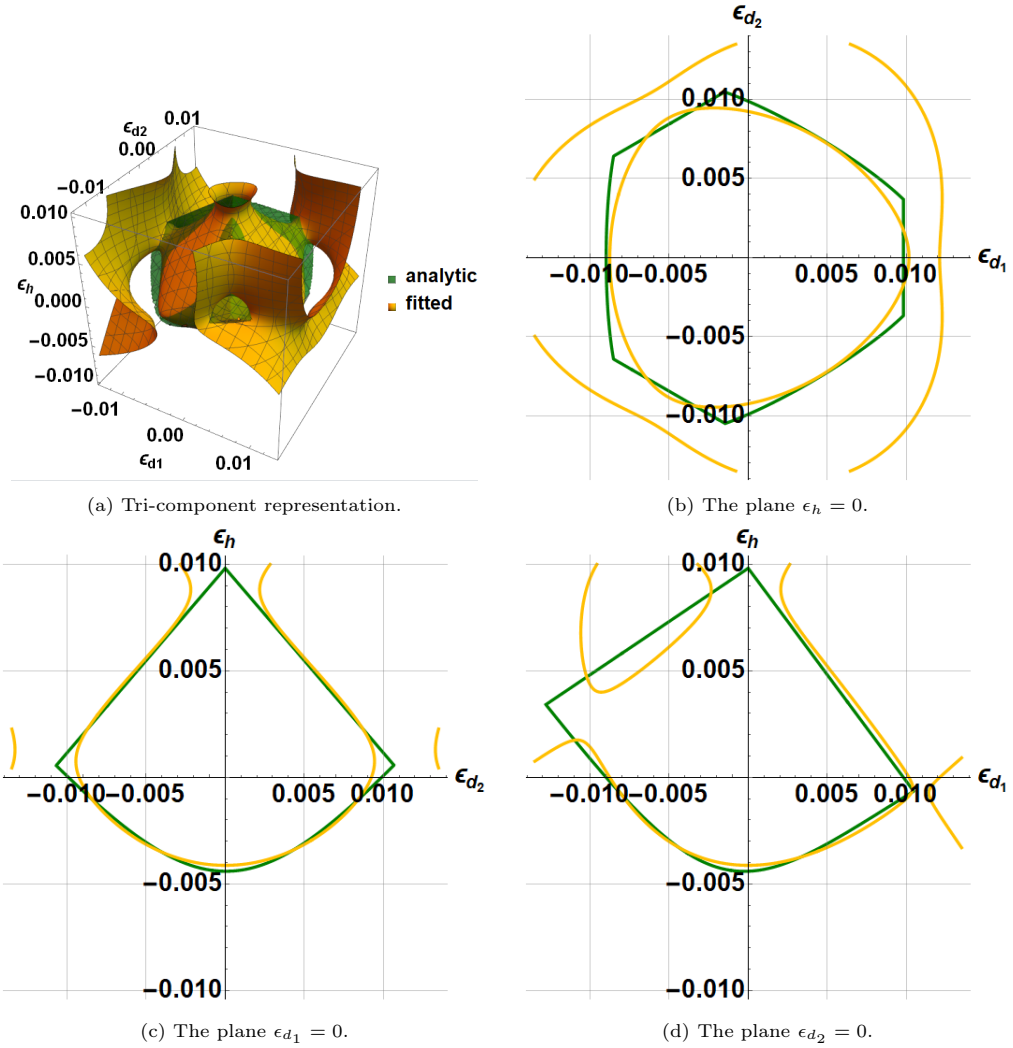

(a) Tri-component representation.

(b) The plane $\epsilon_h = 0$.

(c) The plane $\epsilon_{d_1} = 0$.

(d) The plane $\epsilon_{d_2} = 0$.

Figure 3.29: The threshold surface of the a triangular lattice (green) and the fitted surface (orange).

Lemma 3.5.2. *We the log-sum-exp (LSE) function as follows [131]:*

$$\mathrm{LSE}\left(x_1, \ldots, x_n\right) = \log\left(\exp\left(x_1\right) + \cdots + \exp\left(x_n\right)\right)$$

The function in $\mathbb{R}^n$ domain is an approximation of the maximum $\max_i x_i$ with the following bounds:

$$\max\left\{x_1, \ldots, x_n\right\} \leq \mathrm{LSE}\left(x_1, \ldots, x_n\right) \leq \max\left\{x_1, \ldots, x_n\right\} + \log(n) \tag{3.28}$$

The function has the propriety of being strictly convex.

LSE is one of approaches that are used to have a smooth approximation of the maximum function, and has many uses, particularly in optimisation problems. We can tighten the bounds in the inequality (3.28) by introducing a coefficient $\lambda > 0$ as follows:

$$\max\left\{x_1, \ldots, x_n\right\} \leq \frac{1}{\lambda}\,\mathrm{LSE}\left(\frac{x_1}{\lambda}, \ldots, \frac{x_n}{\lambda}\right) \leq \max\left\{x_1, \ldots, x_n\right\} + \frac{\log(n)}{\lambda},$$

hence, in our case, we approximate the function $F_{pb}(\underset{\sim}{\varepsilon})$ with the following function $\tilde{F}_{pb}(\underset{\sim}{\varepsilon})$:

$$\tilde{F}_{pb}(\underset{\sim}{\varepsilon}) = \frac{1}{\lambda}\left(\exp(\lambda P_1) + \exp(\lambda P_2) + \exp(\lambda P_3) + \exp(\lambda P_{pb})\right)$$

λ is set 0.0085. The approximating is done to the surface coming from $\tilde{F}_{pb}(\underset{\sim}{\varepsilon}) = Y$ instead of the one coming from $F_{pb}(\underset{\sim}{\varepsilon}) = Y$. The same set of harmonic parameters as before is considered.

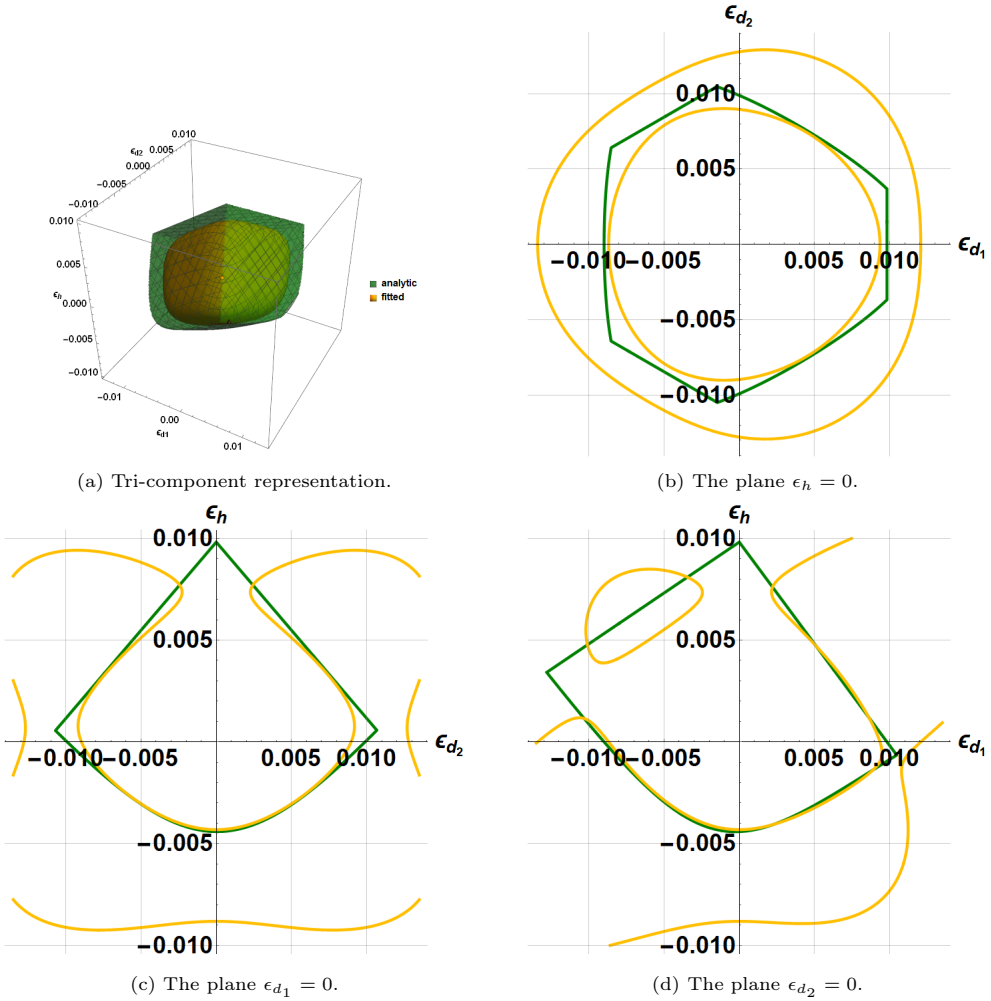

(a) Tri-component representation.

(b) The plane $\epsilon_h = 0$.

(c) The plane $\epsilon_{d_1} = 0$.

(d) The plane $\epsilon_{d_2} = 0$.

Figure 3.30: The threshold surface of the triangular lattice (green) and the fitted surface (orange) after smoothing the function.

Although, the surface is smoothed, identifying the surface of the threshold is difficult (cf. figure 3.30). Assuming having too large a set of parameters, (which leads to unwanted solutions), the 1st and 2nd degree polynomials are of no use in modelling the anisotropy we are looking for, we will remove them from the set of independent variables. Consequently, only the terms associated with 3rd and 4th degree polynomials will be taken into account. The number of independent parameters is therefore reduced from 10 to 7:

$$\{S_1^{8,3}, S_1^{6,3}, \alpha^{8,4}, \alpha^{8,2}, \alpha^{8,0}, \alpha^{6,2}, \alpha^{6,0}\}, \tag{3.29}$$

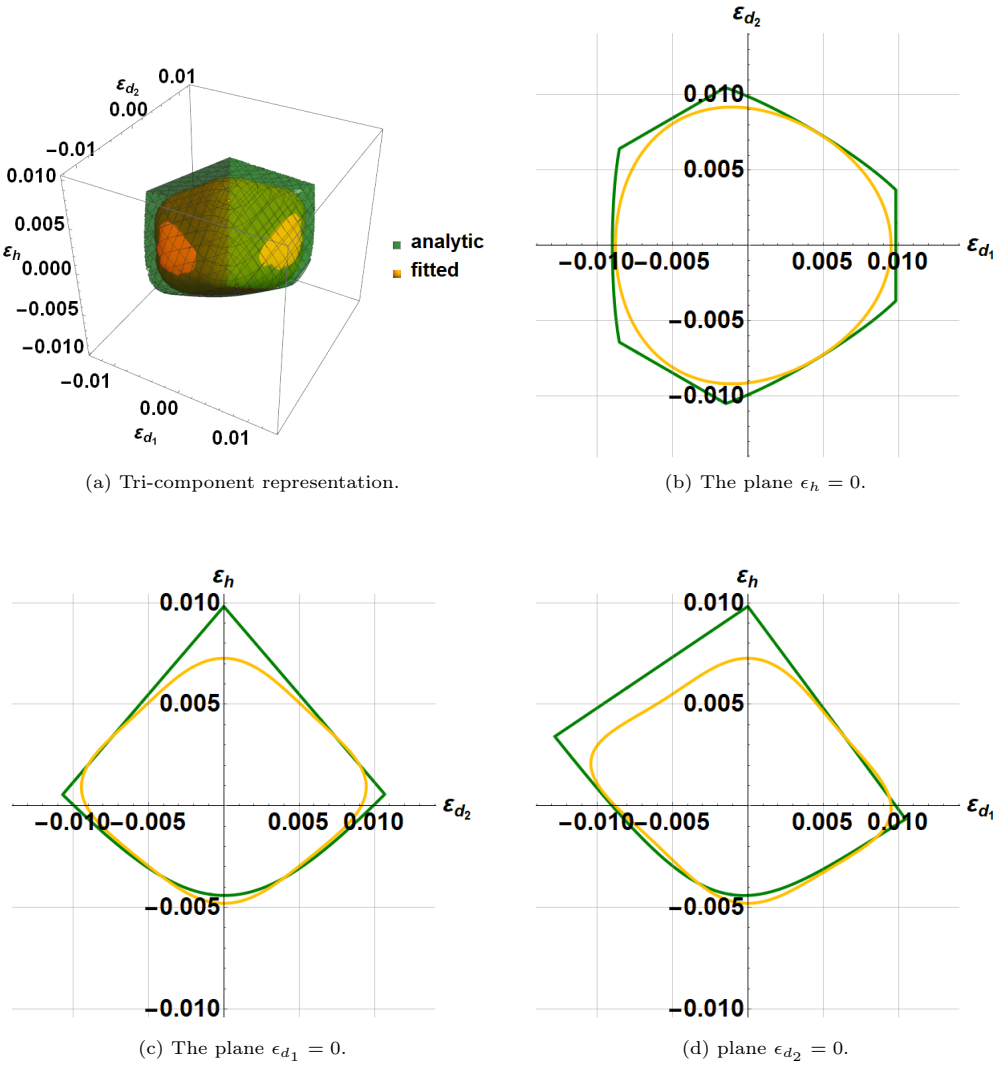

(a) Tri-component representation.

(b) The plane $\epsilon_h = 0$.

(c) The plane $\epsilon_{d_1} = 0$.

(d) plane $\epsilon_{d_2} = 0$.

Figure 3.32: The threshold surface of the a triangular lattice green and the fitted surface orange (smoothed version).

As the figure 3.32 shows, this assumption leads to a physical solution. As it is already mentioned, a more accurate fit can be obtained by taking into account polynomials of higher degree. The value of the corresponding harmonic parameters are given in the following table (for $F_{TW4}(\underset{\sim}{\varepsilon}) = Y$):

$S_1^{8,3}$	$S_1^{6,3}$	$\alpha^{8,4}$	$\alpha^{8,2}$	$\alpha^{8,0}$	$\alpha^{6,2}$	$\alpha^{6,0}$
2.76×10^{11}	-3.68×10^{8}	1.92×10^{12}	6.79×10^{12}	1.93×10^{13}	-1.74×10^{10}	-6.25×10^{10}

We can try to directly identify the surface $F_{pb}(\underset{\sim}{\varepsilon}) = Y$ (unsmoothed) from the reduced set of harmonic parameters (3.29) (see figure 3.34). Better result than the previous one is obtained though, the convexity is not respected. In the end, we were able to identify a fairly complicated surface as a special case of our generalised threshold function with just 7 parameters. The value of the corresponding harmonic parameters are given in the following table:

$S_1^{8,3}$	$S_1^{6,3}$	$\alpha^{8,4}$	$\alpha^{8,2}$	$\alpha^{8,0}$	$\alpha^{6,2}$	$\alpha^{6,0}$
3.62×10^{11}	-3.93×10^{8}	1.64×10^{12}	6.25×10^{12}	1.47×10^{13}	-1.4×10^{10}	-7.47×10^{10}

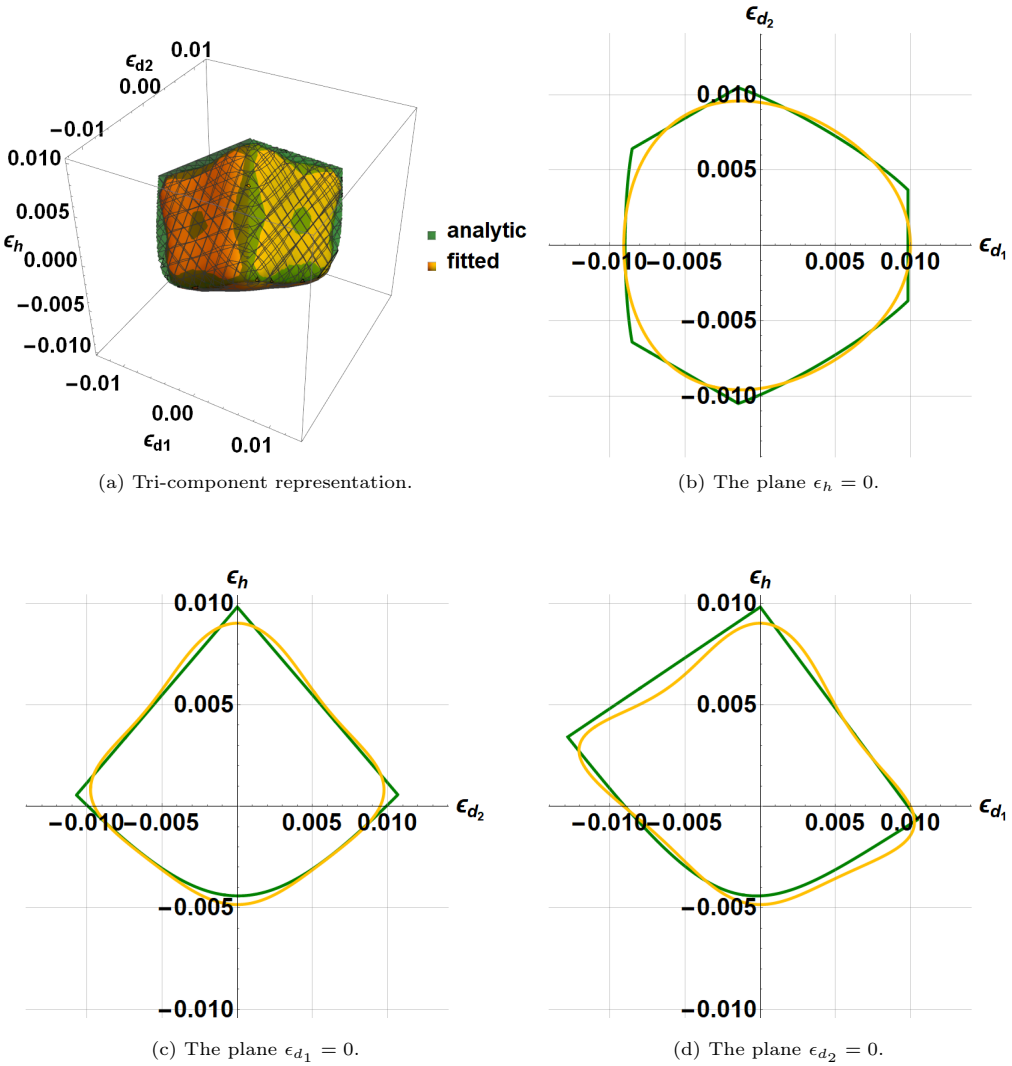

(a) Tri-component representation.

(b) The plane $\epsilon_h = 0$.

(c) The plane $\epsilon_{d_1} = 0$.

(d) The plane $\epsilon_{d_2} = 0$.

Figure 3.34: The threshold surface of the a triangular lattice (green) and the fitted surface (orange) after smoothing the function.

3.6 Synthesis

The following statements allow to summarise in a concise manner this chapter:

- The established analysis in both chapter 1 and 2, guided us to propose a general threshold criterion named *Tsai-wu 4*. It a polynomial function of degree 1 to 4 in $\underset{\sim}{\sigma}$. For each degree, material tensors of order $(2, 4, 6, 8)$ are considered.
- The harmonic decomposition allowed to look for the set of all situations that TW4 can describe. It starts with anisotropic properties (in $\mathbb{R}^2$) in section 3.2.1 where it confirms the link between harmonic decomposition and the representation theory. Furthermore, the harmonic decomposition with respect to $\mathbb{R}^3$ (considering harmonic basis), allowed us to give all the possible symmetry classes of threshold surface associated to TW4.
- As it was done before, the explicit algebraic harmonic decomposition of the 6th and 8th order tensor were established in section 3.3 (for 2nd and 4th order tensor it is already done [13]). A demonstration, on how the threshold surface shape (anisotropy and loading symmetry) changes with presence/absence of some harmonic tensors, is provided. Lastly, approximation of some selected threshold criterion was done in section 3.5, and which validates the obtained results from representation theory in section 3.2.1.

The threshold function approximated in section 3.5.4 will be implemented as constraints in a topology optimisation problem in the next part of the manuscript.

Part II

Towards Stress based topology optimisation

Chapter 4

Topology optimisation : methods and algorithms

Contents

In mechanical engineering, it is important to derive the best performance from a design of manufactured structure. This can be done through engineering experience by doing experimental or numerical tests. However, for complex applications, it is not intuitive hence, it is time-consuming and expensive. To address the problem, it turns out that the whole process can be automated by solving a mathematical structural optimisation problem. Since the middle the 20th century, many numerical methods [123] for structural optimisation, with a solid mathematical background, have emerged. It all started with: (i) firstly with *parametric optimisation* where only the engineering variables are optimised (thickness, radius, truss layout design, ... etc). (ii) Then with the *shape optimisation* in which the geometry of the boundary is optimised [67]. (iii) Finally to arrive at the *topology optimisation* where the presence of matter is determined [31]. The figure 4.1 shows the difference between the three types of structural optimisation.

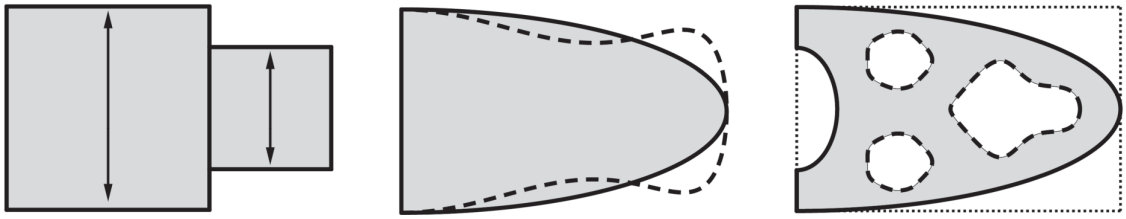

(a) Parametric optimization. (b) Shape optimization. (c) Topological optimization.

Figure 4.1: The three types of structural optimisation [5].

A structural optimisation problem is defined by the following elements [2]:

- **A physical model** describing the mechanical behaviour of the structure, often in the form of partial differential equations.
- **An objective function** derived from a mathematical representation of topology (or the shape).
- **Constraints** which define a set of admissible solutions (manufacturing constraints, mechanical strength, ...etc). The set of possible solutions that satisfy the constraints is called *feasible domain.*

In our study, only the *topology optimisation* for 2D elasticity problems will be featured. On years 1990s, topology optimisation has reach a high level maturity where it is possible to be used in various industrial applications. Now, lot of tools are available in different commercial finite element software (Abaqus, Ansys, Nastran, ... etc).

This chapter focuses on giving a brief overview about the topology optimisation. In the first section, some aspects on what are the most popular methods to parametrise the topology will be shown. In the second section, some examples of different objective functions are discussed. It is important to point out that the mentioned functions will be the encountered ones in our optimisation problems. In the third section, different numerical algorithms are described. In the fourth section, some explanations about the numerical difficulties that are present in stress constrained topology optimisation are given. Lastly, in the fifth section, we will speak about including anisotropy in a topology optimisation problem by adding other optimisation variables (e.g. orientation). The last section is a general conclusion which justifies the choice of the topology optimisation problem and the resolution algorithm used un this thesis.

4.1 Topology optimisation

The topology optimization is defined as a set of computational methods used in engineering to determine the optimal distribution of material within a given design space. It aims to find the most efficient and lightweight configuration of a structure while meeting certain constraints (e.g. manufacturing constraints). Generally a topology optimisation problem is written as follows:

$$\begin{cases} \min\limits_{\Omega_{mat}} \mathcal{J}(\underline{u}_{\Omega_{mat}}, \Omega_{mat}), & \\ \text{Constraints}, & \end{cases} \qquad \Omega_{mat} \subset \Omega, \tag{4.1}$$

where Ω is the design space, Ω_{mat} is the subspace of Ω where the material is being distributed, $\mathcal{J}$ is the objective function. $\underline{u}_{\Omega_{mat}}$ is the displacement and it is dependent on Ω_{mat}. The problem can be subjected to constraints (volume, geometry, ... etc). The figure 4.2 shows an example of an optimal material distribution for a linear elasticity problem where stiffness is maximised under a volume constraint.

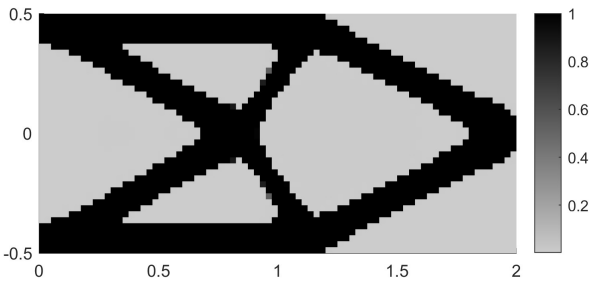

Figure 4.2: Optimal distribution of an isotropic material for a cantilever beam (elasticity). The compliance is considered as the objective function to minimize, subjected to a volume constraint. The black area indicates the presence of material, the grey one indicates absence of material.

Lot of resolution algorithms are available in the literature [189]. They depend on the optimisation problem and on the chosen parameters. Numerical difficulties are encountered [163, 56], it is important to see how different authors managed to address them.

4.2 Parametrisation of the topology

In a topology optimisation problem, one can ask the following question: "How to mathematically parametrise the topology ?". Different methods exist, the first one is the *density based* method. The second one is the *level-set* [9]. In this section, some details about each method are provided. It is important to point out that it exists a third method called *phase field* [36] that however be detailed in this section.

4.2.1 Density based method

In density based methods the presence of material is indicated explicitly by a parameter field denoted $\chi(\underline{x})$. In a position[1] $\underline{x}$, $\chi(\underline{x}) = 1$ indicates the presence of the material, $\chi(\underline{x}) = 0$ indicates void (absence of the material). In a physical model, the effective properties are pondered by the density variable. For example, in an elasticity problem the optimised stiffness tensor $\underset{\approx}{C}(\underline{x})$ is given as follows:

$$\underset{\approx}{C}(\underline{x}) = \chi(\underline{x})\underset{\approx}{C}^0, \tag{4.2}$$

where $\underset{\approx}{C}^0$ is the the material stiffness tensor. The problem here is ill-posed due the fact that χ is a discrete variable (0 or 1) and due the fact that when $\chi(\underline{x}) = 0$, the elasticity problem (or the physical model) can not be defined. To address this, one can relax the problem by replacing χ with $\rho \in [0, 1]$, hence in the previous example, the optimised stiffness tensor $\underset{\approx}{C}(\underline{x})$ is given as follows:

$$\underset{\approx}{C}(\underline{x}) = [\epsilon + (1 - \epsilon)\rho(\underline{x})]\underset{\approx}{C}^0. \tag{4.3}$$

where ϵ, generally set to 10^{-6}, is the Ersatz stiffness [159]. Therefore, the role of ϵ is avoid having a null stiffness. Allowing $\rho(\underline{x})$ to be valued in the interval $[0, 1]$ involves intermediate densities appearing in the optimal topologies. In the literature [5], it is considered as a mixture of material and void. It can describe a microstructure (e.g. a unit cell of a lattice material [42, 53]). In this case, it is known as *homogenisation method*. Some difficulties are encountered on how the relationship between the density and microstructure is defined and also on how the passage from a continuous material to a discontinuous one is done (the process is known as *dis-homogenisation*). The reader may refer to the following references [77, 119, 104, 181] for more details.

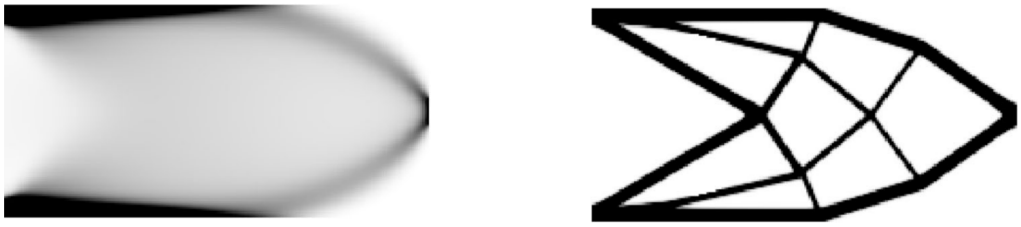

(a) No penalisation. (b) SIMP penalisation $p = 3$.

Figure 4.3: The topology of an optimised beam [194].

In order to eliminate the intermediate, penalisation techniques are used. they force the density to converge to either 0 ot 1. Several techniques are available: (i) the first one called 'SIMP' (Simple Isotropic Material Penalisation) [162]. (ii) The second one is RAMP (Rational Approximation of Material Properties) [177] and (iii) the third one is SINH [39]. In a case where the penalisation is enabled, the equation (4.3) becomes:

$$\underset{\approx}{C}(\underline{x}) = [\epsilon + (1 - \epsilon)f(\rho(\underline{x}))]\underset{\approx}{C}_0, \tag{4.4}$$

$$where, \underbrace{f(\rho) = \rho^p}_{\text{SIMP}}; \qquad \underbrace{f(\rho) = \frac{\rho}{1 + p(1 - \rho)}}_{\text{RAMP}}; \qquad \underbrace{f(\rho) = \frac{\sinh(p\rho)}{\sinh(p)}}_{\text{SINH}}. \tag{4.5}$$

[1] Given a structure domain subdivided by finite elements, $\chi(\underline{x})$ is a local variable constant in each element which indicates the presence/absence of material

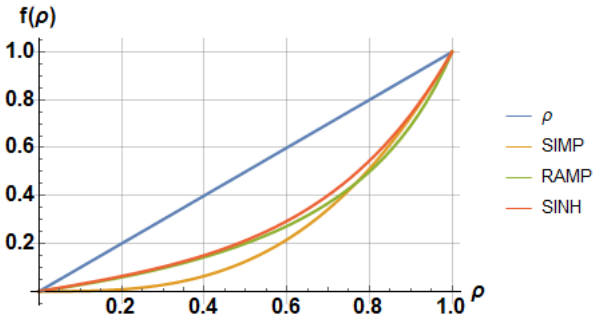

Figure 4.4: Difference between the 3 penalisation techniques for $p = 3$.

The figure 4.4 shows that the 3 penalisation techniques are similar. SIMP remains the most popular and generally the penalisation parameter p is set to 3. The figure 4.3 shows us the effect of the SIMP penalisation on the obtained result. All density based methods have advantages of being simple to understand and easy for numerical implementation. However, when a penalisation technique is applied, the boundaries of the optimal topology are not clear where some remaining intermediate densities can be found. Therefore, the obtained results will need to be post-processed [200]. Some numerical difficulties are encountered [163] such as *checkerboards* issue and some remaining intermediate densities, to overcome these problems different filters are used such as *regularisation* and *heaviside* filters.

4.2.2 Level set method

In the level-set parametrisation, the distribution of the material $\Omega_{mat} \subset \Omega$ ($\Omega = \Omega_{mat} \cup \bar{\Omega}_{mat}$ is the design space) is defined by an implicit function $\phi(\underline{x})$. The boundaries of Ω_{mat} corresponds to the intersections of the level zero with the surface of $\phi(\underline{x})$. Mathematically, the function $\phi : \Omega \mapsto \mathbb{R}$ verifies:

$$\begin{cases} \phi(\underline{x}) < 0 & \text{if } \underline{x} \in \bar{\Omega}_{mat}, \\ \phi(\underline{x}) = 0 & \text{if } \underline{x} \in \partial\Omega_{mat}, \\ \phi(\underline{x}) \geq 0 & \text{if } \underline{x} \in \Omega_{mat}. \end{cases} \tag{4.6}$$

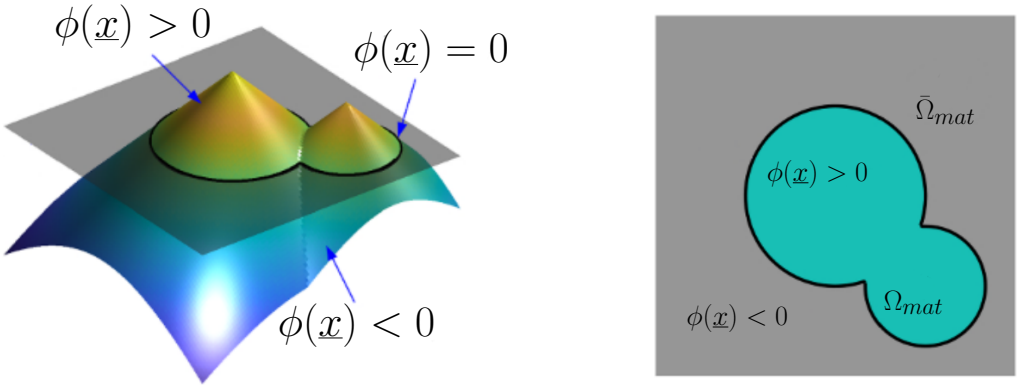

Figure 4.5: The representation of Ω_{mat} with the level-set method ($\Omega = \Omega_{mat} \cup \bar{\Omega}_{mat}$) [106].

The equation (4.6) indicates that the material is present when $\phi(\underline{x}) > 0$. (see figure 4.5). When $\phi(\underline{x}) < 0$ there is void. With the level-set method, the optimisation is assimilated to dynamical problem [106, 56] where in each iteration the form of $\Omega_{mat}(t)$, defined by $\phi(\underline{x})$, evolves with time t following a normal velocity denoted $v(\underline{x}, t)$ evaluated as the descent direction calculated from the shape derivative of the objective function using Hadamard's boundary variation method. The evolution of Ω_{mat} is determined by solving the following advection equation:

$$\frac{\partial \phi}{\partial t} + v(t, x)|\nabla \phi| = 0 \quad \forall \underline{x} \in \Omega, \tag{4.7}$$

During the evolution of Ω_{mat} , the topology can changes only by eliminating holes. This means that using the shape derivative cannot create holes, therefore, it is important, in the initialisation, to put enough holes in order to obtain better results. In a case where no holes are introduced in the initial distribution of the material, a shape optimisation problem is being dealt with. The hole problem can be addressed by using the *topological derivative* [153] (or alongside of shape derivative) which is capable of creating holes.

Concluding remarks

The density-based method is best candidate for all featured topology optimisation problems in this document. The main reason is that it has the ability to include anisotropy (if it is desired). In other terms, additional variables (to the topology), such as orientation of the material or anisotropy parameters, can be considered. This can be done with both homogenisation and SIMP method. The reader is invited to read section 4.6. The level-set is able to include some aspects of anisotropy [6, 165] however, despite the numerical difficulties [163], density based methods are much simpler to implement numerically.

4.3 Objective function and optimisation constraints

In our study, three main aspects are brought to light: volume, rigidity and mechanical strength. The volume represents the amount of volume that the material occupies in the the design space. The rigidity is defined as *compliance* which is the work of the external forces (an energy). The mechanical strength consists of a criterion that must be satisfied in the obtained topology (after solving the optimisation problem). All these three aspects are somehow linked to each other e.g. with the lower volume, the lower the rigidity. In this section, a description on each aspect is given.

4.3.1 Compliance

It is known as the work of external forces. The most popular problem in topology optimisation is the minimisation of the compliance subjected to a defined volume. The volume (less that the volume of the design space) must be imposed in order avoid trivial solution (which is presence of the material in whole design space). With SIMP method the optimisation problem is given by:

$$\begin{cases} \min\limits_{\rho\in[0,1]} \mathcal{C}(\underline{\mathrm{u}}), \\ \dfrac{1}{V_\Omega}\displaystyle\int_\Omega \rho \ \mathrm{dv} = \eta, \end{cases} \tag{4.8}$$

where in an elasticity problem,

$$\mathcal{C}(\underline{\mathrm{u}}) = \int_\Omega \underset{\sim}{\sigma}(\underline{\mathrm{u}}) : \underset{\sim}{\varepsilon}(\underline{\mathrm{u}}) \ \mathrm{dv}, \tag{4.9}$$

with V_Ω as the volume of the design space, $\eta = \dfrac{V_0}{V_\Omega}$, V_0 is the objective volume and $\underline{\mathrm{u}}$ is the displacement vector, solution of the elasticity problem (more details are found in section 5.1). The optimisation problem (4.8) can be solved with multiple algorithms. It has a lot of mathematical particular properties especially for optimality criteria and for gradient-based algorithms [5, 146] which simplify the problem and make the implementation more convenient.

4.3.2 Volume

The volume represents the amount of volume that the material occupies in the the design space. In SIMP method, it is defined by:

$$V_{\Omega_{mat}} = \int_\Omega \rho \ \mathrm{dv}, \tag{4.10}$$

The volume can be used as a constraint usually in the compliance minimisation [146, 42] (see equation (4.8)). It can be considered as an objective function in volume (or mass) minimisation problems [143, 186] subjected to inequality constraints in rigidity or in mechanical strength (or both). This kind of problem is very useful because the mechanical strength is usually known (defined by a criterion). It is also useful when the required rigidity (or compliance) is known and the corresponding volume is unknown. The idea is to reduce of volume while maintaining the required rigidity and the required mechanical strength. The problem is often solved with gradient based algorithm in both SIMP and level-set methods.

4.3.3 Threshold function

It is related to a strength criterion, defined by a threshold function (see part I), that is featured in a topology optimisation problem. It is known in the literature as stress based topology optimisation where the mechanical strength (threshold function) is either employed as an objective function [128, 8] or as a constraint [141, 159, 186, 55, 81]. It is more practical to solve a volume minimisation problem instead of minimising an equivalent stress field (e.g. Von Mises) due to fact that the mechanical limit strength is always known (e.g. when the max

Von Mises stress field reach the threshold). If we minimise the threshold function (as an objective function) we might stumble into a local minima that do not satisfy the mechanical strength [143].

A stress based topology optimisation problems can be solved with both SIMP and level-set methods. A special attention is brought to stress topology optimisation with SIMP where several numerical issues are encountered. Meanwhile, the issues are less pronounced for level-set method (due to the absence of intermediate densities). Lot of approaches are established to tackle these issues [64, 65, 77, 185], more details are available in section 4.5.

Multiple criteria has been implemented, Giraldo et al. [80] regrouped multiple threshold functions in a single one. The regrouped threshold functions were: Von-Mises, Drucker-Prager, Tresca, Mohr-Coulomb, Bresler-Pister and Willam-Warnke.Some anisotropic criteria are found, Tsai-Hill was implemented by Silva et al. [164]. Tsai-Wu was also implemented by Mirzendehdel et al. [128, 187]. It is worth noting that Tsai-Wu cannot be implemented directly. The reason is that it is non-homogenous polynomial which leads to counter intuitive design in the topology optimisation problem. A *safety factor* is introduced to overcome the difficulty.

Concluding remarks

As a stress constrained topology optimisation problem, volume minimisation was the most studied one in the literature. As stated in section 4.3.2, the main reason is that the mechanical strength is usually known (defined by a criterion). The concept is to remove material while maintaining the required mechanical strength. This problem may be subjected to rigidity (compliance) constraint if needed and it will be formulated in next chapter. It can be solved with a gradient based or a metaheuristic algorithms. More details about resolution algorithms are available in following section.

4.4 Algorithms for structural optimisation

For topology optimisation problems, it exists several numerical algorithms as ways to solve them. Some of them are very flexible [57] where they can be adapted for several aspects such as manufacturing constraints and frequency responses. Some of them are too restrictive [146] as they are suited for only one problem with one defined method. Therefore, the choice of an algorithm is very dependent on the chosen method and on the proposed problem. Three main families exist: (1) Optimality criteria, (2) Metaheuristic and (3) Gradient-based (also known as mathematical programming [123]). Each algorithm has its advantages and disadvantages hence, it is important to have a background for each one. In this section, an overview on some of most popular algorithms is provided. For our study, we justify our choice of the algorithm of resolution at the end in the concluding remarks.

4.4.1 Optimality criteria

Optimality criteria algorithms derive or state conditions characterising the optimal design, then find or change the design to satisfy them while indirectly optimising the structure [123]. These conditions are often based on Kuhn-Tucker optimality conditions. It is usually used for compliance minimisation to obtain optimal layout design of trusses [145, 110, 31]. It is also used in topology optimisation. Sigmund, in his work [162], used a heuristic optimality criterion to obtain optimal material distribution for an elasticity problem. Allaire et al. [4] did the same by introducing *alternate direction* algorithm. The same algorithm is also used for the simultaneous optimization of topology and material anisotropy [146] (a proof of convergence can be found in the reference). Optimality criteria has the advantage of being robust and cheap comparing to other algorithms, however they are only restricted to compliance minimisation and cannot, for example, treat mechanical strength as constraints.

4.4.2 Metaheuristic

It consists of algorithms that are mainly inspired by nature, physics and biological evolution. These algorithms have the ability to solve optimisation problem without need to calculate gradient of the objective function. Therefore, they can be applied to any optimisation without the design variables being continuous. For structural optimisation, different problems with different constraints (mechanical strength, ... etc) can be solved. Lot of algorithms are found in the literature. A popular one is the evolutionary structural optimisation (ESO) [197]. The concept consists of removing, in each iteration, the ineffective material elements for the objective function. What remains enables us to achieve an optimal design. One issue with this algorithm is that it could lead to a truss-like design. To address that, bidirectional evolutionary structural optimisation (BESO) [199] was introduced where the material can be removed and added at the same time hence, it allows for a better convergence to a local minimum to obtain better designs.

In the literature, one can find Genetic algorithm (GA), it consists of a stochastic global search method that mimics the metaphor of natural biological evolution [190]. The set of design variable is considered as population is created. The concept is to select, for each generation, the fittest set of solutions. Mutation and crossover are applied to seek improvement for the the selected set of solutions. As metaheuristic algorithm, Ant Colony Optimisation (ACO) [108] and Particle Swarm Optimisation (PSO) [122] can be used for topology optimisation. They both are nature algorithms that emulates the social behaviour of animals such as insects swarming (ACO) and birds flocking (PSO) searching for food. The concept is that a group artificial ants or particles cooperate to solve a combinatorial problem by exchanging information which allows to remove/add material to the design space.

Despite the advantages, these algorithms are computationally expensive for high dimensional problem (i.e. large number of FEM elements) because of the sharp rise in the number of combination problems where, for each one, the objective function must be evaluated.

4.4.3 Gradient based

It is also known as *mathematical programming*. Generally, the concept [123] is to obtain information from conditions around the current design point in the design space in order to look for: (i) decent direction and (ii) how far to go for best descent. The process is repeated until no more reduction is produced in the iterations within some selected tolerance. One of the classical algorithms is *gradient* algorithm [2] which can only be applied to non-constrained optimisation problems. If the constraints are present, *projected gradient* algorithm can be used. In each iteration the solution is projected into feasible domain (where the constraints are satisfied). However, the projection operators can only be defined for certain constraints [3] (e.g. bounds constraint ($0 \leq \rho \leq 1$)) and not for all. Therefore, other flexible algorithms are found in literature [132]. They belong to what so-called *non-linear mathematical programming*. The non linear part is represented by the addition of non-linear equality and inequality constraints. Multiple approaches are available such as Sequential Linear Programming (SLP), Sequential Quadratic Programming (SQP), Augmented Lagrangian, convex approximations [178], Null-space gradient flow[71], ... etc.

Gradient-based algorithms are known to be very flexible. they can treat different optimisation problems with different constraints (multi-constrainted topology optimisation problems [57]). However, the evaluation of the derivative is not straightforward. From an engineering point of view, it is difficult to implement it using commercial software. It can be also expensive specially in case of slow convergence. In complex application, the *Sensitivity Analysis*, which is often required for the numerical implementation of the algorithm, can be "tedious" . This problem can be tackled by using automatic differentiation tools [10].

In this subsection, an overview on some popular gradient-based algorithm is provided. The first one is the convex approximation, the second one is the augmented Lagrangian and the last is the null-space gradient flow. For our study, we justify our choice in the conclusion.

Convex approximation

For an optimisation problem, the idea behind these algorithms is to establish several sub-problems and solve them. These sub-problems are approximations proven to be convex. Several algorithms are available in the literature. One of them is the CONvex LINear approximation (CONLIN) [69]. The concept is to perform, in each iteration, the linearisation process (first order Taylor expansion) and select an appropriate approximation scheme so the resulting problem is convex. An application on truss structures is available [40]. Another algorithm is found and it is the Method of the Moving Asymptotes (MMA) [178]. The idea remains the same as before except that the approximation process is more general. Another variant is proposed and it is called GCMMA (Globally Convergent MMA) [179]. The choice between the two (MMA and GCMMA) is dependant on the proposed optimisation problem. If the the objective function is not stable and fluctuates a lot then GCMMA is recommanded. If it is stable and does not fluctuate a lot then MMA is the better choice. If the problem presents multiple variables (e.g. topology and material orientation) one can use SplitMMA [187]. It allows establishing a sub-problem for each variable and they can be treated separately with a chosen approach (MMA or GCMMA) depending on the variation of the objective function. The MMA algorithms has proven to be efficient for topology optimisation problems and they is very often used for complex applications [185, 203].

Remark It is important to point out that more algorithm are available [69] such as sequential linear approximation (SLP), sequential quadratic approximation (SQP). They are based on approximation which is linear (first order Taylor expansion) for SLP and quadratic (second order Taylor expansion) for SQP. These algorithms are implemented in IPOPT libraries they are used in topology optimisation problems. In the literature [30], another algorithm called Method of Feasible Direction (MFD) can be used. It is a modified version of SLP and SQP based on the concept of marge maximisation [69] and it is proven to be efficient for handling large number of constraints.

Augmented Lagrangian

In an optimisation problem, there exists a way of taking into account the constraints: the Lagrangian approach [2]. It has the property of changing a constrained optimisation problem to an unconstrained one with a different objective function. To clarify, we consider the following problem:

$$\begin{cases} \min\limits_{p} \mathcal{J}(p), \\ f(p) = 0, \end{cases} \tag{4.11}$$

where $\mathcal{J}$ is the objective function, h is an equality constraint function and p is the optimisation variable. The Lagrangian function is given by:

$$\mathcal{L}(p, \lambda) = \mathcal{J}(p) + \lambda f(p), \tag{4.12}$$

where λ is the Lagrange multiplier. It is proven that the equivalent problem [2, 132] to (4.11) is:

$$\max_{\lambda} \min_{p} \mathcal{L}(p, \lambda) \tag{4.13}$$

and it corresponds to looking for a saddle point (P^*, λ^*) (see figure 4.6). The optimisation is transformed into a free one at a cost adding another variable which is λ. One can see that if the constraints are verified the Lagrangian becomes the objective function. This can only be the case if the right value of λ is found. The Lagrangian can be extended to multiple equality and inequality constraints by simply adding more Lagrange multipliers. The inequality can be transformed into equality constraint using the so-called slack variables [32] (an example is shown in section 5.4). The problem (4.13) can be solved using Uzawa algorithm. It defines an updating strategy to the Lagrange multipliers and other non-physical parameters in order to find the saddle point. The implementation of Uzawa algorithm is simple however, the algorithm has issues [69], the convergence is slow, the constraints are not strictly respected and oscillations to the optimisation variable could occur because of the difficulty of defining non-physical parameters.

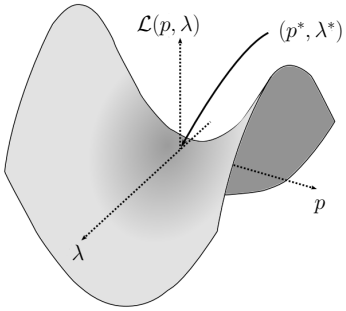

Figure 4.6: Graphical representation of a saddle point [106].

The problem (4.11) can be solved with what so-called penalisation algorithm [106]. Same as previous approach, it transforms a constrained optimisation problem into a unconstrained one. The equivalent problem is given by:

$$\min_{p} \left(\mathcal{J}(p) + \frac{1}{\epsilon} f(p)^2 \right) \tag{4.14}$$

where ϵ is a penalisation parameter. The greater the value of $\frac{1}{\epsilon}$ ($\epsilon \to 0$), the more importance is attached to the constraint. Therefore, solving (4.14) is easy by simply choosing a sufficiently small value of ϵ (e.g. using gradient algorithm) however, the problem appeared to be poorly conditioned [2] which makes to choice of ϵ difficult. If ϵ is too small, numerical errors (Rounding, ...) can therefore be very pronounced. It is important also to keep in mind that multiple equality and inequality constraints can be added by simply introducing more penalised terms to problem (4.14).

To address the problem in both previous algorithms (Uzawa and penalisation), *Augmented Lagrangian* was proposed. It is a combination of both Uzawa and penalisation algorithms. For problem (4.11), the augmented Lagrangian consists of adding a penalisation parameter to the Lagrangian as follows:

$$\mathcal{L}(p, \lambda, b) = \mathcal{J}(p) + \lambda f(p) + \frac{b}{2} f(p)^2, \tag{4.15}$$

where b is a penalisation parameter. The equivalent problem remains the same (looking for saddle point). It is important to point out that the augmented Lagrangian is a regularised version of the basic Lagrangian of

type Moreau-Yosida, more details are found in [41]. b does not need to be importantly high (it is penalisation problem) but it has an important role in the updating scheme of λ. A very detailed algorithm for an optimisation problem is available in section 5.2.

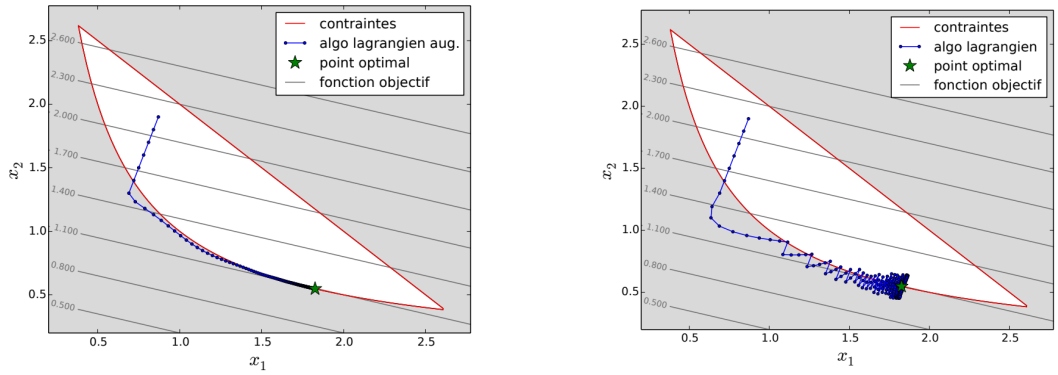

(a) Augmented Lagrangian.

(b) Uzawa

Figure 4.7: An example showing the difference in convergence between Uzawa and augmented Lagrangian algorithms in the optimisation variable space [69].

The augmented Lagrangian algorithm, has the advantage of being easy to implement. comparing to Uzawa algorithm, it converges faster due to the improved updating scheme leading directly to the right value of λ. An example of comparison is found in [69] where the figure 4.7 shows the convergence history in the variable space. Some disadvantages are present. A lot of non-physical parameters has to be chosen (in a kind of arbitrary manner) and can influence greatly the convergence history and the obtained results.

Null-space gradient flow

As gradient based algorithm, a list of algorithms was briefly reviewed such as augmented Lagrangian, MMA, SLP, SQP and MFD. All these algorithms have non-physical parameters and tuning them is not an easy task and it is time consuming. An algorithm called Null-space gradient flow was proposed [71]. The algorithm is based on a dynamical system approaches to non-linear constrained optimization. It is not very common within topology optimisation community. The main advantage is that it does not need tuning due to the fact that the only non-physical parameter is the descent step (very intuitive to adjust). It is also effective when it comes to inequality constraints, the algorithm has the option to not use the slack variables and it shows faster saturation[2]. It can be used for topology optimisation problems [70] and it is proven to be efficient.

Concluding remarks

For stress based topology optimisation, MMA remains the most efficient and most commonly used as an algorithm of resolution. It is used in augmented Lagrangian [81] when the stress are local. It is also used directly when the local stresses are aggregated [186] (more details are given in the next section). The classical gradient algorithm can be also used [55] in augmented Lagrangian for local stresses, however, it is not common and few explicit algorithm are provided. All featured optimisation problems in this document will be solved by augmented Lagrangian with the classical gradient. For pedagogical purposes, the explicit algorithm with explicit derived expressions will be provided and tested.

4.5 Stress constrained topology optimisation

The most encountered optimisation problem in the literature is the volume minimisation subjected to stress constraints. This problem can be solved using with different methods (SIMP, Level-set) and with different algorithms (BESO [196], augmented Lagrangian [141], MMA [186], ...). In this section a special attention is given to the problem when SIMP method is used, it is given as follows:

$$\begin{cases} \min\limits_{\rho\in[0,1]} \int_\Omega \rho \, \mathrm{dv}, \\ g_j = \left(\dfrac{\sigma_j^{eq}}{\sigma_{lim}} - 1 \right) \leq 0 \quad \forall \underline{\mathrm{x}} \in \Omega_{mat} := \{\underline{\mathrm{x}} \in \Omega, \rho \neq 0\} \end{cases} \tag{4.16}$$

[2]the inequality constraint is saturated when it is brought close to its bounds, e.g. $x < 1$ is saturated when $x = 0.999$

where N_e is the total number of elements in FEM analysis and σ_j^{eq} is an equivalent stress (e.g. Von Mises) evaluated on element$j$ ($j = 1, 2, ..., N_e$). Solving this directly does not lead to a black/white solution because several numerical difficulties need to be addressed. In this section, a brief overview of these numerical difficulties is given, together with the different approaches to solve them.

4.5.1 Micro and Macro stress

In SIMP approach, $\rho = 1$ means that the material is present and the evaluated by what so-called *macro* stress it is the same as in equation (4.4) and it given by:

$$\underset{\sim}{\sigma}^{mac} = \rho^p \underset{\approx}{\mathrm{C}}^0 : \underset{\sim}{\varepsilon}. \tag{4.17}$$

However, the intermediates densities, in the literature, is often refereed to composite microstructure. The stress described in SIMP method (equation (4.17)) fails to predict the real stress in the microstructure and could lead to all void design (trivial solution) [185]. Lot of authors have proposed the so-called *micro stress* and it is based on a studied model of microstructure. Donders [77] used homogenisation method to optimise periodic lattice structure. In the optimisation process, she introduced the corrector tensors, obtained from a unit cell problem, to evaluate the micro stress. Duysinx et al. [65] provided a mathematical formulas to compute the micro stress for rank 2 composites, it is given by:

$$\underset{\sim}{\sigma}^{mic} = \frac{\rho^p}{\rho^q} \underset{\approx}{\mathrm{C}}^0 : \underset{\sim}{\varepsilon}, \tag{4.18}$$

where q is an exponent to be chosen. Due to its simplicity, it is widely used in several studies [159, 81]. Verbat et al. [186] mentioned 2 rules for a local stress, it should: (i) be inversely proportional to the density, (ii) converge to a finite stress as the density reaches zero. To respect the second rule, they set $p = q$. A difficulty arises for this definition and it is that the stress is non-zero when $\rho = 0$ which leads the algorithm to be unable to remove materials. The problem is known as *singular optima* and *relaxation* approaches are introduced to tackle the difficulty. The reader is invited to see section 4.5.3 for more details.

4.5.2 Vanishing constraints

The proposed problem in (4.16) belongs to a class called *mathematical program with vanishing constraints* (MPVC) [1]. This terminology comes form the fact that some constraints should not exist (or be considered) in some parts of the feasible domain. In our case, when $\rho = 0$ the constraints (g_j) should not exist because the material is not present. This is a problem because, numerically, when $\rho = 0$ the material is present and it is infinitely compliant. This means that the constraint will be evaluated in the whole design space Ω and consequently leading to numerical issues. To avoid the problem [51], the constraints g_j are modified and replaced by $\bar{g}$ as follows:

$$\bar{g}_j = \rho_j g_j = \rho_j \left(\frac{\sigma_j^{eq}}{\sigma_{lim}} - 1 \right) \quad \forall \underline{\mathrm{x}} \in \Omega \tag{4.19}$$

g_j is simply multiplied by ρ_j, so when $\rho = 0$, $\bar{g} = 0$ hence, the constraint vanishes. By doing so, it allows us to define the constraints in the whole design space Ω. Another approach is proposed by Giraldo-Londono et al. [80]. It is the *polynomial vanishing constraints* and it is given by:

$$\bar{g}_j = \rho_j^p g_j (g_j^2 + 1) \quad \forall \underline{\mathrm{x}} \in \Omega, \tag{4.20}$$

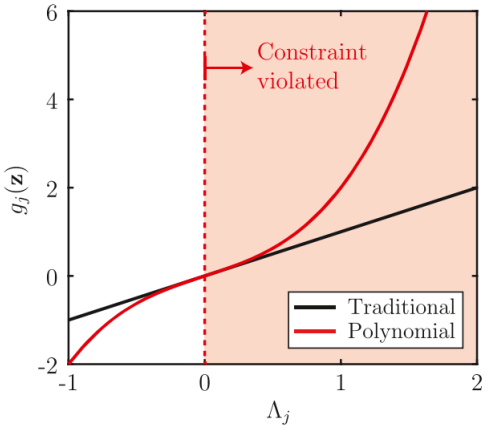

Figure 4.8: Comparison between the "traditional" (equation (4.19)) and "polynomial" (equation (4.20)) vanishing constraints [81].

where p is the SIMP exponent, it helps correlating the constraints to the density. $\bar{g}_j$ is a polynomial of degree 3 on g_j. Comparing to previous one in equation (4.19) (indicated traditional in figure 4.8), polynomial vanishing constraints conserve the limit and penalise the violation severely. The cubic polynomial adds more non-linearity to the constraints but it helps finding an optimal design at a faster pace.

Remark : It is important to point that "vanishing constraints" does not solve the problem of singular optima which is explained in the next section.

4.5.3 Singular optima

In a stress constrained topology optimisation, the singular optima defined by presence of the solution (optimal design) in a degenerate subspace in the feasible domain. It was observed by Cheng et al. [51] in truss structure optimisation. The best way to describe that is the two-bar truss example explained by Verbat et al. [186].

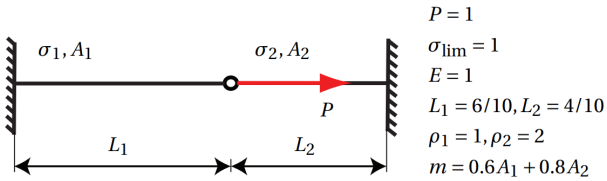

(a) The two-bar truss problem

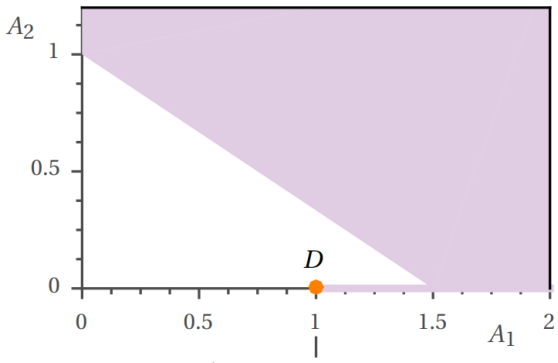

(b) Feasible domain

Figure 4.9: The two-bar truss example [186]

The point D in figure 4.9b is the solution to the truss problem, and it is situated in degenerate subspace ($\mathbb{R}$) of the feasible domain ($\mathbb{R}^2$). Therefore, with a gradient-based algorithm, it is not possible to reach the solution D. The only way to do so, is to pass through violated domain (where the constraints are not satisfied) therefore, the constraints need to be relaxed. Lot of *relaxation* approaches are found in the literature. Cheng et al. [50] proposed the ε-relaxation. It was first introduced truss optimisation and later then to topology optimisation [141]. Bruggi et al. proposed [38] the *qp*-relaxation. It is particular case of ε-relaxation and it is related to the defined micro stress in equation (4.18). It is mentioned in section 4.5.1 that in order to respect the rule regarding the micro stress, $q = p$ should be verified, it is what caused the singular optima problem. For the *qp*-relaxation, q is lower than p ($q < p$) where, generally, it is set $p - q = 0.5$ [81]. The reader is recommanded to read [185] for more details. Another approach called *aggregation* is used to reduce the number of constraints as well as playing a role (optionally) in the relaxation of constraints is details in next section.

4.5.4 Aggregation

In the problem (4.16), the constraints are local, it means that a constraint is present on each element (supposedly linear elements). In order calculate the gradient of the objective function FEM analysis has to be done for each constraint. This leads to high computational cost. One can look for the maximum stress but numerical instabilities could be encountered due to the fact that the max stress could change from one position to another. Moreover, the max function is not differentiable [161]. To reduce the number of constraints, aggregation approaches are proposed, they are widely used for stress constrained topology optimisation [55] and they are also used as a regularisation approach in some non-smooth optimisation problems [157, 48]. There is the *p-norm* [65], the *upper Kreisselmeier–Steinhauser* (KS) [109]. These functions are a smooth differentiable approximation of the max function. By applying to the local constraints, the resulting problem will have only one constraint and a gradient-based algorithm can be used to solve it. Both approaches have the similar effects and they can be combined with a relaxation approach.

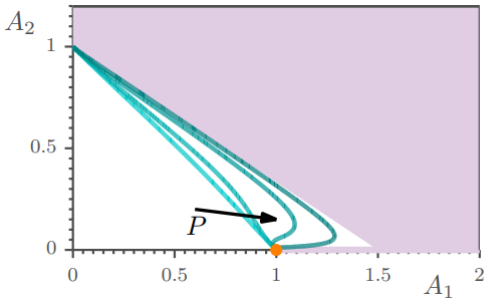

Figure 4.10: The boundaries of the relaxed feasible domain of the bar-truss problem with respect to a varying parameter [186].

A variant of p-norm and upper-KS function [186] called *p-mean* and *lower-KS* (respectively). They both represent a lower bound approximation of the max function and it is found out that they can play the double role of aggregation and relaxation. This means that, when using p-mean and lower-KS, relaxation is not needed. This is important because it reduces the number of parameters for the optimisation problem. It appears that the relaxation with p-mean and lower-KS is an particular adaptive case (to the number of elements) of ϵ-relaxation approach. The figure 4.10 shows the boundaries of relaxed feasible domain of the bar-truss problem using the Lower-KS function.

The aggregation proved to work very well using gradient based-method, however, the main disadvantage of the aggregation is that it underestimates the maximum stress field. This problem has been tackled using what so-called rectifier [133, 198]. It consists of multiplying the aggregation value by a term which is dependent on the ratio of the actual maximum and aggregated value. Another disadvantage regarding the aggregation, it is the disability to have control over the whole design space. It means that only the regions where the stress concentration occurs are taken into account.

It important to point out that it exist other alternative ways to reduce the number of constraints, one of them is the augmented Lagrangian [159, 81]. It has the properties of transforming a constrained problem into an unconstrained one. The computational cost is reduced because only one FEM analysis is required for all the constraints to calculate the gradient of the augmented Lagrangian (in each iteration). Bruggi proposed a strategy called *active stress constraints* where only the constraints that are violated or close to being violated are taken into account. This strategy works well with a coarse mesh however, with a refined mesh the number of constraint could still be important. A block aggregation strategy was attempted by Paris et al. [138] in order to have more control when using aggregation approach. The constraints number is reduced but they are highly non-linear (due to aggregation) which could lead to an important computational cost.

Concluding remarks

For our study, the chosen problem is the volume minimisation with aggregated strength constraints, the reason is that the aggregation can play a double role relaxation and reducing the number to constraints into one. Therefore, the number of parameters is reduced by picking ($p = q$) for the micro-stress. The lower KS-function will be used instead of the p-mean because of fact that the local constraints do not need be strictly positive hence, it can be applied directly (unlike the p-mean). The main disadvantage of using the aggregation that it gives a highly non-linear constraint which could slow down the convergence speed.

4.6 Including anisotropy

Considering anisotropic material opens the possibility to add more optimisation variables (additional to the topology) to the optimisation problem. In this section, a brief overview, on how different authors manage to do it, is given for several range applications. The additional parameters depend on the context of the application (composite laminate, 3D printing, ...). The main parameters, when an anisotropic material is considered, are mainly the orientation and the stiffness (elasticity) tensor. The section starts by considering a fixed anisotropy where the optimisation is only performed with respect to the topology. Then the orientation is added. Some numerical details need to be considered when optimising for topology and orientation. Lastly, the optimisation with respect to elasticity tensor (considering only elasticity problems), where a lot of strategies are found in the literature, is presented.

4.6.1 Fixed anisotropy

Fixed anisotropy means that an anisotropic material is considered in the elasticity problem and the optimisation problem is only performed with respect to the topology. The problem can solved in both SIMP and level-set

method. In terms of equations for any available algorithm, the only thing that changes is the form of the elasticity tensor and the obtained optimal design is dependent on the material orientation. The figure 4.11 shows the results of compliance minimisation for a cantilever elasticity problem [146], considering unidirectional carbon/epoxy composite material. It is noticed that 2 different results are obtained considering an orientation angle of 0° and 45° with respect to fixed reference frame.

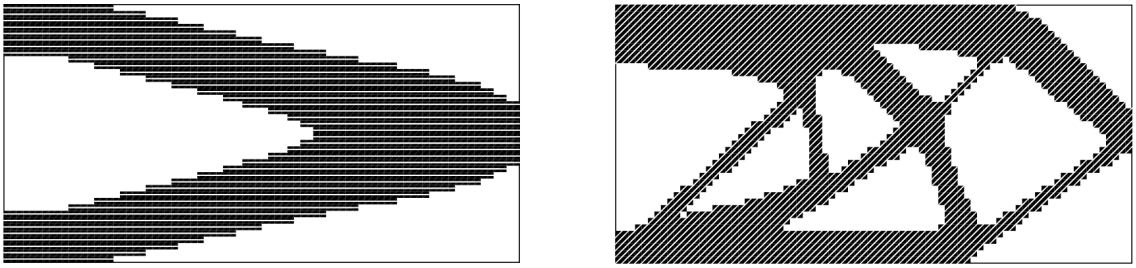

(a) 0° (b) 45°

Figure 4.11: Optimal design from compliance minimisation for cantilever elasticity problem with respect to material orientation[146].

It is important to mention that anisotropy can be exhibited by the mechanical strength. Indeed, a material can have an isotropic elasticity tensor with an anisotropic mechanical strength described by an anisotropic criterion. An example is given with equilateral triangular lattice [103] where its threshold function is approximated by TW4 in section **??**. Another example is found in an additive manufacturing (AM) application [128]. In order to manufacture a mechanical part, layer are deposited with 2 alternated orientations (45°/-45°), the effective stiffness is isotropic, however, because of AM flows, the mechanical strength is anisotropic.

The next sections gives some details on to get better performance from anisotropy by adding more optimisation variables.

4.6.2 Optimisation with respect to topology and orientation

In addition to the topology, orientation can be added as an optimisation variable when anisotropic material is considered. It is proven that it could allow drawing better performance. Concurrent topology and orientation optimisation is possible with both SIMP[3] and level-set method. For density based method, the orientation is a local variable in each element (like the density). One of early studies was done by Pederson et al. [140], they proved that he optimal orientation for an orthotropic material is the one of the principal direction of stress tensor field (or strain tensor field). This is valid only when in a single load case (it is not valid for multiple loads). Ranaivomiarana [146], used the polar parametrisation (see section 3.3.6) to establish the optimal orientation using optimality criteria conditions.It was found out that, in a case, the optimal material orientation in stiffness is aligned with the direction of the principal stress which has the greatest absolute value. And in another case, the optimal material orientation in stiffness is not aligned with the direction of the principal stress. Its value is the greatest absolute value of the principal stress added with a certain angle depending on the material properties and on the spherical and deviatoric part of the stress tensor. The main advantage of this approach relies on the practicality and simplicity for the numerical implementation and moreover, relies on the fact that it leads to a global optimum. Donders [77] used the same approach to optimise, with respect to the orientation, some lattice materials. With the same algorithm (optimality criteria) concurrent topology and orientation optimisation has been done for several applications [146, 151].

The optimisation with respect the orientation using gradient-based algorithm is also possible, Shen et al. [160] proved, in a simple manner, that it is possible to use gradient descent algorithm. One of the numerical issues is that there are a lot of local minima. Discontinuities are observed in the obtained optimal orientation field. Schmidt et al. [156] applied concurrent topology and orientation optimisation for composite fibers (also known as Continuous Fiber Angle Optimization CFAO) using MMA algorithm. In their paper, they explained how they addressed several numerical issues by using filters to tackle the discontinuities and by introducing a numerical strategy to avoid local minima in multiple loads case. An interesting approach is given by [117] for CFAO. In order to apply the concurrent topology and orientation optimisation, a vector parametrisation is used in which the magnitude indicates the presence of material and the direction (of the vector) represents the orientation. The advantage of this approach is that the number of local minima is reduced.

It is worth noting that level-set method can be used for concurrent topology and orientation optimisation. An interesting example is provided by Liu et al. [121]. In their study they point out that the level-set method is well suited for AM applications (e.g. for fused deposition modeling process) where the iso-value contours can gives the deposit path planning. From the iso-value contours the orientation of the material can be derived,

[3]SIMP stands for "simple isotropic material penalisation" but it can be applied to anisotropic material.

therefore, the optimisation with respect to the orientation is possible (together with the topology using shape derivative). Some numerical examples are available in the mentioned reference.

4.6.3 Optimisation with respect to topology and material anisotropy

In topology optimisation problem, the material anisotropy can considered as an additional variable to the topology. In other words, we are looking for an optimal distribution of materials and an optimal tensor elasticity field. Lot of strategies are proposed different studies. One of them is the Multi-scale Topology Optimisation (MTO) [194], it is described by 5 steps [113]: (1) a microstructural analysis (numerical homogenisation) is performed for each distinct microstructure to extract the equivalent elasticity tensor, (2) the elasticity tensors are then used to assemble a global stiffness matrix, (3) a macroscale analysis is carried out, (4) followed by sensitivity analysis, and (5) finally, the micro and macro design variables are updated, subject to various constraints. One of the main difficulties of this strategy is ensuring acceptable connection between the neighbouring microstructures and also reduce computational cost [113, 63]. Homogenisation approach seems to be very similar yet simpler. An example for lattice materials is provided [42] where the density variable ρ is considered as the relative density (see equation (1.50)) of the unit cell (microstructure), the orientation can be set as variable [5, 77], in the mentioned studies, a dis-homogenisation approach is proposed to address the connection issues however, it works only for a limited types of lattice.

Another strategy found in the literature is the Free Material Optimisation (FMO) [206]. In this approach, the optimisation variable is the elasticity tensor. The idea is to design the best material (its mechanical properties and distribution in space) for a given purpose. It should be physically attainable. The attainability requirements consist of the fact that elasticity tensor must be symmetric and positive definite [191]. Therefore, FMO problem belongs to a class of Semi Definite Programming (SDM) and it can be solved with an interior point algorithm [132] or the augmented Lagrangian. Additional constraints can be added such as rigidity and mechanical strength [86]. Lot of applications has been done. Hu et al. [97] combined FMO and dis-homogenisation to obtain optimised cellular structures. Weldeyesus et al. [191] used FMO to optimise laminated plates and shells. FMO has been also used to obtain the design of the ribs of the leading edge of the Airbus A380 [111].

Ranaivomiarana [146] managed to apply concurrent topology and orthotropy optimisation for composite laminates. She used the polar parameterisation of elasticity tensor and considered the anisotropic invariants as optimisation variables. She established optimality criteria to optimise with respect to both topology and orthotropy. It was found out that the obtained optimal materials were not feasible by composite laminates and feasibility constraint needed to be added. Vertonghen [187] continued the study and managed to impose the feasibility constraint using MMA algorithm. He also managed to add the mechanical strength constraints in the topology optimisation problem.

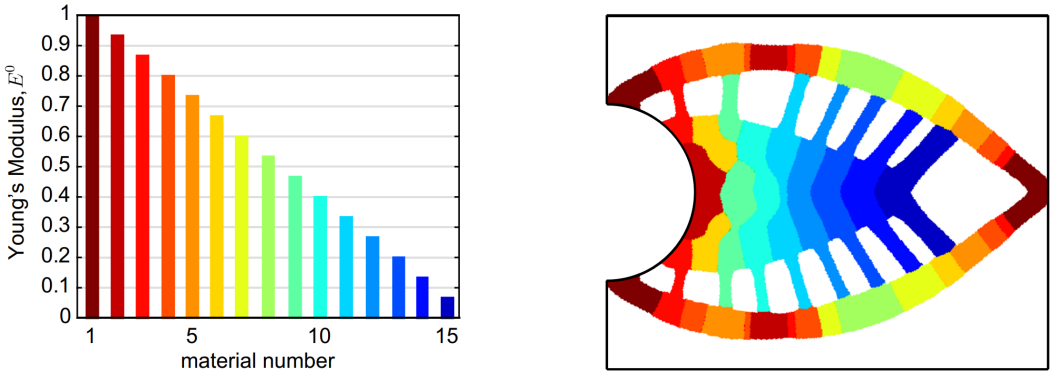

(a) 0° (b) 45°

Figure 4.12: (right) Optimal design of a structure considering multiple material phases. (left) the correspond Young's modulus for each phase (colour) [154].

Finally, it is possible to optimise a structure by taking into account 2 or multiple material phases in the final optimal design. An example is illustrated in figure 4.12. This is known as multi-material topological optimisation (MMTO). The concept is to introduce multiple densities $(\rho_1, \rho_2, ...)$ and use a linear combination of elasticity tensors. The equation (4.21) gives the example of interpolation of 3 phases [192]: void ($\rho_1 = 0$), material A ($\rho_1 = 1$ and $\rho_2 = 1$) and material B ($\rho_1 = 1$ and $\rho_2 = 0$)

$$\underset{\approx}{\mathrm{C}} = \rho_1^p \left[\rho_2^p \underset{\approx}{\mathrm{C}}^A + (1 - \rho_2^P)\, \underset{\approx}{\mathrm{C}}^B \right]. \tag{4.21}$$

The interpolation changes for high number of materials [175]. MMTO can be applied using isotropic or anisotropic materials or both [35]. A MMTO MatLab code "PolyMat" is provided by Sanders et al. [154] for

the interested reader. In the framework of MMTO, Direct material optimisation was proposed by Stegmann and Lund [175] for composite shell structures. It uses the MMTO to find the best ply orientation in a variable stiffness for a constant thickness laminate layup. This approach is extended to Discrete Material and Thickness Optimisation (DMTO) [180] where, in addition to the material distribution, the thickness of laminated composite is optimised.

Concluding remarks

For our study, for TW4, only one anisotropic threshold surface, for an example of lattice material (equilateral triangular lattice), is provided. So, only the orientation can be considered as an additional variable in the topology optimisation problem. SIMP method will be applied where the presence of the material will indicate the presence of lattice (in the microscopic scale). To apply homogenisation or the FMO (or MMTO) approach, several threshold surfaces are required for a given set of triangular lattice materials (a set of geometric parameters for the unit cell). Either way, the dishomogenisation approach must be applied to recover the optimal triangular lattice design obtained from the optimisation process.

4.7 Conclusion

This chapter provides a concise yet rich review about topology optimisation. At first, a general framework was given about the structural optimisation then the main methods to describe a topology of a structure (Density and Level-set) were presented. In the topology optimisation problem, a brief definition is given regarding three main aspects: (i) Mass, (ii) rigidity and (iii) mechanical strength. One of these aspects will be considered in the objective function and the others will be included as constraints. It is more convenient to pick the volume (or mass) as the objective function subjected mechanical strength constraints. This is because of the fact that the mechanical strength is always known (defined by a criterion). Additional constraints can be imposed such as the rigidity (stiffness or compliance). Because the SIMP method is chosen to solve the optimisation problem, an overview on different encountered numerical problems and on different solutions to tackle them, is given. For mechanical strength constraint, it appears that the aggregation is useful to transform the problem with N_e local constraints (N_e is the number of elements in FEM analysis) to a problem with only one constraint. Also, the aggregation can be used as a relaxation approach which allows obtaining the 0/1 optimal design. After reviewing most of resolution algorithms, the augmented Lagrangian is chosen because it is simple to implement. For pedagogical purposes, a classical gradient is used to minimise the augmented Lagrangian since it is not often used for stress based topology optimisation. To include anisotropy, the orientation (only) might be considered as an additional optimisation variable to topology, if needed. In the next chapter, a more detailed and explicit formulation to the optimisation problem is provided. Numerical examples will be discussed.

Chapter 5

Stress based topology optimisation

Contents

In the part 1, a 4th degree generalised polynomial threshold criterion (TW4) was proposed for architectured material where the harmonic decomposition showed its versatility. In section 3.5, TW4 proved to be capable of approximating the threshold surface established from studying the equilateral triangular 2D lattice [103] considering plasticity and buckling instabilities. Lattice materials are known to have very interesting properties such as good stiffness/weight ratio [142]. Optimising their properties is absolutely worth it and this can be done with the help topology optimisation tools. However, they have a particular mechanical behaviour where two mode ruins: plasticity (or brittleness) in tension and buckling in compression. Considering a local mechanical strength constraint is necessary. The objective of this chapter is to implement, as constraints, the approximated threshold surface for the triangular lattice (section 3.5.4) in a topology optimisation problem. Three aspects are focused on: mass, rigidity and mechanical strength. SIMP method will be used where the presence of material means the presence of lattice at the microscale level. The mentioned numerical difficulties presented section 4.5, will be detailed again in a more explicit manner. Additional to topology, the orientation could be considered an optimisation variable if is required.

The outline of chapter is as follows: the first section 5.2 , will explain, in a detailed manner, the augmented Lagrangian algorithm for a general constrained optimisation problem. In the next section 5.3, a full description of the optimisation problem that will solved with the augmented Lagrangian. It consist of a volume minimisation problems in which different constraints will be imposed in each case. More details, on how the numerical problems are dealt with, will be presented. The implementation of various threshold criteria, which are will be considered in the mechanical strength constraints, is provided. In section 5.4, the augmented Lagrangian (explained in section 5.2) is applied the proposed problems. A more explicit algorithm is provided. Finally, the section 5.5, will give and explain the different obtained results.

Remark: It important to point out, that it is possible to use homogenisation method (instead of SIMP). To do so, multiple threshold surfaces, for different geometric parameters of the unit cell, need to be established. For this case, multiple strategies can employed such as the multi scale topology optimisation (MTO) or concurrent topology and anisotropy optimisation. etc.

5.1 Elasticity problem and SIMP formulation

The physical model of all featured topology optimisation problems in this manuscript, is the linear elasticity. Let's consider Ω the structure domain with boundaries $\partial\Omega$ illustrated in figure 5.1. Γ_D denotes a part of boundaries where displacements are imposed (Dirichlet boundary conditions). Γ_N denotes free (no applied forces) boundaries and the boundaries where a line force is applied (a single load case). The volumic forces are not present. The linear elasticity equilibrium problem is given by:

$$\begin{cases} \underset{\sim}{\mathrm{div}}(\underset{\sim}{\sigma}(\underline{u})) = \underline{0} & \underline{x} \in \Omega, \\ \underset{\sim}{\sigma}(\underline{u}) = \underset{\approx}{C} : \underset{\sim}{\varepsilon}(\underline{u}) & \underline{x} \in \Omega, \\ \underset{\sim}{\varepsilon}(\underline{u}) = \dfrac{1}{2}(\underset{\sim}{\nabla}(\underline{u}) + \underset{\sim}{\nabla}(\underline{u})^T) & \underline{x} \in \Omega \\ \underset{\sim}{\sigma}(\underline{u})\cdot\underline{n} = \underline{t} & \underline{x} \in \Gamma_N \\ \underline{u} = \underline{0} & \underline{x} \in \Gamma_D \end{cases} \tag{5.1}$$

where $\underline{x}$ is the vector position, $\underline{u}$ is the displacement field, $\underset{\sim}{\varepsilon}(\underline{u})$ is the strain tensor, $\underline{t}$ is line force and $\underset{\sim}{\sigma}(\underline{u})$ is the cauchy stress tensor where, under plane stress assumption, it is given by:

$$[\underset{\sim}{\sigma}] = \begin{pmatrix} \sigma_{11} & \sigma_{12} \\ \sigma_{12} & \sigma_{22} \end{pmatrix} \tag{5.2}$$

The equation system (5.1) represents the equilibrium in its strong form. In order to apply finite element analysis, a weak form (or variational form) needs to be established. Let U_{ad} be the space of kinematically admissible space of displacement field $\underline{v}$ for the considered problem:

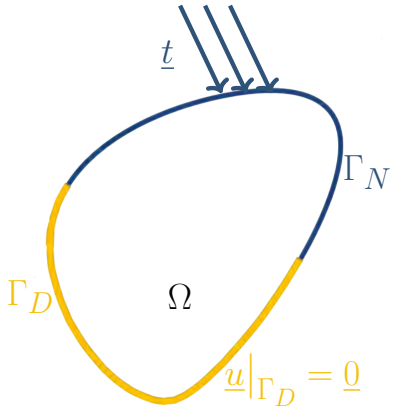

Figure 5.1: The structure Ω and its boundaries

$$U_{ad} = \{\underline{v} = (v_1, v_2); v_i \in H^1(\Omega); \underline{v} = \underline{0} \text{ on } \Gamma_D\} \tag{5.3}$$

The first equation in system (5.1) is picked, we multiply it by $\underline{v} \in U_{ad}$ and we integrate in all domain Ω:

$$\begin{aligned} \int_\Omega \underline{v}.\underset{\sim}{\mathrm{div}}(\underset{\sim}{\sigma})\ \mathrm{dv} &= -\int_\Omega \underset{\sim}{\varepsilon}(\underline{v}) : \underset{\sim}{\sigma}(\underline{u})\ \mathrm{dv} + \int_{\partial\Omega} \underline{v}\cdot(\underset{\sim}{\sigma}(\underline{u})\cdot\underline{n})\ \mathrm{ds} \\ &= -\int_\Omega \underset{\sim}{\sigma}(\underline{u}) : \underset{\sim}{\varepsilon}(\underline{v})\ \mathrm{dv} + \int_{\Gamma_N} \underline{t}\cdot\underline{v}\ \mathrm{ds}, \end{aligned} \tag{5.4}$$

The variational form of the equilibrium problem is:

$$a(\underline{u}, \underline{v}) = L(\underline{v}) \qquad \forall \underline{v} \in U_{ad}. \tag{5.5}$$

where

$$\begin{cases} a(\underline{u}, \underline{v}) = \displaystyle\int_\Omega \underset{\sim}{\varepsilon}(\underline{u}) : \underset{\approx}{C} : \underset{\sim}{\varepsilon}(\underline{v})\ \mathrm{dv} \\ L(\underline{v}) = \displaystyle\int_{\Gamma_N} \underline{v}\cdot\underline{t}\ \mathrm{ds} \end{cases} \tag{5.6}$$

For topology optimisation problem, SIMP method is used. A parameter denoted $\rho(\underline{x})$ is introduced in the weak form of equilibrium equations. It is introduced in the material elasticity tensor $\underset{\approx}{C}$ as follows:

$$\underset{\approx}{C} = \rho^p \underset{\approx}{C}^0 \tag{5.7}$$

where $\underset{\approx}{C}^0$ is the material elasticity tensor, p is the penalisation exponent generally set as $p = 3$. $\rho(\underline{x})$ indicates the presence and the absence of the material in Ω. When $\rho(\underline{x}) = 0$ there is void, when $\rho = 1$ there is material. p plays the important role of eliminating the intermediate densities ($\rho \in]0, 1[$) which, in our case, will not have a physical meaning. The weak form of equilibrium equation, in SIMP method, is introduced as follows:

$$a_\rho(\underline{u}, \underline{v}) = L(\underline{v}) \qquad \forall \underline{v} \in U_{ad}. \tag{5.8}$$

where

$$a_\rho(\underline{u}, \underline{v}) = \rho_\epsilon \int_\Omega \underset{\sim}{\varepsilon}(\underline{u}) : \underset{\approx}{C}^0 : \underset{\sim}{\varepsilon}(\underline{v}) \, \mathrm{dv}, \tag{5.9}$$

where

$$\rho_\epsilon = (\epsilon + (1 - \epsilon))\rho^p), \tag{5.10}$$

ϵ, generally set to 10^{-6}, is the Ersatz stiffness [159]. It is specifically added to equation (5.8) in order to avoid having a null elasticity tensor and have an unique solution. The equation (5.8) will be the physical model of the topology optimisation problem. The next section, treats a general topology optimisation problem in the framework of augmented Lagrangian.

5.2 General optimisation problem using augmented Lagrangian

All featured problems in this document will be solved with the augmented Lagrangian algorithm. It is worth to give a general framework by posing a general optimisation problem and by giving a general algorithm. Derivatives are needed for the gradient descent therefore, sensitivity analysis has to be established in order to be able to implement the algorithm. The following optimisation problem is proposed as follows:

$$\begin{cases} \min\limits_{\rho \in [0,1]} \mathcal{J}(\underline{u}, \rho) = \min\limits_{\rho \in [0,1]} \displaystyle\int_\Omega j(\underline{u}, \rho) \, \mathrm{dv}, \\ \underline{f}(\underline{u}, \rho) = 0, \\ \underline{h}(\underline{u}, \rho) \leq 0, \\ a_\rho(\underline{u}, \underline{v}) = L(\underline{v}) \qquad \forall \underline{v} \in U_{ad}, \end{cases} \tag{5.11}$$

where $\underline{f}(\underline{u}) \in \mathbb{R}^\zeta$ and $\underline{h}(\underline{u}) \in \mathbb{R}^\eta$ are continuos functions describing the $(\zeta + \eta)$ equality and inequality constraints respectively. $\mathcal{J}(\underline{u}, \rho)$ is the objective function. The inequality constraints are treated by introducing the so called *slack variables* included in $\underline{s} \in \mathbb{R}^\eta$. The problem (5.11) is equivalent to the one in (5.12):

$$\begin{cases} \min\limits_{\rho \in [0,1]} \mathcal{J}(\underline{u}, \rho) = \min\limits_{\rho \in [0,1]} \displaystyle\int_\Omega j(\underline{u}, \rho) \, \mathrm{dv}, \\ \underline{f}(\underline{u}, \rho) = 0, \\ \underline{h}_s(\underline{u}, \rho) = \underline{h}(\underline{u}) + \underline{s} = 0, \quad s_i \geq 0, \\ a_\rho(\underline{u}, \underline{v}) = L(\underline{v}) \qquad \forall \underline{v} \in U_{ad}, \end{cases} \tag{5.12}$$

The slack variables allow transforming the inequality constraints into equality ones. All the elements of $\underline{s}$ must be positive otherwise the inequality constraints are not verified. The augmented Lagrangian is introduced as follows:

$$\begin{aligned} \mathcal{L}(\underline{u}, \underline{q}, \rho, \underline{s}, \underline{\lambda}_f, \underline{\lambda}_h) = \mathcal{J}(\underline{u}, \rho) + \underline{q} \cdot \underline{\mathrm{div}}(\underset{\sim}{\sigma}(\underline{u})) \ldots \\ \cdots + \underline{\lambda}_f \cdot \underline{f}(\underline{u}, \rho) + \underline{\lambda}_h \cdot \underline{h}_s(\underline{u}, \rho) + \frac{\underline{b}_f}{2} \cdot (\underline{f}(\underline{u}, \rho) \circledast \underline{f}(\underline{u}, \rho)) + \frac{\underline{b}_h}{2} \cdot (\underline{h}_s(\underline{u}, \rho) \circledast \underline{h}_s(\underline{u}, \rho)), \\ = \mathcal{J}(\underline{u}, \rho) - \rho_\epsilon \int_\Omega \underset{\sim}{\varepsilon}(\underline{u}) : \underset{\approx}{C}^0 : \underset{\sim}{\varepsilon}(\underline{q}) \, \mathrm{dv} + \int_{\Gamma_N} \underline{t} \cdot \underline{q} \, \mathrm{ds} \ldots \\ \cdots + \underline{\lambda}_f \cdot \underline{f}(\underline{u}, \rho) + \underline{\lambda}_h \cdot \underline{h}_s(\underline{u}, \rho) + \frac{\underline{b}_f}{2} \cdot (\underline{f}(\underline{u}, \rho) \circledast \underline{f}(\underline{u}, \rho)) + \frac{\underline{b}_h}{2} \cdot (\underline{h}_s(\underline{u}, \rho) \circledast \underline{h}_s(\underline{u}, \rho)), \end{aligned} \tag{5.13}$$

where $\underline{\lambda}_f \in \mathbb{R}^\zeta$ and $\underline{\lambda}_h \in \mathbb{R}^\eta$ are Lagrange multipliers that enforce all the constraints. $\underline{b}_f \in \mathbb{R}^\zeta$ and $\underline{b}_h \in \mathbb{R}^\eta$ are penalisation coefficients, $\underline{q} \in U_{ad}$ is also a Lagrange multiplier that enforces the constraint that $\underline{u}$ is solution

of elasticity problem, $\circledast$ refers to the Hadamard product [34], which is the element-wise product between two vectors (or matrices), for example:

$$\begin{pmatrix} f_1 \\ f_2 \end{pmatrix} \circledast \begin{pmatrix} h_1 \\ h_2 \end{pmatrix} = \begin{pmatrix} f_1 h_1 \\ f_2 h_2 \end{pmatrix}. \tag{5.14}$$

The equivalent problem to (5.12) is:

$$\begin{cases} \max\limits_{\underline{\mathrm{q}}, \underline{\lambda}_f, \underline{\lambda}_h} \min\limits_{\rho, \underline{\mathrm{s}}} \mathcal{L}(\underline{\mathrm{u}}, \underline{\mathrm{q}}, \rho, \underline{\mathrm{s}}, \underline{\lambda}_f, \underline{\lambda}_h), \\ 0 \leq \rho \leq 1 \text{ and } \underline{\mathrm{s}} \geq 0, \end{cases} \tag{5.15}$$

by introducing the augmented Lagrangian the constrained problem (5.12) is transformed into the unconstrained problem (5.15) at the cost of having more variables (which are the Lagrange multipliers). The bounds constraints on ρ and $\underline{\mathrm{s}}$ can be taken into account by means of applying a projection into feasible domain space. It is important to point out, that minimising with respect to $\underline{\mathrm{s}}$ will affect only the inequality constraints by saturating them (i.e. bring them close to the limit of the inequality).

5.2.1 Sensitivity analysis

Solving the problem (5.11) consists of finding saddle point of the augmented Lagrangian in equation (5.15). This will require establishing the optimality criteria conditions (stationarity conditions [2]) which will be useful later for the implementation of the algorithm. Before anything and for the sake of clarification, it is worth giving some notions about *Differentiability* which play a key role to establish the sensitivity analysis of the problem (5.15).

Definition 5.2.1. *A function F, defined in the neighbourhood of $u \in V$ into $\mathbb{R}$, is differentiable in sense of Gateaux if for any direction $\hat{u} \in V$, the following limit exists:*

$$\langle F'(u), \hat{u} \rangle = \lim_{\delta \to 0^+} \frac{F(u + \delta \hat{u}) - F(u)}{\delta} = F'(u) \cdot \hat{u}, \tag{5.16}$$

Remarks:

- if $V = \mathbb{R}$ then $F'(u) = \dfrac{dF(u)}{du}$.
- if $V = \mathbb{R}^n$ then;

$$F'(u) = \underline{\nabla}(F(u)) = \begin{pmatrix} \dfrac{\partial F(u)}{\partial u_1} \\ \vdots \\ \dfrac{\partial F(u)}{\partial u_n} \end{pmatrix}.$$

The derivative in the sense of Gateaux is also know as *directional derivative* [205]. The main interest of introducing it, is that it allows establishing the sensitivity analysis in a simple and convenient way when the augmented Lagrangian (or the Lagrangian).

Calculating the derivatives of the objective function and the constraints with respect to the variables ρ and $\underline{\mathrm{u}}$, is needed. One can see that $\underline{\mathrm{u}}$ is indirectly dependent on ρ through the elasticity problem therefore, the derivatives are not established in a straightforward manner. The derivatives can be calculated [5] by using composition rule. It consists of calculating the directional derivative $\langle \mathcal{J}(\underline{\mathrm{u}}, \rho), \hat{\underline{\mathrm{u}}} \rangle$ and then $\langle \underline{\mathrm{u}}, \hat{\rho} \rangle$ where $\hat{\underline{\mathrm{u}}} \in U_{ad}$ and $\hat{\rho} \in [0, 1]$ are directions. It appeared that it is not practical because there is no direct expression for $\langle \underline{\mathrm{u}}, \hat{\rho} \rangle$ (calculating it is possible but very expensive because infinite number (or high) of directions needs to be explored).

Another way of calculating the derivative and it is by using *adjoint stat problem*. It consists of introducing $\underline{\mathrm{q}} \in U_{aq}$ solution of the adjoint problem in a way that it allows calculating the derivative of objective function with respect to ρ directly. The adjoint problem is established through the variational formulation (weak form) of the elasticity problem.

In a simple manner, the adjoint problem can be established using the Lagrangian (or the augmented Lagrangian). Indeed, it was proven [5, 2] that $\underline{\mathrm{q}}$ is actually the solution of the adjoint problem. As remind, it is also the Lagrange multiplier that enforces the fact that $\underline{\mathrm{u}}$ is the solution of the elasticity problem. Considering finding the saddle point of the following augmented Lagrangian in equation (5.13), the weak form of the elasticity adjoint problem is one of the optimality criteria conditions given by the following directional derivative:

$$\langle \frac{\partial \mathcal{L}(\underline{\mathrm{u}}, \underline{\mathrm{q}}, \rho, \underline{\lambda}_f, \underline{\lambda}_h)}{\partial \underline{\mathrm{u}}}, \hat{\underline{\mathrm{u}}} \rangle = 0, \qquad \forall \hat{\underline{\mathrm{u}}} \in U_{ad}, \tag{5.17}$$

where $\underline{\mathrm{q}} \in U_{ad}$ is determined by solving adjoint problem (5.17), $\underline{\hat{\mathrm{u}}} \in U_{ad}$ is the direction of derivative. It is important to point out that $\underline{\lambda}_f$, $\underline{\lambda}_f$, $\underline{\mathrm{b}}_f$ and $\underline{\mathrm{b}}_h$ are arbitrary chosen[1] at the first iteration. Their updating scheme is explained in section 5.2.2. The derivative of the augmented Lagrangian with respect to ρ is given as follows:

$$\langle \frac{d\mathcal{L}(\underline{\mathrm{u}},\underline{\mathrm{q}},\rho,\underline{\lambda}_f,\underline{\lambda}_h)}{d\rho},\hat{\rho}\rangle = \langle \frac{\partial\mathcal{L}(\underline{\mathrm{u}},\underline{\mathrm{q}},\rho,\underline{\lambda}_f,\underline{\lambda}_h)}{\partial\rho},\hat{\rho}\rangle + \cancelto{0}{\langle \frac{\partial\mathcal{L}(\underline{\mathrm{u}},\underline{\mathrm{q}},\rho,\underline{\lambda}_f,\underline{\lambda}_h)}{\partial\underline{\mathrm{u}}}, \frac{\partial\underline{\mathrm{u}}}{\partial\rho}(\hat{\rho})\rangle} + \cancelto{0}{\langle \frac{\partial\mathcal{L}(\underline{\mathrm{u}},\underline{\mathrm{q}},\rho,\underline{\lambda}_f,\underline{\lambda}_h)}{\partial\underline{\mathrm{q}}}, \frac{\partial\underline{\mathrm{q}}}{\partial\rho}(\hat{\rho})\rangle}, \tag{5.18}$$

one can observe that the second term and the third term will lead to the weak form of the adjoint and elasticity problem respectively. If we consider that fact that $\underline{\mathrm{q}}$ is the solution of the adjoint problem and $\underline{\mathrm{u}}$ is solution of the elasticity problem then the second and third term are null. Hence, the conclusion is that:

$$\langle \frac{d\mathcal{L}(\underline{\mathrm{u}},\underline{\mathrm{q}},\rho,\underline{\lambda}_f,\underline{\lambda}_h)}{d\rho},\hat{\rho}\rangle = \langle \frac{\partial\mathcal{L}(\underline{\mathrm{u}},\underline{\mathrm{q}},\rho,\underline{\lambda}_f,\underline{\lambda}_h)}{\partial\rho},\hat{\rho}\rangle, \tag{5.19}$$

The equation (5.19) means that total derivative of the augmented Lagrangian is simply its derivative considering $\underline{\mathrm{u}}$ and $\underline{\mathrm{q}}$ constant. This is only true when $\underline{\mathrm{u}}$ and $\underline{\mathrm{q}}$ are solutions to (5.8) and (5.17).

Lastly, when using the augmented Lagrangian, the sensitivity analysis consists of establishing the adjoint problem and calculating the derivative with respect to ρ. For our general problem (5.15), the adjoint problem is as follows:

$$\begin{aligned}\int_\Omega \rho_\epsilon \underset{\sim}{\varepsilon}(\underline{\mathrm{q}}) : \underset{\approx}{\mathrm{C}}^0 : \underset{\sim}{\varepsilon}(\underline{\hat{\mathrm{u}}})\ \mathrm{dv} = &\int_\Omega \frac{\partial j(\underline{\mathrm{u}},\rho)}{\partial\underline{\mathrm{u}}}\cdot\underline{\hat{\mathrm{u}}}\ \mathrm{dv} + (\underline{\lambda}_f + \underline{\mathrm{b}}_f \circledast \underline{\mathrm{f}}(\underline{\mathrm{u}},\rho))\cdot(\frac{\partial\underline{\mathrm{f}}(\underline{\mathrm{u}},\rho)}{\partial\underline{\mathrm{u}}}\cdot\underline{\hat{\mathrm{u}}}) \\ &+ (\underline{\lambda}_h + \underline{\mathrm{b}}_h \circledast \underline{\mathrm{h}}_s(\underline{\mathrm{u}},\rho))\cdot(\frac{\partial\underline{\mathrm{h}}_s(\underline{\mathrm{u}},\rho)}{\partial\underline{\mathrm{u}}}\cdot\underline{\hat{\mathrm{u}}})\end{aligned} \qquad \forall\underline{\hat{\mathrm{u}}} \in U_{ad}, \tag{5.20}$$

The derivative with respect to ρ is given by:

$$\begin{aligned}\langle \frac{\partial\mathcal{L}(\underline{\mathrm{u}},\underline{\mathrm{q}},\rho,\underline{\lambda}_f,\underline{\lambda}_h)}{\partial\rho},\hat{\rho}\rangle = &\int_\Omega \frac{\partial j(\underline{\mathrm{u}},\rho)}{\partial\rho}\hat{\rho}\ \mathrm{dv} - (1-\epsilon)p\int_\Omega \rho^{p-1}\underset{\sim}{\varepsilon}(\underline{\mathrm{u}}) : \underset{\approx}{\mathrm{C}}^0 : \underset{\sim}{\varepsilon}(\underline{\mathrm{q}})\hat{\rho}\ \mathrm{dv} \\ &+ (\underline{\lambda}_f + \underline{\mathrm{b}}_f \circledast \underline{\mathrm{f}}(\underline{\mathrm{u}},\rho))\cdot\frac{\partial\underline{\mathrm{f}}(\underline{\mathrm{u}},\rho)}{\partial\rho}\hat{\rho} + (\underline{\lambda}_h + \underline{\mathrm{b}}_h \circledast \underline{\mathrm{h}}_s(\underline{\mathrm{u}},\rho))\cdot\frac{\partial\underline{\mathrm{h}}_s(\underline{\mathrm{u}},\rho)}{\partial\rho}\hat{\rho},\end{aligned} \tag{5.21}$$

the derivative (5.21) will be used to minimise the augmented Lagrangian.

Remarks:

- It is important to point out that $\underline{\lambda}_f$, $\underline{\lambda}_h$, $\underline{\mathrm{b}}_f$, $\underline{\mathrm{b}}_h$ are not yet determined. Their updating scheme is detailed in the next section.
- If $(\underline{\mathrm{u}}^*,\underline{\mathrm{q}}^*,\underline{\lambda}_f^*,\underline{\lambda}_h^*)$ correspond to a case where all the constraints are verified one can see that:

$$\langle \frac{\partial\mathcal{L}(\underline{\mathrm{u}}^*,\underline{\mathrm{q}}^*,\rho,\underline{\lambda}_f^*,\underline{\lambda}_h^*)}{\partial\rho},\hat{\rho}\rangle = \langle \frac{\partial\mathcal{J}(\underline{\mathrm{u}}^*,\rho)}{\partial\rho},\hat{\rho}\rangle,$$

  which means that if the values $\underline{\lambda}_f^*, \underline{\lambda}_h^*$ are found, the minimisation of the augmented Lagrangian is the minimisation of the objective function.
- In a case where the orientation denoted θ (for example) is considered as additional variable to ρ in the optimisation problem, the derivative of the augmented Lagrangian with respect to θ, given below, will be calculated in the same way as with respect ρ:

$$\langle \frac{d\mathcal{L}(\underline{\mathrm{u}},\underline{\mathrm{q}},\rho,\theta,\underline{\lambda}_f,\underline{\lambda}_h)}{d\theta},\hat{\theta}\rangle = \langle \frac{\partial\mathcal{L}(\underline{\mathrm{u}},\underline{\mathrm{q}},\rho,\theta,\underline{\lambda}_f,\underline{\lambda}_h)}{\partial\theta},\hat{\theta}\rangle, \tag{5.22}$$

  hence:

$$\begin{aligned}\langle \frac{\partial\mathcal{L}(\underline{\mathrm{u}},\underline{\mathrm{q}},\rho,\theta,\underline{\lambda}_f,\underline{\lambda}_h)}{\partial\theta},\hat{\theta}\rangle = &\int_\Omega \frac{\partial j(\underline{\mathrm{u}},\rho,\theta)}{\partial\theta}\hat{\theta}\ \mathrm{dv} + \int_\Omega \rho_\epsilon \underset{\sim}{\varepsilon}(\underline{\mathrm{u}}) : \frac{\partial\underset{\approx}{\mathrm{C}}^0}{\partial\theta} : \underset{\sim}{\varepsilon}(\underline{\mathrm{q}})\hat{\theta}\ \mathrm{dv} \\ &+ (\underline{\lambda}_f + \underline{\mathrm{b}}_f \circledast \underline{\mathrm{f}}(\underline{\mathrm{u}},\rho,\theta))\cdot\frac{\partial\underline{\mathrm{f}}(\underline{\mathrm{u}},\rho,\theta)}{\partial\theta}\hat{\theta} + (\underline{\lambda}_h + \underline{\mathrm{b}}_h \circledast \underline{\mathrm{h}}_s(\underline{\mathrm{u}},\rho,\theta))\cdot\frac{\partial\underline{\mathrm{h}}_s(\underline{\mathrm{u}},\rho,\theta)}{\partial\rho}\hat{\theta},\end{aligned} \tag{5.23}$$

[1] the choice can influence the convergence

5.2.2 Augmented Lagrangian algorithm

The purpose of the algorithm is to find the saddle point which is supposed to correspond to $(\underline{u}^*, \underline{q}^*, \rho^*, \underline{\lambda}_f^*, \underline{\lambda}_h^*)$. It is shown in the section 5.2.1 shows that $\underline{u}^*, \underline{q}^*$ are respectively the solutions to the adjoint and the elasticity problem. What remains is to give the updating scheme of $\underline{\lambda}_f$ and $\underline{\lambda}_h$. The concept of augmented Lagrangian resides on two main steps:

1. For $\underline{\lambda}_f, \underline{\lambda}_h, \underline{b}_f, \underline{b}_h$ fixed, A minimisation of the augmented Lagrangian with respect to ρ and $\underline{s}$ is applied (e.g. using gradient, MMA, ...).
2. For $\underline{u}, \underline{q}$ fixed, a maximisation with respect to $\underline{\lambda}_f$ and $\underline{\lambda}_h$ is applied.

At an iteration n, the density, slack variables, displacement and the Lagrange multipliers are denoted $(\rho^n, \underline{s}^n, \underline{u}^n, \underline{q}^n, \underline{\lambda}_f^n, \underline{\lambda}_h^n)$. $\underline{u}^n$ and $\underline{q}^n$ are determined by solving the the elasticity and the adjoint problem considering ρ^n.

• The minimisation with respect to ρ is done with the projected gradient (it is projected because of bound constraints). From directional derivative (5.21), the direction $\hat{\rho}$ that minimise the augmented Lagrangian is given as follows:

$$\begin{aligned}\hat{\rho} = -\Bigg[&\frac{\partial j(\underline{u},\rho)}{\partial \rho} - (1-\epsilon)p\rho^{p-1}\underset{\sim}{\varepsilon}(\underline{u}) : \underset{\approx}{\mathrm{C}^0} : \underset{\sim}{\varepsilon}(\underline{q}) + (\underline{\lambda}_f + \underline{b}_f \circledast \underline{\mathrm{f}}(\underline{u})) \cdot \frac{\partial \underline{\mathrm{f}}(\underline{u},\rho)}{\partial \rho} \\ &+ (\underline{\lambda}_h + \underline{b}_h \circledast \underline{\mathrm{h}}_s(\underline{u})) \cdot \frac{\partial \underline{\mathrm{h}}_s(\underline{u},\rho)}{\partial \theta}\Bigg]\end{aligned} \tag{5.24}$$

Hence the updating of ρ^n is given as follows:

$$\rho^{n+1} = \max(0, \min(\rho^n + \tau\hat{\rho}^n, 1)) \tag{5.25}$$

where $\tau > 0$ is the step which is chosen sufficiently small to assure the convergence. Using max/min ρ is projected[2] in $[0, 1]$ to take into account the bounds constraints.

• The value of $\underline{s}^n$ that minimise the augmented Lagrangian is given explicitly [159] as follows:

$$\underline{s}^n = \max\left[\underline{0}, -(\underline{\lambda}_h^n \oslash \underline{b}_h + \underline{\mathrm{h}}(\underline{u}^n, \rho^n))\right], \tag{5.26}$$

where $\oslash$ is the Hadamart division [34] which is the element-wise division , for example:

$$\begin{pmatrix} f_1 \\ f_2 \end{pmatrix} \oslash \begin{pmatrix} h_1 \\ h_2 \end{pmatrix} = \begin{pmatrix} f_1/h_1 \\ f_2/h_2 \end{pmatrix}. \tag{5.27}$$

It is important to keep in mind that minimise with respect to $\underline{s}$ means saturating the inequality constraints. Same as for ρ, the max function is used here to take into account the bounds constraints $s_i \geq 0$.

• Speaking of $\underline{\lambda}_f^n, \underline{\lambda}_h^n$, it is proved from the optimality conditions from both the augmented Lagrangian and the Lagrangian (the basic one) [3, 132] that:

$$\begin{cases} \underline{\lambda}_f^* = \underline{\lambda}_f^n + \underline{b}_f \circledast \underline{\mathrm{f}}(\underline{u}^n, \rho^n), \\ \underline{\lambda}_h^* = \underline{\lambda}_h^n + \underline{b}_h \circledast \underline{\mathrm{h}}_s(\underline{u}^n, \rho^n), \end{cases} \tag{5.28}$$

where $\underline{\lambda}_f^*$ and $\underline{\lambda}_h^*$ are the optimal Lagrangian multipliers (which correspond to the saddle point). The equation (5.28) give us two important information [3]:

1. The values of the $\underline{b}_f$ and $\underline{b}_h$ do not need to be very important (have very high value) to enforce the constraints.
2. The updating of scheme of $\underline{\lambda}_f^n$ and $\underline{\lambda}_h^n$ is given as follows:

$$\begin{aligned} \underline{\lambda}_f &= \underline{\lambda}_f^n + \underline{b}_f \circledast \underline{\mathrm{f}}(\underline{u}^n, \rho^n), \\ \underline{\lambda}_h &= \underline{\lambda}_h^n + \underline{b}_h \circledast \underline{\mathrm{h}}_s(\underline{u}^n, \rho^n), \end{aligned} \tag{5.29}$$

[2] The reason why it is called projected gradient.

• Depending on convergence, the penalisation coefficients $\underline{b}_f$ and $\underline{b}_h$ require neither a very high nor a very low value. In an attempt to have better convergence [132], *only for the violated constraints*, the values $\underline{b}_f$ and $\underline{b}_h$ gradually increase as the iterations go on in the following way:

$$\begin{aligned} b_{f_i}^{n+1} &= \min(b_{max}, \alpha b_{f_i}^n) \text{ if } f_i \neq 0 \ \forall i \in \{1, 2, ..., \zeta\}, \\ b_{h_j}^{n+1} &= \min(b_{max}, \alpha b_{h_j}^n) \text{ if } (h_j + s_j) \geq 0 \ \forall j \in \{1, 2, ..., \eta\}, \end{aligned} \tag{5.30}$$

where $\alpha > 1$ is chosen close to 1 (generally $\alpha = 1.1$), b_{max} is maximum value that penalisation coefficient can take. One should note that if the value b_{max} is very high, convergence problems could occur.

At iteration 0, the initial values $\rho^0, \underline{\lambda}_f^0, \underline{\lambda}_h^0, \underline{b}_f^0, \underline{b}_h^0$ must be set. Also the values of τ, α, b_{max} has to be set. To solve problem (5.11) (equivalent to (5.15)), the algorithm 1 is used. It stops when the number of iteration has reached a chosen max.

Regularisation filter

When using the density method, the penalisation causes the so-called *Checkerboards* problem (see figure 5.2). To tackle the problem, regularisation filters [163] are used. The one that it is applied for the all presented optimisation problems in this document, is based on the Helmholtz equation [115] as follows:

$$\begin{cases} -R^2 \Delta(\rho_f) + \rho_f = \rho & \Omega \\ \dfrac{\partial \rho_f}{\partial \underline{n}} = 0 & \partial\Omega \end{cases} \tag{5.31}$$

where R is the radius of the filter. By solving the equation, the obtained ρ_f has smooth and regularised distribution of ρ over Ω. In algorithm 1 the regularisation filter with radius R is defined by $\mathcal{F}_R$. It is worth noting that the same filter is also used for the orientation field [117] (of the material) to avoid discontinuities.

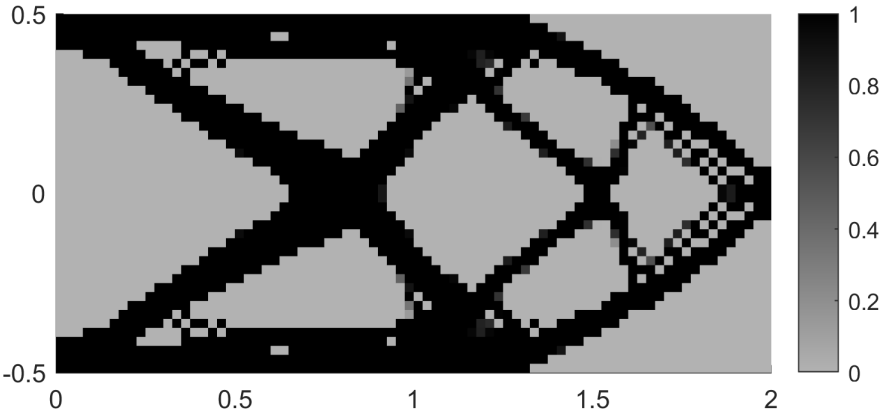

Figure 5.2: Checkers boards issue in the optimal distribution of an isotropic material for cantilever beam (compliance minimisation subjected to volume constraints).

Algorithm 1 Augmented Lagrangian algorithm: general optimisation problem

1. Define the algorithm parameters $iter_{max}, \tau, \alpha, R,$.
2. Initialise the field $\rho(\underline{x})$ and the value of $p, \underline{\lambda}_f, \underline{\lambda}_h, \underline{b}_f, \underline{b}_h, \epsilon$.
3. Precomputations:
   $\underline{u} \leftarrow$ Ela_FE(ρ) % Elasticity problem, equation (5.8)
   $\underline{s} \leftarrow \max[\underline{0}, -(\underline{\lambda}_h \oslash \underline{b}_h + \underline{h}(\underline{u}, \rho))]$
4. For j=1 to $iter_{max}$:
   | $\underline{q} \leftarrow$ Adj_FE($\underline{u}, \rho, \underline{\lambda}_f, \underline{\lambda}_h, , \underline{b}_f, \underline{b}_h$) % Adjoint elasticity problem, equation (5.20)
   | $\hat{\rho} \leftarrow -\left[\frac{\partial j(\underline{u},\rho)}{\partial \rho} - (1-\epsilon)p\rho^{p-1}\underset{\sim}{\varepsilon}(\underline{u}) : \underset{\approx}{C}^0 : \underset{\sim}{\varepsilon}(\underline{q}) + (\underline{\lambda}_f + \underline{b}_f \circledast \underline{f}(\underline{u})) \cdot \frac{\partial \underline{f}(\underline{u},\rho)}{\partial \rho} + (\underline{\lambda}_h + \underline{b}_h \circledast \underline{h}_s(\underline{u})) \cdot \frac{\partial \underline{h}_s(\underline{u},\rho)}{\partial \rho}\right]$
   | $\bar{\rho} \leftarrow \max(\min(\rho + \tau \frac{\mathcal{F}_R(\hat{\rho})}{\max(|\mathcal{F}_R(\hat{\rho})|)}, 1), 0)$
   | $\underline{u} \leftarrow$ Ela_FE($\bar{\rho}$)
   | $\underline{s} \leftarrow \max[\underline{0}, -(\underline{\lambda}_h \oslash \underline{b}_h + \underline{h}(\underline{u}, \bar{\rho}))]$
   | $\underline{\lambda}_f \leftarrow \underline{\lambda}_f + \underline{b}_f \circledast \underline{f}(\underline{u}, \bar{\rho})$
   | $\underline{\lambda}_h \leftarrow \underline{\lambda}_h + \underline{b}_h \circledast \underline{h}_s(\underline{u}, \bar{\rho})$
   | for $i = 1$ to ζ: % ζ is the number of equality constraints
   | | If $| f_i(\underline{u}, \bar{\rho})| \leq 10^{-3}$
   | | | $b_{f_i} = \min(b_{max}, \alpha b_{f_i}^n)$
   | for $i = 1$ to η: % η is the number of inequality constraints
   | | If $h_i(\underline{u}, \bar{\rho}) \geq 0$
   | | | $b_{h_i} = \min(b_{max}, \alpha b_{h_i})$

5.3 Mass minimisation subjected to compliance and mechanical strength constraints

It is mentioned in chapter 4 that it is more convenient to treat a volume minimisation for topology optimisation problem. This is because of the fact that the mechanical strength limit is known by the definition of the associated criterion. Compliance constraints also will be added because the mechanical strength does not guarantee the rigidity if it is required. For the volume minimisation problem, 3 cases are treated:

1. *Problem 1*: volume minimisation with compliance constraint.
2. *Problem 2*: volume minimisation with mechanical strength constraints.
3. *Problem 3*: volume minimisation with both compliance and mechanical strength constraints.

To avoid redundancy, only the resolution algorithm for the problem 3 will be provided. The problem 1 and 2 are particular cases of of problem 3. Therefore, their resolution algorithm can directly deduced by applying simple simplification (make a coefficient null). Speaking of mechanical strength constraints, in order to reduce the number of mechanical strength, an aggregation function will be used. All details about measuring stress and the aggregation will be provided. When it comes to the anisotropy, it can be included by considering anisotropic material or considering anisotropic criteria (or both). The orientation of the material (with respect to fixed reference) can be considered an additional optimisation variable.

All the points mentioned above will be covered in this section.

5.3.1 Optimisation problem

The volume minimisation problem is considered as follows:

$$\begin{cases} \min\limits_{\rho\in[0,1]} \displaystyle\int_\Omega \rho \ \mathrm{dv}, \\ \beta g = \beta \left(\dfrac{\sigma_{eq}}{\sigma_{lim}} - 1 \right) \leq 0 \ \forall \ \underline{\mathrm{x}} \in \Omega_{mat} := \{\underline{\mathrm{x}} \in \Omega, \rho \neq 0\}, \\ \dfrac{\gamma}{\mathcal{C}_0} (\displaystyle\int_{\Gamma_N} \underline{\mathrm{u}} \cdot \underline{\mathrm{t}} \ \mathrm{ds} - 1) \ \mathrm{ds} \leq 0, \\ a_\rho(\underline{\mathrm{u}}, \underline{\mathrm{v}}) = L(\underline{\mathrm{v}}) \quad \forall \ \underline{\mathrm{v}} \in U_{ad}, \end{cases} \tag{$\mathbb{P}$}$$

where ρ is the density, $\underline{\mathrm{u}}$ is the displacement vector, $\underline{\mathrm{t}}$ is applied line force on part of Γ_N (details are in section 5.1). $\mathcal{C}_0$ is the imposed compliance value. σ_{eq} is the equivalent stress associated to a threshold criterion defined by the equation $\frac{F(\underset{\sim}{\sigma})}{\sigma_{lim}} = 1$. σ_{eq} could be a safety factor in a case where the threshold function cannot be implemented directly (more details in section 5.3.2). β and γ are simplification coefficients where the following three particular cases are found:

$$\begin{cases} \min\limits_{\rho\in[0,1]} \displaystyle\int_\Omega \rho \ \mathrm{dv}, \\ \dfrac{\gamma}{\mathcal{C}_0} (\displaystyle\int_{\Gamma_N} \underline{\mathrm{u}} \cdot \underline{\mathrm{t}} \ \mathrm{ds} - 1) \ \mathrm{ds} \leq 0, \\ a_\rho(\underline{\mathrm{u}}, \underline{\mathrm{v}}) = L(\underline{\mathrm{v}}) \quad \forall \ \underline{\mathrm{v}} \in U_{ad}, \end{cases} \tag{$\mathbb{P}_1$}$$

Problem 1: volume minimisation with compliance constraints ($\beta = 0, \gamma = 1$).

$$\begin{cases} \min\limits_{\rho\in[0,1]} \displaystyle\int_\Omega \rho \ \mathrm{dv}, \\ g = \left(\dfrac{\sigma_{eq}}{\sigma_{lim}} - 1 \right) \leq 1 \ \forall \ \underline{\mathrm{x}} \in \Omega_{mat}, \\ a_\rho(\underline{\mathrm{u}}, \underline{\mathrm{v}}) = L(\underline{\mathrm{v}}) \quad \forall \ \underline{\mathrm{v}} \in U_{ad}, \end{cases} \tag{$\mathbb{P}_2$}$$

Problem 2: volume minimisation with mechanical strength constraints($\beta = 1, \gamma = 0$).

$$\begin{cases} \min\limits_{\rho\in[0,1]} \displaystyle\int_\Omega \rho \ \mathrm{dv}, \\ g = \left(\dfrac{\sigma_{eq}}{\sigma_{lim}} - 1 \right) \leq 1 \ \forall \ \underline{\mathrm{x}} \in \Omega_{mat}, \\ \dfrac{1}{\mathcal{C}_0} (\displaystyle\int_{\Gamma_N} \underline{\mathrm{u}} \cdot \underline{\mathrm{t}} \ \mathrm{ds} - 1) \ \mathrm{ds} \leq 0, \\ a_\rho(\underline{\mathrm{u}}, \underline{\mathrm{v}}) = L(\underline{\mathrm{v}}) \quad \forall \ \underline{\mathrm{v}} \in U_{ad}, \end{cases} \tag{$\mathbb{P}_3$}$$

Problem 3: volume minimisation with both compliance and mechanical strength constraints($\beta = 1, \gamma = 1$).

Using augmented Lagrangian, solving the problems ($\mathbb{P}_1$), ($\mathbb{P}_2$) and ($\mathbb{P}_3$) is equivalent to solving ($\mathbb{P}$) considering $\{\beta, \gamma\} \in \{\{0,1\},\{1,0\},\{1,1\}\}$. It is important to point out that the problem, at this form, cannot be solved because of several numerical issues concerning the evaluation of the mechanical strength constraints (see section 4.5 for more details). In problem ($\mathbb{P}$), the mechanical strength defined by g, will have modifications, the process is detailed in the next subsection.

5.3.2 The evaluation of mechanical strength constraints

In problem ($\mathbb{P}$), the mechanical strength constraints are defined by g as follows:

$$g = \left(\frac{\sigma_{eq}}{\sigma_{lim}} - 1 \right) \leq 0 \ \forall \ \underline{\mathrm{x}} \in \Omega_{mat} := \{\underline{\mathrm{x}} \in \Omega, \rho \neq 0\}, \tag{5.32}$$

To overcome numerical difficulties, 3 major aspects need to be treated:

- Vanishing constraints.
- Measuring the stress.
- Aggregation.

Vanishing constraints

Starting by the first one, the problem ($\mathbb{P}$) is considered of class MPVC [1]. The reason is due to the fact that g can only be evaluated the presence of the material (Ω_{mat}). In order the be able to evaluate the constraint in whole domain (Ω), g is multiplied by ρ, therefore the constraints is defined by $\bar{g}$:

$$\bar{g} = \rho g = \rho \left(\frac{\sigma_{eq}}{\sigma_{lim}} - 1 \right), \tag{5.33}$$

by multiplying by ρ the constraint g will vanish when the material is absent $\rho = 0$.

Measuring the stress

When using SIMP method intermediate densities will appear along the iterations and it corresponds to a composite material (microstructure). When measuring the stress tensor, it is important to distinguish between the so-called macro-stress and micro-stress tensor. The reason is that the macro-stress (same as in equation (5.7)) given by:

$$\underset{\sim}{\sigma}^{mac} = \rho^p \underset{\approx}{\mathrm{C}}^0 : \underset{\sim}{\varepsilon}, \tag{5.34}$$

fails to predict the real stress in the microstructure and could lead to all void design (trivial solution) [185]. Therefore, for intermediate densities, the micro-stress is introduced where a simple mathematical formulas is provided [64] for rank 2 composite materials and will be used to compute $\bar{g}$, it is given by:

$$\underset{\sim}{\sigma}^{mic} = \frac{\rho^p}{\rho^q} \underset{\approx}{\mathrm{C}}^0 : \underset{\sim}{\varepsilon}, \tag{5.35}$$

where q is an exponent to be chosen. Verbat et al. [186] mentioned 2 rules for a local stress: (i) it should be inversely proportional to the density, (ii) converges to a finite stress as the density reaches zero. To respect the second rule, we choose $p = q$.

Aggregation

Choosing $p = q$ when evaluating mechanical strength constraints leads to so-called singular optima described in section 4.5.3. To overcome the problem a relaxation approach is applied. For the problem ($\mathbb{P}$), aggregation over Ω is applied on the constraint $\bar{g}$ by using the Lower-KS function:

$$\Psi^L_{KS}(\bar{g}) = \frac{1}{\mu} \ln\left(\frac{1}{V_\Omega} \int_\Omega \exp(\mu \bar{g}) \, \mathrm{dv}\right) \tag{5.36}$$

where μ is a parameter. The Lower-KS function is a conservative (lower) approximation of the max function, it has the following property:

$$\lim_{\mu \to \infty} \Psi^L_{KS}(\bar{g}) = \max_\Omega(\bar{g}) \tag{5.37}$$

The figure 5.3 shows an example where the max of 3 functions (in black) is approximated with the lower-KS. The greater μ the better the accuracy.

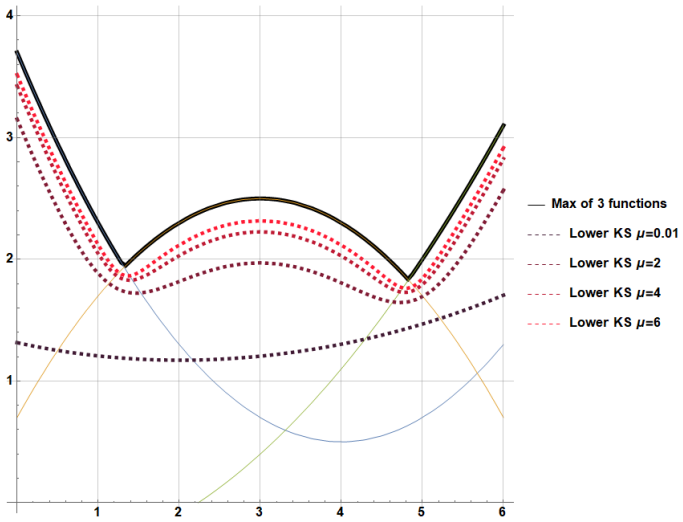

Figure 5.3: The max of 3 functions (in black) is approximated using the lower-KS function.

It is important to point out that $\bar{g}$ designs local constraints[3]. The aggregation has the double role of reducing the number of constraints to 1 and of relaxation (see section 4.5.4). However, the constraint becomes highly non-linear which leads to a convergence problems (slow and unstable convergence).

[3]numerically, it means that it has to be considered for each element (FEM analysis)

Considering all numerical difficulties, the mechanical constraints in problem ($\mathbb{P}$), will replaced by $\Psi^L_{KS}(\bar{g})$ given by equation (5.36). The resolution algorithm is explicitly provided in section (5.4). The following derivatives are useful for the sensitivity analysis:

$$\frac{\partial \Psi^L_{KS}(\bar{g})}{\partial \underset{\sim}{\sigma}} = \frac{\displaystyle\int_\Omega \exp(\mu \bar{g}) \rho \frac{\partial g}{\partial \underset{\sim}{\sigma}} \, \mathrm{dv}}{\displaystyle\int_\Omega \exp(\mu \bar{g}) \, \mathrm{dv}} \tag{5.38}$$

5.3.3 Threshold criteria

A brief description on the some threshold criteria that will be implemented and tested in our optimisation problem. Their derivative with respect to $\underset{\sim}{\sigma}$ will be given, enabling the sensitivity analysis to be established. Three threshold criteria will be implemented: Von Mises, Tsai-Wu (TW2) and Tsai-Wu 4 (TW4).

Von-Mises

It is isotropic criterion used for isotropic material. It is based on the energy distortion (see section 1.1.1. Its threshold function is given by:

$$\sigma_{eq} = \sqrt{2 \underset{\sim}{\mathrm{s}}^{mic} : \underset{\sim}{\mathrm{s}}^{mic}}, \tag{5.39}$$

where $\underset{\sim}{\mathrm{s}}^{mic} = \underset{\sim}{\sigma}^{mic} - \dfrac{\mathrm{tr}(\underset{\sim}{\sigma}^{mic})}{2} \underset{\sim}{\mathrm{I}}$ is deviatoric part of $\underset{\sim}{\sigma}^{mic}$. The following derivatives with respect to $\underset{\sim}{\sigma}^{mic}$ are useful for the sensitivity analysis:

$$\frac{\partial g}{\partial \underset{\sim}{\sigma}^{mic}} = \frac{\rho}{\sigma_{lim}} \frac{\partial \sigma_{eq}}{\partial \underset{\sim}{\sigma}^{mic}} \quad ; \quad \frac{\partial \sigma_{eq}}{\partial \underset{\sim}{\sigma}^{mic}} = \frac{2 \underset{\sim}{\mathrm{s}}^{mic}}{\sigma_{eq}}. \tag{5.40}$$

Tsai-Wu

It is a degree 2 polynomial generalised criterion, it is used for orthotropic material (e.g. unidirectional composites). The criterion is given by:

$$\underset{\sim}{\sigma}^{mic} : \underset{\approx}{\mathrm{M}} : \underset{\sim}{\sigma}^{mic} + \underset{\sim}{\mathrm{m}} : \underset{\sim}{\sigma}^{mic} - 1 = 0 \tag{5.41}$$

where tensors $\underset{\approx}{\mathrm{M}}$ and $\underset{\sim}{\mathrm{m}}$ include the material parameters in the following way:

$$\begin{aligned}
&M_{1111} = \frac{1}{X_t X_c}, && M_{2222} = \frac{1}{Y_t Y_c}, && m_{11} = \frac{X_c - X_t}{X_t X_c}, \\
&M_{1122} = \frac{1}{2\sqrt{X_t X_c Y_t Y_c}}, && M_{1212} = \frac{1}{4S^2}, && m_{22} = \frac{Y_c - Y_t}{Y_t Y_c}, \\
&M_{1112} = 0, && M_{1222} = 0, && m_{12} = 0,
\end{aligned}$$

where X_t and X_c are respectively the magnitude of the tension and compressive strength allowable along the fiber direction, whereas Y_t and Y_c are the ones in the transverse direction. S is the shear tensile stress. It important to point out that the threshold function in a non homogeneous polynomial. Implementing the threshold function directly leads to counter intuitive design [128]. To overcome this limitation safety factor denoted κ is introduced as solution of the following equation:

$$\mathcal{A}\, \kappa^2 + \mathcal{B}\, \kappa - 1 = 0, \tag{5.42}$$

where $\mathcal{A} = \underset{\sim}{\sigma}^{mic} : \underset{\approx}{\mathrm{M}} : \underset{\sim}{\sigma}^{mic}$ and $\mathcal{B} = \underset{\sim}{\mathrm{m}} : \underset{\sim}{\sigma}^{mic}$. The solution of the above equation is given by:

$$\kappa = \frac{-\mathcal{B} + \sqrt{\mathcal{B}^2 + 4\mathcal{A}}}{2\mathcal{A}} \tag{5.43}$$

κ is the positive root of equation (5.42). It can be interpreted as a stress tensor multiplier. In case where the mechanical strength are satisfied, $\kappa \geq 1$. It means the stress tensor in within threshold surface in the stress space (defined by equation (5.41)). In the opposite case, $\kappa < 1$ indicates failure. κ cannot be implemented directly due to the fact that it leads to a load dependent solutions [85]. Adding to that, in low stress state, the safety will be high which could lead to having overflow problem when applying of the aggregation. Instead,

to tackle these problems, it is more convenient to use the inverse the safety factor κ to define the mechanical strength in the following way:

$$\bar{g} = \rho g = \left(\frac{1}{\kappa} - 1\right). \tag{5.44}$$

From our perspective, this form gives us advantages. The mechanical strength constraint is respected when $\frac{1}{\kappa} \leq 1$. In the low stress state, $\frac{1}{\kappa}$ has small values. Therefore, it is more suitable for using the aggregation function where the lower-KS function can be used directly as it is described in equation (5.36). The following derivatives are useful for establishing the sensitivity analysis:

$$\begin{aligned} &\frac{\partial g}{\partial \underset{\sim}{\sigma}^{mic}} = -\rho \frac{1}{\kappa^2} \frac{\partial \kappa}{\partial \underset{\sim}{\sigma}^{mic}} \\ &\frac{\partial \kappa}{\partial \underset{\sim}{\sigma}^{mic}} = \frac{\partial \kappa}{\partial \mathcal{A}} \frac{\partial \mathcal{A}}{\partial \underset{\sim}{\sigma}^{mic}} + \frac{\partial \kappa}{\partial \mathcal{B}} \frac{\partial \mathcal{B}}{\partial \underset{\sim}{\sigma}^{mic}} \end{aligned} \quad \left| \quad \begin{aligned} &\frac{\partial \kappa}{\partial \mathcal{A}} = \frac{2\mathcal{A}(\mathcal{A}^2 + 4\mathcal{A})^{-\frac{1}{2}} - (-\mathcal{B} + \sqrt{\mathcal{B}^2 + 4\mathcal{A}})}{2\mathcal{A}^2} \\ &\frac{\partial \kappa}{\partial \mathcal{B}} = \frac{-1 + (\mathcal{B}^2 + 4\mathcal{A})^{-\frac{1}{2}} \mathcal{B}}{2\mathcal{A}} \end{aligned} \right| \quad \begin{aligned} &\frac{\partial \mathcal{A}}{\partial \underset{\sim}{\sigma}^{mic}} = 2\underset{\approx}{\mathrm{M}} : \underset{\sim}{\sigma}^{mic} \\ &\frac{\partial \mathcal{B}}{\partial \underset{\sim}{\sigma}^{mic}} = \underset{\sim}{\mathrm{m}} \end{aligned} \tag{5.45}$$

Tsai-Wu 4

It was proven in chapter 2 that the threshold surface established from triangular equilateral lattice cannot be generated by Tsai-Wu threshold criterion. For that reason Tsai-Wu 4 (TW4) was proposed in chapter 2.4 as non-homogeneous polynomial of degree 4. The harmonic decomposition has enabled us to establish the set of all possible symmetries that the associated threshold surface can have. With the lowest number of coefficients, TW4 was able to approximate well the threshold surface established from an equilateral triangular lattice with tension/compression asymmetry. TW4 is given by:

$$F(\underset{\sim}{\sigma}) = \underset{\approx\approx\approx}{\mathrm{A}}^{8} \cdot (\underset{\sim}{\sigma} \otimes \underset{\sim}{\sigma} \otimes \underset{\sim}{\sigma} \otimes \underset{\sim}{\sigma}) + \underset{\approx\approx\approx}{\mathrm{B}}^{6} \cdot (\underset{\sim}{\sigma} \otimes \underset{\sim}{\sigma} \otimes \underset{\sim}{\sigma}) + \underset{\approx}{\mathrm{E}} :: (\underset{\sim}{\sigma} \otimes \underset{\sim}{\sigma}) + \underset{\sim}{\mathrm{F}} : \underset{\sim}{\sigma}, \tag{5.46}$$

where the tensors $\underset{\approx\approx\approx}{\mathrm{A}}, \underset{\approx\approx\approx}{\mathrm{B}}, \underset{\approx}{\mathrm{E}}$ and $\underset{\sim}{\mathrm{F}}$ include material parameters, they are defined by their harmonic parameters (see chapter **??** for more details). Same as Tsai-Wu, the threshold function is a non-homogenous polynomial function thus, it cannot be implemented directly. Safety factor κ is used and in this case it is the solution of the following quartic equation:

$$\mathcal{A}\ \kappa^4 + \mathcal{B}\ \kappa^3 + \mathcal{E}\ \kappa^2 + \mathcal{F}\ \kappa - 1 = 0, \tag{5.47}$$

where:

$$\mathcal{A} = \underset{\approx\approx\approx}{\mathrm{A}}^{8} \cdot (\underset{\sim}{\sigma} \otimes \underset{\sim}{\sigma} \otimes \underset{\sim}{\sigma} \otimes \underset{\sim}{\sigma}) \quad \underset{\approx\approx\approx}{\mathrm{B}}^{6} \cdot (\underset{\sim}{\sigma} \otimes \underset{\sim}{\sigma} \otimes \underset{\sim}{\sigma}) \quad \underset{\approx\approx\approx}{\mathrm{B}}^{6} \cdot (\underset{\sim}{\sigma} \otimes \underset{\sim}{\sigma} \otimes \underset{\sim}{\sigma}) \quad \mathcal{F} = \underset{\sim}{\mathrm{F}} : \underset{\sim}{\sigma} \tag{5.48}$$

4 analytic solutions can be established [52, 101]. The case of the threshold surface approximated in section **??**, the following simplification can be applied:

$$\mathcal{E} = \mathcal{F} = 0 \tag{5.49}$$

which means that in this case the safety factor κ is the solution of the following equation:

$$\mathcal{A}\ \kappa^4 + \mathcal{B}\ \kappa^3 - 1 = 0, \tag{5.50}$$

the 4 analytic solution $\{\kappa_1, \kappa_2, \kappa_3, \kappa_4\}$ are established using Mathematica and providied in appendix (with their derivatives with respect to $\mathcal{A}$ and $\mathcal{B}$). Knowing that $\mathcal{A} > 0$, the positivity conditions[4], the 4 four solution are:

$$\begin{cases} \kappa_1 > 0 \rightarrow \emptyset \\ \kappa_2 > 0 \rightarrow \mathcal{B} < 0 \\ \kappa_3 > 0 \rightarrow \mathcal{B} > 0 \\ \kappa_4 > 0 \rightarrow \emptyset \end{cases} \quad \mathcal{A} > 0, \tag{5.51}$$

One can see that there is only one positive solution. It is κ_2 if $\mathcal{B} < 0$ or κ_3 if $\mathcal{B} > 0$.

5.4 Resolution algorithm

As a resolution algorithm, two cases are distinguished:

1. Topology optimisation: The minimisation is performed only with respect to density ρ. It can be considered for an isotropic case or for a fixed anisotropic case (fixed orientation).
2. Simultaneous topology and orientation (ot the material) optimisation: The minimisation is performed only with respect to density ρ and θ simultaneously. It can only be consider for anisotropic cases.

[4] Established using the available tools in Mathematica

5.4.1 Topology optimisation

Taking into account the evaluation numerical issues in section 5.3.2, the final version of the topology optimisation problem is:

$$\begin{cases} \min\limits_{\rho\in[0,1]} \displaystyle\int_\Omega \rho \ \mathrm{dv}, \\ \beta \Psi^L_{KS}(\bar{g}) \leq 1, \\ \dfrac{\gamma}{\mathcal{C}_0}\left(\displaystyle\int_{\Gamma_N} \underline{\mathrm{u}} \cdot \underline{\mathrm{t}} \ \mathrm{ds} - 1\right) \mathrm{ds} \leq 0, \\ a_\rho(\underline{\mathrm{u}}, \underline{\mathrm{v}}) = L(\underline{\mathrm{v}}) \quad \forall \ \underline{\mathrm{v}} \in U_{ad}, \end{cases} \tag{$\overline{\mathbb{P}}$}$$

where $\bar{g} = \rho g$ and $\Psi^L_{KS}(\bar{g})$ is given by equation (5.36). As recall, the three particular cases of problem $\overline{\mathbb{P}}$ are given bellow:

$$\begin{cases} \min\limits_{\rho\in[0,1]} \displaystyle\int_\Omega \rho \ \mathrm{dv}, \\ \dfrac{1}{\mathcal{C}_0}\left(\displaystyle\int_{\Gamma_N} \underline{\mathrm{u}} \cdot \underline{\mathrm{t}} \ \mathrm{ds} - 1\right) \mathrm{ds} \leq 0, \\ a_\rho(\underline{\mathrm{u}}, \underline{\mathrm{v}}) = L(\underline{\mathrm{v}}) \quad \forall \ \underline{\mathrm{v}} \in U_{ad}, \end{cases} \tag{$\overline{\mathbb{P}}_1$}$$

Problem 1: volume minimisation with compliance constraints ($\beta = 0, \gamma = 1$).

$$\begin{cases} \min\limits_{\rho\in[0,1]} \displaystyle\int_\Omega \rho \ \mathrm{dv}, \\ \Psi^L_{KS}(\bar{g}) \leq 1, \\ a_\rho(\underline{\mathrm{u}}, \underline{\mathrm{v}}) = L(\underline{\mathrm{v}}) \quad \forall \ \underline{\mathrm{v}} \in U_{ad}, \end{cases} \tag{$\overline{\mathbb{P}}_2$}$$

Problem 2: volume minimisation with mechanical strength constraints($\beta = 1, \gamma = 0$).

$$\begin{cases} \min\limits_{\rho\in[0,1]} \displaystyle\int_\Omega \rho \ \mathrm{dv}, \\ \Psi^L_{KS}(\bar{g}) \leq 1, \\ \dfrac{1}{\mathcal{C}_0}\left(\displaystyle\int_{\Gamma_N} \underline{\mathrm{u}} \cdot \underline{\mathrm{t}} \ \mathrm{ds} - 1\right) \mathrm{ds} \leq 0, \\ a_\rho(\underline{\mathrm{u}}, \underline{\mathrm{v}}) = L(\underline{\mathrm{v}}) \quad \forall \ \underline{\mathrm{v}} \in U_{ad}, \end{cases} \tag{$\overline{\mathbb{P}}_3$}$$

Problem 3: volume minimisation with both compliance and mechanical strength constraints($\beta = 1, \gamma = 1$).

Solving the problems ($\overline{\mathbb{P}}_1$), ($\overline{\mathbb{P}}_2$) and ($\overline{\mathbb{P}}_3$), is solving the problem ($\overline{\mathbb{P}}$) considering $\{\beta, \gamma\} \in \{\{0,1\},\{1,0\},\{1,1\}\}$.

From now on, we start applying the augmented Lagrangian as it is described in section 5.2. Using the slack variables (s_1 and s_2 in (5.52)), the inequality constraints are turned into equality constraints. The equivalent problem to ($\overline{\mathbb{P}}$) is given by:

$$\begin{cases} \min\limits_{\rho\in[0,1]} \displaystyle\int_\Omega \rho \ \mathrm{dv}, \\ \beta \left[\Psi^L_{KS}(\bar{g}) + s_1\right] = 0 \quad s_1 \geq 0, \\ \gamma \left[\dfrac{1}{\mathcal{C}_0}\left(\displaystyle\int_{\Gamma_N} \underline{\mathrm{u}} \cdot \underline{\mathrm{t}} \ \mathrm{ds} - 1\right) \mathrm{ds} + s_2\right] = 0 \quad s_2 \geq 0, \\ a_\rho(\underline{\mathrm{u}}, \underline{\mathrm{v}}) = L(\underline{\mathrm{v}}) \quad \forall \ \underline{\mathrm{v}} \in U_{ad}, \end{cases} \tag{5.52}$$

The augmented Lagrangian is given by:

$$\begin{aligned} \mathcal{L}(\underline{\mathrm{u}}, \underline{\mathrm{q}}, \rho, \underline{\mathrm{s}}, \underline{\lambda}, \underline{\mathrm{b}}) = & \frac{1}{V_\Omega} \int_\Omega \rho \ \mathrm{dv} - \int_\Omega \rho \underset{\sim}{\varepsilon}(\underline{\mathrm{u}}) : \underset{\approx}{\mathrm{C}}^0 : \underset{\sim}{\varepsilon}(\underline{\mathrm{q}}) \ \mathrm{dv} + \int_{\Gamma_N} \underline{\mathrm{t}} \cdot \underline{\mathrm{q}} \ \mathrm{ds} \\ & + \beta \left[\lambda_1 (\Psi^L_{KS}(\bar{g}) + s_1) + \frac{b_1}{2} (\Psi^L_{KS}(\bar{g}) + s_1)^2\right] \\ & + \gamma \left[\lambda_2 \left(\frac{1}{\mathcal{C}_0}\left(\int_{\Gamma_N} \underline{\mathrm{t}} \cdot \underline{\mathrm{u}} \ \mathrm{ds} - 1\right) + s_2\right) + \frac{b_2}{2} \left(\frac{1}{\mathcal{C}_0}\left(\int_{\Gamma_N} \underline{\mathrm{t}} \cdot \underline{\mathrm{u}} \ \mathrm{ds} - 1\right) + s_2\right)^2\right]. \end{aligned} \tag{5.53}$$

where $\underline{\mathrm{s}} = \begin{bmatrix} s_1 \\ s_2 \end{bmatrix}, \underline{\lambda} = \begin{bmatrix} \lambda_1 \\ \lambda_2 \end{bmatrix}, \underline{\mathrm{b}} = \begin{bmatrix} b_1 \\ b_2 \end{bmatrix}$. The augmented allows transforming a constrained optimisation problem into an unconstrained one, However, Lagrangian multipliers are added as additional variables. The following problem is equivalent to ($\overline{\mathbb{P}}$):

$$\begin{cases} \max\limits_{\underline{\mathrm{q}}, \underline{\lambda}} \min\limits_{\rho, \underline{\mathrm{s}}} \mathcal{L}(\underline{\mathrm{u}}, \underline{\mathrm{q}}, \rho, \underline{\mathrm{s}}, \underline{\lambda}, \underline{\mathrm{b}}), \\ 0 \leq \rho \leq 1 \text{ and } \underline{\mathrm{s}} \geq 0, \end{cases} \tag{5.54}$$

Before providing the resolution algorithm, sensitivity analysis has to be done. As it described in section 5.2.1. Let's start by calculating the directional derivative of $\mathcal{L}$ with respect to $\underline{u}$:

$$\langle \frac{\partial \mathcal{L}(\underline{u},\underline{q},\rho,\underline{s},\underline{\lambda},\underline{b})}{\partial \underline{u}}, \underline{\hat{u}} \rangle = -\int_\Omega \rho_\epsilon \underset{\sim}{\varepsilon}(\underline{q}) : \underset{\approx}{C}^0 : \underset{\sim}{\varepsilon}(\underline{\hat{u}}) \, dv + \beta(\lambda_1 + b_1(\Psi_{KS}^L(\bar{g}) + s_1)) \frac{\int_\Omega \exp(k\bar{g}) \rho \frac{\partial g}{\partial \underset{\sim}{\sigma}^{mic}} : \underset{\sim}{\sigma}^{mic}(\underline{\hat{u}}) \, dv}{\int_\Omega \exp(k\bar{g}) \, dv}$$
$$+ \gamma(\lambda_2 + b_2(\frac{1}{C_0}(\int_{\Gamma_N} \underline{t} \cdot \underline{u} \, ds - 1) + s_2)) \frac{\int_{\Gamma_N} \underline{t} \cdot \underline{\hat{u}} \, ds}{\mathcal{C}_0},$$

where $\frac{\partial \bar{g}}{\partial \underset{\sim}{\sigma}^{mic}}$ is provided in section 4.3.3. The weak form of adjoint elasticity problem, given below, is established by considering $\langle \frac{\partial \mathcal{L}(\underline{u},\underline{q},\rho,\underline{s},\underline{\lambda},\underline{b})}{\partial \underline{u}}, \underline{\hat{u}} \rangle = 0$:

$$\begin{aligned} \int_\Omega \rho_\epsilon \underset{\sim}{\varepsilon}(\underline{q}) : \underset{\approx}{C}^0 : \underset{\sim}{\varepsilon}(\underline{\hat{u}}) \, dv =& \beta(\lambda_1 + b_1(\Psi_{KS}^L(\bar{g}) + s_1)) \frac{\int_\Omega \exp(\mu\bar{g}) \rho \frac{\partial g}{\partial \underset{\sim}{\sigma}^{mic}} : \underset{\sim}{\sigma}^{mic}(\underline{\hat{u}}) \, dv}{\int_\Omega \exp(\mu\bar{g}) \, dv} \\ &+ \gamma(\lambda_2 + b_2(\frac{1}{\mathcal{C}_0}(\int_{\Gamma_N} \underline{t} \cdot \underline{u} \, ds - 1) + s_2)) \frac{\int_{\Gamma_N} \underline{t} \cdot \underline{\hat{u}} \, ds}{\mathcal{C}_0} \qquad \forall \underline{\hat{u}} \in U_{ad}, \end{aligned} \tag{5.55}$$

remark: The following formulas is useful and it can be proved by the definition 5.2.1:

$$\langle \frac{\partial \underset{\sim}{\sigma}(\underline{u})}{\partial \underline{u}}, \underline{\hat{u}} \rangle = \underset{\sim}{\sigma}(\underline{\hat{u}}) \qquad ; \qquad \langle \frac{\partial \underset{\sim}{\varepsilon}(\underline{u})}{\partial \underline{u}}, \underline{\hat{u}} \rangle = \underset{\sim}{\varepsilon}(\underline{\hat{u}})$$

The directional derivative with respect to ρ is needed for the minimisation using projected gradient. As it is detailed in section 5.2.1, when $\underline{q}$ is solution of (5.55):

$$\begin{aligned} \langle \frac{d\mathcal{L}(\underline{u},\underline{q},\rho,\underline{s},\underline{\lambda},\underline{b})}{d\rho}, \hat{\rho} \rangle = \langle \frac{\partial \mathcal{L}(\underline{u},\underline{q},\rho,\underline{s},\underline{\lambda},\underline{b})}{\partial \rho}, \hat{\rho} \rangle =& \frac{1}{V_\Omega} \int_\Omega \hat{\rho} \, dv - \int_\Omega (1-\epsilon) p \rho^{p-1} \underset{\sim}{\varepsilon}(\underline{u}) : \underset{\approx}{C}^0 : \underset{\sim}{\varepsilon}(\underline{q}) \hat{\rho} \, dv \\ &+ \beta(\lambda_1 + b_1(\Psi_{KS}^L(\bar{g}) + s_1)) \frac{\int_\Omega \exp(\mu\bar{g}) g \hat{\rho} \, dv}{\int_\Omega \exp(\mu\bar{g}) \, dv}. \end{aligned} \tag{5.56}$$

Hence, the direction $\hat{\rho}$ that minimises $\mathcal{L}(\underline{u},\underline{q},\rho,\underline{s},\underline{\lambda},\underline{b})$ (considering $\underline{\lambda}$ and $\underline{b}$ constant):

$$\hat{\rho} = -\left[\frac{1}{V_\Omega} - (1-\epsilon) p \rho^{p-1} \underset{\sim}{\varepsilon}(\underline{u}) : \underset{\approx}{C}^0 : \underset{\sim}{\varepsilon}(\underline{q}) + \beta(\lambda_1 + b_1(\Psi_{KS}^L(\bar{g}) + s_1)) \frac{\exp(\mu\bar{g}) g}{\int_\Omega \exp(\mu\bar{g}) \, dv} \right]. \tag{5.57}$$

The minimisation with respect to $\underline{s}$ and the updating scheme of $\underline{\lambda}$ is provided in the following algorithm:

Algorithm 2 Augmented Lagrangian algorithm: Volume minimisation

1. Define the algorithm parameters $iter_{max}, \tau, R, b_{max}, \alpha$.
2. Initialise the field $\rho(\underline{x})$ and the value of $p, \underline{\lambda}, \underline{b}, \epsilon$.
3. Precomputations:
   $\underline{u} \leftarrow$ Ela_FE(ρ) % Elasticity problem, equation (5.8)
   $\bar{g} \leftarrow \rho g(\underline{u})$ % g id given by the two equations (5.33) or (5.44) (depending on threshold criterion)
   $s_1 \leftarrow \max\left[0, -\left(\frac{\lambda_1}{b_1} + \beta \Psi^L_{KS}(\bar{g})\right)\right]$
   $s_2 \leftarrow \max\left[0, -\left(\frac{\lambda_2}{b_2} + \frac{\gamma}{\mathcal{C}_0}\left(\int_{\Gamma_N} \underline{u} \cdot \underline{t} \, \mathrm{ds} - 1\right)\right)\right]$
4. For j=1 to $iter_{max}$:
   $\underline{q} \leftarrow$ Adj_FE($\underline{u}, \rho, \underline{s}, \underline{\lambda}, \underline{b}$) % Adjoint elasticity problem, equation (5.55)
   $\hat{\rho} \leftarrow -\left[\frac{1}{V_\Omega} - (1-\epsilon) p \rho^{p-1} \underset{\sim}{\varepsilon}(\underline{u}) : \underset{\approx}{\mathrm{C}}^0 : \underset{\sim}{\varepsilon}(\underline{q}) + \beta(\lambda_1 + b_1(\Psi^L_{KS}(\bar{g}) + s_1)) \frac{\exp(\mu \bar{g}) g}{\int_\Omega \exp(\mu \bar{g}) \, \mathrm{dv}}\right]$
   $\bar{\rho} \leftarrow \max(\min(\rho + \tau \frac{\mathcal{F}_R(\hat{\rho})}{\max(|\mathcal{F}_R(\hat{\rho})|)}, 1), 0)$
   $\underline{u} \leftarrow$ Ela_FE($\bar{\rho}$)
   $\bar{g} \leftarrow \bar{\rho} g(\underline{u})$
   $s_1 \leftarrow \max\left[0, -\left(\frac{\lambda_1}{b_1} + \beta \Psi^L_{KS}(\bar{g})\right)\right]$
   $s_2 \leftarrow \max\left[0, -\left(\frac{\lambda_2}{b_2} + \frac{\gamma}{\mathcal{C}_0}\left(\int_{\Gamma_N} \underline{u} \cdot \underline{t} \, \mathrm{ds} - 1\right) \, \mathrm{ds}\right)\right]$
   $\lambda_1 \leftarrow \lambda_1 + b_1 \beta(\Psi^L_{KS}(\bar{g}) + s_1)$
   $\lambda_2 \leftarrow \lambda_2 + b_2 \frac{\gamma}{\mathcal{C}_0}\left(\int_{\Gamma_N} \underline{u} \cdot \underline{t} \, \mathrm{ds} - 1\right)$
   if $\beta \Psi^L_{KS}(\bar{g}) + s_1 > 0$:
      $b_1 \leftarrow \min[b_{max}, \alpha b_1]$
   if $\frac{\gamma}{\mathcal{C}_0}\left(\int_{\Gamma_N} \underline{u} \cdot \underline{t} \, \mathrm{ds} - 1\right) + s_2 > 0$:
      $b_2 \leftarrow \min[b_{max}, \alpha b_2]$

5.4.2 Simultaneous topology and orientation optimisation

Adding the orientation as an optimisation variable allows us to obtain the better performance from anisotropic material. It is particularly useful for a variety of applications where architectured materials are involved, such as unidirectional oriented fibre composites. It is also practical especially with the fast development of additive manufacturing methods. The concurrent topology and orientation optimisation is possible only if one of material tensors (describing stiffness and/or mechanical strength) is anisotropic. In this section, θ denotes the orientation of the material with respect to fixed reference. The following problem is posed:

$$\begin{cases} \min\limits_{\rho,\theta} \int_\Omega \rho \, \mathrm{dv}, \\ \beta \Psi^L_{KS}(\bar{g}) \leq 1, \\ \frac{\gamma}{\mathcal{C}_0}\left(\int_{\Gamma_N} \underline{u} \cdot \underline{t} \, \mathrm{ds} - 1\right) \, \mathrm{ds} \leq 0, \\ a_\rho(\underline{u}, \underline{v}) = L(\underline{v}) \quad \forall \, \underline{v} \in U_{ad}, \\ 0 \leq \rho \leq 1, \quad -3\frac{\pi}{2} < \theta < 3\frac{\pi}{2}, \end{cases} \tag{$\overline{\mathbb{O}}$}$$

As a recall, the three particular cases of problem $\overline{\mathbb{O}}$ are given bellow:

$$\begin{cases} \min\limits_{\rho,\theta} \int_\Omega \rho \ \mathrm{dv}, \\ \dfrac{\gamma}{\mathcal{C}_0}\left(\int_{\Gamma_N} \underline{\mathrm{u}} \cdot \underline{\mathrm{t}} \ \mathrm{ds} - 1\right) \mathrm{ds} \leq 0, \\ a_\rho(\underline{\mathrm{u}}, \underline{\mathrm{v}}) = L(\underline{\mathrm{v}}) \quad \forall \ \underline{\mathrm{v}} \in U_{ad}, \\ 0 \leq \rho \leq 1, \quad -3\dfrac{\pi}{2} < \theta < 3\dfrac{\pi}{2}, \end{cases} \tag{$\overline{\mathbb{O}}_1$}$$

Problem 1: volume minimisation with compliance constraints ($\beta = 0, \gamma = 1$).

$$\begin{cases} \min\limits_{\rho,\theta} \int_\Omega \rho \ \mathrm{dv}, \\ \beta \Psi^L_{KS}(\bar{g}) \leq 1, \\ a_\rho(\underline{\mathrm{u}}, \underline{\mathrm{v}}) = L(\underline{\mathrm{v}}) \quad \forall \ \underline{\mathrm{v}} \in U_{ad}, \\ 0 \leq \rho \leq 1, \quad -3\dfrac{\pi}{2} < \theta < 3\dfrac{\pi}{2}, \end{cases} \tag{$\overline{\mathbb{O}}_2$}$$

Problem 2: volume minimisation with mechanical strength constraints($\beta = 1, \gamma = 0$).

$$\begin{cases} \min\limits_{\rho,\theta} \int_\Omega \rho \ \mathrm{dv}, \\ \Psi^L_{KS}(\bar{g}) \leq 1, \\ \dfrac{1}{\mathcal{C}_0}\left(\int_{\Gamma_N} \underline{\mathrm{u}} \cdot \underline{\mathrm{t}} \ \mathrm{ds} - 1\right) \mathrm{ds} \leq 0, \\ a_\rho(\underline{\mathrm{u}}, \underline{\mathrm{v}}) = L(\underline{\mathrm{v}}) \quad \forall \ \underline{\mathrm{v}} \in U_{ad}, \\ 0 \leq \rho \leq 1, \quad -3\dfrac{\pi}{2} < \theta < 3\dfrac{\pi}{2}, \end{cases} \tag{$\overline{\mathbb{O}}_3$}$$

Problem 3: volume minimisation with both compliance and mechanical strength constraints($\beta = 1, \gamma = 1$).

Solving the problems ($\overline{\mathbb{O}}_1$), ($\overline{\mathbb{O}}_2$) and ($\overline{\mathbb{O}}_3$), is solving the problem ($\overline{\mathbb{O}}$) considering $\{\beta, \gamma\} \in \{\{0,1\},\{1,0\},\{1,1\}\}$. One can see that θ has bounds. It allows having more freedom design when minimising the objective and the constraints. The polar parameterisation [75, 184], described briefly in section 2.2.3 is used to explicitly express the orientation dependence of all material tensors.

From now on, the augmented Lagrangian is applied, after transforming the inequality constraints into equality constraints by the mean of the slack variables (see equation (5.52)), the associated augmented Lagrangian is given as follows:

$$\begin{aligned} \mathcal{L}(\underline{\mathrm{u}}, \underline{\mathrm{q}}, \rho, \theta, \underline{\mathrm{s}}, \underline{\lambda}, \underline{\mathrm{b}}) = & \frac{1}{V_\Omega} \int_\Omega \rho \ \mathrm{dv} - \int_\Omega \rho_\epsilon \underset{\sim}{\varepsilon}(\underline{\mathrm{u}}) : \underset{\approx}{\mathrm{C}^0} : \underset{\sim}{\varepsilon}(\underline{\mathrm{q}}) \ \mathrm{dv} + \int_{\Gamma_N} \underline{\mathrm{t}} \cdot \underline{\mathrm{q}} \ \mathrm{ds} \\ & + \beta \left[\lambda_1 (\Psi^L_{KS}(\bar{g}) + s_1) + \frac{b_1}{2} (\Psi^L_{KS}(\bar{g}) + s_1)^2 \right] \\ & + \gamma \left[\lambda_2 \left(\frac{1}{\mathcal{C}_0} \left(\int_{\Gamma_N} \underline{\mathrm{t}} \cdot \underline{\mathrm{u}} \ \mathrm{ds} - 1 \right) + s_2 \right) + \frac{b_2}{2} \left(\frac{1}{\mathcal{C}_0} \left(\int_{\Gamma_N} \underline{\mathrm{t}} \cdot \underline{\mathrm{u}} \ \mathrm{ds} - 1 \right) + s_2 \right)^2 \right]. \end{aligned} \tag{5.58}$$

The equivalent problem to ($\overline{\mathbb{O}}$) is given by:

$$\begin{cases} \max\limits_{\underline{\mathrm{q}}, \underline{\lambda}} \min\limits_{\rho, \theta, \underline{\mathrm{s}}} \mathcal{L}(\underline{\mathrm{u}}, \underline{\mathrm{q}}, \rho, \underline{\mathrm{s}}, \underline{\lambda}, \underline{\mathrm{b}}), \\ 0 \leq \rho \leq 1, \ -3\dfrac{\pi}{2} < \theta < 3\dfrac{\pi}{2} \text{ and } \ \underline{\mathrm{s}} \geq 0, \end{cases} \tag{5.59}$$

Before providing the resolution algorithm, sensitivity analysis has to be done. The sensitivity analysis is very similar the one in section 5.4.1. To avoid redundancy, we have the following statement:

- The adjoint problem is the same as in equation (5.55), it must be keep in mind that the changes coming from the orientation θ (in addition to ρ and $\underline{\mathrm{s}}$) must be taken into account.
- The directional derivative with respect to ρ remains also the same the on in equation (5.60).

What's remaining is the directional derivative of the augmented Lagrangian with respect to θ, it is given by:

$$\begin{aligned} \left\langle \frac{d\mathcal{L}(\underline{\mathrm{u}}, \underline{\mathrm{q}}, \rho, \underline{\mathrm{s}}, \underline{\lambda}, \underline{\mathrm{b}})}{d\theta}, \hat{\theta} \right\rangle = \left\langle \frac{\partial \mathcal{L}(\underline{\mathrm{u}}, \underline{\mathrm{q}}, \rho, \underline{\mathrm{s}}, \underline{\lambda}, \underline{\mathrm{b}})}{\partial \theta}, \hat{\theta} \right\rangle = & \frac{1}{V_\Omega} \int_\Omega \hat{\rho} \ \mathrm{dv} - \int_\Omega \rho_\epsilon \ \underset{\sim}{\varepsilon}(\underline{\mathrm{u}}) : \frac{\partial \underset{\approx}{\mathrm{C}^0}}{\partial \theta} : \underset{\sim}{\varepsilon}(\underline{\mathrm{q}}) \hat{\theta} \ \mathrm{dv} \\ & + \beta(\lambda_1 + b_1(\Psi^L_{KS}(\bar{g}) + s_1)) \frac{\displaystyle\int_\Omega \exp(\mu \bar{g}) \rho \frac{\partial g}{\partial \theta} \hat{\theta} \ \mathrm{dv}}{\displaystyle\int_\Omega \exp(\mu \bar{g}) \ \mathrm{dv}}. \end{aligned} \tag{5.60}$$

Hence, the direction $\hat{\theta}$ that minimises $\mathcal{L}(\underline{u}, \underline{q}, \rho, \theta, \underline{s}, \underline{\lambda}, \underline{b})$ (considering $\underline{\lambda}$ and $\underline{b}$ constant):

$$\hat{\theta} = -\left[-\rho_\epsilon \underset{\sim}{\varepsilon}(\underline{u}) : \frac{\partial \underset{\approx}{C}^0}{\partial \theta} : \underset{\sim}{\varepsilon}(\underline{q}) + \beta(\lambda_1 + b_1(\Psi_{KS}^L(\bar{g}) + s_1)) \frac{\exp(\mu \bar{g}) \rho \dfrac{\partial g}{\partial \theta}}{\displaystyle\int_\Omega \exp(\mu \bar{g}) \, \mathrm{dv}} \right]. \tag{5.61}$$

The following algorithm for concurrent topology and orientation optimisation is given:

Algorithm 3 Augmented Lagrangian algorithm: Concurrent topology and orientation optimisation

1. Define the algorithm parameters $iter_{max}, \tau_\rho, \tau_\theta, R, b_{max}, \alpha$.
2. Initialise the field $\rho(\underline{x})$, $\theta(\underline{x})$ and the value of $p, \underline{\lambda}, \underline{b}, \epsilon$.
3. Precomputations:

   $\underline{u} \leftarrow$ Ela_FE(ρ, θ) % Elasticity problem, equation (5.8)

   $\bar{g} \leftarrow \rho g(\underline{u})$ % g id given by the two equations (5.33) or (5.44) (depending on threshold criterion)

   $s_1 \leftarrow \max\left[0, -\left(\dfrac{\lambda_1}{b_1} + \beta \Psi_{KS}^L(\bar{g})\right)\right]$

   $s_2 \leftarrow \max\left[0, -\left(\dfrac{\lambda_2}{b_2} + \dfrac{\gamma}{\mathcal{C}_0}\left(\displaystyle\int_{\Gamma_N} \underline{u} \cdot \underline{t} \, \mathrm{ds} - 1\right)\right)\right]$

4. For j=1 to $iter_{max}$:

   $\underline{q} \leftarrow$ Adj_FE$(\underline{u}, \rho, \theta, \underline{s}, \underline{\lambda}, \underline{b})$ % Adjoint elasticity problem, equation (5.55)

   $\hat{\rho} \leftarrow -\left[\dfrac{1}{V_\Omega} - (1-\epsilon) p \rho^{p-1} \underset{\sim}{\varepsilon}(\underline{u}) : \underset{\approx}{C}^0 : \underset{\sim}{\varepsilon}(\underline{q}) + \beta(\lambda_1 + b_1(\Psi_{KS}^L(\bar{g}) + s_1)) \dfrac{\exp(\mu \bar{g}) g}{\displaystyle\int_\Omega \exp(\mu \bar{g}) \, \mathrm{dv}}\right]$

   $\bar{\rho} \leftarrow \max(\min(\rho + \tau \dfrac{\mathcal{F}_R(\hat{\rho})}{\max(|\mathcal{F}_R(\hat{\rho})|)}, 1), 0)$

   $\hat{\theta} \leftarrow -\left[-\rho_\epsilon \underset{\sim}{\varepsilon}(\underline{u}) : \dfrac{\partial \underset{\approx}{C}^0}{\partial \theta} : \underset{\sim}{\varepsilon}(\underline{q}) + \beta(\lambda_1 + b_1(\Psi_{KS}^L(\bar{g}) + s_1)) \dfrac{\exp(\mu \bar{g}) \rho \dfrac{\partial g}{\partial \theta}}{\displaystyle\int_\Omega \exp(\mu \bar{g}) \, \mathrm{dv}}\right]$

   $\bar{\theta} \leftarrow \max(\min(\theta + \tau \dfrac{\mathcal{F}_R(\hat{\theta})}{\max(|\mathcal{F}_R(\hat{\theta})|)}, 3\dfrac{\pi}{2}), -3\dfrac{\pi}{2})$

   $\underline{u} \leftarrow$ Ela_FE$(\bar{\rho}, \bar{\theta})$

   $\bar{g} \leftarrow \bar{\rho} g(\underline{u})$

   $s_1 \leftarrow \max\left[0, -\left(\dfrac{\lambda_1}{b_1} + \beta \Psi_{KS}^L(\bar{g})\right)\right]$

   $s_2 \leftarrow \max\left[0, -\left(\dfrac{\lambda_2}{b_2} + \dfrac{\gamma}{\mathcal{C}_0}\left(\displaystyle\int_{\Gamma_N} \underline{u} \cdot \underline{t} \, \mathrm{ds} - 1\right) \mathrm{ds}\right)\right]$

   $\lambda_1 \leftarrow \lambda_1 + b_1 \beta(\Psi_{KS}^L(\bar{g}) + s_1)$

   $\lambda_2 \leftarrow \lambda_2 + b_2 \dfrac{\gamma}{\mathcal{C}_0}\left(\displaystyle\int_{\Gamma_N} \underline{u} \cdot \underline{t} \, \mathrm{ds} - 1\right)$

   if $\beta \Psi_{KS}^L(\bar{g}) + s_1 > 0$:

   $\quad b_1 \leftarrow \min[b_{max}, \alpha b_1]$

   if $\dfrac{\gamma}{\mathcal{C}_0}\left(\displaystyle\int_{\Gamma_N} \underline{u} \cdot \underline{t} \, \mathrm{ds} - 1\right) + s_2 > 0$:

   $\quad b_2 \leftarrow \min[b_{max}, \alpha b_2]$

5.5 Results and Discussion

In this section the 3 problems ($\overline{\mathbb{P}}_1$), ($\overline{\mathbb{P}}_2$) and ($\overline{\mathbb{P}}_3$) will be solved. Many cases are distinguished. In first one, the optimisation with isotropic stiffness and isotropic strength is performed. The effect of the aggregation and the constraints are investigated closely. The second case treat the optimisation considering isotropic material with a fixed (fixed orientation) anisotropic strength.

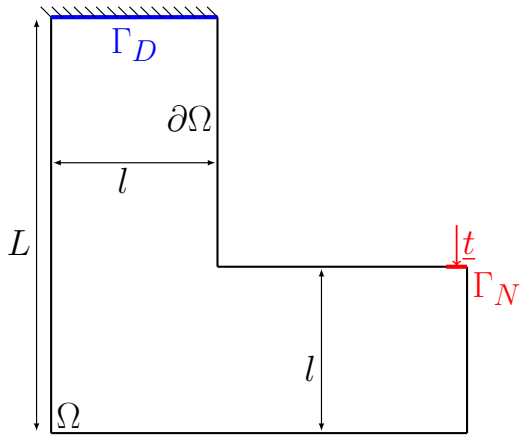

Figure 5.4: The L-shaped beam linear elasticity problem.

For the model, the L-shaped beam problem, illustrated in figure 5.4, will be considered. The structure domain Ω subdivided into n_e linear quadrilateral elements (Q4). All details about the finite element discretisation, optimisation and the algorithm parameters are resumed in the following table:

Model	
Model	Plane stress (linear elasticity)
Element type	Q4
Mesh	Linear quadrilateral elements $n_e = 10000$.
Dimensions	$L = 100mm$, $l = 40mm$
Load	A distributed force over Γ_N, No volumic forces.
optimisation parameters	
Minimum density (Ersat parameter)	$\epsilon = 10^{-6}$
Initial density	Uniform distributed density $\rho(\underline{x}) = 1\ \forall \underline{x} \in \Omega$
Density filter	Based on Helmholtz PDE (equation (5.31)) with radius $R = 2mm$
Algorithm settings	
Algorithm	Augmented Lagrangian
Parameters	$\alpha = 1.1, \tau \in [0.05, 0.3]$
Initial Lagrange multipliers and penalisation coefficients	$\lambda_1 = \lambda_2 = 0.1, b_1 = b_2 = 0.1, b_{max} = 3$

Table 5.1: Numerical model and optimisation settings

ρ is a local variable constant in each element which indicates the presence/absence of material. The algorithm is implemented using FEniCS, a python library for finite element analysis.

5.5.1 Topology optimisation with isotropic material and strength

In the following, the case of isotropic stiffness with isotropic strength is considered. The material parameters are defined by E Young's modulus, ν Poisson's coefficient and σ_{lim} is the tensile limit stress. The values are displayed in table 5.2. To describe the strength, the Von Mises criterion is used with fictitious tensile stress. Its implementation is straight forward and it is detailed in section 5.3.3.

E [MPa]	ν	σ_{lim} [MPa]	$\underline{t}$ [N]
69.7	0.29	45	93.5

Table 5.2: Problem parameters

Let's focus on the problem ($\overline{\mathbb{P}}_2$). The strength stresses are aggregated using the lower KS function, which is a smooth approximation to the max function. As shown in equation (5.37), μ plays an important role, the larger it is, the closer it is to the maximum. It must not be very high, otherwise convergence problems arise (due to high non-linearity). Consequently, μ must be chosen wisely. In order to have a hunch about the suitable values of μ to choose, the initial state of the optimisation problem where $\rho(\underline{x}) = 1 \forall \underline{x} \in \Omega$ is considered. After solving the elasticity, the normalised Von Mises stress field $\frac{\sigma_{eq}}{\sigma_{lim}}$ (normalised with respect σ_{lim}) is illustrated in the figure 5.5. The max value is around 1.55 in the corner.

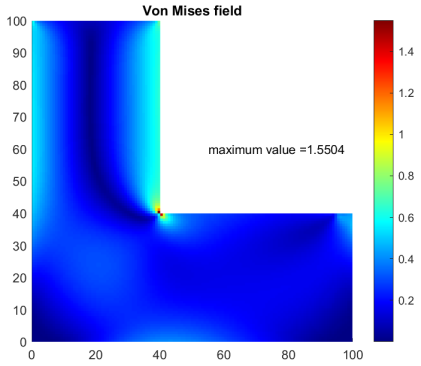

Figure 5.5: Normalised Von Mises stress field $\frac{\sigma_{eq}}{\sigma_{lim}}$ where $\rho(\underline{x}) = 1 \forall \underline{x} \in \Omega$.

The following function is evaluated (keep in mind $\rho(\underline{x}) = 1 \ \forall \underline{x} \in \Omega$):

$$\frac{\Psi_{KS}^{L}(\bar{g}+1)}{\bar{g}_{max}+1} = \frac{\Psi_{KS}^{L}(\sigma_{eq}/\sigma_{lim})}{\sigma_{eq}^{max}/\sigma_{lim}} \tag{5.62}$$

The above function is the ratio between the aggregated normalised stress field and the non-aggregated one. The figure 5.6 shows its variation according to μ. The dashed line (value 1) corresponds to the max stress field. It is observed that the greater μ, the closer the aggregated field to 1 (max). One can see that aggregation grows very fast at the beginning ($\mu < 40$) then, it slows down. To choose a reasonable value for μ, we opt for those corresponding to around the ratio 0.9 (meaning 90% of the maximum value). The values chosen are $\mu = \{40, 50, 60\}$ as those for which the problem ($\overline{\mathbb{P}}_2$) will be solved.

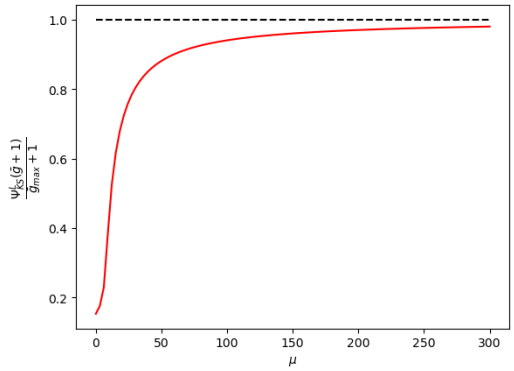

Figure 5.6: Variation of $\frac{\Psi_{KS}^{L}(\bar{g}+1)}{\bar{g}_{max}+1}$ according to μ.

The figures 5.7, 5.8 and 5.9, show the results for solving the problem ($\overline{\mathbb{P}}_2$) considering $\mu = \{40, 50, 60\}$ respectively. The three optimal design are similar where they all have a rounded corner to avoid stress concentration. As μ get greater, the final volume also get slightly higher. This can be explained by the fact that more volume is needed to reduce the maximum stress as it approaches 1. The design plays an important role. One can see a

gap appearing (right of superior part of structure) when $\mu = 60$ which the design more rounded in the corner thus reducing maximum stress.

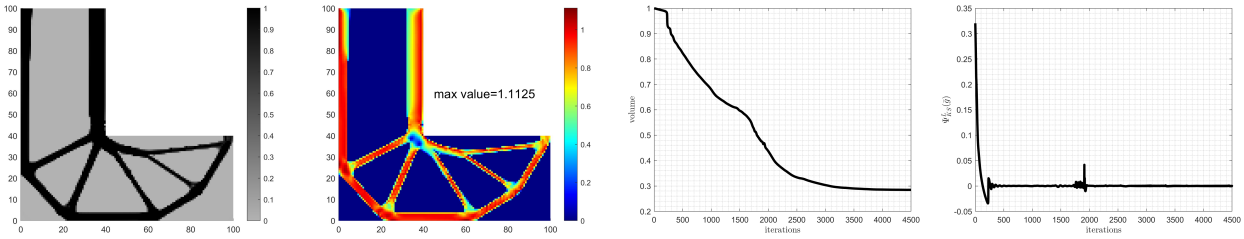

(a) Density field (b) Normalised stress field $\frac{\sigma_{eq}}{\sigma_{lim}}$ (c) volume history (d) Strength $\Psi^L_{KS}(\bar{g})$ history

Figure 5.7: The Results of solving problem ($\overline{\mathbb{P}}_2$) for $\mu = 40$. The final values: $V_{\Omega_{mat}} = 28.4\%$, $\mathcal{C} = 36.00$ mJ, $\frac{\sigma_{eq}^{max}}{\sigma_{lim}} = 1.11$

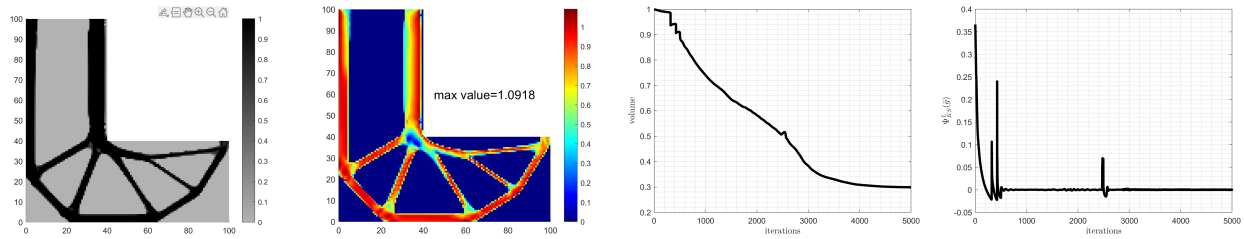

(a) Density field (b) Normalised stress field $\frac{\sigma_{eq}}{\sigma_{lim}}$ (c) volume history (d) Strength $\Psi^L_{KS}(\bar{g})$ history

Figure 5.8: The Results of solving problem ($\overline{\mathbb{P}}_2$) for $\mu = 50$. The final values: $V_{\Omega_{mat}} = 29.90\%$, $\mathcal{C} = 36.05$ mJ, $\frac{\sigma_{eq}^{max}}{\sigma_{lim}} = 1.09$

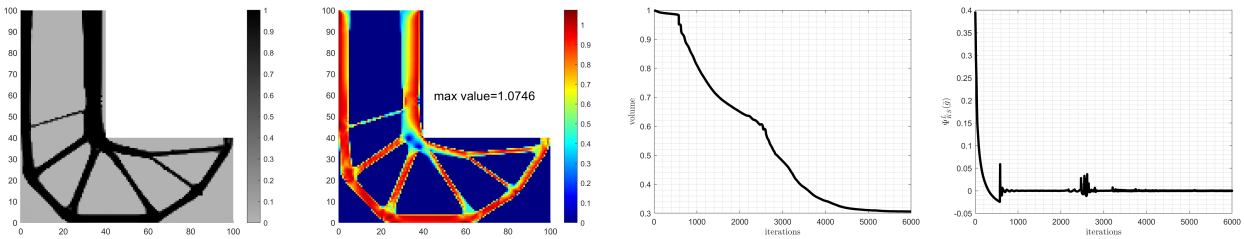

(a) Density field (b) Normalised stress field $\frac{\sigma_{eq}}{\sigma_{lim}}$ (c) volume history (d) Strength $\Psi^L_{KS}(\bar{g})$ history

Figure 5.9: The Results of solving problem ($\overline{\mathbb{P}}_2$) for $\mu = 60$. The final values: $V_{\Omega_{mat}} = 30.06\%$, $\mathcal{C} = 36.00$ mJ, $\frac{\sigma_{eq}^{max}}{\sigma_{lim}} = 1.07$

When looking at the convergence history for three figures, one can see that they are kind of similar. The volume decreases at the beginning at very slow pace then it accelerates. The reason is because of strength constraint. Being violated at beginning, the algorithm prioritises minimising the strength constraint (over the volume) until it is saturated (inequality). Once done, the priority is progressively given to minimising the volume. It is important to note that the priority mechanism is driven by the Lagrange multipliers, which can be interpreted as sensitivity parameter in relation to the constraints [4]. The higher μ is, the greater the number of iterations required to converge. Indeed, as μ increases, the constraint becomes increasingly non-linear. Some peaks can be found when looking to strength history, this is explained by fact that stress concentrations could occur when looking for optimal design. In an attempt to avoid the convergence problems, caused by these peaks, the step τ must be chosen small enough and the descent direction must be normalised with respect to its max absolute value (see algorithm 2). Although the strength constraints are checked at the end, the maximum stress field is always greater than 1 (but close). This illustrates one of the disadvantages of using aggregation.

From now on, The focus is on problem ($\overline{\mathbb{P}}_3$), the inequality constraints are currently the mechanical strength and the stiffness. Previously, after solving the problem ($\overline{\mathbb{P}}_2$), the strength constraint is satisfied, though, it is assumed that it is not stiff enough. The final compliance was around 36.0 mJ therefore, in problem ($\overline{\mathbb{P}}_3$), $\mathcal{C}_0 = 25$ mJ will be imposed as a rigidity (or stiffness) constraint.

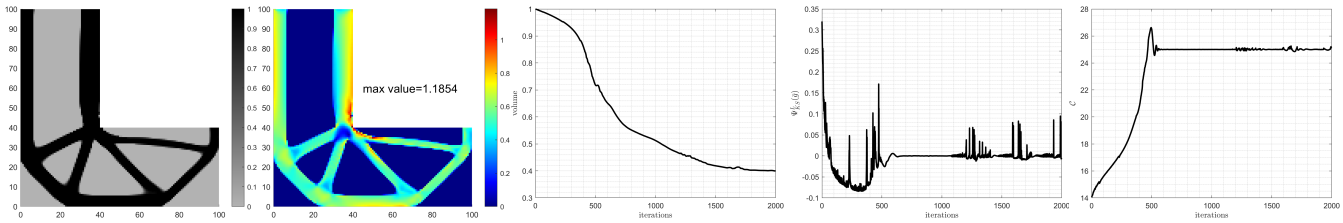

(a) Density field (b) Normalised stress field $\frac{\sigma_{eq}}{\sigma_{lim}}$ (c) volume history (d) Strength $\Psi^L_{KS}(\bar{g})$ history (e) compliance $\mathcal{C}$ history

Figure 5.10: The Results of solving problem ($\overline{\mathbb{P}}_3$) for $\mu = 40$. The final values: $V_{\Omega_{mat}} = 40.01\%$, $\mathcal{C} = 25.00$ mJ, $\frac{\sigma_{eq}^{max}}{\sigma_{lim}} = 1.19$

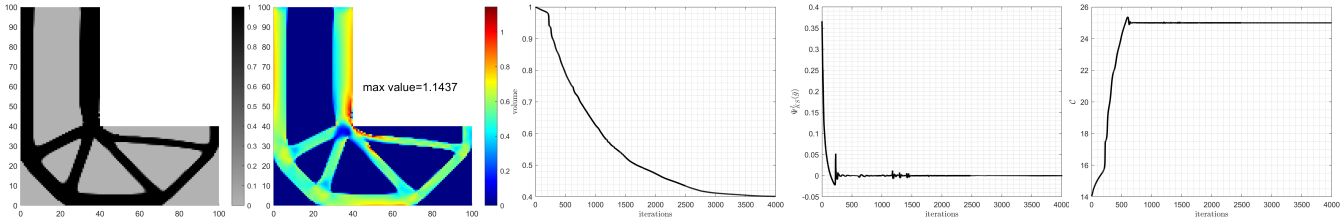

(a) Density field (b) Normalised stress field $\frac{\sigma_{eq}}{\sigma_{lim}}$ (c) volume history (d) Strength $\Psi^L_{KS}(\bar{g})$ history (e) compliance $\mathcal{C}$ history

Figure 5.11: The Results of solving problem ($\overline{\mathbb{P}}_3$) for $\mu = 50$. The final values: $V_{\Omega_{mat}} = 40.13\%$, $\mathcal{C} = 25.00$ mJ, $\frac{\sigma_{eq}^{max}}{\sigma_{lim}} = 1.14$

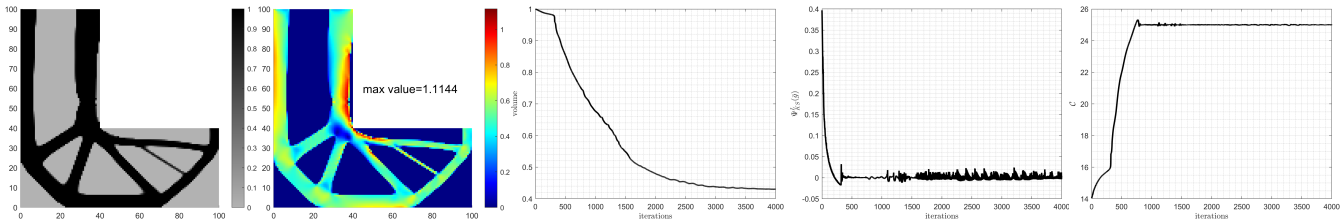

(a) Density field (b) Normalised stress field $\frac{\sigma_{eq}}{\sigma_{lim}}$ (c) volume history (d) Strength $\Psi^L_{KS}(\bar{g})$ history (e) compliance $\mathcal{C}$ history

Figure 5.12: The Results of solving problem ($\overline{\mathbb{P}}_3$) for $\mu = 60$. The final values: $V_{\Omega_{mat}} = 43.03\%$, $\mathcal{C} = 25.00$ mJ, $\frac{\sigma_{eq}^{max}}{\sigma_{lim}} = 1.11$

The results are illustrated in figure 5.10, 5.11 and 5.12 for $\mu = \{40, 50, 60\}$ respectively. The final volume is higher due to the presence of stiffness constraint. The maximum values of the equivalent stress field is higher than the ones obtained with problem ($\overline{\mathbb{P}}_2$). This is explained by the fact that the aggregated strength constraint is evaluated over larger volume Ω_{mat}. It is also due the fact that the stress field is not close to 1 over all Ω_{mat} unlike what's found after solving problem ($\overline{\mathbb{P}}_2$). In any case, the same effect is present: the greater the μ, the closer the maximum normalised Von Mises stress is to 1.

Looking to convergence history, one can see that it is faster because the minimum volume, imposed by stiffness constraint, is more than sufficient to satisfy the aggregated strength constraint. At the beginning, the stiffness inequality constraint is satisfied thus, it was inactive. As a result of the decrease in volume, compliance increases until it reaches the required (imposed) value, then remains close to this value; the stiffness inequality constraint remains therefore close to saturation. The mechanism of deactivating and saturating the inequality constraints is driven by the slack variables. For the aggregated strength constraints, some peaks are observed in their convergence history especially in figure 5.10 (where they are more present). It is explained by the fact to step τ was little higher than it needs to be (τ was higher in 5.10 thus, fast convergence and many peaks). As it is mentioned before, to avoid the problems caused by these peaks, the step τ must be chosen small enough and the descent direction must be normalised with respect to its max value (see algorithm 2). The figure 5.14 show the the influence of the constraints on the obtained optimal design from the volume minimisation problem.

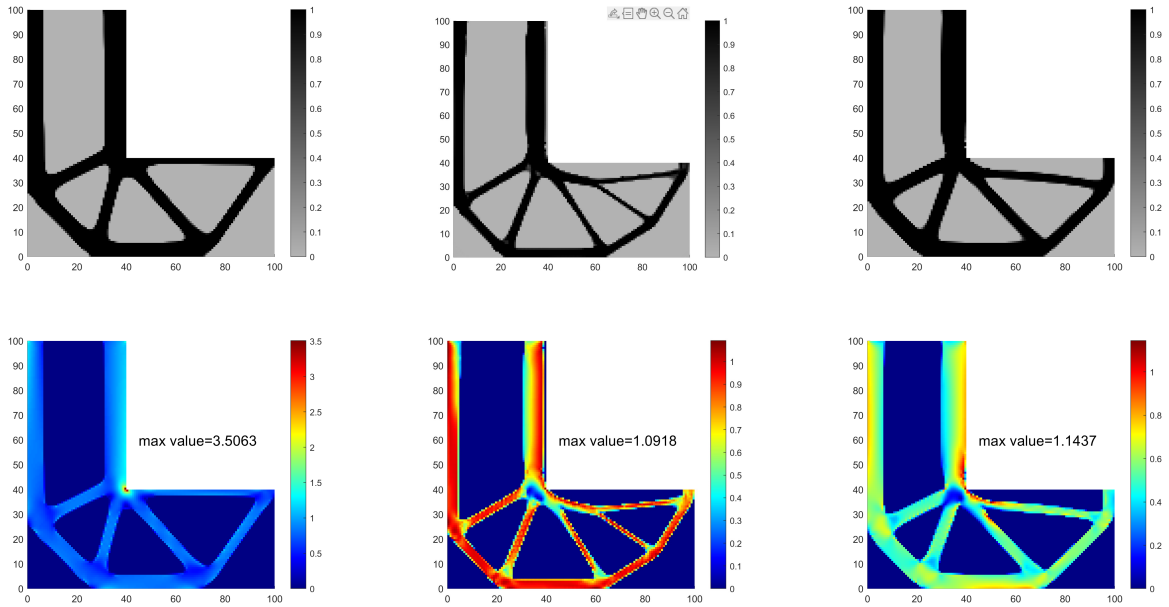

Problem $\overline{\mathbb{P}}_1$: $V_{\Omega_{mat}} = 38.15\%$, $\mathcal{C} = 25$ mJ, $\frac{\sigma_{eq}^{max}}{\sigma_{lim}} = 3.60$

Problem $\overline{\mathbb{P}}_2$: $V_{\Omega_{mat}} = \%$, $\mathcal{C} = 36.05$ mJ, $\frac{\sigma_{eq}^{max}}{\sigma_{lim}} = 1.09$

Problem $\overline{\mathbb{P}}_3$: $V_{\Omega_{mat}} = 40.13\%$, $\mathcal{C} = 25$ mJ, $\frac{\sigma_{eq}^{max}}{\sigma_{lim}} = 1.14$

Figure 5.14: Influence of the optimisation problem ($\overline{\mathbb{P}}_1$, $\overline{\mathbb{P}}_2$ and $\overline{\mathbb{P}}_3$) with an isotropic material and a Von Mises criterion.

5.5.2 Stress based topology optimisation with isotropic stiffness and fixed anisotropic strength

A particular case where the stiffness is isotropic and the strength is anisotropic is treated for problems $\overline{\mathbb{P}}_2$ and $\overline{\mathbb{P}}_3$. It important to keep in mind that this case is possible, an example is given in an additive manufacturing application [128]. The same L-shaped beam problem is considered (details are available in table 5.2). For mechanical strength, the Tsai-Wu threshold criterion (TW2) is considered. Its implementation is possible using the safety factor (see section 5.3.3). Both problems ($\overline{\mathbb{P}}_2$) and ($\overline{\mathbb{P}}_3$) will be solved for $\mu = 50$. The following material and problem parameters are given in the following table:

E [MPa]	ν	$\underline{t}$ [N]
69.7	0.29	40

Table 5.3: Problem parameters

X_t [MPa]	X_c [MPa]	Y_t [MPa]	Y_c [MPa]	S [MPa]
79.2	140	118.4	152	40

Table 5.4: Tsai-Wu material parameters

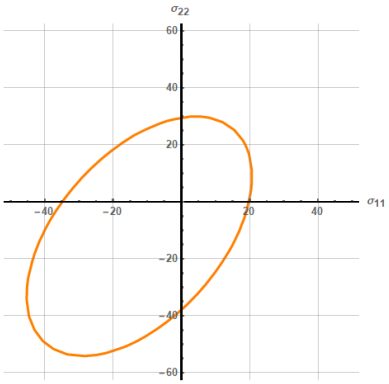

Figure 5.15: The ($\sigma_{11} - \sigma_{22}$) plane cut of the TW2 threshold surface associated to mentioned parameters in table 5.4)

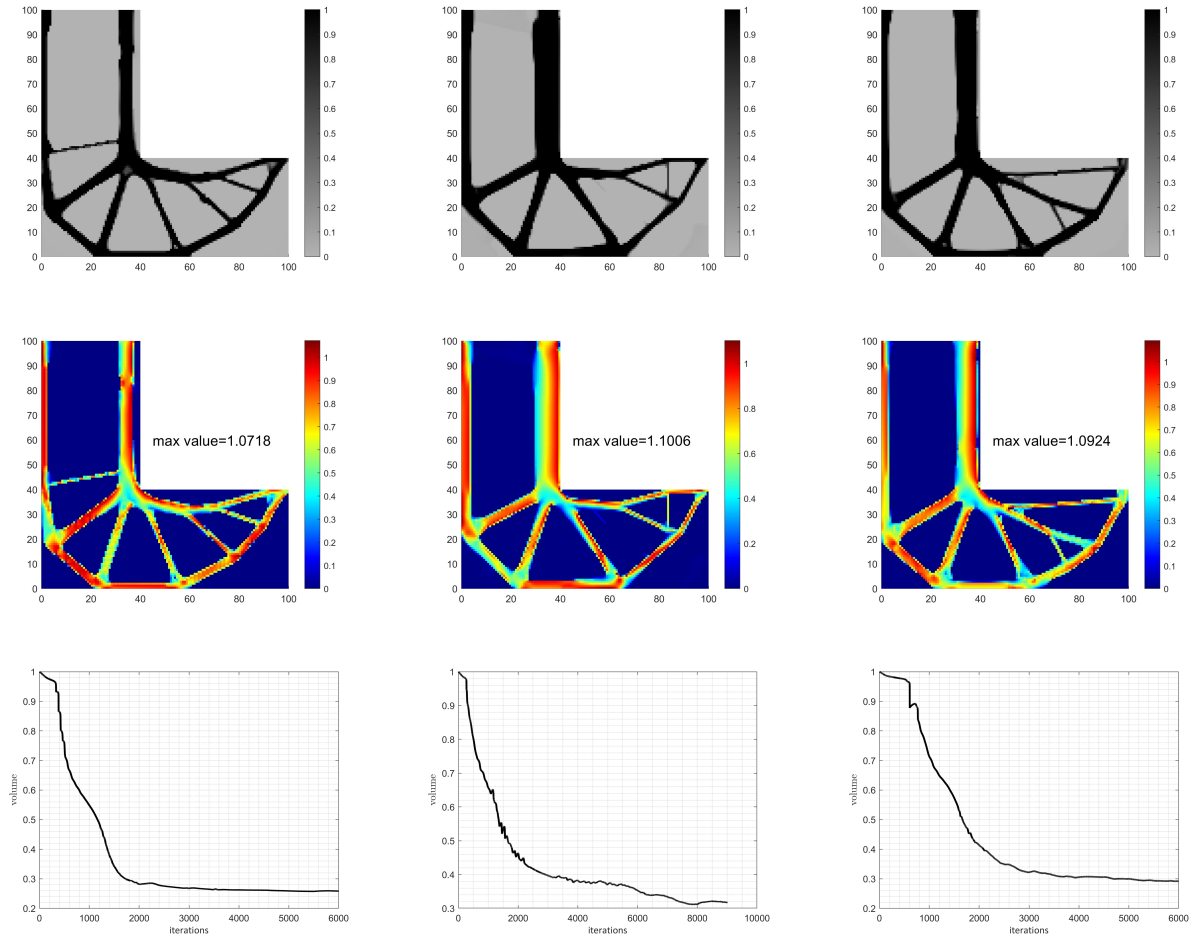

θ=0° ,$V_{\Omega_{mat}} = 25.89\%$, $\mathcal{C} = 8.94$ mJ, $\left(\frac{1}{\kappa}\right)_m ax = 1.07$

θ=60° ,$V_{\Omega_{mat}} = 31.72\%$, $\mathcal{C} = 6.77$ mJ, $\left(\frac{1}{\kappa}\right)_m ax = 1.10$

θ=90° ,$V_{\Omega_{mat}} = 29.18\%$, $\mathcal{C} = 7.63$ mJ, $\left(\frac{1}{\kappa}\right)_m ax = 1.09$

Figure 5.18: The Results of solving problem ($\overline{\mathbb{P}}_2$) considering Tsai-Wu criterion for $\mu = 50$ and for the material orientations: 0°, 60° and 90° . The first row of figures are density field. The second row, $\frac{1}{\kappa}$ strength indicator field. The volume history.

The figure 5.18 shows the results (problem ($\overline{\mathbb{P}}_2$)) for the three material orientations 0°, 60° and 90°. By changing the orientation different optimal designs and TW2 fields are obtained however, they remain similar. This because the micro stress tensor field σ^{mic} does not change with the orientation due the fact that the stiffness is isotropic.

The figure 5.18 illustrates the results (problem ($\overline{\mathbb{P}}_3$)) for the three material orientations 0°, 60° and 90°. where, this time, rigidity constraint is imposed. Same as before the results are different for each orientation, however some similarities are present due to isotropic stiffness. Looking at $\frac{1}{\kappa}$ strength indicator field, some tension/compression dissymmetry are present some parts of the optimal design. This is clearer in the upper part of the design space, where the $\frac{1}{\kappa}$ field on the left (compression) is less pronounced than on the right (tension).

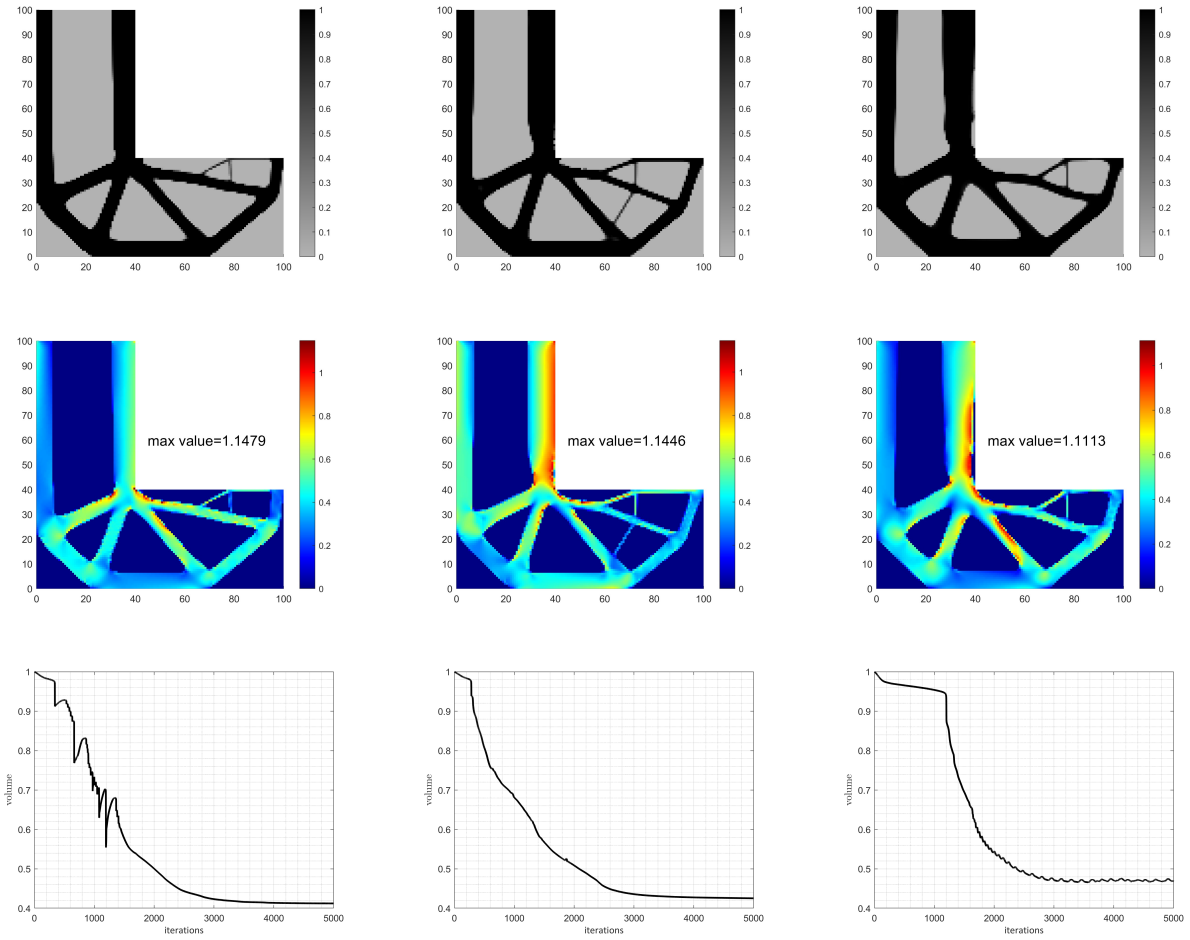

θ=0° ,$V_{\Omega_{mat}} = 41.26\%$, $\mathcal{C} = 4.5$ mJ, $\left(\frac{1}{\kappa}\right)_{max} = 1.14$

θ=60° ,$V_{\Omega_{mat}} = 42.56\%$, $\mathcal{C} = 4.5$ mJ, $\left(\frac{1}{\kappa}\right)_{max} = 1.14$

θ=90° ,$V_{\Omega_{mat}} = 46.86\%$, $\mathcal{C} = 4.5$ mJ, $\left(\frac{1}{\kappa}\right)_{max} = 1.11$

Figure 5.21: The Results of solving problem ($\overline{\mathbb{P}}_2$) considering Tsai-Wu criterion for $\mu = 50$ and for the material orientations: 0°, 60° and 90° . The first row of figures are density field. The second row, $\frac{1}{\kappa}$ strength indicator field. The volume history.

5.6 Synthesis

The following statements allow to summarise this chapter:

- For pedagogical purposes, the general framework of augmented Lagrangian is explained in a concise manner. An algorithm is provided to solve a general constrained optimisation problem.
- Three volume minimisation problems with different constraints (stiffness and strength constraints only) has been solved. the augmented Lagrangian algorithm allowed condensing the three optimisation problems into one main parametric problem. For the strength constraints all details about threshold functions, aggregation and addressing numerical issues were explained. An explicit algorithm is provided for both topology optimisation and concurrent topology and orientation optimisation (in case of included anisotropy).
- Some results are discussed L-shaped beam elasticity. Interesting designs with rounded corner were obtained for both problem 1 and problem 2. Only the topology optimisation is performed for the two following cases:
  1. The first case is the topology optimisation considering isotropic stiffness and isotropic mechanical strength (Von Mises threshold criterion). A closer look was given the influence of the aggregation parameter and the constraints.
  2. The second case is the topology optimisation considering isotropic stiffness and fixed anisotropic mechanical strength (TW2 threshold criterion). Different results were obtained for different orientations. The designs obtained are similar (especially when stiffness constraint is imposed) because the stress tensor field is not affected by the change in orientation due to the isotropic stiffness.

Chapter 6

Conclusion and Perspectives

6.1 Conclusion

The two main objectives of the carried out study in this document were (i) to establish a threshold criterion for lattice then, (ii) to implement it a topology optimisation problem. The purpose is to obtain optimised lattice structure design. With all mentioned work in this document, The first objective was achieved thanks to the proposal and the study of TW4 polynomial threshold function. With regard to the second objective, significant progress has been made, with an algorithm having been proposed and proven to work for stress constrained topology optimisation. What remains to be done is to implement the TW4 function and perform simultaneous topology and orientation optimisation.

In the first part of the study, a review was done about different threshold criteria available in the literature (mostly in plasticity studies of bulk materials), it led us to conclude that there exist some approaches that used to establish a threshold criterion when the anisotropy of the material in known. The main approaches are representation theory, linear transformation and high degree polynomials. For lattice materials, a review is provided, on how some authors manage to establish threshold criteria taking into account plasticity with or without buckling. It was found out that they are non-smooth max functions (thus, non smooth threshold surface) due to using beam theory as model. Tension/compression asymmetry is present when buckling instabilities are taken into account (in parallel with plasticity). It was concluded that to theoretically define a threshold function for lattice materials, polynomials meet all the requirements and may be sufficient to generate at least an approximately smooth threshold surface.

A framework has been established for anisotropy in the stress space. The harmonic basis allows to interpret geometrically a threshold surface with two main point of views: anisotropy and loading symmetry. Mathematically, the links, between writing H-invariant functions from group representation theory and polynomial nth order tensor tensor, is detailed. More precisely we have seen how from representation theory, how to obtain an H-invariant tensor polynomial from a suitable structure tensor (harmonic tensors). However, one step in the process remains tedious, namely the establishment of an integrity base, and as a tool it is neither accessible nor user-friendly for anyone.

Consequently (opposite what is done with representation theory), a general high polynomial threshold function of degree 4 is proposed and named *TW4*. 4 material tensors were present of orders 2, 4, 6, 8 with total of 34 material parameters (which is a lot). However, with the help of harmonic decomposition of all 4 tensor, which is established the three step methodology (section 3.3.2), H-invariant polynomial functions are much easy to establish (by simple eliminations) and it was found out that they are linked to the representation theory. Moreover, all possible threshold surface group symmetries can be found with the clips product (section 3.2.3). Interesting shapes have been found when they are driven by harmonic parameters, making it possible to find possible cases of loading symmetry under hydrostatic pressure. Lastly, approximation of some selected threshold criterion was done in section 3.5, and which validates the obtained results from representation theory in section 3.2.1. The threshold surface established by Jeanneau [102] for 2D equilateral triangular lattice was successfully approximated with only 7 material parameters.

In part 2 of the study, a state of art about topology optimisation was provided. The main approaches on how to parameter the topology of structure (SIMP, level-set) were explained. An overview on different algorithm that are used to solve different optimisation problems were provided. A special attention is brought to augmented Lagrangian which is used to solve all featured problems in our study. For the objective and the constraints, 3 aspects were focused on: volume (or mass), stiffness (rigidity) and mechanical strength.

Speaking mechanical strength, several numerical issues were encountered and addressed by different authors

especially when SIMP method. The stress tensor need to be evaluated differently when intermediate densities are present. Relaxation approaches must be used to avoid singular optima problem. The high number of strength constraints (due to the fact that they are local) will induce an expensive computational cost. Aggregation (using KS-function) remains one of best solution to tackle the problem. Easy to use, it is also used as a relaxation approach which comes makes it more convenient however, some disadvantages are present such us losing control over the design space.

Including anisotropy (stiffness or strength or both), opens the possibility to add (to the topology) more variables to the optimisation problem which allows getting better performance in the obtained optimal designs. It is often performed with SIMP (or homogenisation)method due its simple implementation. The additional variable consists generally of considering the orientation or the material itself the reader is invited to read section for more details 4.6.

The proposed problem in the study, was the volume minimisation subject to aggregated strength and stiffness constraints. The problem was solved by the augmented Lagrangian algorithm using SIMP method. The strategy is that the presence of material, in the design space, means the presence of lattice at the microscale level. For pedagogical purposes, the general framework of the algorithm is explained in a simple manner, explicit algorithm is provided for both topology optimisation and concurrent topology and orientation optimisation. Some obtained results were discussed to validate the algorithm where a close look was paid to the influence of aggregation parameter and to the type of constraints (stiffness and strength). It is important to point out that the implementation of TW4, provided in section 5.3.3, is not yet tested. It is the same thing with the concurrent topology and orientation optimisation.

6.2 Perspectives

As perspectives for the first part of the study, it would be interesting to establish threshold surface for hexachiral 2D lattice, depicted in figure 2.2a, and attempt to approximate its threshold surface taking into account it symmetry classes (which is Z_6). It would also be interesting to impose convexity conditions in the identification process. Bower et al. [37] studied the same quartic polynomial function as TW4 and established convexity conditions. These conditions are necessary but not sufficient, hence it is worth it looking again into it. Lastly, a generalisation to $\mathbb{R}^3$ is possible. It means that the stress tensor $\underset{\sim}{\sigma} \in S^2(\mathbb{R}^3)$. With such tensor space, the rules are little different when it comes to harmonic decomposition where a nth order harmonic tensor will contain $2n+1$ element (parameter). The determination of H-invariant function is possible though it is different where the so-called *Covariant* basis need to be established for each harmonic tensor. More details are found in [137]. It would be even more complicated if Kelvin basis is considered where $\{\underset{\sim}{\sigma}\} \in \mathbb{R}^6$.

As perspectives for the second part, it would be interesting, in case of successful implementation of TW4, to apply a dishomogenisation approach [195, 77] to obtain the optimal lattice structure. Considering a sufficient scale separation, numerical tests must be performed to see if there is conformity with the continuous optimal structure design. Moreover, Jeanneau, in his thesis [102], managed to established an analytical expression between the geometric parameters of the lattice unit cell and the elasticity tensor. For the same set of parameters (geometric), several threshold surfaces can be establish and interpolated. This means that it is possible to use homogenisation method [77] for the problem ($\overline{\mathbb{P}}$) (and for ($\overline{\mathbb{O}}$)). The optimisation with respect to the anisotropy is also possible. Using the polar parameterisation, it is possible to optimise with respect to anisotropic invariant like it was done composite laminate by Ranaivomiarana [146] and Vertonghen [187]. For dishomogenisation, clustering approaches [113, 97] can be used to the optimised lattice structure for optimised elasticity tensor field. It is possible to use Multi-material optimisation where, for example, two lattice materials are considered (e.g. two equilateral triangular lattices with different wall thickness). The fact that it is possible to establish threshold criteria for lattice materials can potentially open up the possibility of finding new coherent designs in terms of mechanical strength.

Part III

Appendices

Appendix A

Orthogonal groups O(2), O(3)

i Basic properties of groups

i.1 Invariant algebra

Let $(\mathbb{V}, \rho)$ be a linear representation of $G = \mathrm{O}(2)$ or $G = \mathrm{SO}(2)$. The action of G on $\mathbb{V}$ induces a linear representation of G on the algebra $\mathbb{R}[\mathbb{V}]$ of polynomials functions on $\mathbb{V}$, which will be denoted by $\star$, and which is given by

$$(g \star p)(\underline{\mathrm{v}}) := p(\rho(g)^{-1}\underline{\mathrm{v}}). \tag{A.1}$$

The invariant algebra of $\mathbb{V}$ under the group G, denoted by $\mathbf{Inv}(\mathbb{V}, G)$ (and more usually by $\mathbb{R}[\mathbb{V}]^G$ in the Mathematical community), is defined as

$$\mathbf{Inv}(\mathbb{V}, G) := \{\, p \in \mathbb{R}[\mathbb{V}], \quad g \star p = p, \, \forall g \in G \,\}.$$

It is a subalgebra of $\mathbb{R}[\mathbb{V}]$, which is furthermore *finitely generated*, thanks to Hilbert's theorem [**? ?**]. Moreover, since the group action on polynomials preserves vector spaces of *homogeneous polynomials of given degrees*, it can always be generated by homogeneous polynomial invariants.

Definition i.1 (Integrity basis)**.** *A finite set of G-invariant homogeneous polynomials $\{ J_1, \ldots, J_N \}$ over $\mathbb{V}$ is a* generating set *(also called an* integrity basis*) of the invariant algebra $\mathbf{Inv}(\mathbb{V}, G)$ if any G-invariant polynomial J over $\mathbb{V}$ is a polynomial function in $J_1, \ldots, J_N$, i.e if J can be written as*

$$J(\underline{\mathrm{v}}) = P(J_1(\underline{\mathrm{v}}), \ldots, J_N(\underline{\mathrm{v}})), \qquad \underline{\mathrm{v}} \in \mathbb{V},$$

where P is a polynomial function in N variables. An integrity basis is minimal *if no proper subset of it is an integrity basis.*

ii The orthogonal group in $\mathbb{R}^2$: O(2)

We have the following properties

Proposition ii.1.

$$\begin{cases} \forall \mathbf{g} \in \mathrm{O}(2), \ \mathbf{g}\mathrm{Z}_k\mathbf{g}^T = \mathrm{Z}_k \\ \forall \mathbf{g} \in \mathrm{O}(2), \ \mathbf{g}\mathrm{D}_k^{\underline{\mathrm{n}}}\mathbf{g}^T = \mathrm{D}_k^{\mathbf{g}\cdot\underline{\mathrm{n}}} \end{cases}$$

Proof. It is sufficient to understand how the generators of each kind of group are transformed by conjugacy.
• Z_k
We have

$$\mathrm{Gen}\,(\mathrm{Z}_k) = \mathbf{r}(\frac{2\pi}{k}) = \mathbf{r}(-\frac{2\pi}{k})$$

Hence

$$\mathrm{Gen}\,(\mathbf{g}\mathrm{Z}_k\mathbf{g}^T) = \mathbf{g}\mathbf{r}(\frac{2\pi}{k})\mathbf{g}^T = \begin{cases} \mathbf{r}(\frac{2\pi}{k}), & \text{if } \det \mathbf{g} = 1 \\ \mathbf{r}(-\frac{2\pi}{k}), & \text{if } \det \mathbf{g} = -1 \end{cases}$$

Since the generator are unchanged, the resulting group is the same.
• $\mathrm{D}_k^{\underline{\mathrm{n}}}$
We have

$$\mathrm{Gen}\,(\mathrm{D}_k^{\underline{\mathrm{n}}}) = \{\mathbf{r}(\frac{2\pi}{k}), \boldsymbol{\pi}(\underline{\mathrm{n}})\} = \{\mathbf{r}(-\frac{2\pi}{k}), \boldsymbol{\pi}(\underline{\mathrm{n}})\}$$

For the rotational generator, the situation has been dealt with. We now need to consider how the mirror line is transformed

$$\mathbf{g}\boldsymbol{\pi}(\underline{\mathrm{n}})\mathbf{g}^T = \mathbf{g}\left(\underset{\sim}{\mathrm{I}} - 2\underline{\mathrm{n}}\otimes\underline{\mathrm{n}}\right)\mathbf{g}^T = \underset{\sim}{\mathrm{I}} - 2(\mathbf{g}\underline{\mathrm{n}})\otimes(\mathbf{g}\underline{\mathrm{n}})$$

Hence

$$\mathrm{Gen}\left(\mathbf{g}\mathrm{D}_k^{\underline{\mathrm{n}}}\mathbf{g}^T\right) = \{\mathbf{r}(\frac{2\pi}{k}), \boldsymbol{\pi}(\mathbf{g}\underline{\mathrm{n}})\} = \mathrm{Gen}\left(\mathrm{D}_k^{\mathbf{g}\underline{\mathrm{n}}}\right)$$

□

It can also be observed that the conugacy modulo O(2) and SO(2) are equivalent.

Remark ii.2. *The following classes* $\{[\mathbb{1}], [\mathrm{Z}_k], [\mathrm{SO}(2)], [\mathrm{O}(2)]\}_{k>1}$ *contain one element, while* $[\mathrm{Z}_2^\pi], [\mathrm{D}_k]$ *contains an infinite number of members. This is partially related to the fact that in* $\mathbb{R}^2$ *all the rotation are along a same* axis. *As soon as axes or planes are to be specified, the conjugation classes will contain an infinite number of elements. Indeed,* $[\mathrm{Z}_k]$ *in* O(3)*, as will be seen later, is a class not reduced to a single element.*

It can be observed that

Proposition ii.3. $\mathrm{Orb}(\underset{\sim}{\sigma}, \mathrm{O}(2)) = \mathrm{Orb}(\underset{\sim}{\sigma}, \mathrm{SO}(2))$

Proof. It sufficient to show that for any $\underset{\sim}{\sigma}$ it exists θ such that

$$\mathbf{r}(\theta)\star\underset{\sim}{\sigma} = \boldsymbol{\pi}(\underline{\mathrm{n}})\star\underset{\sim}{\sigma}$$

This is direct since $\underset{\sim}{\sigma}$ is at least orthotropic, as such, it exists $\underline{\mathrm{v}}$ such aas

$$\boldsymbol{\pi}(\underline{\mathrm{v}})\star\underset{\sim}{\sigma} = \underset{\sim}{\sigma}$$

Hence

$$\boldsymbol{\pi}(\underline{\mathrm{n}})\star\underset{\sim}{\sigma} = \boldsymbol{\pi}(\underline{\mathrm{n}})\star\left(\boldsymbol{\pi}(\underline{\mathrm{v}})\star\underset{\sim}{\sigma}\right) = (\boldsymbol{\pi}(\underline{\mathrm{n}}).\boldsymbol{\pi}(\underline{\mathrm{v}}))\star\underset{\sim}{\sigma}$$

and $\boldsymbol{\pi}(\underline{\mathrm{n}}).\boldsymbol{\pi}(\underline{\mathrm{v}}) \in \mathrm{SO}(2)$. Direct computation shows that θ depends on $\underset{\sim}{\sigma}$ and that

$$\theta = \frac{-2\sigma_{12}}{\sigma_{11} - \sigma_{22}}$$

□

iii The orthogonal group in $\mathbb{R}^3$: O(3)

iii.1 Some theorems

Lemma iii.1. *The action of* O(3) *on* $\mathbb{R}^3$ *can be reduced to* SO(3)*.*

Proof. Consider a non-null vector $\underline{\mathrm{k}}$ of $\mathbb{R}^3$, its symmetry group is $\mathrm{G}_{\underline{\mathrm{k}}} = \mathrm{O}(2)(-, \underline{\mathrm{k}})$. In the notation $\underline{\mathrm{k}}$ indicates the axis of rotational invaraince. This symmetry group also contains mirror planes of symmetry with respect to $\underline{\mathrm{n}}$, with $\underline{\mathrm{n}}\cdot\underline{\mathrm{k}} = 0$. These elements are improper, ie. $\det\boldsymbol{\pi}(\underline{\mathrm{n}}) = -1$. Consider now $\mathbf{g} \in \mathrm{O}(3)/\mathrm{SO}(3)$, that is an improper element of O(3), we have

$$\mathbf{g}\star\underline{\mathrm{k}} = \mathbf{g}\star(\boldsymbol{\pi}(\underline{\mathrm{n}})\star\underline{\mathrm{k}}) = (\mathbf{g}\cdot\boldsymbol{\pi}(\underline{\mathrm{n}}))\star\underline{\mathrm{k}}$$

In the last expression, $\mathbf{g}\cdot\boldsymbol{\pi}(\underline{\mathrm{n}})$ is an element of O(3) whose determinant is 1. There therefore exists a rotation $\mathbf{r} \in \mathrm{SO}(3)$ such that $\mathbf{r} = \mathbf{g}\cdot\boldsymbol{\pi}(\underline{\mathrm{n}})$. Therefore, any element of $\mathbf{g} \in \mathrm{O}(3)/\mathrm{SO}(3)$ is seen as an element of SO(3) by $\underline{\mathrm{k}}$ □

iii.2 subgroups

The following different tables (Table A.1,-A.2,-A.3) detail the physical characteristics of the 32 crystallographic point groups of type I, II and III. In these tables, the correspondence between the Golubtisky's notations and the crystallographers' ones such as the Hermann–Maugin or the Schonflies systems are provided. Note also that the column *System* refers to the Bravais lattice, and *Space Groups* indicates the reference of the space groups having this group as its point group (see [176] for instance).

Type I closed subgroups					
System	Hermann-Maugin	Schonflies	Golubitsky	Nature	Space Groups
Triclinic	1	Z_1	$\mathbb{1}$	CP	1
Monoclinic	2	Z_2	Z_2	CP	3-5
Orthotropic	222	D_2	D_2	C	16-24
Trigonal	3	Z_3	Z_3	CP	143-146
Trigonal	32	D_3	D_3	C	149-155
Tetragonal	4	Z_4	Z_4	CP	75-80
Tetragonal	422	D_4	D_4	C	89-98
Hexagonal	6	Z_6	Z_6	CP	168-173
Hexagonal	622	D_6	D_6	C	177-182
	∞	Z_∞	SO(2)	CP	
	$\infty 2$	D_∞	O(2)	C	
Cubic	23	T	$\mathbb{T}$	C	195-199
Cubic	432	O	$\mathbb{O}$	C	207-214
	532	I	$\mathbb{I}$	C	
	$\infty\infty$		SO(3)	C	

Table A.1: Type I closed subgroups: designation and characteristics (C = Chiral, P=Polar).

Type II closed subgroups					
System	Hermann-Maugin	Schonflies	Golubitsky	Nature	Space Group
Triclinic	$\bar{1}$	Z_i	Z_2^c	I	2
Monoclinic	$2/m$	Z_{2h}	$Z_2 \times Z_2^c$	I	10-15
Orthotropic	mmm	D_{2h}	$D_2 \times Z_2^c$	I	47-74
Trigonal	$\bar{3}$	S_6, Z_{3i}	$Z_3 \times Z_2^c$	I	147-148
Trigonal	$\bar{3}m$	D_{3d}	$D_3 \times Z_2^c$	I	162-167
Tetragonal	$4/m$	Z_{4h}	$Z_4 \times Z_2^c$	I	83-88
Tetragonal	$4/mmm$	D_{4h}	$D_4 \times Z_2^c$	I	123-142
Hexagonal	$6/m$	Z_{6h}	$Z_6 \times Z_2^c$	I	175-176
Hexagonal	$6/mmm$	D_{6h}	$D_6 \times Z_2^c$	I	191-194
	∞/m	$Z_{\infty h}$	$SO(2) \times Z_2^c$	I	
	∞/mm	$D_{\infty h}$	$O(2) \times Z_2^c$	I	
Cubic	$m\bar{3}$	T_h	$\mathbb{T} \times Z_2^c$	I	200-206
Cubic	$m\bar{3}m$	O_h	$\mathbb{O} \times Z_2^c$	I	221-230
	$\bar{5}\bar{3}m$	I_h	$\mathbb{I} \times Z_2^c$	I	
	$\infty/m\infty/m$		O(3)	I	

Table A.2: Type II closed subgroups: designation and characteristics (I = Centrosymetric).

Type III closed subgroups					
System	Hermann-Maugin	Schonflies	Golubitsky	Nature	Space Groups
Monocinic	m	Z_s	Z_2^-	P	6-9
Orthotropic	$2mm$	Z_{2v}	D_2^v	P	25-46
Trigonal	$3m$	Z_{3v}	D_3^v	P	156-161
Tetragonal	$\bar{4}$	S_4	Z_4^-		81-82
Tetragonal	$4mm$	Z_{4v}	D_4^v	P	99-110
Tetragonal	$\bar{4}2m$	D_{2d}	D_4^h		111-122
Hexagonal	$\bar{6}$	Z_{3h}	Z_6^-		174
Hexagonal	$6mm$	Z_{6v}	D_6^v	P	183-186
Hexagonal	$\bar{6}2m$	D_{3h}	D_6^h		187-190
Cubic	$\bar{4}3m$	T_d	O^-		215-220
	∞m	$\mathrm{Z}_{\infty v}$	$\mathrm{O}(2)^-$	P	

Table A.3: Type III closed subgroups: designation and characteristics (P=Polar).

In the following table a set of generators is detailed for each finite O(3)-closed subgroups.

Group	Order	Generators
Z_2^-	2	$\boldsymbol{\pi}(\underline{\mathrm{e}}_3)$
$\mathrm{Z}_n,\ n \geq 2$	n	$\mathbf{r}\left(\underline{\mathrm{e}}_3; {}^{2\pi}/_{n}\right)$
$\mathrm{D}_n,\ n \geq 2$	$2n$	$\mathbf{r}\left(\underline{\mathrm{e}}_3; {}^{2\pi}/_{n}\right),\ \mathbf{r}(\underline{\mathrm{e}}_1; \pi)$
$\mathrm{Z}_{2n}^-,\ n \geq 2$	$2n$	$-\mathbf{r}\left(\underline{\mathrm{e}}_3; {}^{\pi}/_{n}\right)$
$\mathrm{D}_{2n}^h,\ n \geq 2$	$4n$	$-\mathbf{r}\left(\underline{\mathrm{e}}_3; {}^{\pi}/_{n}\right),\ \mathbf{r}(\underline{\mathrm{e}}_1, \pi)$
$\mathrm{D}_n^v,\ n \geq 2$	$2n$	$\mathbf{r}\left(\underline{\mathrm{e}}_3; {}^{2\pi}/_{n}\right),\ \boldsymbol{\pi}(\underline{\mathrm{e}}_1)$
$\mathbb{T}$	12	$\mathbf{r}(\underline{\mathrm{e}}_3; \pi),\ \mathbf{r}(\underline{\mathrm{e}}_1; \pi),\ \mathbf{r}(\underline{\mathrm{e}}_1 + \underline{\mathrm{e}}_2 + \underline{\mathrm{e}}_3; {}^{2\pi}/_{3})$
$\mathbb{O}$	24	$\mathbf{r}(\underline{\mathrm{e}}_3; {}^{\pi}/_{2}),\ \mathbf{r}(\underline{\mathrm{e}}_1; \pi),\ \mathbf{r}(\underline{\mathrm{e}}_1 + \underline{\mathrm{e}}_2 + \underline{\mathrm{e}}_3; {}^{2\pi}/_{3})$
$\mathbb{O}^-$	24	$-\mathbf{r}(\underline{\mathrm{e}}_3; {}^{\pi}/_{2}),\ \boldsymbol{\pi}(\underline{\mathrm{e}}_2 - \underline{\mathrm{e}}_3)$
$\mathbb{I}$	60	$\mathbf{r}(\underline{\mathrm{e}}_3; \pi),\ \mathbf{r}(\underline{\mathrm{e}}_1 + \underline{\mathrm{e}}_2 + \underline{\mathrm{e}}_3; {}^{2\pi}/_{3}), \mathbf{r}(\underline{\mathrm{e}}_1 + \phi\underline{\mathrm{e}}_3; {}^{2\pi}/_{5}) \quad \phi := (1+\sqrt{5})/2$

Table A.4: Generators of finite closed O(3)-subgroups.

Appendix B

Explicit harmonic decomposition

i The CGHD of $\mathbb{W}_4$

First let us introduce the following notation:

$$\underset{\approx}{\mathrm{A}}\cdot^{8}(\underset{\sim}{\rho}\otimes\underset{\sim}{\sigma}\otimes\underset{\sim}{\tau}\otimes\underset{\sim}{\eta})=\underset{\sim}{\rho}:(\underset{\sim}{\sigma}:\underset{\approx}{\mathrm{A}}:\underset{\sim}{\eta}):\underset{\sim}{\tau} \tag{B.1}$$

which reads, in components,

$$A_{(ij)(kl)(mn)(op)}\sigma_{(ij)}\rho_{(kl)}\tau_{(km)}\eta_{(op)}$$

Here, only the case $\underset{\sim}{\sigma}=\underset{\sim}{\rho}=\underset{\sim}{\tau}=\underset{\sim}{\eta}$ will be considered, which leads to

$$A_{\underline{(ij)}\ \underline{(kl)}\ \underline{(mn)}\ \underline{(op)}}\sigma_{(ij)}\sigma_{(kl)}\sigma_{(km)}\sigma_{(op)} \tag{B.2}$$

The coefficients of the fourth-order polynomial in $\underset{\sim}{\sigma}$ are contained in the 8th-order tensor $\underset{\approx}{\mathrm{A}}\in\mathbb{W}_4$. We recall that this space has the following structure $\mathbb{W}_4=S^4(S^2(\mathbb{R}^2))$. The index symmetry group of $\underset{\approx}{\mathrm{A}}$ is

$$\mathbb{G}(\underset{\approx}{\mathrm{A}})=\mathfrak{S}_4\otimes\mathrm{Z}_2.$$

where $\mathfrak{S}_4$ is the symmetric group on 4 elements and corresponds to the permutation of the underlines blocks appearing in Equation 3.6. The group Z_2 corresponds to the index symmetries of $\underset{\sim}{\sigma}$ indicated by parentheses in Equation 3.6. The resulting number of index symmetries of $\underset{\approx}{\mathrm{A}}$ is $\#\mathbb{G}(\underset{\approx}{\mathrm{A}})=4!.2^4=384$ and a set of generators of $\mathbb{G}(\underset{\approx}{\mathrm{A}})$ is given by:

$$\mathrm{Gen}\left(\mathbb{G}(\underset{\approx}{\mathrm{A}})\right)=\{(12),(13)(24),(15)(26),(17)(28)\}\,.$$

Knowing $\mathbb{G}(\underset{\approx}{\mathrm{A}})$, let us establish the harmonic decomposition of $\underset{\approx}{\mathrm{A}}$.

Let's apply the algorithm introduced in subsection 3.3.2 to the current situation. The first step has already been done in subsection 3.3.3. Hence only the second and the third steps will be considered.

i.1 Block decomposition of $\underset{\approx\approx\approx}{\mathrm{A}}$

The introduction of the decomposition $\underset{\sim}{\sigma}$ in Equation B.2 induces the following partition

$$
\begin{aligned}
\underset{\sim}{\sigma} : (\underset{\sim}{\sigma} : \underset{\approx\approx\approx}{\mathrm{A}} : \underset{\sim}{\sigma}) : \underset{\sim}{\sigma} = (\underset{\sim}{\sigma}^{(2)} + \underset{\sim}{\sigma}^{(0)}) : \Big[(\underset{\sim}{\sigma}^{(2)} + \underset{\sim}{\sigma}^{(0)}) : \underset{\approx\approx\approx}{\mathrm{A}} : (\underset{\sim}{\sigma}^{(2)} + \underset{\sim}{\sigma}^{(0)}) \Big] : (\underset{\sim}{\sigma}^{(2)} + \underset{\sim}{\sigma}^{(0)}),& \\
= \underset{\sim}{\sigma}^{(2)} : (\underset{\sim}{\sigma}^{(2)} : \underset{\approx\approx\approx}{\mathrm{A}} : \underset{\sim}{\sigma}^{(2)}) : \underset{\sim}{\sigma}^{(2)}& \\
+ \underset{\sim}{\sigma}^{(2)} : (\underset{\sim}{\sigma}^{(2)} : \underset{\approx\approx\approx}{\mathrm{A}} : \underset{\sim}{\sigma}^{(2)}) : \underset{\sim}{\sigma}^{(0)} + \underset{\sim}{\sigma}^{(2)} : (\underset{\sim}{\sigma}^{(2)} : \underset{\approx\approx\approx}{\mathrm{A}} : \underset{\sim}{\sigma}^{(0)}) : \underset{\sim}{\sigma}^{(2)} + \underset{\sim}{\sigma}^{(2)} : (\underset{\sim}{\sigma}^{(0)} : \underset{\approx\approx\approx}{\mathrm{A}} : \underset{\sim}{\sigma}^{(2)}) : \underset{\sim}{\sigma}^{(2)} + \underset{\sim}{\sigma}^{(0)} : (\underset{\sim}{\sigma}^{(2)} : \underset{\approx\approx\approx}{\mathrm{A}} : \underset{\sim}{\sigma}^{(2)}) : \underset{\sim}{\sigma}^{(2)}& \\
+ \underset{\sim}{\sigma}^{(2)} : (\underset{\sim}{\sigma}^{(2)} : \underset{\approx\approx\approx}{\mathrm{A}} : \underset{\sim}{\sigma}^{(0)}) : \underset{\sim}{\sigma}^{(0)} + \underset{\sim}{\sigma}^{(2)} : (\underset{\sim}{\sigma}^{(0)} : \underset{\approx\approx\approx}{\mathrm{A}} : \underset{\sim}{\sigma}^{(2)}) : \underset{\sim}{\sigma}^{(0)} + \underset{\sim}{\sigma}^{(0)} : (\underset{\sim}{\sigma}^{(2)} : \underset{\approx\approx\approx}{\mathrm{A}} : \underset{\sim}{\sigma}^{(2)}) : \underset{\sim}{\sigma}^{(0)} + \underset{\sim}{\sigma}^{(2)} : (\underset{\sim}{\sigma}^{(0)} : \underset{\approx\approx\approx}{\mathrm{A}} : \underset{\sim}{\sigma}^{(0)}) : \underset{\sim}{\sigma}^{(2)} + \underset{\sim}{\sigma}^{(0)} : (\underset{\sim}{\sigma}^{(2)} : \underset{\approx\approx\approx}{\mathrm{A}}& \\
+ \underset{\sim}{\sigma}^{(2)} : (\underset{\sim}{\sigma}^{(0)} : \underset{\approx\approx\approx}{\mathrm{A}} : \underset{\sim}{\sigma}^{(0)}) : \underset{\sim}{\sigma}^{(0)} + \underset{\sim}{\sigma}^{(0)} : (\underset{\sim}{\sigma}^{(2)} : \underset{\approx\approx\approx}{\mathrm{A}} : \underset{\sim}{\sigma}^{(0)}) : \underset{\sim}{\sigma}^{(0)} + \underset{\sim}{\sigma}^{(0)} : (\underset{\sim}{\sigma}^{(0)} : \underset{\approx\approx\approx}{\mathrm{A}} : \underset{\sim}{\sigma}^{(2)}) : \underset{\sim}{\sigma}^{(0)} + \underset{\sim}{\sigma}^{(0)} : (\underset{\sim}{\sigma}^{(0)} : \underset{\approx\approx\approx}{\mathrm{A}} : \underset{\sim}{\sigma}^{(0)}) : \underset{\sim}{\sigma}^{(2)}& \\
+ \underset{\sim}{\sigma}^{(0)} : (\underset{\sim}{\sigma}^{(0)} : \underset{\approx\approx\approx}{\mathrm{A}} : \underset{\sim}{\sigma}^{(0)}) : \underset{\sim}{\sigma}^{(0)}&
\end{aligned}
\tag{B.3}
$$

This expression can be reformulated from the following property

$$
\underset{\sim}{\sigma}^{(o)} : (\underset{\sim}{\sigma}^{(p)} : \underset{\approx\approx\approx}{\mathrm{A}} : \underset{\sim}{\sigma}^{(q)}) : \underset{\sim}{\sigma}^{(r)} = \underset{\sim}{\sigma}^{(o)} : (\underset{\sim}{\sigma}^{(p)} : \underset{\approx\approx\approx}{\mathrm{A}}^{o,p,q,r} : \underset{\sim}{\sigma}^{(q)}) : \underset{\sim}{\sigma}^{(r)}, \qquad \forall p,q,r \in \{0,2\}.
$$

in which

$$
\underset{\approx\approx\approx}{\mathrm{A}}^{o,p,q,r} = \underset{\approx\approx\approx}{\mathrm{A}} \overset{8}{\circ} (\underset{\approx}{\mathrm{P}}^{o} \otimes \underset{\approx}{\mathrm{P}}^{p} \otimes \underset{\approx}{\mathrm{P}}^{q} \otimes \underset{\approx}{\mathrm{P}}^{r}) \quad \forall o,p,q,r \in \{0,2\} \tag{B.4}
$$

with the definition

$$
\left(\underset{\approx\approx\approx}{\mathrm{A}} \overset{8}{\circ} (\underset{\approx}{\mathrm{O}} \otimes \underset{\approx}{\mathrm{P}} \otimes \underset{\approx}{\mathrm{Q}} \otimes \underset{\approx}{\mathrm{R}}) \right)_{ijklmnop} = A_{pqrstuvw} O_{pqij} P_{rskl} Q_{tumn} R_{vwop}.
$$

Proceeding this way, 16 different blocks have been obtained. As for $\underset{\approx\approx\approx}{\mathrm{B}}$, only the tensors $\underset{\approx\approx\approx}{\mathrm{A}}^{2,2,2,2}$ and $\underset{\approx\approx\approx}{\mathrm{A}}^{0,0,0,0}$ satisfy the index symmetries of $\mathbb{W}_4$. Other blocks have lower symmetries and need to be symmetrised

$$
\begin{aligned}
\underset{\approx\approx\approx}{\mathrm{A}}^{(2222)} &= \underset{\approx\approx\approx}{\mathrm{A}}^{2,2,2,2} \\
\underset{\approx\approx\approx}{\mathrm{A}}^{(2220)} &= \underset{\approx\approx\approx}{\mathrm{A}}^{2,2,2,0} + \underset{\approx\approx\approx}{\mathrm{A}}^{2,2,0,2} + \underset{\approx\approx\approx}{\mathrm{A}}^{2,0,2,2} + \underset{\approx\approx\approx}{\mathrm{A}}^{0,2,2,2)} \\
\underset{\approx\approx\approx}{\mathrm{A}}^{(2200)} &= \underset{\approx\approx\approx}{\mathrm{A}}^{2,2,0,0} + \underset{\approx\approx\approx}{\mathrm{A}}^{2,0,2,0} + \underset{\approx\approx\approx}{\mathrm{A}}^{0,2,2,0} + \underset{\approx\approx\approx}{\mathrm{A}}^{2,0,0,2} + \underset{\approx\approx\approx}{\mathrm{A}}^{0,2,0,2} + \underset{\approx\approx\approx}{\mathrm{A}}^{0,0,2,2} \\
\underset{\approx\approx\approx}{\mathrm{A}}^{(2000)} &= \underset{\approx\approx\approx}{\mathrm{A}}^{2,0,0,0} + \underset{\approx\approx\approx}{\mathrm{A}}^{0,2,0,0} + \underset{\approx\approx\approx}{\mathrm{A}}^{0,0,2,0} + \underset{\approx\approx\approx}{\mathrm{A}}^{0,0,0,2} \\
\underset{\approx\approx\approx}{\mathrm{A}}^{(0000)} &= \underset{\approx\approx\approx}{\mathrm{A}}^{0,0,0,0}
\end{aligned}
$$

At the end,

$$
\underset{\approx\approx\approx}{\mathrm{A}} = \underset{\approx\approx\approx}{\mathrm{A}}^{(2222)} + \underset{\approx\approx\approx}{\mathrm{A}}^{(2220)} + \underset{\approx\approx\approx}{\mathrm{A}}^{(2200)} + \underset{\approx\approx\approx}{\mathrm{A}}^{(2000)} + \underset{\approx\approx\approx}{\mathrm{A}}^{(0000)}
$$

which means that $\mathbb{W}_4$ has been split into 5 orthogonal subspaces, i.e

$$
\mathbb{W}_4 = \mathbb{W}_4^4 \oplus \mathbb{W}_4^3 \oplus \mathbb{W}_4^2 \oplus \mathbb{W}_4^1 \oplus \mathbb{W}_4^0, \qquad (\underset{\approx\approx\approx}{\mathrm{A}}^{(2222)}, \underset{\approx\approx\approx}{\mathrm{A}}^{(2220)}, \underset{\approx\approx\approx}{\mathrm{A}}^{(2200)}, \underset{\approx\approx\approx}{\mathrm{A}}^{(2000)}, \underset{\approx\approx\approx}{\mathrm{A}}^{(0000)}) \in (\mathbb{W}_4^4 \times \mathbb{W}_4^3 \times \mathbb{W}_4^2 \times \mathbb{W}_4^1 \times \mathbb{W}_4^0)
\tag{B.5}
$$

in which the number k in $\mathbb{W}_4^k$ indicates the number of occurrences of the space $\mathbb{K}^2$ in the underlying tensor product. This decomposition should be compared with the expression given by the lemma 3.2.3, i.e.

$$
\mathbb{W}_4 \simeq S^4(\mathbb{K}^2) \oplus S^3(\mathbb{K}^2) \oplus S^2(\mathbb{K}^2) \oplus \mathbb{K}^2 \oplus \mathbb{K}^0 \tag{B.6}
$$

i.2 Clebsch-Gordan harmonic decomposition

The blocks $\underset{\approx\approx\approx}{\mathrm{A}}^{(opqr)}$ we have obtained are not O(2)-irreducible and should therefore be decomposed further. The first step to compute their explicit harmonic decomposition is to determine their harmonic structure. This structure is a consequence of Equation B.5 and Equation B.6. For $\mathbb{W}_4^1$ and $\mathbb{W}_4^0$, the results are straightforward,

$$
\mathbb{W}_4^1 \simeq \mathbb{K}^2, \ \mathbb{W}_4^0 \simeq \mathbb{K}^0,
$$

whereas for the other three spaces, they are obtained by applying the formula of the lemma 3.2.4

$$\mathbb{W}_4^4 \simeq \mathbb{K}^8 \oplus \mathbb{K}^4 \oplus \mathbb{K}^0,\ \mathbb{W}_4^3 \simeq \mathbb{K}^6 \oplus \mathbb{K}^2,\ \mathbb{W}_4^2 \simeq \mathbb{K}^4 \oplus \mathbb{K}^0.$$

It results that the harmonic structure of $\mathbb{W}_4$ is:

$$\mathbb{W}_4 \simeq \mathbb{K}^8 \oplus \mathbb{K}^6 \oplus 2\mathbb{K}^4 \oplus 2\mathbb{K}^2 \oplus 3\mathbb{K}^0, \quad \dim(\mathbb{W}_4) = 15$$

as already known from Proposition 3.2.5 but, now, we know explicitly in which elementary block each harmonic tensor is located.

a) The space $\mathbb{W}_4^0$ Since $\underset{\approx\approx\approx}{\mathrm{A}}^{(0000)} \in \mathbb{W}_4^0 \simeq \mathbb{K}^0$ this term is isotropic and reduces to a unique scalar that will be denoted $\alpha^{8,0}$. Let us insert the expression of $\underset{\approx}{\mathrm{P}}^{(0)}$ into the definition of $\underset{\approx\approx\approx}{\mathrm{A}}^{(0000)}$

$$\begin{aligned}
\underset{\approx\approx\approx}{\mathrm{A}}^{(0000)} &= \underset{\approx\approx\approx}{\mathrm{A}} \overset{8}{\circ} (\underset{\approx}{\mathrm{P}}^{(0)} \otimes \underset{\approx}{\mathrm{P}}^{(0)} \otimes \underset{\approx}{\mathrm{P}}^{(0)} \otimes \underset{\approx}{\mathrm{P}}^{(0)}) = \frac{1}{16} \underset{\approx\approx\approx}{\mathrm{A}} \overset{8}{\circ} \left[(\underset{\sim}{\mathrm{I}} \otimes \underset{\sim}{\mathrm{I}}) \otimes (\underset{\sim}{\mathrm{I}} \otimes \underset{\sim}{\mathrm{I}}) \otimes (\underset{\sim}{\mathrm{I}} \otimes \underset{\sim}{\mathrm{I}}) \otimes (\underset{\sim}{\mathrm{I}} \otimes \underset{\sim}{\mathrm{I}}) \right] \\
&= \frac{1}{16} \left(\underset{\approx\approx\approx}{\mathrm{A}} \overset{8}{\circ} \left[\underset{\sim}{\mathrm{I}} \otimes \underset{\sim}{\mathrm{I}} \otimes \underset{\sim}{\mathrm{I}} \otimes \underset{\sim}{\mathrm{I}} \right] \right) \underset{\sim}{\mathrm{I}} \otimes \underset{\sim}{\mathrm{I}} \otimes \underset{\sim}{\mathrm{I}} \otimes \underset{\sim}{\mathrm{I}} \\
&= \frac{1}{16} \alpha^{8,0} \underset{\sim}{\mathrm{I}} \otimes \underset{\sim}{\mathrm{I}} \otimes \underset{\sim}{\mathrm{I}} \otimes \underset{\sim}{\mathrm{I}} \\
&= \frac{1}{4} \alpha^{8,0} \underset{\approx}{\mathrm{P}}^{(0)} \otimes \underset{\approx}{\mathrm{P}}^{(0)}
\end{aligned}$$

Hence the following parameterisation is obtained

$$\underset{\approx\approx\approx}{\mathrm{A}}^{(0000)} = \frac{1}{4} \alpha^{8,0} \underset{\approx}{\mathrm{P}}^{(0)} \otimes \underset{\approx}{\mathrm{P}}^{(0)},$$

and conversely the scalar we are looking for is determined as

$$\alpha^{8,0} = \underset{\sim}{\mathrm{I}} : (\underset{\sim}{\mathrm{I}} : \underset{\approx\approx\approx}{\mathrm{A}} : \underset{\sim}{\mathrm{I}}) : \underset{\sim}{\mathrm{I}} = \mathrm{tr}_{12}^{(4)}(\underset{\approx\approx\approx}{\mathrm{A}})$$

in which $\mathrm{tr}_{ab}^{(n)}$ stands for the nth-order iterated trace on the index ab, and should not be confused with the n-th power of tr_{ab}.

b) The space $\mathbb{W}_4^1$ The term $\underset{\approx\approx\approx}{\mathrm{A}}^{(2000)} \in \mathbb{W}_4^1$ will be treated in two stages. First the harmonic term $\underset{\approx\approx\approx}{\mathrm{A}}^{2,0,0,0}$ will be proceed, and then its expression symmetrised to obtained $\underset{\approx\approx\approx}{\mathrm{A}}^{(2000)}$.

From its harmonic structure, we know that $\underset{\approx\approx\approx}{\mathrm{A}}^{2,0,0,0}$ is parameterised by a second order harmonic tensor $\underset{\sim}{\mathrm{h}}^{8,1} \in \mathbb{K}^2$. As in the previous paragraph, let's start by inserting the expression for $\underset{\approx}{\mathrm{P}}^{(0)}$ into the definition of $\underset{\approx\approx\approx}{\mathrm{A}}^{2,0,0,0}$.

$$\begin{aligned}
\underset{\approx\approx\approx}{\mathrm{A}}^{2,0,0,0} &= \underset{\approx\approx\approx}{\mathrm{A}} \overset{8}{\circ} (\underset{\approx}{\mathrm{P}}^{(2)} \otimes \underset{\approx}{\mathrm{P}}^{(0)} \otimes \underset{\approx}{\mathrm{P}}^{(0)} \otimes \underset{\approx}{\mathrm{P}}^{(0)}) = \frac{1}{8} \underset{\approx\approx\approx}{\mathrm{A}} \overset{8}{\circ} \left[\underset{\approx}{\mathrm{P}}^{(2)} \otimes (\underset{\sim}{\mathrm{I}} \otimes \underset{\sim}{\mathrm{I}}) \otimes (\underset{\sim}{\mathrm{I}} \otimes \underset{\sim}{\mathrm{I}}) \otimes (\underset{\sim}{\mathrm{I}} \otimes \underset{\sim}{\mathrm{I}}) \right] \\
&= \frac{1}{8} \left(\underset{\approx\approx\approx}{\mathrm{A}} \overset{8}{\circ} \left[\underset{\approx}{\mathrm{P}}^{(2)} \otimes \underset{\sim}{\mathrm{I}} \otimes \underset{\sim}{\mathrm{I}} \otimes \underset{\sim}{\mathrm{I}} \right] \right) \underset{\sim}{\mathrm{I}} \otimes \underset{\sim}{\mathrm{I}} \otimes \underset{\sim}{\mathrm{I}} \\
&= \frac{1}{8} \underset{\sim}{\mathrm{h}}^{8,1} \otimes \underset{\sim}{\mathrm{I}} \otimes \underset{\sim}{\mathrm{I}} \otimes \underset{\sim}{\mathrm{I}} \\
&= \frac{1}{4} \underset{\sim}{\mathrm{h}}^{8,1} \otimes \underset{\sim}{\mathrm{I}} \otimes \underset{\approx}{\mathrm{P}}^{(0)}
\end{aligned}$$

Hence the following parameterisation is obtained

$$\underset{\approx\approx\approx}{\mathrm{A}}^{2,0,0,0} = \frac{1}{4} \underset{\sim}{\mathrm{h}}^{6,1} \otimes \underset{\sim}{\mathrm{I}} \otimes \underset{\approx}{\mathrm{P}}^{(0)},$$

and conversely the harmonic tensor we are looking for is determined as

$$\underset{\sim}{\mathrm{h}}^{8,1} = \underset{\approx}{\mathrm{P}}^{(2)} : (\underset{\sim}{\mathrm{I}} : \underset{\approx\approx\approx}{\mathrm{A}} : \underset{\sim}{\mathrm{I}}) : \underset{\sim}{\mathrm{I}} = \underset{\approx}{\mathrm{P}}^{(2)} : \left(\mathrm{tr}_{12}^{(3)} (\underset{\approx\approx\approx}{\mathrm{A}}) \right).$$

The parameterisation of $\underset{\approx\approx\approx}{\mathrm{A}}^{(2000)}$ can now be obtained by symmetrisation

$$\begin{aligned} \underset{\approx\approx\approx}{\mathrm{A}}^{(2000)} &= \underset{\approx\approx\approx}{\mathrm{A}}^{2,0,0,0} + \underset{\approx\approx\approx}{\mathrm{A}}^{0,2,0,0} + \underset{\approx\approx\approx}{\mathrm{A}}^{0,0,2,0} + \underset{\approx\approx\approx}{\mathrm{A}}^{0,0,0,2} \\ &= \underbrace{\left(\varsigma_{(e)} + \varsigma_{(13)(24)} + \varsigma_{(15)(26)} \right) + \varsigma_{(17)(28)}}_{\tau_4} \star \underset{\approx\approx\approx}{\mathrm{A}}^{2,0,0,0} \end{aligned}$$

in which τ_4 is the symmetrisation operator from $\mathbb{K}^2 \otimes S^3(\mathbb{R}^2)$ to $\mathbb{W}_4^1$.

c) The space $\mathbb{W}_4^2$ As for the previous situation, the term $\underset{\approx\approx\approx}{\mathrm{A}}^{(2200)} \in \mathbb{W}_4^2$ will be treated in two stages. First the harmonic term $\underset{\approx\approx\approx}{\mathrm{A}}^{2,2,0,0}$ will be proceed, and then its expression symmetrised to obtained $\underset{\approx\approx\approx}{\mathrm{A}}^{(2200)}$. The harmonic structure of $\underset{\approx\approx\approx}{\mathrm{A}}^{2,2,0,0}$ contains two terms $\underset{\approx}{\mathrm{H}}^{8,2} \in \mathbb{K}^4$ and $\alpha^{8,2} \in \mathbb{K}^0$. The insertion of $\underset{\approx}{\mathrm{P}}^{(0)}$ into the definition of $\underset{\approx\approx\approx}{\mathrm{A}}^{2,2,0,0}$ allows to write

$$\begin{aligned} \underset{\approx\approx\approx}{\mathrm{A}}^{2,2,0,0} &= \underset{\approx\approx\approx}{\mathrm{A}} \overset{8}{\circ} (\underset{\approx}{\mathrm{P}}^{(2)} \otimes \underset{\approx}{\mathrm{P}}^{(2)} \otimes \underset{\approx}{\mathrm{P}}^{(0)} \otimes \underset{\approx}{\mathrm{P}}^{(0)}) = \frac{1}{4} \underset{\approx\approx\approx}{\mathrm{A}} \overset{8}{\cdot} (\underset{\approx}{\mathrm{P}}^{(2)} \otimes \underset{\approx}{\mathrm{P}}^{(2)} \otimes (\underset{\sim}{\mathrm{I}} \otimes \underset{\sim}{\mathrm{I}}) \otimes (\underset{\sim}{\mathrm{I}} \otimes \underset{\sim}{\mathrm{I}})) \\ &= \frac{1}{4} \left[\underset{\approx}{\mathrm{P}}^{(2)} : (\underset{\sim}{\mathrm{I}} : \underset{\approx\approx\approx}{\mathrm{A}} : \underset{\sim}{\mathrm{I}}) : \underset{\approx}{\mathrm{P}}^{(2)} \right] \otimes \underset{\sim}{\mathrm{I}} \otimes \underset{\sim}{\mathrm{I}} \\ &= \frac{1}{2} \underset{\approx}{\mathrm{Q}}^{8,2} \otimes \underset{\sim}{\mathrm{I}} \otimes \underset{\sim}{\mathrm{I}} \\ &= \underset{\approx}{\mathrm{Q}}^{8,2} \otimes \underset{\approx}{\mathrm{P}}^{(0)} \end{aligned}$$

The eighth-order tensor $\underset{\approx\approx\approx}{\mathrm{A}}^{2,2,0,0}$ can thus be reduced to a fourth-order one $\underset{\approx}{\mathrm{Q}}^{8,2}$ element of $S^2(\mathbb{K}^2)$, i.e.

$$\underset{\approx}{\mathrm{Q}}^{8,2} = \underset{\approx}{\mathrm{P}}^{(2)} : (\underset{\sim}{\mathrm{I}} : \underset{\approx\approx\approx}{\mathrm{A}} : \underset{\sim}{\mathrm{I}}) : \underset{\approx}{\mathrm{P}}^{(2)} = \underset{\approx}{\mathrm{P}}^{(2)} : \left(\mathrm{tr}_{12}^{(2)} (\underset{\approx\approx\approx}{\mathrm{A}}) \right) : \underset{\approx}{\mathrm{P}}^{(2)},$$

but, unlike the previous situations, this tensor is not O(2)-irreducible and must therefore be redecomposed. Using a procedure described in [13], and recalled in section ii, it can be demonstrated that

$$\underset{\approx}{\mathrm{Q}}^{6,2} = \underset{\approx}{\mathrm{H}}^{6,2} + \frac{\alpha^{6,2}}{2} \underset{\approx}{\mathrm{P}}^{(2)}, \quad \text{with } (\underset{\approx}{\mathrm{H}}^{6,2}, \alpha^{6,2}) \in \mathbb{K}^4 \times \mathbb{K}^0$$

with:

$$\alpha^{6,2} = \underset{\approx}{\mathrm{P}}^{(2)} :: \underset{\approx}{\mathrm{Q}}^{6,2}, \qquad \underset{\approx}{\mathrm{H}}^{6,2} = \underset{\approx}{\mathrm{Q}}^{6,2} - \frac{\alpha^{6,2}}{2} \underset{\approx}{\mathrm{P}}^{(2)},$$

hence, putting all the pieces together,

$$\underset{\approx\approx\approx}{\mathrm{A}}^{2,2,0,0} = \left(\underset{\approx}{\mathrm{H}}^{6,2} + \frac{\alpha^{6,2}}{2} \underset{\approx}{\mathrm{P}}^{(2)} \right) \otimes \underset{\approx}{\mathrm{P}}^{(0)}$$

The ultimate expression is obtained by symmetrising the last one

$$\underset{\approx\approx\approx}{\mathrm{A}}^{(2200)} = \tau_{22} \star \underset{\approx\approx\approx}{\mathrm{A}}^{2,2,0,0}$$

in which

$$\tau_{22} = (\varsigma_{(e)} + \varsigma_{(35)(46)} + \varsigma_{(37)(48)} + \varsigma_{(15)(26)} + \varsigma_{(17)(28)} + \varsigma_{(15)(26)(37)(48)})$$

c) The space $\mathbb{W}_4^3$ As for the previous situations, the term $\underset{\approx\approx\approx}{\mathrm{A}}^{(2220)} \in \mathbb{W}_3^3$ will be treated in two stages. First the harmonic term $\underset{\approx\approx\approx}{\mathrm{A}}^{0,2,2,2}$ will be proceed, and then its expression symmetrised to obtained $\underset{\approx\approx\approx}{\mathrm{A}}^{(2220)}$. The harmonic structure of $\underset{\approx\approx\approx}{\mathrm{A}}^{0,2,2,2}$ is a little more complex because it contains two terms $\underset{\approx\approx\approx}{\mathrm{S}}^{6,3} \in \mathbb{K}^6$ and $\underset{\sim}{\mathrm{h}}^{6,3} \in \mathbb{K}^2$. The insertion of $\underset{\approx}{\mathrm{P}}^{(0)}$ into the definition of $\underset{\approx\approx\approx}{\mathrm{A}}^{0,2,2,2}$ allows to write

$$\begin{aligned}
\underset{\approx\approx\approx}{\mathrm{A}}^{0,2,2,2} &= \underset{\approx\approx\approx}{\mathrm{A}} \overset{8}{\circ} (\underset{\approx}{\mathrm{P}}^{(0)} \otimes \underset{\approx}{\mathrm{P}}^{(2)} \otimes \underset{\approx}{\mathrm{P}}^{(2)} \otimes \underset{\approx}{\mathrm{P}}^{(2)}) = \frac{1}{2}\underset{\approx\approx\approx}{\mathrm{A}} \overset{8}{\cdot} ((\underset{\sim}{\mathrm{I}} \otimes \underset{\sim}{\mathrm{I}}) \otimes \underset{\approx}{\mathrm{P}}^{(2)} \otimes \underset{\approx}{\mathrm{P}}^{(2)} \otimes \underset{\approx}{\mathrm{P}}^{(2)}) \\
&= \frac{1}{2}\underset{\sim}{\mathrm{I}} \otimes \left[\left(\underset{\approx}{\mathrm{P}}^{(2)} : (\underset{\approx\approx\approx}{\mathrm{A}} : \underset{\sim}{\mathrm{I}}) : \underset{\approx}{\mathrm{P}}^{(2)} \right) : \underset{\approx}{\mathrm{P}}^{(2)} \right] \\
&= \frac{1}{2}\underset{\sim}{\mathrm{I}} \otimes \underset{\approx\approx\approx}{\mathrm{Q}}^{8,3}
\end{aligned}$$

The eighth-order tensor $\underset{\approx\approx\approx}{\mathrm{A}}^{0,2,2,2}$ can thus be reduced to a sixth-order one $\underset{\approx\approx\approx}{\mathrm{Q}}^{8,3}$ element of $S^3(\mathbb{K}^2)$, i.e.

$$\underset{\approx\approx\approx}{\mathrm{Q}}^{8,3} = \underset{\approx}{\mathrm{P}}^{(2)} : (\underset{\approx\approx\approx}{\mathrm{A}} : \underset{\sim}{\mathrm{I}}) : \underset{\approx}{\mathrm{P}}^{(2)} = \underset{\approx}{\mathrm{P}}^{(2)} : \left(\mathrm{tr}_{12}(\underset{\approx\approx\approx}{\mathrm{A}}) \right) : \underset{\approx}{\mathrm{P}}^{(2)},$$

but this tensor is not O(2)-irreducible and must therefore be redecomposed. Using a procedure described in [13], and recalled in section ii, it can be demonstrated that

$$\underset{\approx\approx\approx}{\mathrm{Q}}^{8,3} = \underset{\approx\approx\approx}{\mathrm{S}}^{6,3} + \underset{\approx\approx\approx}{\Phi}^{6,3} : \underset{\sim}{\mathrm{h}}^{6,3}, \quad \text{with } (\underset{\approx}{\mathrm{S}}^{6,3}, \underset{\sim}{\mathrm{h}}^{6,3}) \in \mathbb{K}^6 \times \mathbb{K}^2$$

It can be shown that

$$\underset{\approx\approx\approx}{\Phi}^{6,3} : \underset{\sim}{\mathrm{h}}^{6,3} = \frac{1}{3}\tau_3 \star \left[\underset{\sim}{\mathrm{h}}^{6,3} \otimes \underset{\approx}{\mathrm{P}}^{(2)} \right]. \tag{B.7}$$

in which $\tau_3 = (\varsigma_{(e)} + \varsigma_{(13)(24)} + \varsigma_{(15)(26)})$. Once $\underset{\approx\approx\approx}{\Phi}^{6,3}$ identified the converse formula are

$$\underset{\sim}{\mathrm{h}}^{6,3} = \mathrm{tr}_{23}^{(2)}(\underset{\approx\approx\approx}{\mathrm{Q}}^{8,3}), \quad \underset{\approx\approx\approx}{\mathrm{S}}^{6,3} = \underset{\approx\approx\approx}{\mathrm{Q}}^{8,3} - \underset{\approx\approx\approx}{\Phi}^{6,3} : \underset{\sim}{\mathrm{h}}^{6,3}, \tag{B.8}$$

Hence, putting all the pieces together,

$$\underset{\approx\approx\approx}{\mathrm{A}}^{0,2,2,2} = \frac{1}{2}\underset{\sim}{\mathrm{I}} \otimes \left(\underset{\approx\approx\approx}{\mathrm{S}}^{6,3} + \underset{\approx\approx\approx}{\Phi}^{6,3} : \underset{\sim}{\mathrm{h}}^{6,3} \right)$$

The ultimate expression is obtained by symmetrising the last one

$$\underset{\approx\approx\approx}{\mathrm{A}}^{(2220)} = \tau_4 \star \underset{\approx\approx\approx}{\mathrm{A}}^{0,2,2,2}$$

where τ_4 is the symmetrisation operator introduced earlier.

c) The space $\mathbb{W}_4^4$ Unlike the other terms, $\underset{\approx\approx\approx}{\mathrm{A}}^{(2222)} \in \mathbb{W}_4^4$ cannot be reduced to a lower order tensor by contraction with $\underset{\approx}{\mathrm{P}}^{(0)}$. It is minimal for this aspect, although this does not make it O(2)-irreducible. We remind you that:

$$\underset{\approx\approx\approx}{\mathrm{A}}^{(2222)} \simeq \mathbb{K}^8 \oplus \mathbb{K}^4 \oplus \mathbb{K}^0 \tag{B.9}$$

Hence, from the harmonic structure of $\mathbb{W}_4^4$, we know that the harmonic parametrisation is given by three harmonic tensors $\underset{\approx}{\mathrm{E}}^{8,4} \in \mathbb{K}^8$, $\underset{\approx}{\mathrm{H}}^{8,4} \in \mathbb{K}^4$ and $\alpha^{8,4} \in \mathbb{K}^0$ such as

$$\underset{\approx\approx\approx}{\mathrm{A}}^{(2222)} = \underset{\approx\approx\approx}{\mathrm{E}}^{8,4} + \underset{\approx\approx\approx}{\Phi}^{8,4} :: \underset{\approx}{\mathrm{H}}^{8,4} + \alpha^{8,4}\underset{\approx\approx\approx}{\Theta}, \quad \text{with } \left(\underset{\approx\approx\approx}{\mathrm{E}}^{8,4}, \underset{\approx}{\mathrm{H}}^{8,4}, \alpha^{8,4} \right) \in \mathbb{K}^8 \times \mathbb{K}^4 \times \mathbb{K}^0 \tag{B.10}$$

where $\underset{\approx\approx\approx}{\Phi}^{8,3}$ and $\underset{\approx\approx\approx}{\Theta}$ are respectively a 12-th and a 8-th order tensor to be determined which represent, respectively, embeddings from $\mathbb{K}^4$ and $\mathbb{K}^0$ into the tensor space $S^4(\mathbb{K}^2)$.

The same method as in subsection 3.3.3 is applied, it results that

$$\underset{\approx\approx\approx}{\Phi}^{8,4} :: \underset{\approx}{\mathrm{H}}^{8,4} = \tau_2 \star \left(\underset{\approx}{\mathrm{H}}^{8,4} \otimes \underset{\approx}{\mathrm{P}}^2\right) = \frac{1}{2}\left[\underset{\approx}{\mathrm{P}}^2 \otimes \underset{\approx}{\mathrm{H}}^{8,4} + \underset{\approx}{\mathrm{H}}^{8,4} \otimes \underset{\approx}{\mathrm{P}}^2\right], \tag{B.11}$$

$$\alpha^{8,4}\underset{\approx\approx\approx}{\Theta} = \tau_3^\star \left(\alpha^{8,4}\underset{\approx}{\mathrm{P}}^2 \otimes \underset{\approx}{\mathrm{P}}^2\right) = \frac{\alpha^{8,4}}{8}\left[(\underset{\approx}{\mathrm{P}}^2 \otimes \underset{\approx}{\mathrm{P}}^2) + \varsigma_{(35)(46)} \star (\underset{\approx}{\mathrm{P}}^2 \otimes \underset{\approx}{\mathrm{P}}^2) + \varsigma_{(37)(48)} \star (\underset{\approx}{\mathrm{P}}^2 \otimes \underset{\approx}{\mathrm{P}}^2)\right] \tag{B.12}$$

where $\tau_2 = \frac{1}{2}(\varsigma_{(e)} + \varsigma_{(13)(24)(35)(48))})$ and $\tau_3^\star = \frac{1}{3}(\varsigma_{(e)} + \varsigma_{(35)(46)} + \varsigma_{(37)(48)})$.

All this is summarised in the following proposition

Proposition i.1. *The tensor* $\underset{\approx\approx\approx}{\mathrm{A}}$ *admits the uniquely defined Clebsch-Gordan harmonic decomposition associated to the family projectors* $\left(\underset{\approx}{\mathrm{P}}^{(2)}, \underset{\approx}{\mathrm{P}}^{(0)}\right)$*:*

$$\begin{aligned}\underset{\approx\approx\approx}{\mathrm{A}} \;=\; & \underset{\approx\approx\approx}{\mathrm{E}}^{8,4} + \tau_2 \star \left(\underset{\approx}{\mathrm{H}}^{8,4} \otimes \underset{\approx}{\mathrm{P}}^2\right) + \frac{1}{2}\tau_4 \star \left[\underset{\sim}{\mathrm{I}} \otimes \left(\underset{\approx\approx\approx}{\mathrm{S}}^{6,3} + \frac{1}{3}\tau_3 \star \left(\underset{\sim}{\mathrm{h}}^{6,3} \otimes \underset{\approx}{\mathrm{P}}^{(2)}\right)\right)\right] + \tau_{22} \star \left[\left(\underset{\approx}{\mathrm{H}}^{6,2} + \frac{\alpha^{6,2}}{2}\underset{\approx}{\mathrm{P}}^{(2)}\right) \otimes \underset{\approx}{\mathrm{P}}^{(0)}\right] \\ & + \frac{1}{4}\tau_4 \star \left[\underset{\sim}{\mathrm{h}}^{8,1} \otimes \underset{\sim}{\mathrm{I}} \otimes \underset{\approx}{\mathrm{P}}^{(0)}\right] + \frac{1}{4}\alpha^{8,0}\underset{\approx}{\mathrm{P}}^{(0)} \otimes \underset{\approx}{\mathrm{P}}^{(0)} + \alpha^{8,4}\tau_3^\star \star \left(\underset{\approx}{\mathrm{P}}^2 \otimes \underset{\approx}{\mathrm{P}}^2\right),\end{aligned}$$

where $\underset{\sim}{\mathrm{I}}$ *is the identity second order tensor, and with the following symmetrisers:*

- $\tau_2 = \frac{1}{2}(\varsigma_{(e)} + \varsigma_{(13)(24)(35)(48))})$*;*
- $\tau_{22} = (\varsigma_{(e)} + \varsigma_{(35)(46)} + \varsigma_{(37)(48)} + \varsigma_{(15)(26)} + \varsigma_{(17)(28)} + \varsigma_{(15)(26)(37)(48)})$*;*
- $\tau_3 = (\varsigma_{(e)} + \varsigma_{(13)(24)} + \varsigma_{(15)(26)})$*;*
- $\tau_3^\star = \frac{1}{3}(\varsigma_{(e)} + \varsigma_{(35)(46)} + \varsigma_{(37)(48)})$*;*
- $\tau_4 = (\varsigma_{(e)} + \varsigma_{(13)(24)} + \varsigma_{(15)(26)}) + \varsigma_{(17)(28)})$*;*

We have the tensors, $\underset{\approx\approx\approx}{\mathrm{E}}^{8,4} \in \mathbb{K}^8$, $\underset{\approx\approx\approx}{\mathrm{S}}^{8,3} \in \mathbb{K}^6$, $(\underset{\approx}{\mathrm{H}}^{8,4}, \underset{\approx}{\mathrm{H}}^{8,2}) \in (\mathbb{K}^4)^2$, $(\underset{\sim}{\mathrm{h}}^{8,3}, \underset{\sim}{\mathrm{h}}^{8,1}) \in (\mathbb{K}^2)^2$ $(\alpha^{8,4}, \alpha^{8,2}, \alpha^{8,0}) \in (\mathbb{K}^0)^3$. *Those elements are defined from* $\underset{\approx\approx\approx}{\mathrm{A}}$ *as follows:*

$\mathbb{K}^0$	$\mathbb{K}^2$	$\mathbb{K}^4$
$\alpha^{8,0} = \mathrm{tr}^4_{12}(\underset{\approx\approx\approx}{\mathrm{A}})$	$\underset{\sim}{\mathrm{h}}^{8,1} = \underset{\approx}{\mathrm{P}}^{(2)} : (\mathrm{tr}^3_{12}(\underset{\approx\approx\approx}{\mathrm{A}}))$	
$\alpha^{8,2} = \underset{\approx}{\mathrm{Q}}^{8,2} :: \underset{\approx}{\mathrm{P}}^{(2)}$	$\underset{\sim}{\mathrm{h}}^{8,3} = \mathrm{tr}^2_{23}(\underset{\approx\approx\approx}{\mathrm{Q}}^{8,3})$	$\underset{\approx}{\mathrm{H}}^{8,2} = \underset{\approx}{\mathrm{Q}}^{8,2} - \frac{\alpha^{8,2}}{2}\underset{\approx}{\mathrm{P}}^{(2)}$
$\alpha^{8,4} = 2\,\mathrm{tr}_{12}(\mathrm{tr}^3_{23}(\underset{\approx\approx\approx}{\mathrm{A}}^{(2222)}))$		$\underset{\approx}{\mathrm{H}}^{8,4} = \mathrm{tr}_{13}(\mathrm{tr}_{12}(\underset{\approx\approx\approx}{\mathrm{A}}^{(2222)} - \alpha^{8,4}\underset{\approx\approx\approx}{\Theta}))$

$\mathbb{K}^6$	$\mathbb{K}^8$
$\underset{\approx\approx\approx}{\mathrm{S}}^{8,3} = \underset{\approx\approx\approx}{\mathrm{Q}}^{8,3} - \underset{\approx\approx\approx}{\Phi}^{6,3} : \underset{\sim}{\mathrm{h}}^{8,3}$	$\underset{\approx\approx\approx}{\mathrm{E}}^{8,4} = \underset{\approx\approx\approx}{\mathrm{A}}^{(2222)} - \underset{\approx\approx\approx}{\Phi}^{8,4} : \underset{\approx}{\mathrm{H}}^{8,4} - \alpha^{8,4}\underset{\approx\approx\approx}{\Theta}$

where $\underset{\approx}{\mathrm{Q}}^{8,2} = \underset{\approx}{\mathrm{P}}^{(2)} : (\underset{\approx\approx\approx}{\mathrm{A}} : \underset{\sim}{\mathrm{I}}) : \underset{\approx}{\mathrm{P}}^{(2)}$. $\underset{\approx}{\mathrm{Q}}^{8,3} = (\underset{\approx\approx\approx}{\mathrm{A}} : \underset{\sim}{\mathrm{I}}) \overset{6}{\circ} (\underset{\approx}{\mathrm{P}}^{(2)} \otimes \underset{\approx}{\mathrm{P}}^{(2)} \otimes \underset{\approx}{\mathrm{P}}^{(2)})$. *The projectors* $\underset{\approx}{\mathrm{P}}^{(2)}$, $\underset{\approx}{\mathrm{P}}^{(0)}$ *are defined by equation* (2.11). *All blocks* $\underset{\approx\approx\approx}{\mathrm{A}}^{p,q,r,s}$ *are defined by equation* (B.4). $\underset{\approx\approx\approx}{\Phi}^{6,4} : \underset{\approx}{\mathrm{H}}^{8,4}$ *and* $\underset{\approx\approx\approx}{\Theta}$ *are given equations* (B.11) *and* (B.12) *in the appendix i.*

ii Harmonic embedding

Consider $\mathbf{T} \in \mathbb{W}_n$ where $\mathbb{W}_n$ is a space $2n$-th order tensor. We have the isomorphism:

$$\mathbb{W}_n \simeq S^n(\mathbb{K}^2)$$

The index symmetry group of $\mathbf{T} \in \mathbb{W}_n$ is given by:

$$\mathbb{G}(\mathbf{T}) = \mathfrak{S}_n \otimes \mathrm{Z}_2.$$

$$\mathrm{Gen}\left(\mathbb{G}(\mathbf{T}) = \{(12), (13)(24), ..., (1\ (2n-1))(1\ 2n)\}\right.$$

$$\#\mathbb{G}(\mathbb{W}_n) = n!2^n$$

$\mathfrak{S}_n$ is the symmetric group between n elements and Z_2 the cyclic group between 2 elements.

We look for an embedding of $\mathbf{H} \in \mathbb{K}^{2k}$ into $S^n(\mathbb{K}^2)$, denoted by $\Pi(\mathbf{H}, S^n(\mathbb{K}^2))$, or simply Π when the context is clear. To construct such an embedding, we start by considering the $2n$th order tensor $\mathbf{V}$ defined:

$$\mathbf{V} = \mathbf{H} \otimes \underset{\approx}{(\mathrm{P}^2)}^{\otimes q}, \quad \text{with} \mathbf{V} \in \mathbb{V}_{k,n} \simeq \mathbb{K}^{2k} \otimes S^q(S^2(\mathbb{K}^2)) \tag{B.13}$$

in which $q = \frac{n-k}{2}$. The index symmetry group of $\mathbf{V} \in \mathbb{V}_q$ is given by:

$$\mathbb{G}(\mathbf{V}) = \mathfrak{S}_{2k} \times (\mathfrak{S}_q \otimes \mathrm{D}_2).$$

and it contains $(2k)!q!2^3$ elements, i.e.

$$\#\mathbb{G}(\mathbf{V}) = (2k)!q!2^3$$

It should be observed that generally $\mathbb{G}(\mathbf{V})$ is a not a subgroup of $\mathbb{G}(\mathbb{W}_n)$. This is because the harmonic tensor has index symmetries not present in $\mathbb{W}_n$. But $\mathbf{V}$ can be viewed as a particular element of the space $\overline{\mathbb{V}}_{k,n} \simeq S^k(\mathbb{K}^2) \otimes S^q(S^2(\mathbb{K}^2))$, and this time $\mathbb{G}(\overline{\mathbb{V}}_{k,n}) < \mathbb{G}(\mathbb{W}_n)$.

The embedding operator we look for Π is the projection of $\mathbf{V}$ onto $S^n(\mathbb{K}^2)$. It can be obtained using the appropriate Reynolds projector, i.e. as the sum of the index permutations of $\mathbb{G}(\mathbb{W}_n)$:

$$\Pi = \frac{1}{\#\mathbb{G}(\mathbb{W}_n)} \sum_{i=1}^{\#\mathbb{G}(\mathbb{W}_n)} g_i * \mathbf{V} \quad g_i \in \mathbb{G}(\mathbb{W}_n) \tag{B.14}$$

Since by construction $\mathbb{G}(\overline{\mathbb{V}}_{k,n})$ is a subgroup of $\mathbb{G}(\mathbb{W}_n)$, and since $\mathbb{G}(\overline{\mathbb{V}}_{k,n})$ is non-trivial, the number of permutations required can be reduced and *a priori* determined. Hence, by Lagrange Theorem,

$$\mathcal{C}_{k,n} = \frac{\#\mathbb{G}(\mathbb{W}_n)}{\#\mathbb{G}(\overline{\mathbb{V}}_{k,n})} = 2^{n-k-3}\frac{n!}{k!(\frac{n-k}{2})!}$$

in which $\mathcal{C}$ indicates the number of left cosets of $\mathbb{G}(\overline{\mathbb{V}}_{k,n})$ in $\mathbb{G}(\mathbb{W}_n)$. It should be noted that the quotient set $\mathbb{G}(\mathbb{W}_n)/\mathbb{G}(\overline{\mathbb{V}}_{k,n})$ is, generically, not a group. The symmetrisation can hence be reduced to

$$\Pi = \sum_{i=1}^{\#\mathcal{C}_{k,n}} g_i * \mathbf{V} \quad g_i \in \mathcal{C}_{k,n} \tag{B.15}$$

The g_i elements to be considered can be easily determined using a CAS such as Mathematica or GAP. It should be noted that since $\mathbb{G}(\overline{\mathbb{V}}_{k,n}) < \mathbb{G}(\mathbf{V})$, the number of elements to be taken into account in symmetrization can be further reduced.

ii.1 Harmonic embedding of $\mathbb{K}^2 \in S^3(\mathbb{K}^2)$

Consider $\underset{\approx\approx}{\mathrm{T}} \in S^3(\mathbb{K}^2)$, its harmonic parameterisation is realised by two harmonic tensors $\underset{\approx\approx}{\mathrm{S}}^{6,3} \in \mathbb{K}^6$ and $\underset{\sim}{\mathrm{h}}^{6,3} \in \mathbb{K}^2$ such as

$$\underset{\approx\approx}{\mathrm{T}} = \underset{\approx\approx}{\mathrm{S}}^{6,3} + \underset{\approx\approx}{\Phi}^{6,3} : \underset{\sim}{\mathrm{h}}^{6,3},$$

in which $\underset{\approx\approx}{\Phi}^{6,3} \in S^3(\mathbb{K}^2) \otimes \mathbb{K}^2$ is a $8th$-order tensor to be determined.

The index symmetry group of $\mathbb{W}_3$ is

$$\mathbb{G}(\mathbb{W}_3) = \mathfrak{S}_3 \otimes \mathrm{Z}_2.$$

a set of generators of which is given by:

$$\mathrm{Gen}\left(\mathbb{G}(\mathbb{W}_3)\right) = \{(12), (13)(24), (15)(26)\}.$$

which is a group of order 48. Using Mathematica, we can define this group as follows

```
W3=PermutationGroup[{Cycles[{{1, 2}}], Cycles[{{1, 3}, {2, 4}}], Cycles[{{1, 5}, {2, 6}}]}];
```

As obvious the instruction `Cycles[{{}}]` indicates a permutation, and `Cycles[{{1, 3},{2, 4}}]` stands for the operation (13)(24).

The embedding $\underset{\approx\approx}{\Phi}^{6,3} : \underset{\sim}{\mathrm{h}}^{6,3}$ is obtained by some symmetrisation τ of

$$\underset{\approx\approx}{\mathrm{V}} = \underset{\sim}{\mathrm{h}}^{6,3} \otimes \underset{\approx}{\mathrm{P}}^{(2)}$$

The index symmetry group of $\underset{\approx\approx}{\mathrm{V}}$ is given by:

$$\mathbb{G}(\mathbf{V}) = \mathrm{Z}_2 \times \mathrm{D}_2.$$

and it contains 16 elements, i.e.

$$\#\mathbb{G}(\mathbf{V}) = 16$$

Using Mathematica, we can define this group as follows

```
V13=PermutationGroup[{Cycles[{{1, 2}}], Cycles[{{3, 5}, {4, 6}}],  Cycles[{{3, 4}}]}];
```

In this particular case $\mathbb{G}(\mathbf{V})$ is a subgroup of $\mathbb{G}(\mathbb{W}_n)$, as such the left coset approach applies directly, and

$$\mathcal{C}_{1,3} = 3$$

The three left cosets are computed as follows in Mathematica

```
ClasseS3 = Gather[GroupElements[W3], GroupElementQ[V13, PermutationProduct[InversePermutation[#1], #2]]
```

and the following cosert are obtained:

- first coset:

```
{Cycles[{}], Cycles[{{1, 2}}], Cycles[{{3, 4}}], Cycles[{{5, 6}}],
Cycles[{{3, 5, 4, 6}}], Cycles[{{3, 6, 4, 5}}], Cycles[{{1, 2}, {3, 4}}],
Cycles[{{1, 2}, {5, 6}}], Cycles[{{1, 2}, {3, 5, 4, 6}}], Cycles[{{1, 2}, {3, 6, 4, 5}}],
Cycles[{{3, 4}, {5, 6}}], Cycles[{{3, 5}, {4, 6}}], Cycles[{{3, 6}, {4, 5}}],
Cycles[{{1, 2}, {3, 4}, {5, 6}}],  Cycles[{{1, 2}, {3, 5}, {4, 6}}],
Cycles[{{1, 2}, {3, 6}, {4, 5}}]}
```

- second coset:

```
{Cycles[{{1, 3, 2, 4}}], Cycles[{{1, 4, 2, 3}}], Cycles[{{1, 5, 3, 2, 6, 4}}],
Cycles[{{1, 5, 4, 2, 6, 3}}],  Cycles[{{1, 6, 3, 2, 5, 4}}], Cycles[{{1, 6, 4, 2, 5, 3}}],
Cycles[{{1, 3}, {2, 4}}], Cycles[{{1, 4}, {2, 3}}], Cycles[{{1, 5, 3}, {2, 6, 4}}],
Cycles[{{1, 5, 4}, {2, 6, 3}}],  Cycles[{{1, 6, 3}, {2, 5, 4}}], Cycles[{{1, 6, 4}, {2, 5, 3}}],
Cycles[{{1, 3, 2, 4}, {5, 6}}],  Cycles[{{1, 4, 2, 3}, {5, 6}}], Cycles[{{1, 3}, {2, 4}, {5, 6}}],
Cycles[{{1, 4}, {2, 3}, {5, 6}}]}
```

- third coset:

```
{Cycles[{{1, 5, 2, 6}}], Cycles[{{1, 6, 2, 5}}], Cycles[{{1, 3, 5, 2, 4, 6}}],
Cycles[{{1, 3, 6, 2, 4, 5}}], Cycles[{{1, 4, 5, 2, 3, 6}}], Cycles[{{1, 4, 6, 2, 3, 5}}],
 Cycles[{{1, 5}, {2, 6}}], Cycles[{{1, 6}, {2, 5}}], Cycles[{{1, 3, 5}, {2, 4, 6}}],
 Cycles[{{1, 3, 6}, {2, 4, 5}}], Cycles[{{1, 4, 5}, {2, 3, 6}}], Cycles[{{1, 4, 6}, {2, 3, 5}}],
 Cycles[{{1, 5, 2, 6}, {3, 4}}], Cycles[{{1, 6, 2, 5}, {3, 4}}], Cycles[{{1, 5}, {2, 6}, {3, 4}}],
 Cycles[{{1, 6}, {2, 5}, {3, 4}}]}
```

The symmetrisation operator is obtained by choosing a transformation in each coset. Since all the transformations in each coset produce the same effect, let's choose the simplest elements:

$$\{(), (13)(24), (15)(26)\}$$

At the end, the following formula is obtained

$$\underset{\approx\approx}{\Phi}^{6,3} : \underset{\sim}{\mathrm{h}}^{6,3} = \tau_3 \star \left[\underset{\sim}{\mathrm{h}}^{6,3} \otimes \underset{\approx}{\mathrm{P}}^{(2)}\right].$$

with $\tau_3 = \frac{1}{3}(\varsigma_{(e)} + \varsigma_{(13)(24)} + \varsigma_{(15)(26)})$.

To sum up, the determination of the embedding amounts to the search for the symmetrisation of $\mathbf{V}$ such that $\tau \star \mathbf{V} \in \mathbb{W}_n$. The zero trace conditions are satisfied by construction.

ii.2 Harmonic embedding of $\mathbb{K}^4 \in S^4(\mathbb{K}^2)$

Consider $\underset{\approx\approx}{\mathrm{T}} \in S^4(\mathbb{K}^2)$, its harmonic parameterisation is realised by we know that the harmonic parameterisation is given by three harmonic tensors $\underset{\approx}{\mathrm{E}}^{8,4} \in \mathbb{K}^8$, $\underset{\approx}{\mathrm{H}}^{8,4} \in \mathbb{K}^4$ and $\alpha^{8,4} \in \mathbb{K}^0$ such as

$$\underset{\approx\approx}{\mathrm{T}} = \underset{\approx\approx}{\mathrm{E}}^{8,4} + \underset{\approx\approx\approx}{\Phi}^{8,4} :: \underset{\approx}{\mathrm{H}}^{8,4} + \alpha^{8,4} \underset{\approx\approx}{\Theta} \tag{B.16}$$

where $\underset{\approx\approx\approx}{\Phi}^{8,4}$ and $\underset{\approx\approx}{\Theta}$ are respectively a 12-th and a 8-th order tensor to be determined which represent, respectively, embeddings from $\mathbb{K}^4$ and $\mathbb{K}^0$ into the tensor space $S^4(\mathbb{K}^2)$. We will consider here the term $\underset{\approx\approx\approx}{\Phi}^{8,4} :: \underset{\approx}{\mathrm{H}}^{8,4}$.

The index symmetry group of $\mathbb{W}_4$ is

$$\mathbb{G}(\mathbb{W}_4) = \mathfrak{S}_3 \otimes \mathrm{Z}_2.$$

a set of generators of which is:

$$\mathrm{Gen}\left(\mathbb{G}(\mathbb{W}_4)\right) = \{(12), (13)(24), (15)(26)\}.$$

it is a group of order 384. Using Mathematica, this group is set as follows

```
W4=PermutationGroup[{Cycles[{{1, 2}}], Cycles[{{1, 3}, {2, 4}}], Cycles[{{1, 5}, {2, 6}}],
Cycles[{{1, 7}, {2, 8}}]}];
```

The embedding $\underset{\approx\approx\approx}{\Phi}^{8,4} :: \underset{\approx}{\mathrm{H}}^{8,4}$ is obtained by some symmetrisation τ of

$$\underset{\approx\approx\approx}{\mathrm{V}} = \underset{\approx}{\mathrm{H}}^{8,4} \otimes \underset{\approx}{\mathrm{P}}^{(2)}$$

The index symmetry group of $\underset{\approx\approx\approx}{\mathrm{V}}$ is given by:

$$\mathbb{G}(\underset{\approx\approx\approx}{\mathrm{V}}) = \mathfrak{S}_4 \times \mathrm{D}_2.$$

and it contains 192 elements, i.e.

$$\#\mathbb{G}(\underset{\approx\approx\approx}{\mathrm{V}}) = 192$$

Using Mathematica, we can define this group as follows

```
V24 = PermutationGroup[{Cycles[{{1, 2}}], Cycles[{{1, 3}}],
   Cycles[{{2, 4}}],
   Cycles[{{5, 7}, {6, 8}}], Cycles[{{5, 6}}]}]
```

In this case $\mathbb{G}(\underset{\approx\approx\approx}{\mathrm{V}})$ is not a subgroup of $\mathbb{G}(\mathbb{W}_n)$, and the left coset approach can not be directly applied. Let us note anyway that

$$\frac{\#\mathbb{G}(\mathbb{W}_4)}{\#\mathbb{G}(\underset{\approx\approx\approx}{\mathrm{V}})} = 2$$

giving rise to the hope that symmetrisation can be reduced to 2 permutations.

To circumvent this problem, $\underset{\approx\approx\approx}{\mathrm{V}}$ can always be viewed as a particular element of the space $\overline{\mathbb{V}}_{2,4} \simeq S^2(\mathbb{K}^2) \otimes S^2(\mathbb{K}^2)$, and this time $\mathbb{G}(\overline{\mathbb{V}}_{2,4}) < \mathbb{G}(\mathbb{W}_n)$. The left coset approach applies , and

$$\mathcal{C}_{2,4} = 6$$

The sixth left cosets are computed as follows in Mathematica

```
ClasseS6 = Gather[GroupElements[W4], GroupElementQ[V24, PermutationProduct[InversePermutation[#1], #2]]
```

Since each coset contains 64 elements, they will not be reproduced here. Following the set approach as in the previous subsection the following set of representative transformation can be considered

$$\{(), (35)(46), (37)(48), (15)(26), (17)(28), (15)(26)(37)(48)\}$$

Meaning that

$$\mathbb{G}(\mathbb{W}_4) = (e)\mathrm{H} + (35)(46)\mathrm{H} + (37)(48)\mathrm{H} + (15)(26)\mathrm{H} + (17)(28)\mathrm{H} + (15)(26)(37)(48)\mathrm{H}$$

with $\mathrm{H} = \mathbb{G}(\overline{\mathbb{V}}_{2,4})$.

$$\underset{\approx}{\overset{\approx}{\Phi}}^{8,4} :: \underset{\approx}{\mathrm{H}}^{8,4} = \frac{1}{6}\left(\underset{\approx}{\overset{\approx}{\mathrm{V}}} + (35)(46) \star \underset{\approx}{\overset{\approx}{\mathrm{V}}} + (37)(48) \star \underset{\approx}{\overset{\approx}{\mathrm{V}}} + (15)(26) \star \underset{\approx}{\overset{\approx}{\mathrm{V}}} + (17)(28) \star \underset{\approx}{\overset{\approx}{\mathrm{V}}} + (15)(26)(37)(48) \star \underset{\approx}{\overset{\approx}{\mathrm{V}}}\right)$$

Since $\mathbb{G}(\underset{\approx}{\overset{\approx}{\mathrm{V}}}) > \mathbb{G}(\overline{\mathbb{V}}_{2,4})$, the number of terms on the symmetrisation can be reduced.

It can be noticed that

$$(15)(26)(37)(48) \star \underset{\approx}{\overset{\approx}{\mathrm{V}}} = \underset{\approx}{\mathrm{P}}^{(2)} \otimes \underset{\approx}{\mathrm{H}}^{8,4},$$

it results that the index symmetries of $(15)(26)(37)(48) \star \underset{\approx}{\overset{\approx}{\mathrm{V}}}$ are complementary to those of $\underset{\approx}{\overset{\approx}{\mathrm{V}}}$. Same observation can be made with respect to the pairs $(35)(46) \star \underset{\approx}{\overset{\approx}{\mathrm{V}}}, (17)(28) \star \underset{\approx}{\overset{\approx}{\mathrm{V}}}$ and $(37)(48) \star \underset{\approx}{\overset{\approx}{\mathrm{V}}}, (15)(26) \star \underset{\approx}{\overset{\approx}{\mathrm{V}}}$, meaning that

$$\left(\underset{\approx}{\overset{\approx}{\mathrm{V}}} + (15)(26)(37)(48) \star \underset{\approx}{\overset{\approx}{\mathrm{V}}}\right) = \left((35)(46) \star \underset{\approx}{\overset{\approx}{\mathrm{V}}} + (17)(28) \star \underset{\approx}{\overset{\approx}{\mathrm{V}}}\right) = \left((37)(48) \star \underset{\approx}{\overset{\approx}{\mathrm{V}}} + (15)(26) \star \underset{\approx}{\overset{\approx}{\mathrm{V}}}\right)$$

At the end, the following formula is obtained

$$\underset{\approx}{\overset{\approx}{\Phi}}^{8,4} :: \underset{\approx}{\mathrm{H}}^{8,4} = \frac{1}{2}\left((e) + (15)(26)(37)(48)\right) \star \underset{\approx}{\overset{\approx}{\mathrm{V}}} = \tau_2 \star \left(\underset{\approx}{\mathrm{H}}^{8,4} \otimes \underset{\approx}{\mathrm{P}}^{(2)}\right) \tag{B.17}$$

with $\tau_2 = \frac{1}{2}(\varsigma_{(e)} + \varsigma_{(15)(26)(37)(48)})$.

When you look at the final result, you think you could have guessed it beforehand. However, the proposed method is applicable to more general situations and can lead to the development of an algorithm that can be automated.

Appendix C

The 4 solutions of equation (5.51)

$$
\begin{cases}
\kappa_1 = -\dfrac{B}{4A} + \dfrac{1}{2}\sqrt{-\dfrac{4\sqrt[3]{\frac{2}{3}}}{\sqrt[3]{\sqrt{81B^4+768A^3}-9B^2}} + \dfrac{\sqrt[3]{\sqrt{81B^4+768A^3}-9B^2}}{\sqrt[3]{2}3^{2/3}A} + \dfrac{B^2}{4A^2}} - \dfrac{1}{2}\sqrt{\dfrac{4\sqrt[3]{\frac{2}{3}}}{\sqrt[3]{\sqrt{81B^4+768A^3}-9B^2}} + \dfrac{B^2}{2A^2} - \dfrac{\sqrt[3]{\sqrt{81B^4+768A^3}-9B^2}}{\sqrt[3]{2}3^{2/3}A} - \dfrac{B^3}{4A^3\sqrt{-\frac{4\sqrt[3]{\frac{2}{3}}}{\sqrt[3]{\sqrt{81B^4+768A^3}-9B^2}} + \frac{\sqrt[3]{\sqrt{81B^4+768A^3}-9B^2}}{\sqrt[3]{2}3^{2/3}A} + \frac{B^2}{4A^2}}}}}, \\
\kappa_2 = -\dfrac{B}{4A} + \dfrac{1}{2}\sqrt{-\dfrac{4\sqrt[3]{\frac{2}{3}}}{\sqrt[3]{\sqrt{81B^4+768A^3}-9B^2}} + \dfrac{\sqrt[3]{\sqrt{81B^4+768A^3}-9B^2}}{\sqrt[3]{2}3^{2/3}A} + \dfrac{B^2}{4A^2}} + \dfrac{1}{2}\sqrt{\dfrac{4\sqrt[3]{\frac{2}{3}}}{\sqrt[3]{\sqrt{81B^4+768A^3}-9B^2}} + \dfrac{B^2}{2A^2} - \dfrac{\sqrt[3]{\sqrt{81B^4+768A^3}-9B^2}}{\sqrt[3]{2}3^{2/3}A} - \dfrac{B^3}{4A^3\sqrt{-\frac{4\sqrt[3]{\frac{2}{3}}}{\sqrt[3]{\sqrt{81B^4+768A^3}-9B^2}} + \frac{\sqrt[3]{\sqrt{81B^4+768A^3}-9B^2}}{\sqrt[3]{2}3^{2/3}A} + \frac{B^2}{4A^2}}}}}, \\
\kappa_3 = -\dfrac{B}{4A} - \dfrac{1}{2}\sqrt{-\dfrac{4\sqrt[3]{\frac{2}{3}}}{\sqrt[3]{\sqrt{81B^4+768A^3}-9B^2}} + \dfrac{\sqrt[3]{\sqrt{81B^4+768A^3}-9B^2}}{\sqrt[3]{2}3^{2/3}A} + \dfrac{B^2}{4A^2}} - \dfrac{1}{2}\sqrt{\dfrac{4\sqrt[3]{\frac{2}{3}}}{\sqrt[3]{\sqrt{81B^4+768A^3}-9B^2}} + \dfrac{B^2}{2A^2} - \dfrac{\sqrt[3]{\sqrt{81B^4+768A^3}-9B^2}}{\sqrt[3]{2}3^{2/3}A} + \dfrac{B^3}{4A^3\sqrt{-\frac{4\sqrt[3]{\frac{2}{3}}}{\sqrt[3]{\sqrt{81B^4+768A^3}-9B^2}} + \frac{\sqrt[3]{\sqrt{81B^4+768A^3}-9B^2}}{\sqrt[3]{2}3^{2/3}A} + \frac{B^2}{4A^2}}}}}, \\
\kappa_4 = -\dfrac{B}{4A} - \dfrac{1}{2}\sqrt{-\dfrac{4\sqrt[3]{\frac{2}{3}}}{\sqrt[3]{\sqrt{81B^4+768A^3}-9B^2}} + \dfrac{\sqrt[3]{\sqrt{81B^4+768A^3}-9B^2}}{\sqrt[3]{2}3^{2/3}A} + \dfrac{B^2}{4A^2}} + \dfrac{1}{2}\sqrt{\dfrac{4\sqrt[3]{\frac{2}{3}}}{\sqrt[3]{\sqrt{81B^4+768A^3}-9B^2}} + \dfrac{B^2}{2A^2} - \dfrac{\sqrt[3]{\sqrt{81B^4+768A^3}-9B^2}}{\sqrt[3]{2}3^{2/3}A} + \dfrac{B^3}{4A^3\sqrt{-\frac{4\sqrt[3]{\frac{2}{3}}}{\sqrt[3]{\sqrt{81B^4+768A^3}-9B^2}} + \frac{\sqrt[3]{\sqrt{81B^4+768A^3}-9B^2}}{\sqrt[3]{2}3^{2/3}A} + \frac{B^2}{4A^2}}}}}
\end{cases}
$$

Bibliography

[1] W. Achtziger and C Kanzow. Mathematical programs with vanishing constraints: optimality conditions and constraint qualifications. *Mathematical Programming*, 114(1):69–99, 2008.

[2] G. Allaire. *Conception optimale de structures*, volume 58 of *Mathématiques & applications*. Springer Berlin Heidelberg, 2006.

[3] G. Allaire. Optimisation et contrôle. 2021. Lesson notes _eprint: http://www.cmap.polytechnique.fr/ allaire/map435/poly435.pdf.

[4] G. Allaire, Z. Belhachmi, and F. Jouve. The homogenization method for topology and shape optimization. Single and multiple loads case. *Revue Européenne des Éléments Finis*, 5(5-6):649–672, 1996.

[5] G. Allaire, L. Cavallina, N. Miyake, T. Oka, and T. Yachimura. The Homogenization Method for Topology Optimization of Structures: Old and New. *Interdisciplinary Information Sciences*, 25(2):75–146, 2019.

[6] G. Allaire, C. Dapogny, G. Delgado, and G. Michailidis. Multi-phase structural optimization via a level set method. *ESAIM: Control, Optimisation and Calculus of Variations*, 20(2):576–611, 2014. Number: 2 Publisher: EDP Sciences.

[7] G. Allaire, P. Geoffroy-Donders, and O. Pantz. Topology optimization of modulated and oriented periodic microstructures by the homogenization method. *Computers & Mathematics with Applications*, 78(7):2197–2229, 2019.

[8] G. Allaire and F. Jouve. Minimum stress optimal design with the level set method. *Engineering Analysis with Boundary Elements*, 32(11):909–918, 2008.

[9] G. Allaire, F. Jouve, and A. Toader. A level-set method for shape optimization. *Comptes Rendus Mathematique*, 334(12):1125–1130, 2002.

[10] M. Alnæs, A. Logg, K. Ølgaard, M. Rognes, and G. Wells. Unified form language: A domain-specific language for weak formulations of partial differential equations. *ACM Transactions on Mathematical Software*, 40(2):1–37, 2014.

[11] M. Armstrong. *Groups and symmetry*. Springer Science & Business Media, 1997.

[12] M. Ashby. Designing architectured materials. *Scripta Materialia*, 68(1):4–7, 2013.

[13] N. Auffray, H. Abdoul-Anziz, and B. Desmorat. Explicit harmonic structure of bidimensional linear strain-gradient elasticity. *European Journal of Mechanics - A/Solids*, 87:104202, 2021.

[14] N. Auffray, R. Bouchet, and Y. Bréchet. Representation graphique des coefficients d'anisotropies des milieux élastiques généralisés. In *CFM 2009-19ème Congrès Français de Mécanique*. AFM, Maison de la Mécanique, 39/41 rue Louis Blanc-92400 Courbevoie, 2009.

[15] N. Auffray, S. El Ouafa, G. Rosi, and B. Desmorat. Anisotropic structure of two-dimensional linear cosserat elasticity. *Mathematics and Mechanics of Complex Systems*, 2022.

[16] N. Auffray, B. Kolev, and M. Olive. Handbook of bi-dimensional tensors: Part I: Harmonic decomposition and symmetry classes. *Mathematics and Mechanics of Solids*, 22(9):1847–1865, 2017. Publisher: SAGE Publications Ltd STM.

[17] N. Auffray, B. Kolev, and M. Petitot. On anisotropic polynomial relations for the elasticity tensor. *Journal of Elasticity*, 115(1):77–103, 2014.

[18] P. Azzi and M. Olive. Clips operation between type II and type III O(3)-subgroups with application to piezoelectricity. 2022. arXiv:2202.00261 [math-ph].

[19] D. Banabic. *Sheet Metal Forming Processes*. Springer Berlin Heidelberg.

[20] D. Banabic. *Plastic Behaviour of Sheet Metal*, pages 27–140. 05 2010.

[21] F. Barlat, H. Aretz, J. Yoon, M. Karabin, J. Brem, and R. Dick. Linear transfomation-based anisotropic yield functions. *International Journal of Plasticity*, 21:1009–1039, 05 2005.

[22] F. Barlat, H. Aretz, J. Yoon, M. Karabin, J. Brem, and R. Dick. Linear transfomation-based anisotropic yield functions. *International Journal of Plasticity*, 21(5):1009–1039, 2005.

[23] F. Barlat, J. Brem, J. Yoon, K. Chung, R. Dick, D. Lege, F. Pourboghrat, S. Choi, and E. Chu. Plane stress yield function for aluminum alloy sheets - part 1: Theory. *International Journal of Plasticity - INT J PLASTICITY*, 19:1297–1319, 2003.

[24] F. Barlat, D. Lege, and J. Brem. A six-component yield function for anisotropic materials. *International Journal of Plasticity*, 7:693–712, 01 1991.

[25] F. Barlat, Y. Maeda, K. Chung, M. Yanagawa, J. Brem, Y. Hayashida, D. Lege, K. Matsui, S. Murtha, S. Hattori, R. Becker, and S. Makosey. Yield function development for aluminum alloy sheets. *Journal of the Mechanics and Physics of Solids*, 45:1727–1763, 11 1997.

[26] F. Barlat and O. Richmond. Prediction of tricomponent plane stress yield surfaces and associated flow and failure behavior of strongly textured f.c.c. polycrystalline sheets. *Materials Science and Engineering*, 95:15–29, 1987.

[27] F. Barlat, J. Yoon, and O. Cazacu. On linear transformations of stress tensors for the description of plastic anisotropy. *International Journal of Plasticity*, 23(5):876–896, 2007.

[28] J. Barlat, F.and Lian and B. Baudelet. *A Yield Function for Orthotropic Sheets under Plane Stress Conditions*, pages 283–288. 12 1989.

[29] J. Bassani. Yield characterization of metals with transversely isotropic plastic properties. *International Journal of Mechanical Sciences*, 19(11):651–660, 1977.

[30] A. Belegundu, L. Berke, and S. Patnaik. An optimization algorithm based on the method of feasible directions. *Structural optimization*, 9(2):83–88, 1995.

[31] M. Bendsøe. *Optimization of Structural Topology, Shape, and Material*. Springer Berlin Heidelberg, Berlin, Heidelberg, 1995.

[32] D. Bertsekas. *Constrained Optimization and Lagrange Multiplier Methods*. Elsevier, 1982.

[33] J. P. Boehler. *Applications of Tensor Functions in Solid Mechanics*. Springer, Vienna, 1987.

[34] C. Bogusław. Tensor Methods in Computer Vision. In *Object Detection and Recognition in Digital Images*, pages 9–188. John Wiley & Sons, Ltd, 2013. Section: 2.

[35] R. Bohrer and I. Kim. Multi-material topology optimization considering isotropic and anisotropic materials combination. *Structural and Multidisciplinary Optimization*, 64(3):1567–1583, 2021.

[36] B. Bourdin and A. Chambolle. Design-dependent loads in topology optimization. *ESAIM: Control, Optimisation and Calculus of Variations*, 9:19–48, 2003.

[37] M. Bower and D. Koedam. Tensor Polynomial Failure Criterion: Coefficient Limits Based on Convexity Requirements. *Journal of Reinforced Plastics and Composites*, 16(5):435–477, 1997. Publisher: SAGE Publications Ltd STM.

[38] M. Bruggi. On an alternative approach to stress constraints relaxation in topology optimization. *Structural and Multidisciplinary Optimization*, 36(2):125–141, 2008.

[39] T. Bruns. A reevaluation of the SIMP method with filtering and an alternative formulation for solid–void topology optimization. *Structural and Multidisciplinary Optimization*, 30(6):428–436, 2005.

[40] O. Brüls, E. Lemaire, P. Duysinx, and P. Eberhard. Optimization of Multibody Systems and Their Structural Components. In Krzysztof Arczewski, Wojciech Blajer, Janusz Fraczek, and Marek Wojtyra, editors, *Multibody Dynamics*, volume 23, pages 49–68. Springer Netherlands, Dordrecht, 2011. Series Title: Computational Methods in Applied Sciences.

[41] P. Carpentier and G. Cohen. *Décomposition-coordination en optimisation déterministe et stochastique*, volume 81 of *Mathématiques et Applications*. Springer Berlin Heidelberg, Berlin, Heidelberg, 2017.

[42] A. Casalotti, F. D'Annibale, and G. Rosi. Multi-scale design of an architected composite structure with optimized graded properties. *Composite Structures*, 252:112608, 2020.

[43] A. Catapano, B. Desmorat, and P. Vannucci. Invariant formulation of phenomenological failure criteria for orthotropic sheets and optimisation of their strength. *Mathematical Methods in the Applied Sciences*, 35(15):1842–1858, 2012. _eprint: https://onlinelibrary.wiley.com/doi/pdf/10.1002/mma.2530.

[44] O. Cazacu and F. Barlat. Generalization of drucker's yield criterion to orthotropy. *Mathematics and Mechanics of Solids*, 6(6):613–630, 2001.

[45] O. Cazacu and F. Barlat. Application of the theory of representation to describe yielding of anisotropic aluminum alloys. *International Journal of Engineering Science*, 41(12):1367–1385, 2003.

[46] O. Cazacu and F. Barlat. A criterion for description of anisotropy and yield differential effects in pressure-insensitive metals. *International Journal of Plasticity*, 20(11):2027–2045, 2004.

[47] Letian Chen. *Triangular lattice of arbitrary class of 2D elasticity TRIANGULAR LATTICE OF ARBITRARY CLASS OF 2D ELASTICITY*. PhD thesis, 06 2017.

[48] X. Chen, L. Niu, and Y. Yuan. Optimality Conditions and a Smoothing Trust Region Newton Method for NonLipschitz Optimization. *SIAM Journal on Optimization*, 23(3):1528–1552, 2013.

[49] Y. Chen, H. Nassar, and G. Huang. Discrete transformation elasticity: An approach to design lattice-based polar metamaterials. *International Journal of Engineering Science*, 168:103562, 2021.

[50] G. Cheng and X. Guo. ϵ-relaxed approach in structural topology optimization. *Structural optimization*, 13(4):258–266, 1997.

[51] G Cheng and Z. Jiang. Study on topology optimisation with stress constraints. *Engineering Optimization*, 20(2):129–148, 1992.

[52] M. Chávez-Pichardo, M. Martínez-Cruz, A. Trejo-Martínez, D. Martínez-Carbajal, and T. Arenas-Resendiz. A Complete Review of the General Quartic Equation with Real Coefficients and Multiple Roots. *Mathematics*, 10(14):2377, 2022. Number: 14 Publisher: Multidisciplinary Digital Publishing Institute.

[53] P. Coelho, P. Fernandes, J. Guedes, and H. Rodrigues. A hierarchical model for concurrent material and topology optimisation of three-dimensional structures. *Structural and Multidisciplinary Optimization*, 35(2):107–115, 2008.

[54] C. Combescure, P. Henry, and R. Elliott. Post-bifurcation and stability of a finitely strained hexagonal honeycomb subjected to equi-biaxial in-plane loading. *International Journal of Solids and Structures*, 88-89:296–318, 2016.

[55] G. da Silva, N. Aage, A. Beck, and O. Sigmund. Local versus global stress constraint strategies in topology optimization: A comparative study. *International Journal for Numerical Methods in Engineering*, 122(21):6003–6036, 2021.

[56] C. Dapogny and F. Feppon. Shape optimization using a level set based mesh evolution method: an overview and tutorial. 2022. Hal (https://hal.science/hal-03881641).

[57] S. Deng and K. Suresh. Multi-constrained 3D topology optimization via augmented topological level-set. *Computers & Structures*, 170:1–12, 2016.

[58] V. Deshpande, M. Ashby, and N. Fleck. Foam topology: bending versus stretching dominated architectures. *Acta Materialia*, 49(6):1035–1040, 2001.

[59] V. Deshpande, N. Fleck, and M. Ashby. Effective properties of the octet-truss lattice material. *Journal of the Mechanics and Physics of Solids*, 49(8):1747–1769, 2001.

[60] B. Desmorat and N. Auffray. Space of 2D elastic materials: a geometric journey. *Continuum Mechanics and Thermodynamics*, 31(4):1205–1229, 2019.

[61] B. Desmorat, M. Olive, N. Auffray, R. Desmorat, and B. Kolev. Computation of minimal covariants bases for 2D coupled constitutive laws. *International Journal of Engineering Science*, 191:103880, 2023. arXiv:2007.01576 [physics].

[62] D. Drucker. Relation of Experiments to Mathematical Theories of Plasticity. *Journal of Applied Mechanics*, 16(4):349–357, 04 2021.

[63] E. Duriez, J. Morlier, M. Charlotte, and C. Azzaro-Pantel. A well connected, locally-oriented and efficient multi-scale topology optimization (EMTO) strategy. *Structural and Multidisciplinary Optimization*, 64(6):3705–3728, 2021.

[64] P. Duysinx and M. Bendsøe. Topology optimization of continuum structures with local stress constraints. *International Journal for Numerical Methods in Engineering*, 43(8):1453–1478, 1998.

[65] P. Duysinx and O. Sigmund. New developments in handling stress constraints in optimal material distribution. In *7th AIAA/USAF/NASA/ISSMO Symposium on Multidisciplinary Analysis and Optimization*. American Institute of Aeronautics and Astronautics, 1998.

[66] I. Echeta, X. Feng, B. Dutton, R. Leach, and S. Piano. Review of defects in lattice structures manufactured by powder bed fusion. *The International Journal of Advanced Manufacturing Technology*, 106(5):2649–2668, 2020.

[67] M. El-Sayed, T. Sun, and J. Berry. Shape optimization with computational fluid dynamics. *Advances in Engineering Software*, 36(9):607–613, 2005.

[68] D. Fang, X. Cui, Y. Zhang, and H. Zhao. Mechanical Properties and Design of Lattice Composites and Structures. In Han Zhao and N. A. Fleck, editors, *IUTAM Symposium on Mechanical Properties of Cellular Materials*, IUTAM Bookseries, pages 9–18, Dordrecht, 2009. Springer Netherlands.

[69] A. Faure. *Optimisation de forme de matériaux et structures architecturés par la méthode des lignes de niveaux avec prise en compte des interfaces graduées*. PhD thesis, Université de Grenoble-Alpes, 2017.

[70] F. Feppon. *Shape and topology optimization of multiphysics systems*. PhD thesis, Université Paris Saclay, 2019.

[71] F. Feppon, G. Allaire, and C. Dapogny. Null space gradient flows for constrained optimization with applications to shape optimization. *ESAIM: Control, Optimisation and Calculus of Variations*, 26:90, 2020.

[72] N. Fleck, V. Deshpande, and M. Ashby. Micro-architectured materials: past, present and future. *Proceedings of the Royal Society A: Mathematical, Physical and Engineering Sciences*, 466(2121):2495–2516, 2010.

[73] S. Forest, M. Amestoy, G. Damamme, S. Kruch, V. Maurel, and M. Maziere. *Mécanique des milieux continus*. École des Mines de Paris, 2015.

[74] S. Forte and M. Vianello. Symmetry classes for elasticity tensors. *Journal of Elasticity*, 43(2):81–108, May 1996.

[75] S. Forte and M. Vianello. A unified approach to invariants of plane elasticity tensors. *Meccanica*, 49(9):2001–2012, 2014.

[76] M. Louis Maurice François. A new yield criterion for the concrete materials. *Comptes rendus de l'Académie des sciences. Série IIb, Mécanique, physique, chimie, astronomie*, 336(5):417–421, 2008.

[77] P. Geoggroy-Donders. *Homogenization method for topology optimization of structures built with lattice materials*. PhD thesis, Universite Paris-Saclay, 2018.

[78] P. Germain. La méthode des puissances virtuelles en mécanique des milieux continus, premiere partie: théorie du second gradient. *J. Mécanique*, 12(2):235–274, 1973.

[79] L. Gibson and M. Ashby. *Cellular Solids: Structure and Properties*. Cambridge Solid State Science Series. Cambridge University Press, 1997.

[80] O. Giraldo-Londoño and G. Paulino. A unified approach for topology optimization with local stress constraints considering various failure criteria: von Mises, Drucker–Prager, Tresca, Mohr–Coulomb, Bresler–Pister and Willam–Warnke. *Proceedings of the Royal Society A: Mathematical, Physical and Engineering Sciences*, 476(2238):20190861, 2020.

[81] O. Giraldo-Londoño and G. Paulino. PolyStress: a Matlab implementation for local stress-constrained topology optimization using the augmented Lagrangian method. *Structural and Multidisciplinary Optimization*, 63(4):2065–2097, 2021.

[82] I. Gol'denblat and V. Kopnov. Strength of glass-reinforced plastics in the complex stress state. *Polymer Mechanics*, 1(2):54–59, 1965.

[83] M. Golubitsky, I. Stewart, and D. Schaeffer. *Singularities and Groups in Bifurcation Theory: Volume II*, volume 69. Springer Science & Business Media, 2012.

[84] M. Gotoh. A theory of plastic anisotropy based on a yield function of fourth order (plane stress state)—i. *International Journal of Mechanical Sciences*, 19(9):505–512, 1977.

[85] A. Groenwold and R. Haftka. Optimization with non-homogeneous failure criteria like Tsai–Wu for composite laminates. *Structural and Multidisciplinary Optimization*, 32(3):183–190, 2006.

[86] J. Haslinger, M. Kocvara, G. Leugering, and M. Stingl. Multidisciplinary Free Material Optimization. *SIAM Journal on Applied Mathematics*, 70(7):2709–2728, 2010.

[87] A. Hershey. The Plasticity of an Isotropic Aggregate of Anisotropic Face-Centered Cubic Crystals. *Journal of Applied Mechanics*, 21(3):241–249, 06 2021.

[88] T. Hewage, K. Alderson, A. Alderson, and F. Scarpa. Double-negative mechanical metamaterials displaying simultaneous negative stiffness and negative poisson's ratio properties. *Advanced Materials*, 28(46):10323–10332, 2016.

[89] R. Hill. *The Mathematical Theory of Plasticity*. Oxford classic texts in the physical sciences. Clarendon Press, 1950.

[90] R. Hill. Theoretical plasticity of textured aggregates. *Mathematical Proceedings of the Cambridge Philosophical Society*, 85(1):179–191, 1979.

[91] R. Hill. Constitutive modelling of orthotropic plasticity in sheet metals. *Journal of the Mechanics and Physics of Solids*, 38(3):405–417, 1990.

[92] R. Hill. A user-friendly theory of orthotropic plasticity in sheet metals. *International Journal of Mechanical Sciences*, 35(1):19–25, 1993.

[93] R. Hill and E. Orowan. A theory of the yielding and plastic flow of anisotropic metals. *Proceedings of the Royal Society of London. Series A. Mathematical and Physical Sciences*, 193(1033):281–297, 1948.

[94] W. Hosford. A Generalized Isotropic Yield Criterion. *Journal of Applied Mechanics*, 39(2):607–609, 06 1972.

[95] W. Hosford. Comments on anisotropic yield criteria. *International Journal of Mechanical Sciences*, 27(7):423–427, 1985.

[96] W.F. Hosford. *Fundamentals of Engineering Plasticity*. Fundamentals of Engineering Plasticity. Cambridge University Press.

[97] J. Hu, M. Li, X. Yang, and S. Gao. Cellular structure design based on free material optimization under connectivity control. *Computer-Aided Design*, 127:102854, 2020.

[98] M. Huber. Specific work of strain as a measure of material effort. *Archives of Mechanics*, 56:173–190, 2004.

[99] J. Hutchinson and Z. Xue. Metal sandwich plates optimized for pressure impulses. *International Journal of Mechanical Sciences*, 47(4):545–569, 2005.

[100] E Ihrig and M. Golubitsky. Pattern selection with o (3) symmetry. *Physica D: Nonlinear Phenomena*, 13(1-2):1–33, 1984.

[101] S. Janson. Roots of polynomials of degrees 3 and 4, 2010. arXiv:1009.2373 [math] version: 1.

[102] V. Jeanneau. *Tenseur d'élasticité et critère limite d'élasticité des milieux architecturés périodiques*. PhD thesis, Nantes université, 2023.

[103] V. Jeanneau, C. Combescure, and M. Francois. Comportement effectif et limite de linéarité d'un matériau architecturé 2D périodique à celulles triangulaires. CFM 2022 (submitted).

[104] P. Jensen, O. Sigmund, and J. Groen. De-homogenization of optimal 2D topologies for multiple loading cases. *Computer Methods in Applied Mechanics and Engineering*, 399:115426, 2022.

[105] J. Jerphagnon, D. Chemla, and R. Bonneville. The description of the physical properties of condensed matter using irreducible tensors. *Advances in Physics*, 27(4):609–650, 1978.

[106] A. Joubert. Optimisation de formes de structures viscoélastiques sous sollicitations dynamiques.

[107] A. Karafillis and M. Boyce. A general anisotropic yield criterion using bounds and a transformation weighting tensor. *Journal of the Mechanics and Physics of Solids*, 41(12):1859–1886, 1993.

[108] A. Kaveh, B. Hassani, S. Shojaee, and S. Tavakkoli. Structural topology optimization using ant colony methodology. *Engineering Structures*, 30(9):2559–2565, 2008.

[109] G. Kennedy and E. Hicken. Improved constraint-aggregation methods. *Computer Methods in Applied Mechanics and Engineering*, 289:332–354, 2015.

[110] U. Kirsch. *Structural Optimization*. Springer Berlin Heidelberg, Berlin, Heidelberg, 1993.

[111] M. Kocvara, M. Stingl, and J. Zowe. Free material optimization: recent progress. *Optimization*, 57(1):79–100, 2008. Publisher: Taylor & Francis _eprint: https://doi.org/10.1080/02331930701778908.

[112] F. X. Kromm and H. Wargnier. Design Methods for Architectured Materials. In *Architectured Materials in Nature and Engineering: Archimats*, Springer Series in Materials Science, pages 141–171. Springer International Publishing, Cham, 2019.

[113] T. Kumar and K. Suresh. A density-and-strain-based K-clustering approach to microstructural topology optimization. *Structural and Multidisciplinary Optimization*, 61(4):1399–1415, 2020.

[114] P. Köhnen, C. Haase, J. Bültmann, S. Ziegler, J. Schleifenbaum, and W. Bleck. Mechanical properties and deformation behavior of additively manufactured lattice structures of stainless steel. *Materials & Design*, 145:205–217, 2018.

[115] B. Lazarov and O. Sigmund. Filters in topology optimization based on Helmholtz-type differential equations. *International Journal for Numerical Methods in Engineering*, 86(6):765–781, 2011. _eprint: https://onlinelibrary.wiley.com/doi/pdf/10.1002/nme.3072.

[116] A. G. Leacock. A mathematical description of orthotropy in sheet metals. *Journal of the Mechanics and Physics of Solids*, 54(2):425–444, 2006.

[117] J. Lee, D. Kim, T. Nomura, E. Dede, and J. Yoo. Topology optimization for continuous and discrete orientation design of functionally graded fiber-reinforced composite structures. *Composite Structures*, 201:217–233, 2018.

[118] J. Lehman and R. Lakes. Stiff lattices with zero thermal expansion and enhanced stiffness via rib cross section optimization. *International Journal of Mechanics and Materials in Design*, 9(3):213–225, 2013.

[119] D. Li, W. Liao, N. Dai, and Y. Xie. Anisotropic design and optimization of conformal gradient lattice structures. *Computer-Aided Design*, 119:102787, 2020.

[120] S.B. Lin and J.L. Ding. A modified form of hill's orientationdashdependent yield criterion for orthotropic sheet metals. *Journal of the Mechanics and Physics of Solids*, 44(11):1739–1764, 1996.

[121] J. Liu and H. Yu. Concurrent deposition path planning and structural topology optimization for additive manufacturing. *Rapid Prototyping Journal*, 23(5):930–942, 2017. Publisher: Emerald Publishing Limited.

[122] G. Luh, C. Lin, and Y. Lin. A binary particle swarm optimization for continuum structural topology optimization. *Applied Soft Computing*, 11(2):2833–2844, 2011.

[123] J. Lógó and H. Ismail. Milestones in the 150-year history of topology optimization: A review. *Computer Assisted Methods in Engineering and Science*, 2–3(27):97–132, 2020.

[124] J. Meaud, T. Sain, B. Yeom, S. J. Park, A. B. Shoultz, G. Hulbert, Z. Ma, N. A. Kotov, A. J. Hart, E. M. Arruda, and A. M. Waas. Simultaneously high stiffness and damping in nanoengineered microtruss composites. *ACS Nano*, 2014.

[125] A. Mendelson. *Plasticity: Theory and Application*. Macmillan series in applied mechanics. R.E. Krieger Publishing Company, 1983.

[126] M.H.H. Meuwissen. *Yield criteria for anisotropic elasto-plastic metals*. DCT rapporten. Technische Universiteit Eindhoven, 1995. WFW 1995.152.

[127] Z. Mingyang, Y. Zhenyu, L. Zixing, L. Baohua, and H. Xiaofan. Effective elastic properties and initial yield surfaces of two 3d lattice structures. *International Journal of Mechanical Sciences*, 138-139:146–158, 2018.

[128] A. Mirzendehdel, B. Rankouhi, and K. Suresh. Strength-based topology optimization for anisotropic parts. *Additive Manufacturing*, 19:104–113, 2018.

[129] R. Mises. Mechanik der festen körper im plastisch- deformablen zustand. *Nachrichten von der Gesellschaft der Wissenschaften zu Göttingen, Mathematisch-Physikalische Klasse*, 1913:582–592, 1913.

[130] G. Mou, B. Desmorat, R. Turlin, and N. Auffray. On exotic linear materials: 2D elasticity and beyond. *International Journal of Solids and Structures*, 264:112103, 2023.

[131] F. Nielsen and K. Sun. Guaranteed bounds on the Kullback-Leibler divergence of univariate mixtures using piecewise log-sum-exp inequalities. *Entropy*, 18(12):442, 2016. arXiv:1606.05850 [cs, math, stat].

[132] J. Nocedal and S. Wright. *Numerical optimization*. Springer series in operations research. Springer, New York, 2nd ed edition, 2006.

[133] J. Norato, H. Smith, J. Deaton, and R. Kolonay. A maximum-rectifier-function approach to stress-constrained topology optimization. *Structural and Multidisciplinary Optimization*, 65(10):286, 2022.

[134] M. Olive and N. Auffray. Symmetry classes for even-order tensors. *Mathematics and Mechanics of Complex Systems*, 1(2):177–210, 2013.

[135] M. Olive and N. Auffray. Symmetry classes for odd-order tensors. *ZAMM-Journal of Applied Mathematics and Mechanics/Zeitschrift für Angewandte Mathematik und Mechanik*, 94(5):421–447, 2014.

[136] M. Olive, B. Kolev, B. Desmorat, and R. Desmorat. Harmonic Factorization and Reconstruction of the Elasticity Tensor. *Journal of Elasticity*, 132(1):67–101, 2018.

[137] M. Olive, B. Kolev, R. Desmorat, and B. Desmorat. Characterization of the symmetry class of an elasticity tensor using polynomial covariants. *Mathematics and Mechanics of Solids*, 27(1):144–190, 2022.

[138] J. París, F. Navarrina, I. Colominas, and M. Casteleiro. Block aggregation of stress constraints in topology optimization of structures. *Advances in Engineering Software*, 41(3):433–441, 2010.

[139] E. Pasternak and A. Dyskin. *Architectured Materials with Inclusions Having Negative Poisson's Ratio or Negative Stiffness*, pages 51–87. Springer International Publishing, Cham, 2019.

[140] P. Pedersen. On optimal orientation of orthotropic materials. *Structural Optimization*, 1(2):101–106, 1989.

[141] J. Pereira, E. Fancello, and C. Barcellos. Topology optimization of continuum structures with material failure constraints. *Structural and Multidisciplinary Optimization*, 26(1-2):50–66, 2004.

[142] A. Phani and M. Hussein. *Dynamics of Lattice Materials*. Wiley, 2017.

[143] R. Picelli, S. Townsend, C. Brampton, J. Norato, and H. Kim. Stress-based shape and topology optimization with the level set method. *Computer Methods in Applied Mechanics and Engineering*, 329:1–23, 2018.

[144] M. Poncelet, A. Somera, C. Morel, C. Jailin, and N. Auffray. An experimental evidence of the failure of Cauchy elasticity for the overall modeling of a non-centro-symmetric lattice under static loading. *International Journal of Solids and Structures*, 147:223–237, 2018.

[145] W. Prager. *Introduction to Structural Optimization*. Springer Vienna, Vienna, 1972.

[146] N. Ranaivomiarana. *Simultaneous optimization of topology and material anisotropy for aeronautic structures*. PhD thesis, Sorbonne université, 2019.

[147] R. Rivlin and J. Ericksen. Stress-deformation relations for isotropic materials. *Collected Papers of RS Rivlin: Volume I and II*, pages 911–1013, 1997.

[148] G. Rosi and N. Auffray. Continuum modelling of frequency dependent acoustic beam focussing and steering in hexagonal lattices. *European Journal of Mechanics-A/Solids*, 77:103803, 2019.

[149] G. Rosi and N. Auffray. Continuum modelling of frequency dependent acoustic beam focussing and steering in hexagonal lattices. *European Journal of Mechanics - A/Solids*, 77:103803, 2019.

[150] M. Safaei. *Constitutive modelling of anisotropic sheet metals based on a non-associated flow rule*. PhD thesis, 01 2013.

[151] A. Safonov. 3D topology optimization of continuous fiber-reinforced structures via natural evolution method. *Composite Structures*, 215:289–297, 2019.

[152] J. Salençon. About Tresca's Memoirs on the fluidity of solids (1864–1870). *Comptes Rendus. Mécanique*, 349(1):1–7, 2021.

[153] B. Samet, S. Amstutz, and M. Masmoudi. The Topological Asymptotic for the Helmholtz Equation. *SIAM Journal on Control and Optimization*, 42(5):1523–1544, 2003.

[154] E. Sanders, A. Pereira, M. Aguiló, and G. Paulino. PolyMat: an efficient Matlab code for multi-material topology optimization. *Structural and Multidisciplinary Optimization*, 58(6):2727–2759, 2018.

[155] A. Sanyal, J. Scheffelin, and T. Keaveny. The Quartic Piecewise-Linear Criterion for the Multiaxial Yield Behavior of Human Trabecular Bone. *Journal of Biomechanical Engineering*, 137(1):0110091–01100910, 2015.

[156] M. Schmidt, L. Couret, C. Gout, and C. Pedersen. Structural topology optimization with smoothly varying fiber orientations. *Structural and Multidisciplinary Optimization*, 62(6):3105–3126, 2020.

[157] M. Schmidt, G. Fung, and R. Rosales. Fast Optimization Methods for L1 Regularization: A Comparative Study and Two New Approaches. In *Machine Learning: ECML 2007*, Lecture Notes in Computer Science, pages 286–297, Berlin, Heidelberg, 2007. Springer.

[158] J. Schwiedrzik, U. Wolfram, and P. Zysset. A generalized anisotropic quadric yield criterion and its application to bone tissue at multiple length scales. *Biomechanics and Modeling in Mechanobiology*, 12(6):1155–1168, 2013.

[159] F. Senhora, O. Giraldo-Londono, I. Menezes, and G. Paulino. Topology optimization with local stress constraints: a stress aggregation-free approach. *Structural and Multidisciplinary Optimization*, 62(4):1639–1668, 2020.

[160] Y. Shen and D. Branscomb. Orientation optimization in anisotropic materials using gradient descent method. *Composite Structures*, 234:111680, 2020.

[161] M. Shimoda, H. Azegami, and T. Sakurai. Numerical Solution for Min-Max Shape Optimization Problems. (Minimum Design of Maximum Stress and Displacement). *JSME International Journal Series A*, 41(1):1–9, 1998.

[162] O. Sigmund. A 99 line topology optimization code written in matlab. *Structural and Multidisciplinary Optimization*, 21(2):120–127, 2001.

[163] O. Sigmund and J. Petersson. Numerical instabilities in topology optimization: A survey on procedures dealing with checkerboards, mesh-dependencies and local minima. *Structural Optimization*, 16(1):68–75, 1998.

[164] A. Silva, R. Salas, and E. Silva. Topology Optimization of fiber reinforced structures considering stress constraint and optimized penalization. *Composite Structures*, 316:117006, 2023.

[165] R. Sivapuram, P. D. Dunning, and H. Kim. Simultaneous material and structural optimization by multi-scale topology optimization. *Structural and Multidisciplinary Optimization*, 54(5):1267–1281, 2016.

[166] S. Soare. On the use of homogenous polynomials to develop anisotropic yield functions with application to sheet metal forming.

[167] S. Soare. On the use of homogeneous polynomials to develop anisotropic yield functions with applications to sheet forming. *International Journal of Plasticity*, 2008.

[168] S. Soare. A parameter identification scheme for the orthotropic Poly6 yield function satisfying the convexity condition. *European Journal of Mechanics - A/Solids*, 92:104467, 2022.

[169] S. Soare, J. Yoon, and O. Cazacu. On Using Homogeneous Polynomials To Design Anisotropic Yield Functions With Tension/Compression Symmetry/Assymetry. *AIP Conference Proceedings*, 908(1):607–612, 2007.

[170] S. Soare, J. Yoon, and O. Cazacu. On Using Homogeneous Polynomials To Design Anisotropic Yield Functions With Tension/Compression Symmetry/Assymetry. *AIP Conference Proceedings*, 908(1):607–612, 2007.

[171] S. Soare, J. Yoon, and O. Cazacu. On the use of homogeneous polynomials to develop anisotropic yield functions with applications to sheet forming. *International Journal of Plasticity*, 24(6):915–944, 2008.

[172] A. Somera. On the effective elasticity of quasi-periodic lattice materials.

[173] J. Somnic and B. Jo. Status and challenges in homogenization methods for lattice materials. *Materials*, 15(2):605, 2022.

[174] C. Steeves, C. Mercer, E. Antinucci, M. Y. He, and A. Evans. Experimental investigation of the thermal properties of tailored expansion lattices. *International Journal of Mechanics and Materials in Design*, 5(2), 2009.

[175] J. Stegmann and E. Lund. Discrete material optimization of general composite shell structures: DISCRETE MATERIAL OPTIMIZATION OF GENERAL COMPOSITE SHELL STRUCTURES. *International Journal for Numerical Methods in Engineering*, 62(14):2009–2027, 2005.

[176] S. Sternberg. *Group theory and physics*. Cambridge University Press, 1995.

[177] M. Stolpe and K. Svanberg. An alternative interpolation scheme for minimum compliance topology optimization. *Structural and Multidisciplinary Optimization*, 22(2):116–124, 2001.

[178] K. Svanberg. The method of moving asymptotes—a new method for structural optimization. *International Journal for Numerical Methods in Engineering*, 24(2):359–373, 1987.

[179] K. Svanberg. A Class of Globally Convergent Optimization Methods Based on Conservative Convex Separable Approximations. *SIAM Journal on Optimization*, 12(2):555–573, 2002.

[180] S. Sørensen, R. Sørensen, and E. Lund. DMTO – a method for Discrete Material and Thickness Optimization of laminated composite structures. *Structural and Multidisciplinary Optimization*, 50(1):25–47, 2014.

[181] B. Telgen, O. Sigmund, and D. Kochmann. Topology Optimization of Graded Truss Lattices Based on On-the-Fly Homogenization. *Journal of Applied Mechanics*, 89(6):061006, 2022. arXiv:2205.14366 [cond-mat].

[182] C. Truesdell, W. Noll, C. Truesdell, and W. Noll. *The non-linear field theories of mechanics*. Springer, 2004.

[183] E. Uribe-Lam, C. Treviño-Quintanilla, E. Cuan-Urquizo, and O. Olvera-Silva. Use of additive manufacturing for the fabrication of cellular and lattice materials: a review. *Materials and Manufacturing Processes*, 36:257–280, 2021.

[184] P. Vannucci. Plane Anisotropy by the Polar Method*. *Meccanica*, 40(4):437–454, 2005.

[185] A. Verbart. *Topology Optimization with Stress Constraints*. PhD thesis, TU Delft, 2015.

[186] A. Verbart, M. Langelaar, and F. Keulen. A unified aggregation and relaxation approach for stress-constrained topology optimization. *Structural and Multidisciplinary Optimization*, 55(2):663–679, 2017.

[187] L. Vertonghen. *Incorporating strength constraints in a simultaneous material anisotropy and topology optimization of composite laminate structures*. PhD thesis, Sorbonne Université, 2023.

[188] A. Wang and D. McDowell. Yield surfaces of various periodic metal honeycombs at intermediate relative density. *International Journal of Plasticity*, 21(2):285–320, 2005.

[189] C. Wang, Z. Zhao, M. Zhou, O. Sigmund, and X. Zhang. A comprehensive review of educational articles on structural and multidisciplinary optimization. *Structural and Multidisciplinary Optimization*, 64(5):2827–2880, 2021.

[190] S. Wang and K. Tai. Structural topology design optimization using Genetic Algorithms with a bit-array representation. *Computer Methods in Applied Mechanics and Engineering*, 194(36-38):3749–3770, 2005.

[191] A. Weldeyesus and M. Stolpe. Free material optimization for laminated plates and shells. *Structural and Multidisciplinary Optimization*, 53(6):1335–1347, 2016.

[192] C. Woischwill and I. Kim. Multimaterial multijoint topology optimization. *International Journal for Numerical Methods in Engineering*, 115(13):1552–1579, 2018. _eprint: https://onlinelibrary.wiley.com/doi/pdf/10.1002/nme.5908.

[193] J. Woodthorpe and R. Pearce. The anomalous behaviour of aluminium sheet under balanced biaxial tension. *International Journal of Mechanical Sciences*, 12(4):341–347, 1970.

[194] J. Wu, O. Sigmund, and J. Groen. Topology optimization of multi-scale structures: a review. *Structural and Multidisciplinary Optimization*, 63(3):1455–1480, 2021.

[195] J. Wu, W. Wang, and X. Gao. Design and optimization of conforming lattice structures. *IEEE Transactions on Visualization and Computer Graphics*, 27(1):43–56, 2021.

[196] L. Xia, L. Zhang, Q. Xia, and T. Shi. Stress-based topology optimization using bi-directional evolutionary structural optimization method. *Computer Methods in Applied Mechanics and Engineering*, 333:356–370, 2018.

[197] Y. Xie and G. Steven. A simple evolutionary procedure for structural optimization. *Computers & Structures*, 49(5):885–896, 1993.

[198] D. Yang, Ho. Liu, W. Zhang, and S. Li. Stress-constrained topology optimization based on maximum stress measures. *Computers & Structures*, 198:23–39, 2018.

[199] X. Yang, Y. Xie, G. Steven, and O. Querin. Bidirectional Evolutionary Method for Stiffness Optimization. *AIAA Journal*, 37(11):1483–1488, 1999.

[200] G. Yi and N. Kim. Identifying boundaries of topology optimization results using basic parametric features. *Structural and Multidisciplinary Optimization*, 55(5):1641–1654, 2017.

[201] Y. Zhang, X. Qiu, and D. Fang. Mechanical Properties of two novel planar lattice structures. *International Journal of Solids and Structures*, 45(13):3751–3768, 2008.

[202] Y. Zhang, Z. Xue, X. Qiu, and D. Fang. Plastic yield and collapse mechanism of planar lattice structures. *Journal of Mechanics of Materials and Structures - J MECH MATER STRUCT*, 3:1257–1277, 2008.

[203] Z. Zhang, O. Ibhadode, U. Ali, C. Dibia, P. Rahnama, A. Bonakdar, and E. Toyserkani. Topology optimization parallel-computing framework based on the inherent strain method for support structure design in laser powder-bed fusion additive manufacturing. *International Journal of Mechanics and Materials in Design*, 16(4):897–923, 2020.

[204] Q. Zheng. Theory of Representations for Tensor Functions—A Unified Invariant Approach to Constitutive Equations. *Applied Mechanics Reviews*, 47(11):545–587, 1994.

[205] H Zidani. Optimisation quadartique. December 2018. Class lecture, ENSTA Paris.

[206] J. Zowe and M. Kocvara, M. an.d Bendsoe. Free material optimization via mathematical programming. *Mathematical Programming*, 79(1):445–466, 1997.